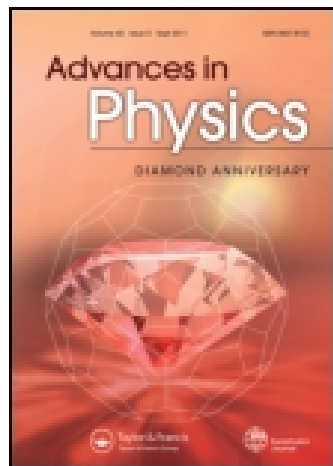


This article was downloaded by: [18.140.1.248]

On: 06 April 2015, At: 15:50

Publisher: Taylor & Francis

Informa Ltd Registered in England and Wales Registered Number: 1072954 Registered office: Mortimer House, 37-41 Mortimer Street, London W1T 3JH, UK



## Advances in Physics

Publication details, including instructions for authors and subscription information:

<http://www.tandfonline.com/loi/tadp20>

### The transition metal dichalcogenides discussion and interpretation of the observed optical, electrical and structural properties

J.A. Wilson<sup>a</sup> & A.D. Yoffe<sup>a</sup>

<sup>a</sup> Cavendish Laboratory, Cambridge

Published online: 02 Jun 2006.

To cite this article: J.A. Wilson & A.D. Yoffe (1969) The transition metal dichalcogenides discussion and interpretation of the observed optical, electrical and structural properties, *Advances in Physics*, 18:73, 193-335, DOI: [10.1080/00018736900101307](https://doi.org/10.1080/00018736900101307)

To link to this article: <http://dx.doi.org/10.1080/00018736900101307>

PLEASE SCROLL DOWN FOR ARTICLE

Taylor & Francis makes every effort to ensure the accuracy of all the information (the "Content") contained in the publications on our platform. However, Taylor & Francis, our agents, and our licensors make no representations or warranties whatsoever as to the accuracy, completeness, or suitability for any purpose of the Content. Any opinions and views expressed in this publication are the opinions and views of the authors, and are not the views of or endorsed by Taylor & Francis. The accuracy of the Content should not be relied upon and should be independently verified with primary sources of information. Taylor and Francis shall not be liable for any losses, actions, claims, proceedings, demands, costs, expenses, damages, and other liabilities whatsoever or howsoever caused arising directly or indirectly in connection with, in relation to or arising out of the use of the Content.

This article may be used for research, teaching, and private study purposes. Any substantial or systematic reproduction, redistribution, reselling, loan, sub-licensing, systematic supply, or distribution in any form to anyone is expressly forbidden. Terms & Conditions of access and use can be found at <http://www.tandfonline.com/page/terms-and-conditions>

## The Transition Metal Dichalcogenides

### Discussion and Interpretation of the Observed Optical, Electrical and Structural Properties

By J. A. WILSON and A. D. YOFFE  
Cavendish Laboratory, Cambridge

#### ABSTRACT

The transition metal dichalcogenides are about 60 in number. Two-thirds of these assume layer structures. Crystals of such materials can be cleaved down to less than 1000 Å and are then transparent in the region of direct band-to-band transitions. The transmission spectra of the family have been correlated group by group with the wide range of electrical and structural data available to yield useful working band models that are in accord with a molecular orbital approach. Several special topics have arisen; these include exciton screening, d-band formation, and the metal/insulator transition; also magnetism and superconductivity in such compounds. High pressure work seems to offer the possibility for testing the recent theory of excitonic insulators.

#### CONTENTS

	PAGE
§ 1. INTRODUCTION.	194
§ 2. THE STRUCTURES OF THE $\text{TX}_2$ DICHALCOGENIDES AND RELATED MATERIALS.	198
§ 3. $\text{TX}_2$ LAYER COMPOUNDS—THE CRYSTALS.	216
§ 4. TRANSMISSION SPECTRA FOR THE LAYER-TYPE TRANSITION METAL DICHALCOGENIDES.	224
§ 5. THE APPROACH TOWARDS A BAND SCHEME FOR THE LAYER-TYPE TRANSITION METAL DICHALCOGENIDES.	233
5.1. General Discussion of Band Formation in Transition Metal Compounds.	233
5.2. The Proposed Banding Arrays for the Layer-type Transition Metal Dichalcogenides.	236
§ 6. THE OPTICAL SPECTRA OF THE <i>Regular</i> LAYERED $\text{TX}_2$ DICHALCOGENIDES RELATED TO THE ABOVE BANDING SCHEME.	240
6.1. The Trigonal Prism Materials.	240
6.1.1. Band positions and transition assignments.	240
6.1.2. The A and B excitons of group VI.	245
6.1.3. Phonon spectra and the indirect edge.	252
6.2. The Group IV Materials.	253
6.3. The Group VIII Layer Materials.	254
6.4. U.V. and Electron Energy Loss Spectra.	257
§ 7. THE ELECTRICAL AND MAGNETIC PROPERTIES OF THE <i>Regular</i> LAYERED $\text{TX}_2$ DICHALCOGENIDES.	260
7.1. The Group IV Materials.	260
7.2. The Trigonal Prism Group VI Materials.	261
7.2.1. General electrical properties.	261
7.2.2. Electromagnetic work on the A and B excitons.	270
7.3. The Regular Group V and Mixed V/VI Materials.	272
7.3.1. Group V materials as antiferromagnetic metals.	272
7.3.2. Group V materials as superconductors.	278
7.3.3. Doped materials, intercalates and exciton screening.	281
7.4. The Group VIII Layer Materials.	286

§ 8. THE OPTICAL AND ELECTRICAL PROPERTIES OF THE <i>Distorted</i> LAYER COMPOUNDS OF GROUPS V, VI AND VII.	287
8.1. $\text{ReS}_2$ , $\text{ReSe}_2$ , $\text{WTe}_2$ , $\beta\text{-MoTe}_2$ , $\text{NbTe}_2$ and $\text{TaTe}_2$ .	287
8.2. $1T\text{-TaS}_2$ and $1T\text{-TaSe}_2$ .	297
§ 9. CAUSE AND EFFECT OF CRYSTAL STRUCTURE CHOICE AMONG THE TRANSITION METAL DICHALCOGENIDES AND HALIDES.	303
9.1. Survey of the Properties of the Transition Metal Dichalcogenides beyond Group VII.	303
9.2. The Development of Crystal Structure through the Transition Metal Dichalcogenides.	316
9.3. Survey of the Properties of the Transition Metal Layer Halides.	322
§ 10. SUMMARY AND CONCLUSION.	328
ACKNOWLEDGMENTS.	329
REFERENCES.	330

## § 1. INTRODUCTION

THE work has centred on the layered transition metal dichalcogenides of groups IV, V, VI and VII, but the non-layered compounds of group VIII are incorporated into this discussion for purposes of comparison and contrast (see table 1).

Periodic Table

IA	IIA											IIIA	IVA	VA	VIA	VIIA	O	
Li <sup>3</sup>	Be <sup>4</sup>											B <sup>5</sup>	C <sup>6</sup>	N <sup>7</sup>	O <sup>8</sup>	F <sup>9</sup>	Ne <sup>10</sup>	
2s	2s <sup>2</sup>											2s <sup>2</sup> 2p	2s <sup>2</sup> 2p <sup>2</sup>	2s <sup>2</sup> 2p <sup>3</sup>	2s <sup>2</sup> 2p <sup>4</sup>	2s <sup>2</sup> 2p <sup>5</sup>	2s <sup>2</sup> 2p <sup>6</sup>	
Na <sup>11</sup>	Mg <sup>12</sup>											Al <sup>13</sup>	Si <sup>14</sup>	P <sup>15</sup>	S <sup>16</sup>	Cl <sup>17</sup>	Ar <sup>18</sup>	
3s	3s <sup>2</sup>	IIIB	IVB	VB	VIB	VIIB	VIII <sup>A</sup>	VIII <sup>B</sup>	VIII <sup>C</sup>	IB	IIB	3s <sup>2</sup> 3p	3s <sup>2</sup> 3p <sup>2</sup>	3s <sup>2</sup> 3p <sup>3</sup>	3s <sup>2</sup> 3p <sup>4</sup>	3s <sup>2</sup> 3p <sup>5</sup>	3s <sup>2</sup> 3p <sup>6</sup>	
K <sup>19</sup>	Ca <sup>20</sup>	Sc <sup>21</sup>	Ti <sup>22</sup>	V <sup>23</sup>	Cr <sup>24</sup>	Mn <sup>25</sup>	Fe <sup>26</sup>	Co <sup>27</sup>	Ni <sup>28</sup>	Cu <sup>29</sup>	Zn <sup>30</sup>	Ga <sup>31</sup>	Ge <sup>32</sup>	As <sup>33</sup>	Se <sup>34</sup>	Br <sup>35</sup>	Kr <sup>36</sup>	
4s	4s <sup>2</sup>	3d	3d <sup>2</sup>	3d <sup>3</sup>	3d <sup>3</sup>	3d <sup>5</sup>	3d <sup>6</sup>	3d <sup>7</sup>	3d <sup>8</sup>	3d <sup>10</sup>	3d <sup>10</sup>	4s <sup>2</sup> 4p	4s <sup>2</sup> 4p <sup>2</sup>	4s <sup>2</sup> 4p <sup>3</sup>	4s <sup>2</sup> 4p <sup>4</sup>	4s <sup>2</sup> 4p <sup>5</sup>	4s <sup>2</sup> 4p <sup>6</sup>	
Rb <sup>37</sup>	Sr <sup>38</sup>	Y <sup>39</sup>	Zr <sup>40</sup>	Nb <sup>41</sup>	Mo <sup>42</sup>	Tc <sup>43</sup>	Ru <sup>44</sup>	Rh <sup>45</sup>	Pd <sup>46</sup>	Ag <sup>47</sup>	Cd <sup>48</sup>	In <sup>49</sup>	Sn <sup>50</sup>	Sb <sup>51</sup>	Te <sup>52</sup>	I <sup>53</sup>	Xe <sup>54</sup>	
5s	5s <sup>2</sup>	4d	4d <sup>2</sup>	4d <sup>3</sup>	4d <sup>5</sup>	4d <sup>6</sup>	4d <sup>7</sup>	4d <sup>8</sup>	4d <sup>10</sup>	4d <sup>10</sup>	4d <sup>10</sup>	5s <sup>2</sup> 5p	5s <sup>2</sup> 5p <sup>2</sup>	5s <sup>2</sup> 5p <sup>3</sup>	5s <sup>2</sup> 5p <sup>4</sup>	5s <sup>2</sup> 5p <sup>5</sup>	5s <sup>2</sup> 5p <sup>6</sup>	
Cs <sup>55</sup>	Ba <sup>56</sup>	La <sup>57</sup>	Hf <sup>72</sup>	Ta <sup>73</sup>	W <sup>74</sup>	Re <sup>75</sup>	Os <sup>76</sup>	Ir <sup>77</sup>	Pt <sup>78</sup>	Au <sup>79</sup>	Hg <sup>80</sup>	Tl <sup>81</sup>	Pb <sup>82</sup>	Bi <sup>83</sup>	Po <sup>84</sup>	At <sup>85</sup>	Rn <sup>86</sup>	
6s	6s <sup>2</sup>	6s <sup>2</sup>	5d	5d <sup>2</sup>	5d <sup>3</sup>	5d <sup>4</sup>	5d <sup>5</sup>	5d <sup>6</sup>	5d <sup>9</sup>	5d <sup>10</sup>	5d <sup>10</sup>	6s <sup>2</sup> 6p	6s <sup>2</sup> 6p <sup>2</sup>	6s <sup>2</sup> 6p <sup>3</sup>	6s <sup>2</sup> 6p <sup>4</sup>	6s <sup>2</sup> 6p <sup>5</sup>	6s <sup>2</sup> 6p <sup>6</sup>	
Fr <sup>87</sup>	Ra <sup>88</sup>	Ac <sup>89</sup>																
7s	7s <sup>2</sup>	7s <sup>2</sup>	Ce <sup>58</sup>	Pr <sup>59</sup>	Nd <sup>60</sup>	Pm <sup>61</sup>	Sm <sup>62</sup>	Eu <sup>63</sup>	Gd <sup>64</sup>	Tb <sup>65</sup>	Dy <sup>66</sup>	Ho <sup>67</sup>	Er <sup>68</sup>	Tm <sup>69</sup>	Yb <sup>70</sup>	Lu <sup>71</sup>		
			4f <sup>2</sup>	4f <sup>3</sup>	4f <sup>4</sup>	4f <sup>5</sup>	4f <sup>6</sup>	4f <sup>7</sup>	4f <sup>7</sup>	4f <sup>8</sup>	4f <sup>10</sup>	4f <sup>10</sup>	4f <sup>12</sup>	4f <sup>13</sup>	4f <sup>14</sup>	4f <sup>14</sup>		
			6s <sup>2</sup>	6s <sup>2</sup>	6s <sup>2</sup>	6s <sup>2</sup>	6s <sup>2</sup>	6s <sup>2</sup>	6s <sup>2</sup>	6s <sup>2</sup>	6s <sup>2</sup>	6s <sup>2</sup>						
			Th <sup>90</sup>	Pa <sup>91</sup>	U <sup>92</sup>	Np <sup>93</sup>	Pu <sup>94</sup>	Am <sup>95</sup>	Cm <sup>96</sup>	Bk <sup>97</sup>	Cf <sup>98</sup>	Es <sup>99</sup>	Fm <sup>100</sup>	Md <sup>101</sup>		Lw <sup>103</sup>		
			-	5f <sup>2</sup>	5f <sup>3</sup>	5f <sup>4</sup>	5f <sup>6</sup>	5f <sup>7</sup>	5f <sup>7</sup>	5f <sup>7</sup>	6d	6d	6d	6d	6d			
			7s <sup>2</sup>	7s <sup>2</sup>	7s <sup>2</sup>	7s <sup>2</sup>	7s <sup>2</sup>											

Table 1. Structure types and electrical character of the transition metal dichalcogenides

M	Crystallographic type			Electrical character	
	X <sub>2</sub>	-S <sub>2</sub>	-Se <sub>2</sub>		-Te <sub>2</sub>
IV d <sup>2</sup>	Ti	L octa	L octa	L octa	Diamagnetic semiconductors. $\rho \gtrsim 1$ ohm-cm, $E_g \sim 0.2-2.0$ ev. Ti, as with all first series metals, yields non-stoichiometric products.
	Zr	L octa	L octa	L octa	
	Hf	L octa	L octa	(L octa)	
V d <sup>3</sup>	V	(L octa)	L octa	L distd. octa	Undistorted compounds are narrow band metals, $\rho \sim 10^{-4}$ ohm-cm. Pauli paramagnetic $\rightarrow$ band antiferromagnetic. Superconducting. Free-carrier absorption in <i>I.R.</i> Others diamagnetic semi-metals. Octa TaS <sub>2</sub> /Se <sub>2</sub> perhaps semiconducting.
	Nb	L trig pr	L trig pr	L distd. octa	
	Ta	L { trig pr (dist) octa	L { trig pr (dist) octa	L distd. octa	
VI d <sup>4</sup>	Cr	---	---	---	(i) The undistorted compounds are diamagnetic semiconductors. $\rho \gtrsim 1$ ohm-cm. $E_{gap} \gtrsim 1.5$ ev, $E_g^{th} \sim 0.15$ ev. (ii) The distorted octahedral structures are semi-metals. $\rho \sim 10^{-3}$ ohm-cm. Diamagnetic, low Seebeck coefficients.
	Mo	L trig pr	L trig pr	L { trig pr distd. octa	
	W	L trig pr	L trig pr	L distd. octa	
VII d <sup>5</sup>	Mn		Pyrites		(i) Mn compounds quasi-ionic antiferromagnetic semiconductors. (ii) TeS <sub>2</sub> possibly also a pyrite form. (iii) ReS <sub>2</sub> and ReSe <sub>2</sub> are small gap semiconductors, diamagnetic, and with no free-carrier absorption.
	Tc	L dist octa	L dist octa	L distd.	
	Re	L dist octa	L dist octa	L distd.	
VIII a d <sup>6</sup>	Fe	Pyrite /	Marcasite		'Non-magnetic' semiconductors
	Ru				
	Os				
VIII b d <sup>7</sup>	Co	Pyrite	{ Pyrite Marcasite	{ Marcasite L octa	Pyrite, marcasite and layer types metallic. CoS <sub>2</sub> ferromagnetic. $\beta$ -RhSe <sub>2</sub> and RhTe <sub>2</sub> superconductors. IrSe <sub>2</sub> types semiconducting.
	Rh	(Pyrite)	{ IrSe <sub>2</sub> Pyrite	{ Pyrite L octa	
	Ir	IrSe <sub>2</sub>	IrSe <sub>2</sub>	L octa	
VIII c d <sup>8</sup>	Ni	Pyrites	Pyrites	L octa	(i) Tellurides, metallic Pauli paramagnetic. $\rho \sim 10^{-5}$ ohm-cm. PdTe <sub>2</sub> superconducting. (ii) PdS <sub>2</sub> /Se <sub>2</sub> semiconducting. $E_g \sim 0.4$ ev. $\rho \sim 1$ ohm-cm. Diamagnetic, PtS <sub>2</sub> /Se <sub>2</sub> large Seebeck coefficients.
	Pd	Layer type showing X-X links		L octa	
	Pt	L octa	L octa	L octa	

L octa : layer structure—octahedral coordination. L trig pr : layer structure—trigonal prism coordination.  
L distd. : layer structure showing distorted coordination. High pressure forms given in table 15(a) p. 304.

The  $\text{TX}_2$  layer materials form a structurally and chemically well-defined family. Electrically, however, they cover a wide spectrum of properties, from an insulator like  $\text{HfS}_2$ , through semiconductors like  $\text{MoS}_2$  and semi-metals like  $\text{WTe}_2$  and  $\text{TcS}_2$ , to true metals like  $\text{NbS}_2$  and  $\text{VSe}_2$ . Several of the materials such as  $\text{TaTe}_2$ ,  $\text{WTe}_2$  and  $\text{ReSe}_2$  show structural distortions that throw their properties out of line as compared with their undistorted analogues. 'Domains' have been observed in  $\text{NbTe}_2$  and  $\text{TaTe}_2$  reminiscent of the deformation twinning observed in  $\text{VO}_2$  below  $68^\circ\text{C}$ .  $1\text{T-TaS}_2$  and  $1\text{T-TaSe}_2$  present a greater problem as their structure appears undistorted when examined by x-rays. Accordingly they should be metals, like  $\text{VSe}_2$ , but in fact they behave optically and magnetically as semiconductors. Electron microscope diffraction patterns do, however, indicate some type of superlattice. All the Nb and Ta materials, whether distorted or not, are superconducting, and the truly metallic ones also show band antiferromagnetism below about  $150^\circ\text{K}$ .

In order to illuminate the origin of these unusual properties more fully, an investigation has been made of the optical properties. Detailed transmission spectra were obtained in the range  $0.5\text{--}5\text{ eV}$  from cleaved crystal specimens. Collectively, these allow band models to be set up for the whole range of compounds. The structural, optical and electrical properties are well accommodated. The diversity of properties arises through the existence of non-bonding d bands and the degree to which they are filled. In these dichalcogenides the d bands are quite wide ( $\sim 1\text{ eV}$ ) and lead to room temperature mobilities  $\sim 100\text{ cm}^2/\text{v-sec}$ . Contrast is made between these materials and the layer dihalides, for which there is a progressive delocalization of the d electrons from say  $\text{MnI}_2$  through  $\text{FeI}_2$  and  $\text{NiI}_2$  to  $\text{TiI}_2$ . It seems possible that this latter material may undergo a semiconductor to metal transition of the Mott type on cooling. The binary layer compounds are in fact ideal for investigating the course of d-band formation since the metal atoms lie in well-defined hexagonal sheets.

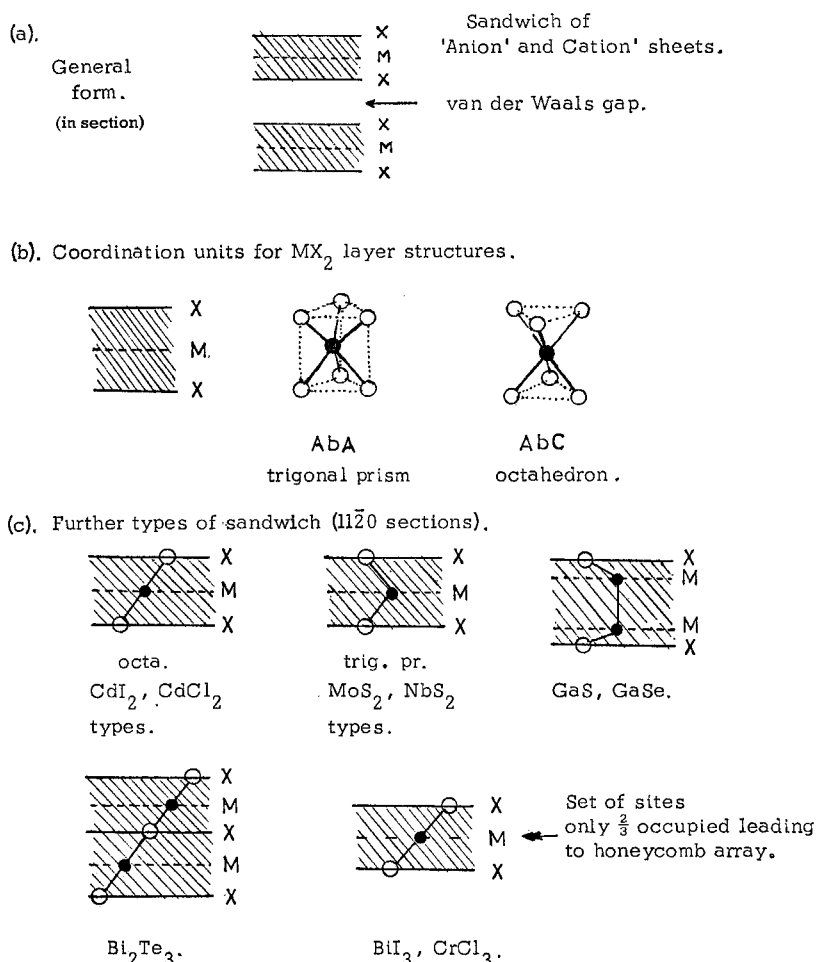
The basic atomic structure of loosely coupled X-M-X atom sheet sandwiches makes such materials extremely anisotropic, both mechanically and electrically. The conductivity perpendicular to the planes is down by a factor of at least  $10^2$  on that in the planes for  $\text{MoS}_2$ , etc., and there is some evidence that the carriers move by hopping rather than a band mechanism in the former direction. Thermal conductivity likewise is low perpendicular to the layers. In layer structures, moreover, the charge carriers and phonons seem to couple in a unique fashion.

In order to view these materials in the wider context of layer materials in general, the behaviour of the non-transition metal layer compounds has also been considered. Preliminary band schemes for several such compounds, e.g.  $\text{GaS}$ ,  $\text{Bi}_2\text{Te}_3$  and  $\text{SnSe}_2$ , are available and a good deal of data has been amassed on the first two. The families of  $\text{GaS}$ ,  $\text{CdI}_2$  and  $\text{BiI}_3$  show excitonic absorption which makes for useful comparison with the excitons of the  $\text{MoS}_2$  (group VI) family. These exciton states are interesting in their own right. For  $\text{MoS}_2$ , etc. they are of rather small radius

and are remarkably stable to pressure, temperature and crystal composition. Only very high concentrations of Ta or Re ( $\sim 1$  at. %) will lead, in say  $WSe_2$ , to a screening out of the excitonic binding interaction.

The non-layered half of the  $TX_2$  dichalcogenide family (prototype  $FeS_2$ ) is equally if not more varied in property from one member to the next than that of the layered compounds. Indeed, it is the progressive filling, within a given structure type, of the narrow non-bonding d bands, coupled with the increasing metal-metal atom orbital overlap between the 3d and 4d or 5d members, which gives the family as a whole a most interesting diversity in unity.

Fig. 1

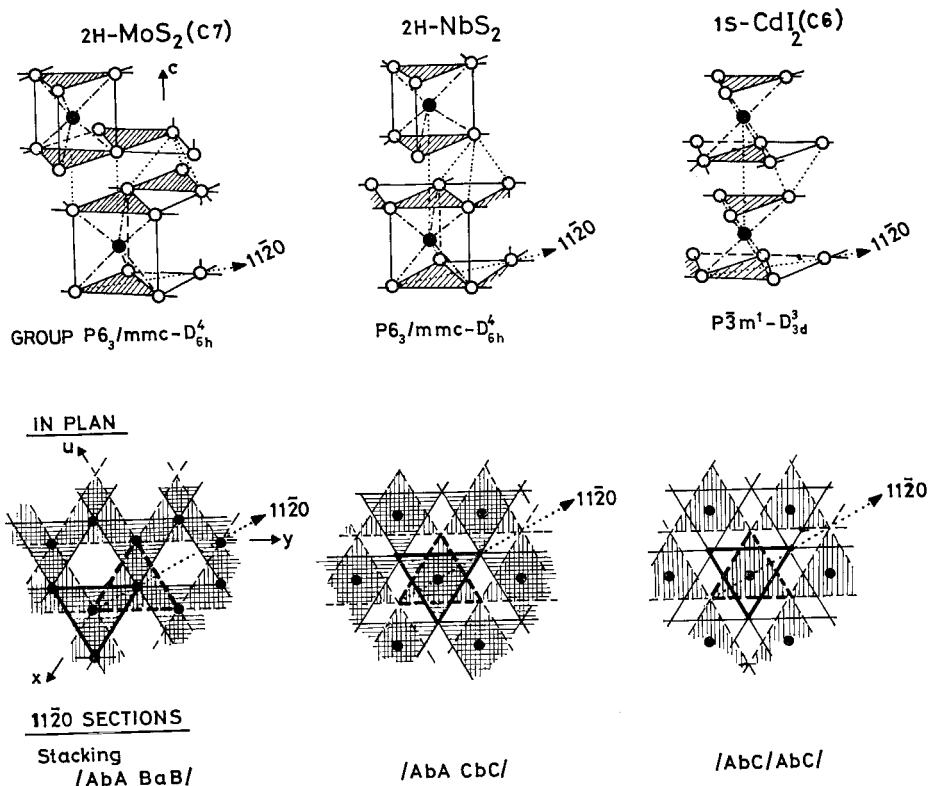


Basic form of layer compounds.

§ 2. THE STRUCTURES OF THE  $\text{TX}_2$  DICHALCOGENIDES  
AND RELATED MATERIALS

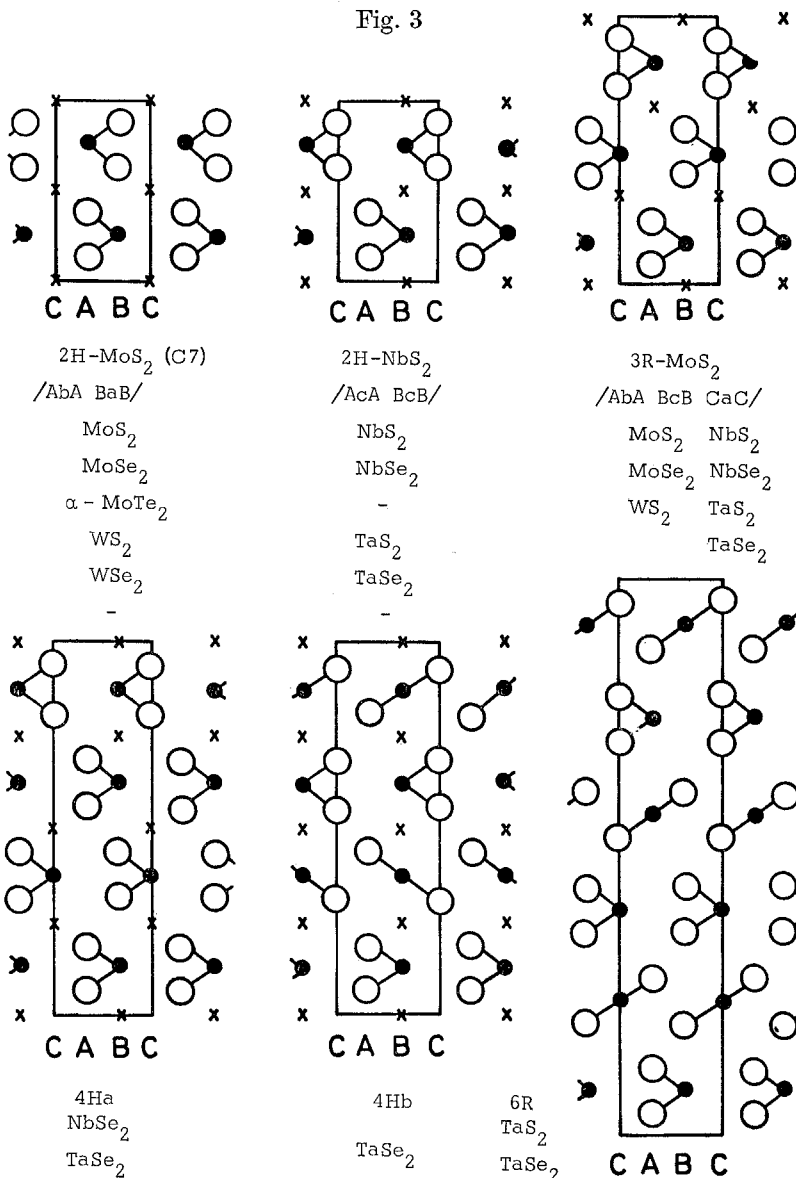
The structures of the  $\text{TX}_2$  dichalcogenides (see table 1) fall into two distinct classes—layered and otherwise. The layered materials arise from the stacking of hexagonally packed planes (not close packed) in the sequence shown in fig. 1 (a). 6:3 coordination results, that around the metal atoms being either trigonal prismatic (e.g.  $\text{MoS}_2$ ,  $\text{NbS}_2$ ) or octahedral (e.g.  $\text{HfS}_2$ ,  $\text{PtS}_2$ ). The coordination around the non-metal is quite lopsided, and this leads to the marked cleavage properties perpendicular to the hexagonal/trigonal symmetry axis ( $z$ ). Several stacking polytypes exist. The commonest stacking of  $\text{NbS}_2$  is one never adopted by the  $\text{MoS}_2$  group VI family. Figure 2 contrasts the structures of the simplest polytypes, both in three dimensions and plan, whilst fig. 3 gives  $11\bar{2}0$  sections for most polytypes so far reported in groups V and VI (Jellinek 1963, Haraldsen 1966, Zvyagin and Soboleva 1967). Several of the  $\text{TX}_2$  materials occur with layer structures that are distorted in some way. The group VIII

Fig. 2



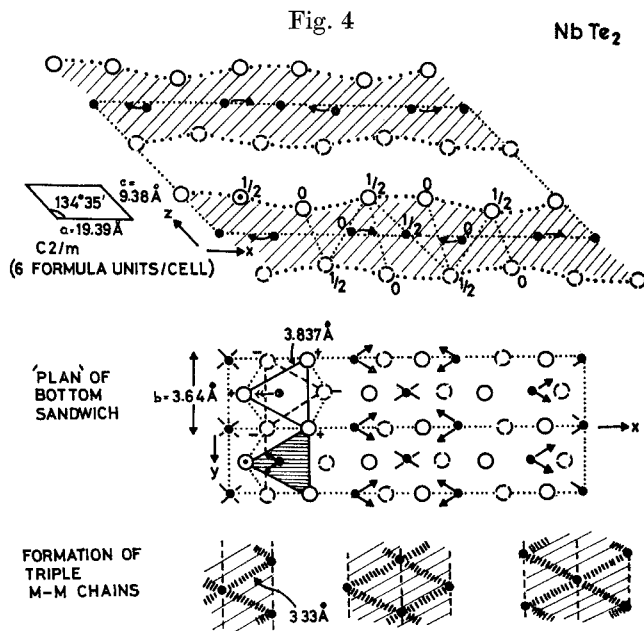
The structures of the 2H- $\text{MoS}_2$ , 2H- $\text{NbS}_2$  and  $\text{CdI}_2$  layer polytypes.

Fig. 3

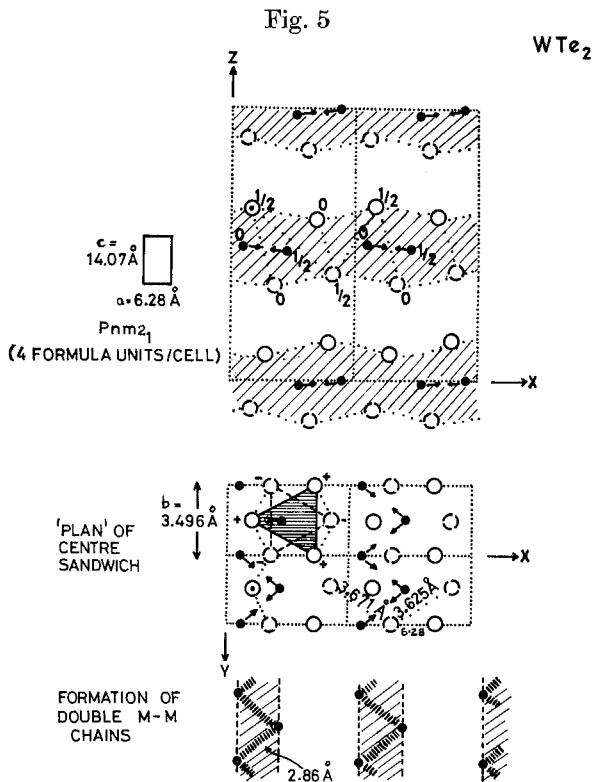


1120 sections of the various stacking polytypes found in the group V and VI  $TX_2$  layer dichalcogenides. ( $c/a$  somewhat reduced.  $C-C = \sqrt{3}a.$ )

layer compounds, and particularly the metallic tellurides, show considerable flattening of the  $TX_2$  sandwich and a contraction of the van der Waals gap. Further, in the layer structures of  $NbTe_2$ ,  $TaTe_2$ ,  $\beta-MoTe_2$ ,  $WTe_2$ ,  $TcS_2$ ,  $TcSe_2$ ,  $ReS_2$ ,  $ReSe_2$  and  $ReTe_2$  the metal atoms are actually displaced from the centre of the coordination units. Short metal-metal distances result with chains of metal atoms running through the structure. The

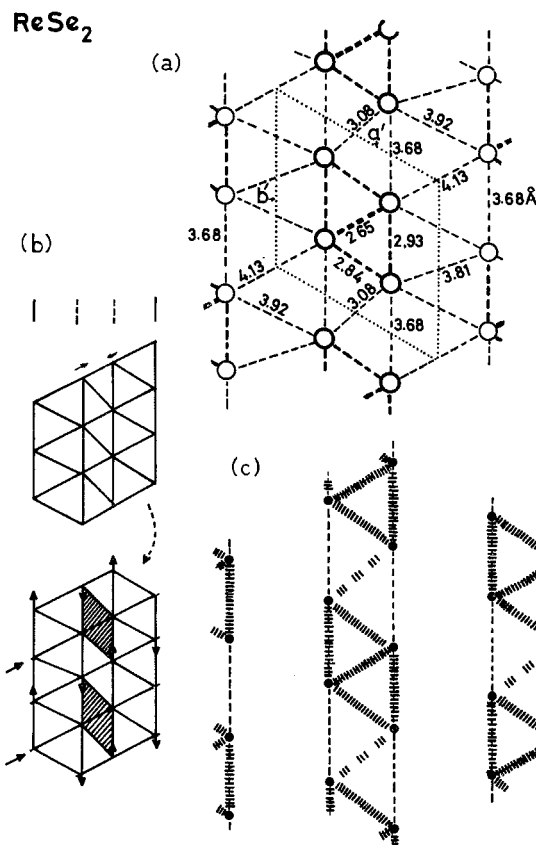


Distorted octahedral layer structure of  $\text{NbTe}_2$  (and  $\text{TaTe}_2$ ). [After Brown 1966 ; note :  $a/\sqrt{3} = 3.73 \text{ \AA}$  as against  $3.64 \text{ \AA}$  for  $b$ .]



Distorted octahedral layer structure of  $\text{WTe}_2$  ( $\beta\text{-MoTe}_2$ ) similar. [After Brown 1966 ; note :  $a/\sqrt{3} = 3.627 \text{ \AA}$  as against  $3.496 \text{ \AA}$  for  $b$ .]

Fig. 6



Distorted octahedral layer structure of ReSe<sub>2</sub>. [After Alcock and Kjekshus 1965.] (a) Single distorted plane of rhenium atoms, (b) progressive distortion from CdI<sub>2</sub>, (c) emphasizing cluster formation in chains.

chalcogenide sheets buckle somewhat to accommodate these shifts. Figures 4, 5 and 6 give interpretations of the reported structures for NbTe<sub>2</sub> (TaTe<sub>2</sub> same), WTe<sub>2</sub>, ( $\beta$ -MoTe<sub>2</sub> similar) and ReSe<sub>2</sub> (to which ReS<sub>2</sub>, TeS<sub>2</sub> and TeSe<sub>2</sub> seem similar). Such refined structural data as exist in the whole range of TX<sub>2</sub> layer dichalcogenides is collected into tables 2 and 3.

The non-layered TX<sub>2</sub> dichalcogenides occur exclusively in groups VII and beyond, and are of four types—pyrites, marcasite, IrSe<sub>2</sub> and PdS<sub>2</sub>. Figure 8 illustrates the manner in which marcasite is related to CdI<sub>2</sub>, whilst fig. 9 shows how pyrites is related to marcasite. The empty van der Waals gap is eliminated from these structures, and in fact they all show strong X-X pairing, particularly the sulphides. The cubic pyrite structure is the

Table 2. Structure parameters for the 'undistorted'  $\text{TX}_2$  layer dichalcogenides (see also fig. 92 and table 18)

(a) Trigonal prism structures (2H polytype)											
	$a$	$c/s$	$c/a$	Coordinate unit angles $\text{XMX} _c \text{XMX} _c$	Coordinate unit sandwich X-M ht.	Coordinate Gap ht.	Inter- v.d.W. layer X-X M-M	$z\text{MX}$ sandwich angle ( $\rho$ )	v.d.W. length ratio ( $\chi$ )	$z\text{OX}$ gap angle ( $\delta$ )	Reference
$d^8$	$\text{NiS}_2$	3.31	5.94	1.796	79° 00' 84° 10'	2.47	3.14	2.80	3.39	5.94	Jellinek <i>et al.</i> (1960)
	$\text{TaS}_2$	3.31 <sub>5</sub>	6.05	1.825							Jellinek (1962)
	$\text{NbSe}_2$	3.45	6.27	1.821	80° 10' 82° 50'	2.60	3.36	2.91	3.52	6.27	Brown and Beemisen (1965)
	$\text{TaSe}_2$	3.436	6.348	1.847	80° 20' 82° 46'	2.59	3.35	3.00	3.59	6.35	Bjerkelund and Kjekshus (1967)
$d^4$	$\text{MoS}_2$	3.1604	6.147	1.945	82° 30' 81° 30'	2.41	3.19	2.96	3.47	6.41	Wildervanck and Jellinek (1964)
	$\text{WS}_2$	3.154	6.181	1.960							Wildervanck and Jellinek (1964)
	$\text{MoSe}_2$	3.288	6.460	1.962	2.49 <sup>†</sup> → 3.23	3.22	3.75				James and Lavik (1963)
	$\alpha\text{-MoTe}_2$	3.286	6.488	1.976	83° 30' 80° 24'	2.73	3.63	3.35	3.92	50° 29' (ideal 54° 45')	Hicks (1964) Puotinen and Newnham (1961)
(b) Octahedral coordination											
$d^8$	$\text{TiS}_2$	3.4048	5.6904	1.670	94° 26'	2.32	2.64	3.05	3.62	5.69	Bernard and Jeannin (1962)
	$\text{ZrS}_2$	3.662	5.813	1.590							(a) McTaggart and Wadsley (1958)
	$\text{HfS}_2$	3.635	5.837	1.606							(b) Greenaway and Nitsche (1965)
	$\text{TiSe}_2$	3.535	6.004	1.698							(b) Greenaway and Nitsche (1965)
	$d^8 \text{ZrSe}_2$	3.770	6.138	1.628							(b) Greenaway and Nitsche (1965)
	$\text{HfSe}_2$	3.748	6.159	1.643							(b) Greenaway and Nitsche (1965)
	$\text{ZrTe}_2$	3.766	6.491	1.724							(b) Greenaway and Nitsche (1965)
$d^8$	$\text{ZrTe}_2$	3.950	6.630	1.678							(b) Greenaway and Nitsche (1965)
	$\text{VSe}_2$	3.35	6.10	1.82							Rost and Gjertsen (1964)
	$\text{VTe}_2$	3.6	6.45	1.8							Grønsvold <i>et al.</i> (1958)
$d^8$	$\text{TaS}_2$	3.346	5.860	1.751							Jellinek (1962)
	$\text{TaSe}_2$	3.477	6.272	1.804							Bjerkelund and Kjekshus (1967)
	$\text{CoTe}_2$	3.86	5.30	1.38							Haraldsen <i>et al.</i> (1956)
$d^8$	$\text{RhTe}_2$	3.92	5.41	1.38							Geller (1955)
	$\text{IrTe}_2$	3.929	5.395	1.373							Hockings and White (1960)
$d^8$	$\text{NiTe}_2$	3.8542	5.2604	1.368	95° 52'	2.596	2.734	2.526	3.41	5.260	Furuseth <i>et al.</i> (1965)
	$\text{PdTe}_2$	4.0365	5.1262	1.270	99° 06'	2.652	2.533	2.593	3.49	5.126	Furuseth <i>et al.</i> (1965)
	$\text{PtS}_2$	3.5432	5.0388	1.422	98° 26'	2.34	2.289	2.750	3.43	5.039	Furuseth <i>et al.</i> (1965)
	$\text{PtSe}_2$	3.7278	5.0813	1.363	95° 44'	2.513	2.592	2.489	3.29	5.081	Furuseth <i>et al.</i> (1965)
	$\text{PtTe}_2$	4.0259	5.2209	1.297	97° 34'	2.676	2.653	2.568	3.46	5.221	Furuseth <i>et al.</i> (1965)
			(ideal 1.633)							(ideal 54° 45')	

Table 3. Further structure parameters for the polytypic and distorted layer dichalcogenides of groups V, VI and VII

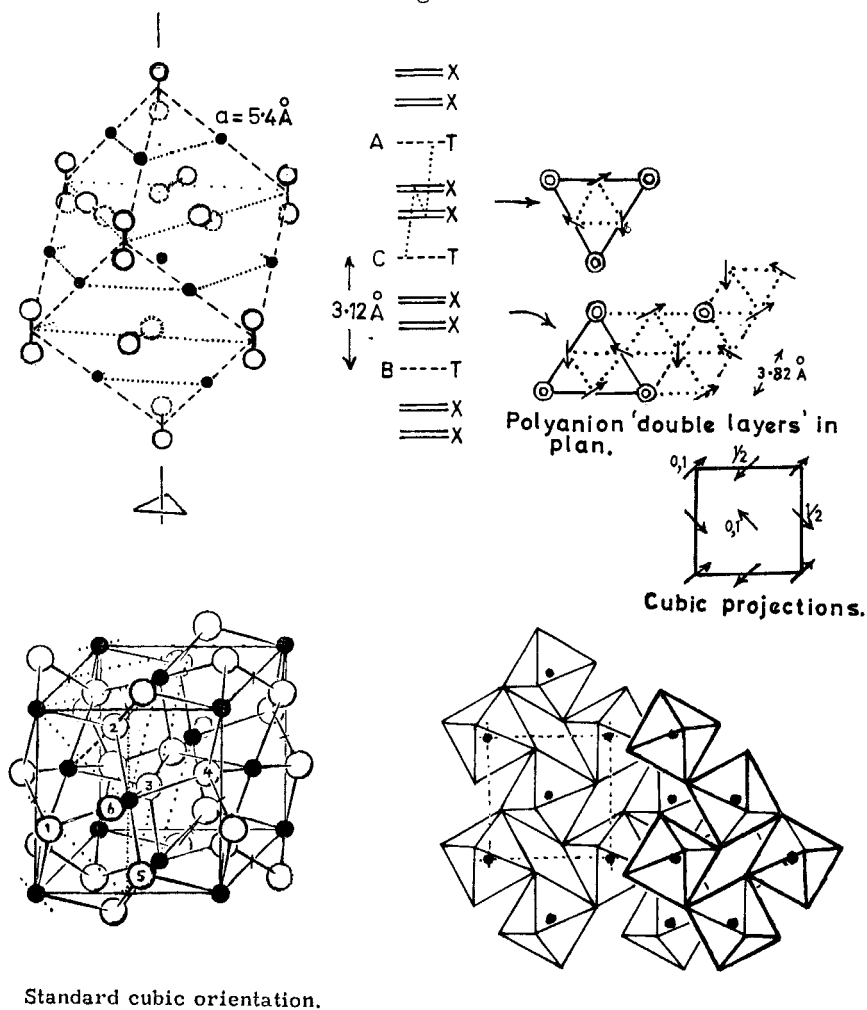
	$a$	$c$	$c/a$	Interbond $\angle_{\parallel c}$	Bonding X-M	Sandwich ht.	Gap v.d.W. ht.	Interlayer X-X M-M	Reference		
Gr VI 2H-MoS <sub>2</sub> 3R-MoS <sub>2</sub>  2H-MoSe <sub>2</sub> 3R-MoSe <sub>2</sub> 2H-WSe <sub>2</sub> 3R-WSe <sub>2</sub> 2H- $\alpha$ MoTe <sub>2</sub> $\beta$ MoTe <sub>2</sub> WTe <sub>2</sub>	3.160	2 × 6.147	2 × 1.945	82° 30'	2.41	3.19	2.96	3.47	Swanson <i>et al.</i> (1955) Takeuchi and Nowacki (1964) Wildervanck and Jellinek (1964) James and Lavik (1963) Towle <i>et al.</i> (1966) Swanson <i>et al.</i> (1958) Wildervanck and Jellinek (1964) Puotinen and Newnham (1963) Brown (1966) Brown (1966)		
	3.164	3 × 6.130	3 × 1.936	81.8° 82.1°	2.41	3.15 <sub>5</sub>	2.98	3.50			
	3.288	2 × 6.460	2 × 1.962	80° 49'	2.49	3.23	3.22	3.75			
	3.292	3 × 6.464	2 × 1.965								
	3.154	2 × 6.181	2 × 1.960								
	3.162	3 × 6.167	3 × 1.950								
	3.517	2 × 6.983	2 × 1.984	83.5°	2.73	3.63	3.35	3.92			
	3.65(av)	2 × 6.913	1.89		{ For $\alpha$ taken average						
	3.65(av)	2 × 7.036	1.93		{ For $c$ taken $c \cdot \sin \beta$ .						
					{ large for octahedral coordinate.						
	Gr V 2H-NbS <sub>2</sub> 3R-NbS <sub>2</sub> 2H-NbSe <sub>2</sub> 3R-NbSe <sub>2</sub> 4H-NbSe <sub>2</sub> 2H-TaS <sub>2</sub> 3R-TaS <sub>2</sub> 2H-TaSe <sub>2</sub> 3R-TaSe <sub>2</sub> 4H-TaSe <sub>2</sub> 1T-TaS <sub>2</sub> 1T-TaSe <sub>2</sub>	3.31	2 × 5.945	2 × 1.796	79° 00'	2.47				5.945	Jellinek <i>et al.</i> (1960) Jellinek <i>et al.</i> (1960) Brown and Beerntsen (1965) Brown and Beerntsen (1965) Brown and Beerntsen (1965) Jellinek (1962) Jellinek (1962) Brown and Beerntsen (1965) Bjerkelund and Kjekshus (1967) Brown and Beerntsen (1965) Jellinek (1962) Bjerkelund and Kjekshus (1967) Brown (1966) Brown (1966)
		3.33	3 × 5.967	3 × 1.783	84° 10'						
3.449		2 × 6.27	2 × 1.821	80° 10'	2.60	3.36	2.91	3.52			
3.45		3 × 6.29	3 × 1.824	82° 50'	2.59	3.32	2.97	3.54			
3.44		4 × 6.31	4 × 1.835		2.60	3.38	2.93	3.55			
3.315		2 × 6.05	2 × 1.826								
3.32		3 × 5.937	3 × 1.797								
3.434		2 × 6.348	2 × 1.849	80° 20'	2.59	3.35	3.00	3.59			
3.455		3 × 6.392	3 × 1.861								
3.46		4 × 6.29	4 × 1.82								
3.346		5.860	1.751								
3.477		6.272	1.804								
Gr VII NbTe <sub>2</sub> TaTe <sub>2</sub>	3.75	6.677	1.78						Alcock and Kjekshus (1965)		
	3.74	6.720	1.80								
ReS <sub>2</sub> ReSe <sub>2</sub>	3.30	6.343	1.92						Alcock and Kjekshus (1965)		

{  $c$  taken as separation of metal sheets.  
 $a$  taken as  $\frac{2}{3}b$  (trigonal cell).

Note  $\alpha$  slightly larger than for trigonal prism forms.  $c/a$  large for an octahedral structure.

{ For  $\alpha$  taken av. Te-Te in layers. For  $c$  taken  $c \cdot \sin \beta$ .

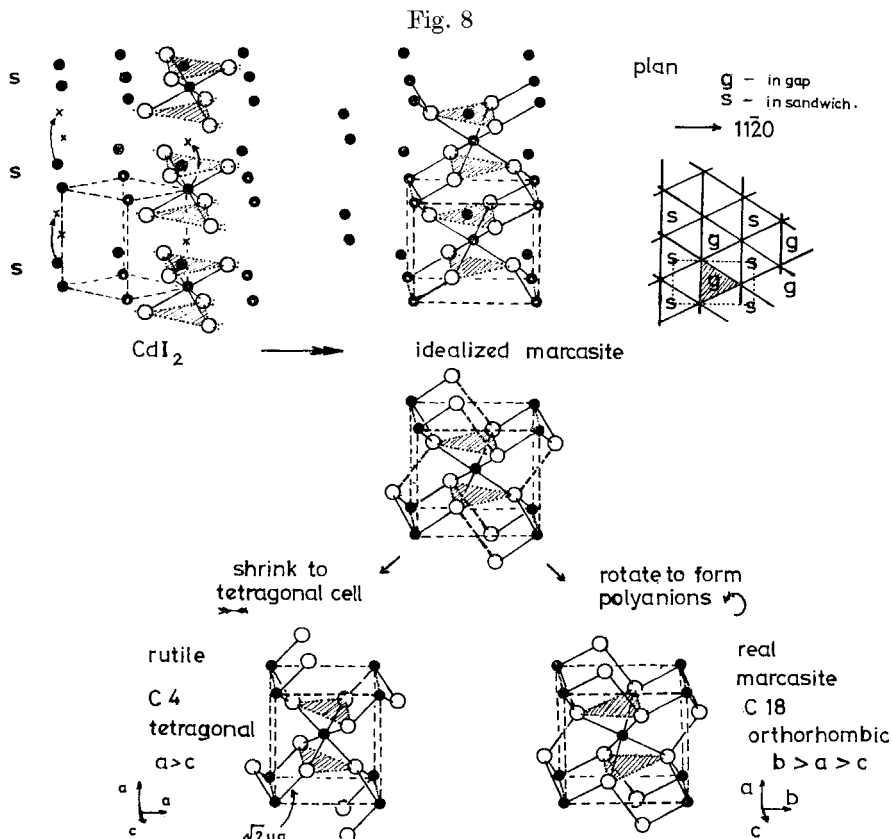
Fig. 7



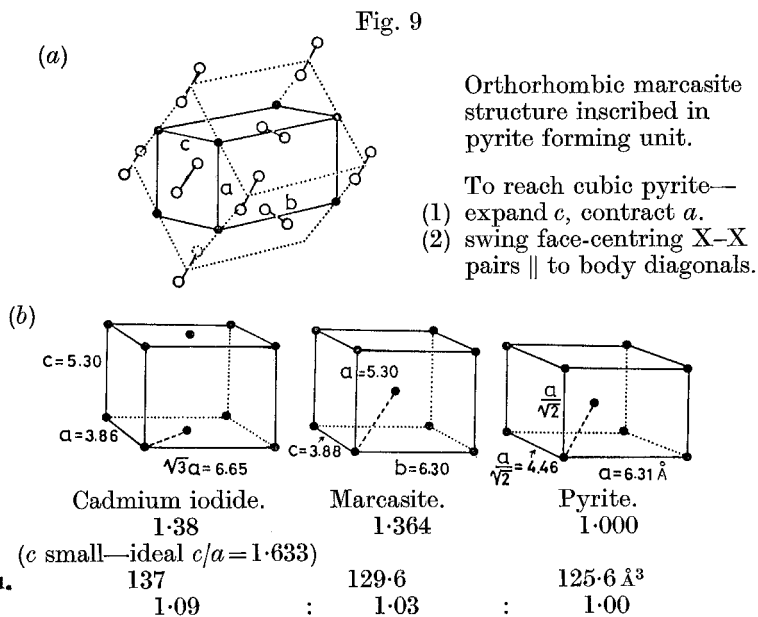
The pyrites structure (C2). [After Hulliger.]

densest and the other three structures are intermediary between the pyrite and  $\text{CdI}_2$  structures, e.g.

(a)	$\text{NiS}_2$ (pyrites)	$\text{PdS}_2$ (special)	$\text{PtS}_2$ ( $\text{CdI}_2$ )
(b)	$\text{RhS}_2$ (pyrites)	$\alpha\text{-RhSe}_2$ ( $\text{IrSe}_2$ )	$\beta\text{-RhTe}_2$ ( $\text{CdI}_2$ )
(c)	h.p. $\text{CoTe}_2$ (pyrites)	l.t. $\text{CoTe}_2$ (marcasite)	h.t. $\text{CoTe}_2$ ( $\text{CdI}_2$ )
	Vol/formula unit		
	62.8	64.8	68.5 $\text{\AA}^3$



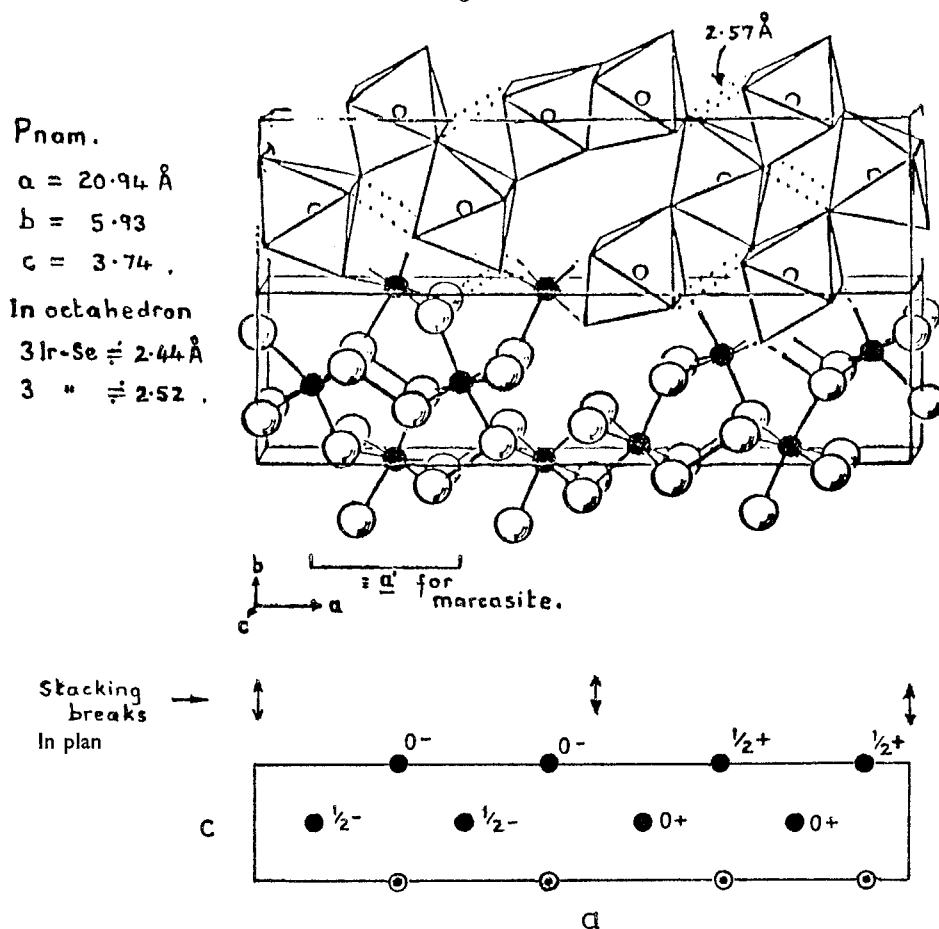
Relation of the marcasite (C18) and rutile (C4) structures to CdI<sub>2</sub> (C6). [After Hulliger and Mooser 1965.] Further details of marcasite structure in fig. 9; of rutile structure in fig. 73.



(a) Relation of the marcasite to the pyrite structure, (b) comparison of the three forms of CoTe<sub>2</sub>.

Figures 10 and 11 show the unusual intermediate structure types of  $\text{IrSe}_2$  and  $\text{PdS}_2$ .

Fig. 10



$\text{IrSe}_2$  structure (orthorhombic). [After Hulliger and Mooser 1965.]

Table 4 provides a collection of lattice parameters for the non-layered compounds to complement tables 2 and 3. Despite their greater density, the metal-metal distance in these non-layered compounds is increased. Figure 12 plots by groups the volume per formula unit, whilst fig. 13 likewise plots the nearest M-M distance for all the  $\text{TX}_2$  materials. Table 5 gives the smallest X-X distance in the various compounds. Note how in the pyrite  $\alpha\text{-RhTe}_2$  the Te-Te pairing is much weakened relative to say  $\text{RuTe}_2$ , although X-X interaction still persists in  $\text{PdTe}_2$  relative to say  $\alpha\text{-MoTe}_2$ .

Table 4. Some structure parameters for the non-layered TX<sub>2</sub> dichalcogenides—including shortest metal-metal distance

(a) Pyrites. Cubic, structure C2. Group T<sub>h</sub><sup>6</sup> (Pa3). Four formula units/cell. Structure parameter *u* yields X-X and T-X distances via  $\sqrt{3}a \cdot (1-2u)$  and  $a(3u^2-2u+\frac{1}{2})^{1/2}$  respectively. Least metal-metal distance =  $\frac{1}{2}\sqrt{(2a^2)}$

	MnS <sub>2</sub>	MnSe <sub>2</sub>	MnTe <sub>2</sub>	TcS <sub>2</sub>			ReS <sub>2</sub>		
<i>a</i>	6.109	6.430	6.951 Å	?			5.57		
M-M	4.319	4.560	4.915				—		
	FeS <sub>2</sub>	FeSe <sub>2</sub>	FeTe <sub>2</sub>	RuS <sub>2</sub>	RuSe <sub>2</sub>	RuTe <sub>2</sub>	OsS <sub>2</sub>	OsSe <sub>2</sub>	OsTe <sub>2</sub>
<i>a</i>	5.405	5.783* <sub>M</sub>	6.292* <sub>M</sub>	5.59	5.921	6.360	5.6075	5.933	6.369 Å
M-M	3.822	4.089	4.499	3.953	4.187	4.497	3.965	4.195	4.503
	CoS <sub>2</sub>	CoSe <sub>2</sub>	CoTe <sub>2</sub>	RhS <sub>2</sub>	β-RhSe <sub>2</sub>	α-RhTe <sub>2</sub>			
<i>a</i>	5.535	5.849 <sub>M</sub>	6.310* <sub>M,C</sub>	5.73	6.092	6.441 <sub>C</sub>			
M-M	3.914	4.136	4.462	4.051	4.307	4.554			
	NiS <sub>2</sub>	NiSe <sub>2</sub>	NiTe <sub>2</sub>						
<i>a</i>	5.685	5.960	6.374* <sub>C</sub> Å						
M-M	4.019	4.214	4.507						
	CuS <sub>2</sub>	CuSe <sub>2</sub>	CuTe <sub>2</sub>						
<i>a</i>	5.790*	6.123* <sub>M</sub>	6.600* <sub>C</sub> ? Å						
M-M	4.093	4.330	4.667						
	ZnS <sub>2</sub>	ZnSe <sub>2</sub>	ZnTe <sub>2</sub>	CdS <sub>2</sub>	CdSe <sub>2</sub>	CdTe <sub>2</sub>	MgTe <sub>2</sub>		
<i>a</i>	5.954*	6.290*	* <sub>C</sub> Å	6.309*	6.615*	* <sub>C</sub> Å	7.025* Å		
M-M	4.210	4.447							

Alternative forms. M : marcasite. C : cadmium iodide. \* : high pressure form.

(b) Marcasites. Orthorhombic, C18. Group D<sub>2h</sub><sup>13</sup> (Pnmm). Two formula units/cell. Structure parameters *x* and *y* yield :

$$X-X (1) = [4x^2a^2 + (1-2y)^2b^2]^{1/2}, \quad M-X (4) = [x^2a^2 + y^2b^2]^{1/2},$$

$$M-X (2) = [(\frac{1}{2}-x)^2a^2 + (\frac{1}{2}-y)^2b^2 + \frac{1}{4}c^2]^{1/2}$$

FeS <sub>2</sub>			FeSe <sub>2</sub>			FeTe <sub>2</sub>			CoTe <sub>2</sub>		
<i>a</i>	<i>b</i>	<i>c</i>	<i>a</i>	<i>b</i>	<i>c</i>	<i>a</i>	<i>b</i>	<i>c</i>	<i>a</i>	<i>b</i>	<i>c</i>
4.436	5.414	3.381	4.791	5.715	3.575	5.340	6.260	3.849	5.301	6.298	3.882 Å

FeS<sub>2</sub><sup>M</sup>: Fe-S 2.23 and 2.25 Å, S-S = 2.21 Å.

(c) IrSe<sub>2</sub>. Orthorhombic. Group D<sub>2h</sub><sup>16</sup> (Pnam). Eight formula units/cell

	<i>a</i>	<i>b</i>	<i>c</i>
RhSe <sub>2</sub>	20.91	5.951	3.709 Å
IrS <sub>2</sub>	19.78	5.624	3.565
IrSe <sub>2</sub>	20.94	5.93	3.74

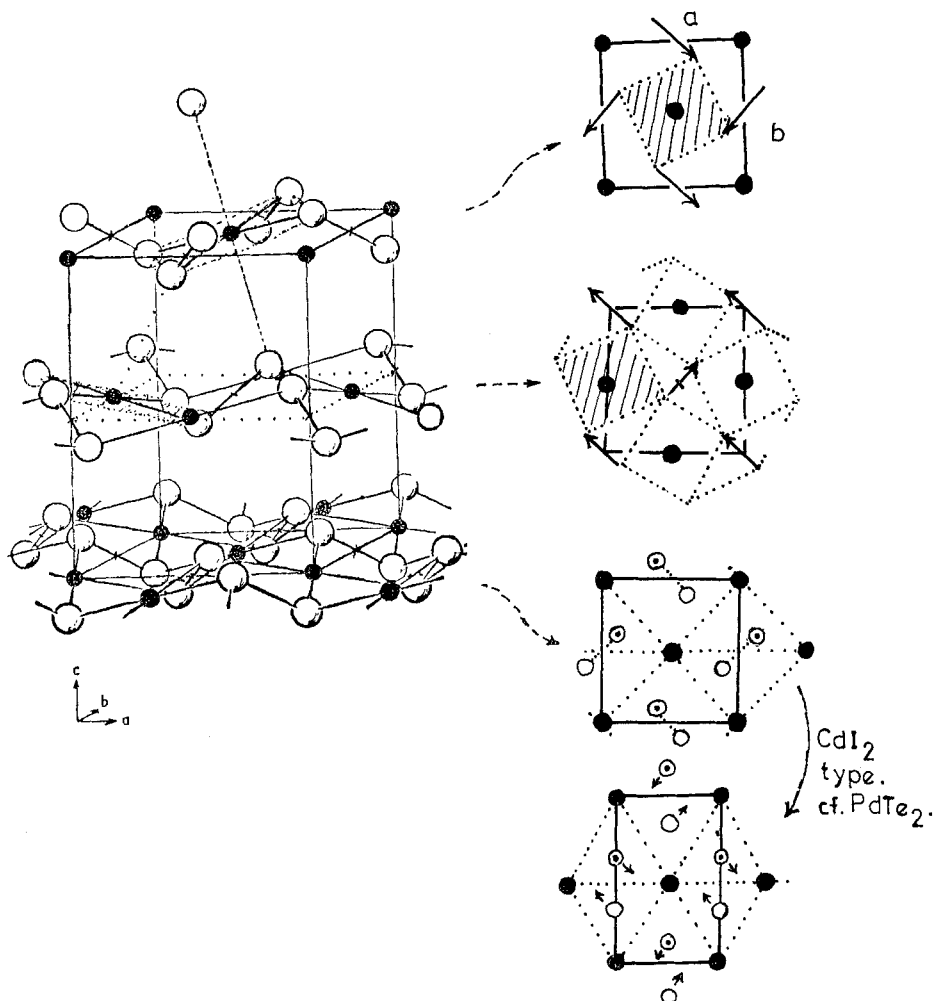
Least M-M ≡ c

IrSe<sub>2</sub>: Ir-Se 3 at ca. 2.44, 3 at ca. 2.52; Se-Se short 2.57, long 3.27 Å.

(d) PdS<sub>2</sub>. Orthorhombic. Group D<sub>2h</sub><sup>15</sup> (Pbca). Four formula units/cell

	<i>a</i>	<i>b</i>	<i>c</i>	Pd-X	X-X <sub>least</sub>	Pd-Pd <sub>least</sub>
PdS <sub>2</sub>	5.460	5.541	7.531	2.30	2.13	3.89 Å
PdSe <sub>2</sub>	5.741	5.866	7.691	2.44	2.36	4.11

Fig. 11

PdS<sub>2</sub> structure (orthorhombic). [After Hulliger and Mooser 1965.]

Short X-X distances are also found in the rutile structure, adopted by many of the TO<sub>2</sub> dioxides. As was shown in fig. 8, the rutile structure (C4) is closely related to that of marcasite (C18). Some of the dioxides also undergo distortion with metal-metal pairing  $\parallel c$  below a certain temperature (e.g. VO<sub>2</sub>, 68°C). Table 6 shows all the structures of the TO<sub>2</sub> dioxides; the more ionic dioxides ZrO<sub>2</sub> and HfO<sub>2</sub> adopt the higher coordination 8:4 fluorite structure. The marcasite structure also can suffer metal-metal bonding  $\parallel c$ , either as alternating contractions (as in the arsenopyrites like RhP<sub>2</sub>), or as a general contraction (in compounds like RuP<sub>2</sub>—isoelectronic with MoS<sub>2</sub>)—see Hulliger (1965). Again isoelectronic with MoS<sub>2</sub> is ZrCl<sub>2</sub>.

Table 5. Least X-X atom distances in the TX<sub>2</sub> dichalcogenides

(a) S-S distances

	MnS <sub>2</sub>	FeS <sub>2</sub>		CoS <sub>2</sub>	NiS <sub>2</sub>	
	2.084	M	P	2.10	2.06	Å
		2.210	2.136			
MoS <sub>2</sub>	TcS <sub>2</sub>	RuS <sub>2</sub>		RhS <sub>2</sub>	PdS <sub>2</sub>	
Through sandwich					Through sandwich	v.d.W.
3.19			2.41		2.13	(3.92)
HfS <sub>2</sub>	ReS <sub>2</sub>	OsS <sub>2</sub>		IrS <sub>2</sub>	PtS <sub>2</sub>	
					Through sandwich	v.d.W.
~3.6			2.43		3.06	3.43

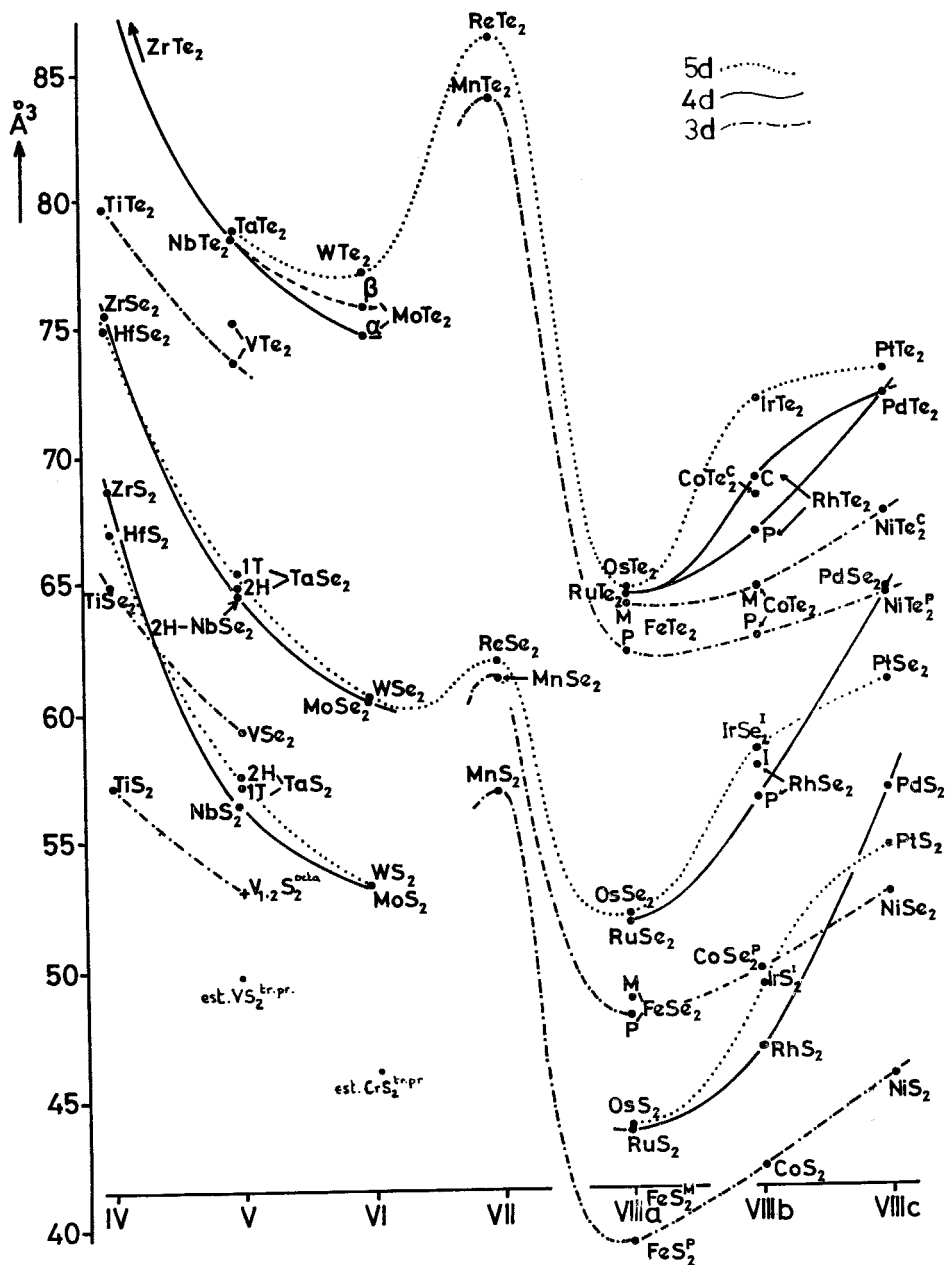
(b) Se-Se distances

	MnSe <sub>2</sub>	FeSe <sub>2</sub>		CoSe <sub>2</sub>		NiSe <sub>2</sub>
	2.38	M	P	M	P	2.394
		2.50		2.53		
	TcSe <sub>2</sub>	RuSe <sub>2</sub>		RhSe <sub>2</sub>		PdSe <sub>2</sub>
				P	I	Through sandwich
			2.46	2.50		2.36
						(3.75)
	ReSe <sub>2</sub>	OsSe <sub>2</sub>		IrSe <sub>2</sub>		PtSe <sub>2</sub>
	v.d.W.			2.57		Through sandwich
~3.3			2.47	(and 3.27)		3.374
						3.29

(c) Te-Te distances

	MnTe <sub>2</sub>	FeTe <sub>2</sub>		CoTe <sub>2</sub>			NiTe <sub>2</sub>	
	2.745	M	P	M	C	P	Through sandwich	v.d.W.
		2.616		2.924			3.48	3.41
α-MoTe <sub>2</sub>	TcTe <sub>2</sub>	RuTe <sub>2</sub>		RhTe <sub>2</sub>		PdTe <sub>2</sub>		
Through sandwich				P	C	Through sandwich	v.d.W.	
3.63			2.64	3.087		3.44	3.49	
	ReTe <sub>2</sub>	OsTe <sub>2</sub>		IrTe <sub>2</sub>			PtTe <sub>2</sub>	
						Through sandwich	v.d.W.	
			2.64			3.53	3.46	

Fig. 12



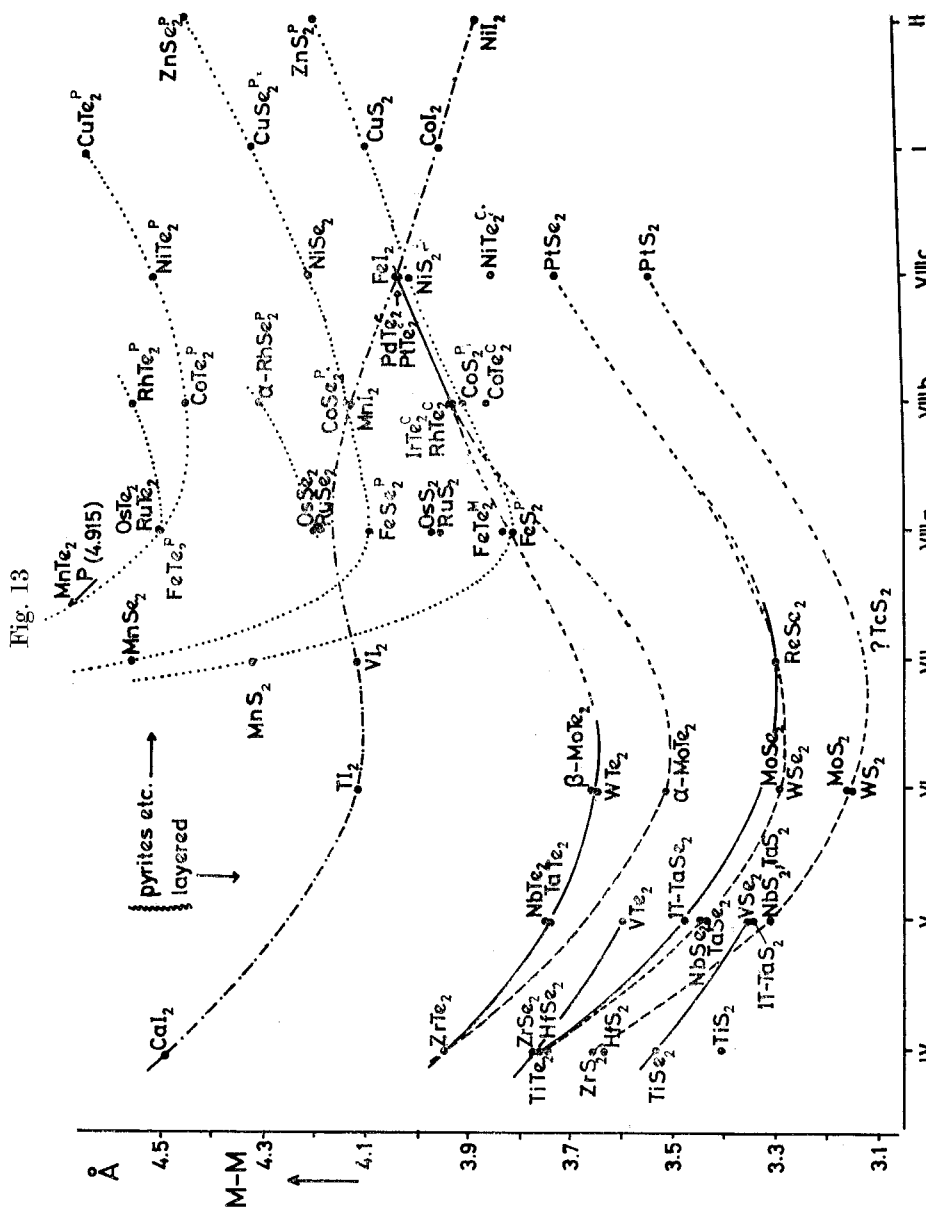


Fig. 13

Plot by group number of the shortest metal-metal distance in the TX<sub>2</sub> dichalcogenides. (Halides in isoelectronic position.)

This layer compound is rather unstable; the anhydrous dihalides of the first period (3d) are more manageable; all crystallize in CdI<sub>2</sub> or related forms. Figure 14 is a plot for the full range of MX<sub>2</sub> layer compounds of *c/a* against the distance between X-X cores (obtained using Waber's core radii, and lattice parameters from Slater (1965), pp. 103 and 308 ff respectively)).



Table 6.  $\text{TO}_2$  dioxide structure types

	Ti	V	Cr	Mn	Fe	Co	Ni
3d	C4 <i>et al.</i>	C4*	C4	C4 <i>et al.</i>	—	—	—
	Zr	Nb	Mo	Tc	Ru	Rh	Pd
4d	C4, C1	C4*	C4*	C4*	C4	C4	—
	Hf	Ta	W	Re	Os	Ir	Pt
5d	C1	C4	C4*	C4* <i>et al.</i>	C4	C4	C4

See Sleight *et al.* 1969.

\* Distorted by metal-metal bonding.

Obviously the extremely anisotropic character of the layer compounds, built in at the atomic level, dominates all the properties of such materials, both mechanical and electrical. The expansion coefficient is about a factor of 10 greater perpendicular to the layers than parallel (Brixner 1963); conversely the velocity of sound in this latter direction is twice that parallel to  $c$  (Guseinov and Rasulov 1966). The thermal conductivity is also up by almost a factor of 10 parallel to the layers. Under applied pressure this factor falls rapidly as the structure stiffens mechanically (Guseinov and Rasulov 1966). Electrical conduction in the two directions is even more different, at least for  $\text{MoS}_2$ , where a difference factor of  $10^3$  seems likely. Another result of the weak van der Waals binding is that the inter-sandwich gap will open up to accept alkali metal ions from ammonia solution. ('Intercalation', c.f. graphite, see p. 285). These intercalates will later be compared to the 'tungsten bronzes'. One problem, particularly with the 3d dichalcogenides, is poor stoichiometry. The  $\text{TX}_2$  structures can readily be transformed (fig. 15) into TX structures like NiAs or NbS by filling the vacant sites of the van der Waals region with metal atoms (Jellinek 1963). Often a continuous solid solution exists (e.g. Ni/Te—Barstad *et al.* 1966), or superlattices may condense out (e.g. Ti/S). Moreover, at a given temperature the equilibrium products may lie far from

Fig. 15

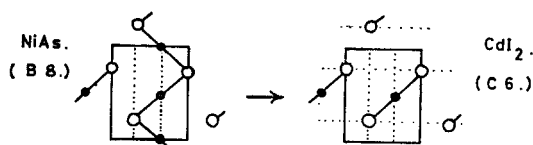
Relation of the  $\text{TX}_2$  layer structures to TX structures.

Table 7. Stacking polytypes of the group VI materials—experimental results

Method of determination	Synthetic material				Natural crystals
	Powder synthesized		High temperature transport 800 to 1050°C		
	Normal pressure	High pressure	Low temperature transport 650 to 800°C	Load microcrystal	Transport crystal
MoS <sub>2</sub>	2H sharp	—	3R/2H diffuse	—	3R (950°C) sharp
	—	—	3R (750°C)	—	—
	—	—	14750 14850 15950	—	—
	—	—	1200 15400 16610 1210	—	—
Optical positions of A and B pair cm <sup>-1</sup>	—	—	1200	—	—
300°K	—	—	15430 16630	—	—
77°K	—	—	1200	—	—
	—	—	Note slightly higher than for natural 3R	—	—
MoSe <sub>2</sub>	3R/(2H) sharp	2H sharp	2H/(3R) diffuse	—	2H sharp
	—	—	3R	—	—
	—	—	Brixner 650°C 12300 12330 12250 14100 14150 14380	—	—
	—	—	1800 1820 2130	—	—
Optical positions of A and B pair cm <sup>-1</sup>	—	12300 14650 1750	12850 12930 12770 14700 14730 14920	—	12320 14410 2090 (900°C)
300°K	—	—	1850 1800 2150	—	12850 15040
77°K	—	—	—	—	2190
	—	—	—	—	14750 15930 1180
	—	—	—	—	15420 17040 1620 ↑ reflc.

WS <sub>2</sub>	x-ray	2H sharp	3R sharp	—	—	3R (900°C) sharp	Composition, +6% Mo ? 2H
	Kikuchi	3R like	—	3R	—	—	—
Optical positions of A and B' pair cm <sup>-1</sup>	300°K	15650 18650 3000	15600 18950 3350	15650 18950 3300	—	—	15.08 17.80 2.72
	77°K	↑ refn. 16190 19530 3340	16220 19530 3310	—	—	—	15.51 18.25 2.74
WS <sub>2</sub>	x-ray	—	—	2H/3R diffuse	—	2H sharp	—
	Kikuchi	—	—	3R 13150 17850 16850 3700	—	—	—
Optical positions of A and B pair and A' cm <sup>-1</sup>	300°K	—	—	13720	—	—	—
	77°K	—	—	18150 17450 3730	13850	18040 17680 18150 17560 3830	—
<p>α-MoTe<sub>2</sub>, all tests give 2H. β form obtained above about 920°C.                      Optical positions of A and B, 300°K 8410 } 2740, 77°K 8980 } 2730 cm<sup>-1</sup>.                      11150 } 11710</p>							

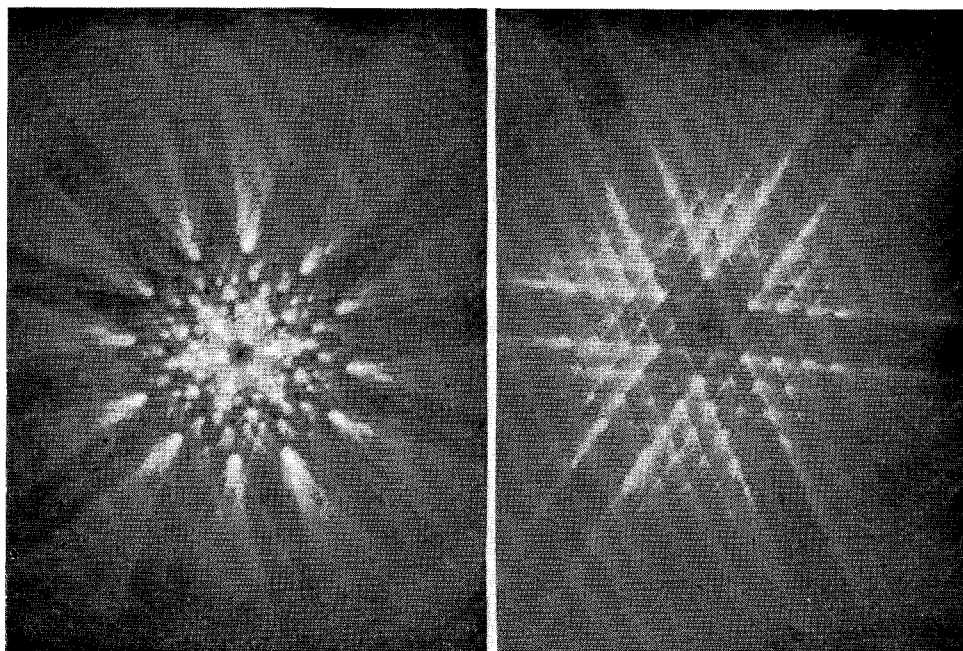
simple stoichiometry, e.g. a 2 to 1 S/Ti powder mixture yields  $\text{TiS}_{1.94}$  at  $800^\circ$  and  $\text{TiS}_{1.92}$  at  $1000^\circ\text{C}$  (Bernard and Jeannin 1962). This non-stoichiometric tendency is least marked for the third period (5d) materials, and for the compounds of group VI. Cleavage of non-stoichiometries like 'VS<sub>2</sub>' or 'CoTe<sub>2</sub>' is noticeably more difficult than for say MoS<sub>2</sub>. The cleavage properties of the stoichiometric materials are indeed quite remarkable. The crystals are not friable and may be pulled apart on sellotape. Through repeated cleaving it is easy to obtain specimens  $200\mu$  square and only  $500\text{ \AA}$  thick. For such a thickness even when the absorption coefficient rises to  $5 \times 10^5\text{ cm}^{-1}$  the crystal will still transmit 2% of the incident light.

### § 3. TX<sub>2</sub> LAYER COMPOUNDS—THE CRYSTALS

Only MoS<sub>2</sub> occurs naturally in appreciable quantities. The other crystals are best obtained by chemical vapour transport (Schafer 1964). The TX<sub>2</sub> dichalcogenides do not in general melt until above  $1000^\circ\text{C}$ , and then only with decomposition. This same technique has been used to obtain anhydrous TX<sub>2</sub> dihalides, and also layer materials like CdI<sub>2</sub> and SnS<sub>2</sub> which could otherwise be grown from solution and the melt respectively. The most convenient carrier gas is iodine, though bromine and chlorine are sometimes required. The carrier concentration was kept low to avoid contamination ( $\sim 1\text{ mg/cm}^3$ ), though Kershaw *et al.* (1967), Hicks (1964) and Conroy and Park (1968) all report remarkably little take up (e.g. iodine in HfS<sub>2</sub>  $\sim 10^{15}$  atoms/cm<sup>3</sup>). With our two-zone furnaces the crystals were typically only 1 to 2 mm across, but this was found quite adequate for our purposes. (Larger crystals up to a centimetre in diameter have been grown in other laboratories.) The group V crystals were particularly easy to obtain. For  $\alpha$ -MoTe<sub>2</sub> crystals with thicknesses of 1 mm were repeatedly obtained, based on clearly marked growth spirals. Crystals of the rhenium compounds grew to very large areas but maintained thicknesses  $\sim 2000\text{ \AA}$  or less. Most of the crystals are quite stable though the groups V and IV compounds tarnish slowly. Additional experimental data concerning crystal growth, etc. is reported elsewhere (Wilson 1969 a).

Naturally occurring MoS<sub>2</sub> has been found in the 3R (Graeser 1964) as well as with the common 2H sandwich stacking (see fig. 3). Our transport crystals of MoS<sub>2</sub> in fact were always of the 3R form. The two types belong to different space groups and their spectra show remarkably different magnitudes of spin-orbit splitting for the pair of excitons situated on the absorption edge (see p. 243). The same has now been found for the MoSe<sub>2</sub> and WS<sub>2</sub> polytypic forms. Table 7 gives the conditions under which the various specimens were obtained and the means by which they were identified. The polytypes are easily distinguishable by (a) the spin-orbit splitting, (b) by x-ray powder analysis (see fig. 18), and (c) in some cases by the form of the Kikuchi banding seen on electron microscope diffraction patterns (e.g. MoS<sub>2</sub>, fig. 16). This latter method is sometimes misleading; thus, although 2H-MoS<sub>2</sub> gives an hexagonal 6-planar star, and 3R-MoS<sub>2</sub> a

Fig. 16



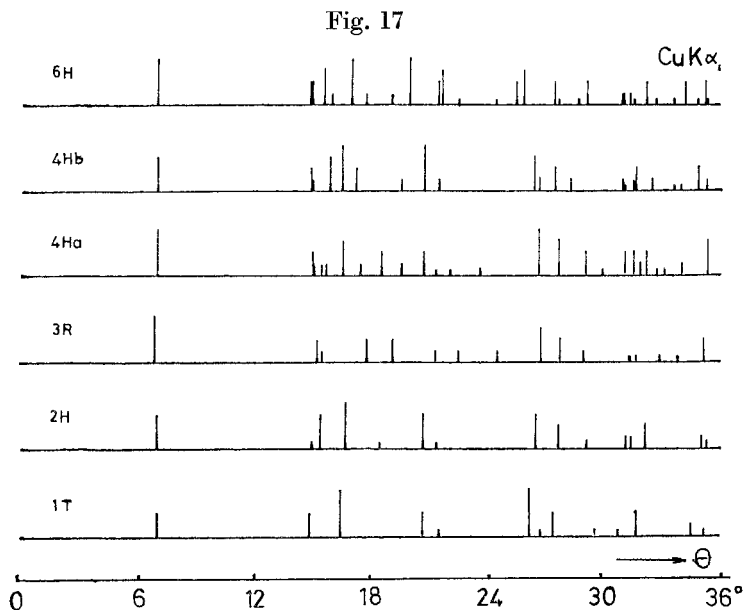
(a)

(b)

Kikuchi bands in (a) 2H and (b) 3R-MoS<sub>2</sub>. (Uyeda 1968—200 kv,  $t \sim 1.2 \mu$ .)

trigonal 3-planar star, HfS<sub>2</sub> gives an hexagonal type pattern, whilst 2H-MoSe<sub>2</sub> gives the trigonal pattern like 3R-MoSe<sub>2</sub>. Though many of our transport crystals were of the 3R type it seems that the 2H form is the stable one to 1000°C. The group VI 3R forms have been synthesized in *powder* form only at high pressure and temperature (Towle *et al.* 1966, Silverman 1967). Such synthesis of the 3R form from the *elements* is much easier than conversion through of the 2H powdered *compound*. 3R-WSe<sub>2</sub> seems very difficult to obtain in pure form, whilst MoTe<sub>2</sub> always occurs in the  $\beta$  form at high temperatures and pressures (Revolinsky and Beerntsen 1966). Several transport crystals were obtained for which both 2H and 3R lines appeared in the x-ray pattern. These stacking mixtures gave exciton peaks intermediate between the extreme positions of 2H and 3R, and at least at 77°K there was no indication of any division of the B peak (see p. 246).

The group V stacking polytypes are also known to show an interesting difference of degree, namely their superconducting transition temperatures. Figure 17 gives the x-ray powder lines expected from six polytypes of TaSe<sub>2</sub>. Some experimental results are shown in fig. 18. It is seen that the line intensities are not consistent: this is due most likely to the impossibility of powdering such flexible crystals. In fig. 19 is given a selection of electron



X-ray powder pattern lines for the polytypes of  $\text{TaSe}_2$ . (Constructed from Bjerkelund and Kjekshus 1967.)

microscope diffraction patterns. It is seen that the majority match the structures discussed earlier. However, the 1T- $\text{TaS}_2$  pattern is at variance with its x-ray pattern, unlike  $\text{VSe}_2$  and  $\text{TaTe}_2$ . Both electron and x-ray patterns are simple for  $\text{VSe}_2$  (like  $\text{HfS}_2$ ); both are complex for  $\text{TaTe}_2$  (like  $\text{WTe}_2$ ). This problem is returned to on p. 297. Bright-field electron micrographs are given in fig. 20. The fluid dislocations and hexagonal networks found in the regular materials have been discussed by Amelinckx (1964). Ribboning is observed in the distorted structures like  $\text{ReSe}_2$ . As seen the 1T- $\text{TaS}_2$  picture appears simpler. The most complex pictures are obtained with  $\text{TaTe}_2$  and particularly  $\text{NbTe}_2$ . 'Domains' are found throughout the crystal and this can result in complex compounded diffraction patterns. It is just possible that these domains invalidate the structure determined by Brown 1966. Kjekshus' Oslo group certainly failed to confirm Brown's result (Selte *et al.* 1966). Many of these points are returned to in detail in § 8.

Mixed crystals of the types  $(\text{W}/\text{Ta})\text{Se}_2$  and  $(\text{W}/\text{Mo})\text{Se}_2$  have been prepared and the micrographs show no indication of segregation. Brixner found smooth parameter and property changes right through these systems (Brixner 1963). The group VI materials, however, will substitute surprisingly little group VII metal (e.g.  $(\text{Mo}/\text{Re})\text{Se}_2 \lesssim 2\% \text{Re}$ —Hicks 1964). Similarly 1T- $\text{TaS}_2$  does not seem to incorporate Hf readily, at least when using the vapour transport process. Such mixed crystals can be satisfactorily analysed to 2% by electron-probe x-ray microanalysis. The composition varies from crystal to crystal, depending on its position of growth in the reaction tube.

Fig. 18

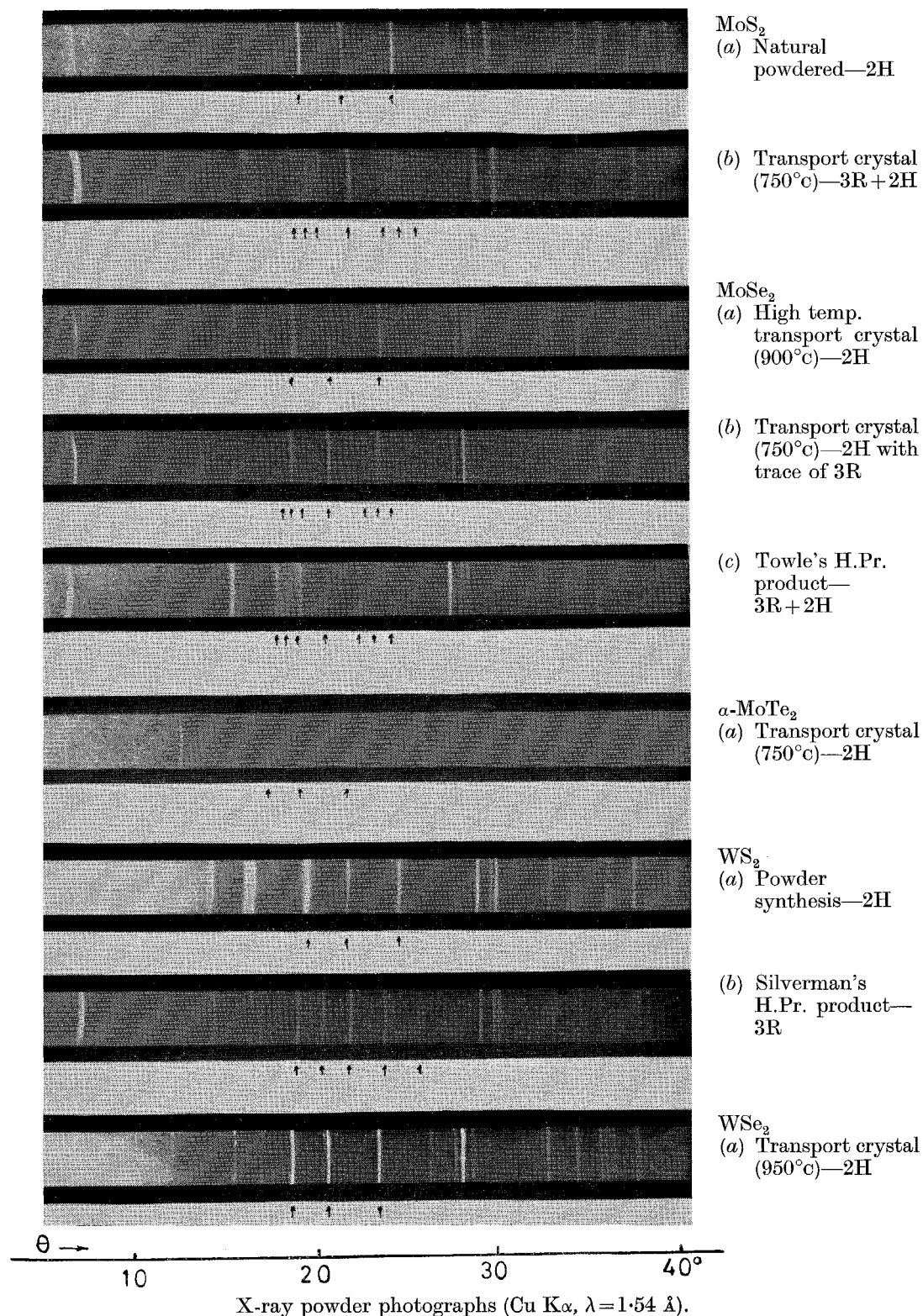


Fig. 18 (continued)

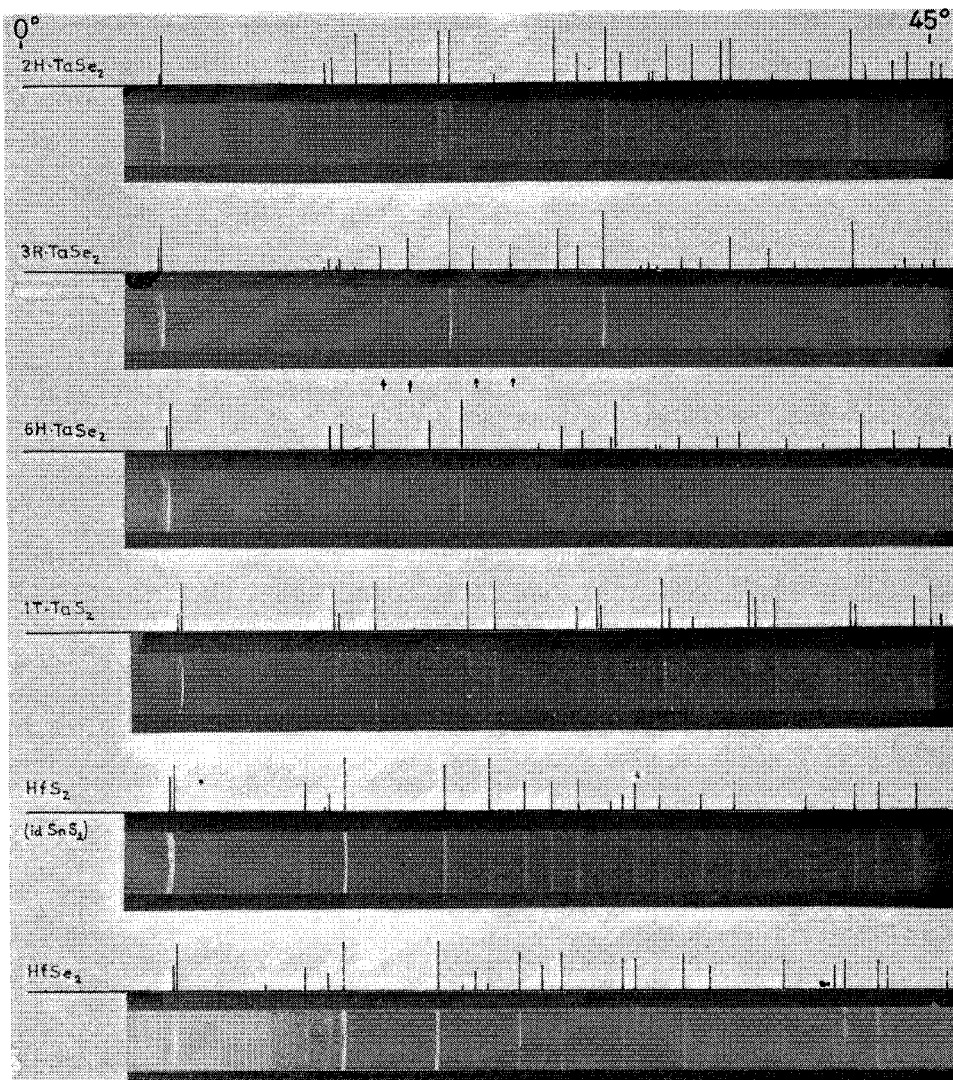
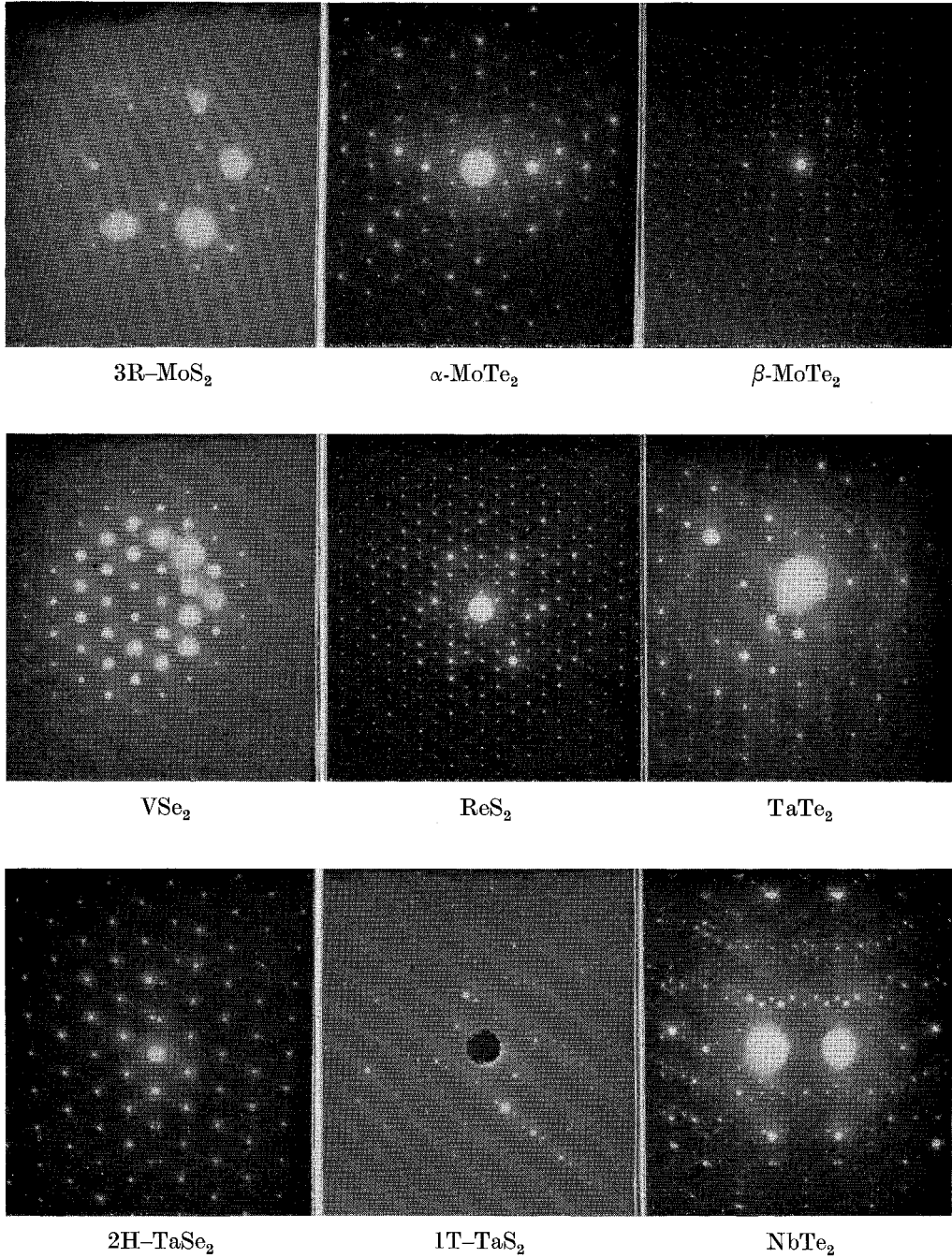
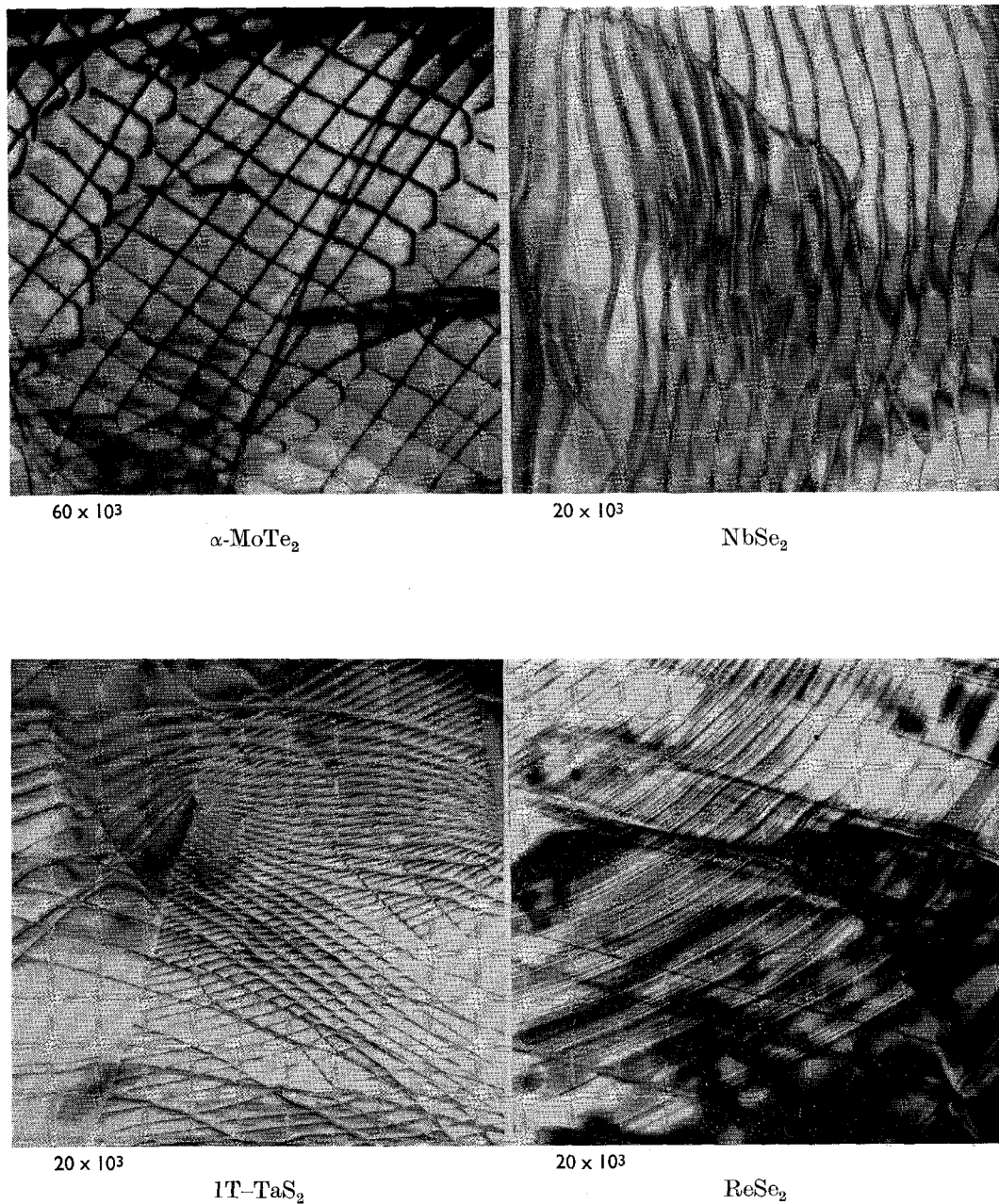
X-ray powder photographs (Cu  $K\alpha$ ,  $\lambda=1.54 \text{ \AA}$ ).

Fig. 19



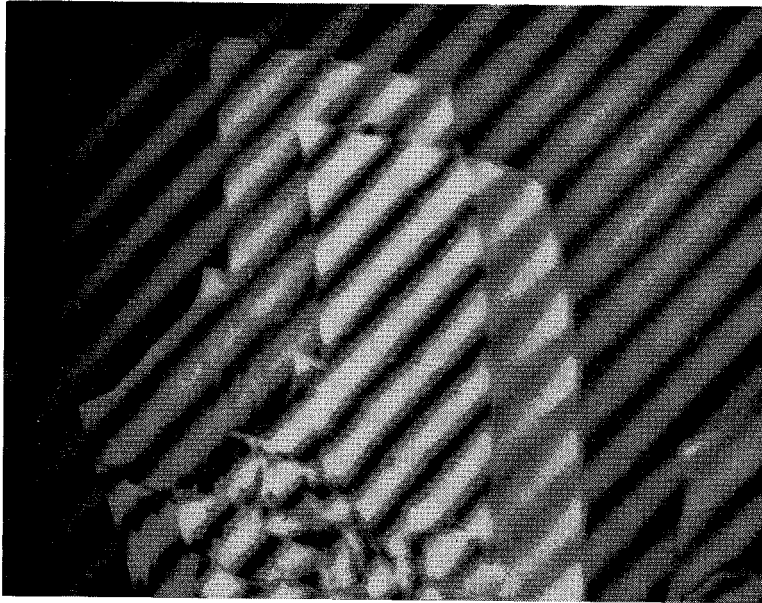
Electron microscope diffraction patterns.

Fig. 20

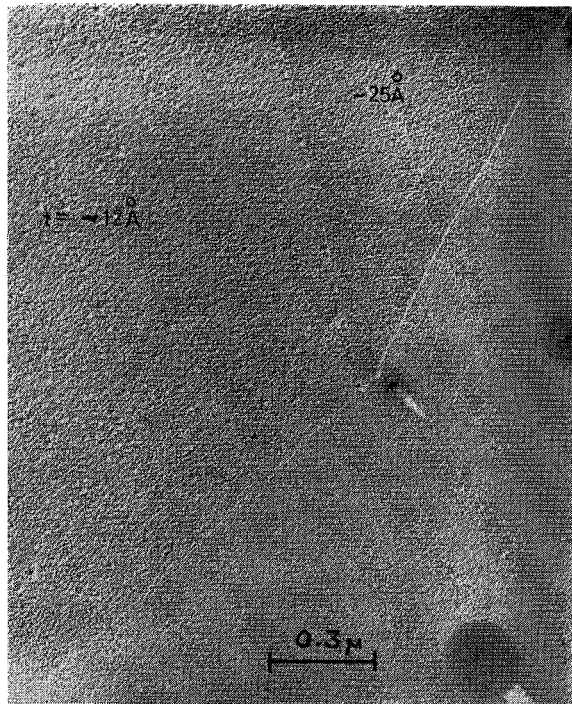


Bright-field dislocation arrays.

Fig. 21



(a)



(b)

- (a) Nomarski thickness fringes for a uniform section of  $\text{TaSe}_2$ . (The crystal is about 1 mm wide and the fringe shift of 21% corresponds to  $t=630 \text{ \AA}$ .)  
 (b) Electron micrograph of a cleaved specimen of  $\text{MoS}_2$  only one and two unit cells thick, measured by the carbon shadowing technique. (By Frindt 1966.)

§ 4. TRANSMISSION SPECTRA FOR THE LAYER-TYPE  
TRANSITION METAL DICHALCOGENIDES

The crystal specimens used for the optical transmission work are obtained by repeated cleaving on sellotape. The very thin cleaved sections can be transferred from the tape to a glass or quartz substrate using trichloroethylene as solvent. Details of this and other experimental techniques are given elsewhere (Wilson, J. A., 1969). Specimens only 500 Å thick can readily be mounted, and may then be used for electrical (Wieting 1968, see p. 271) as well as optical measurements. Crystal thicknesses have been measured using the Nomarski polarizing technique. As seen in fig. 21 (*a*) quite large areas  $\sim 200 \mu$  square cleave at the same thickness. Most of the layer dichalcogenides are strongly coloured in transmission, and the colour changes rapidly with thickness in a characteristic way from material to material. The crystals are highly reflecting also, and even in the high transmission range about 20% reflection occurs, since the refractive index is still  $\sim 2.7$ .

The micro-optical work was carried out on a split-beam spectrophotometer over the range  $\frac{1}{2}$  to  $5\frac{1}{2}$  eV ( $2 \mu$  to 2200 Å), at both room and liquid air temperatures. Experimental details are again given in the above reference, together with an assessment of spectral quality; the peak positions are also detailed there.

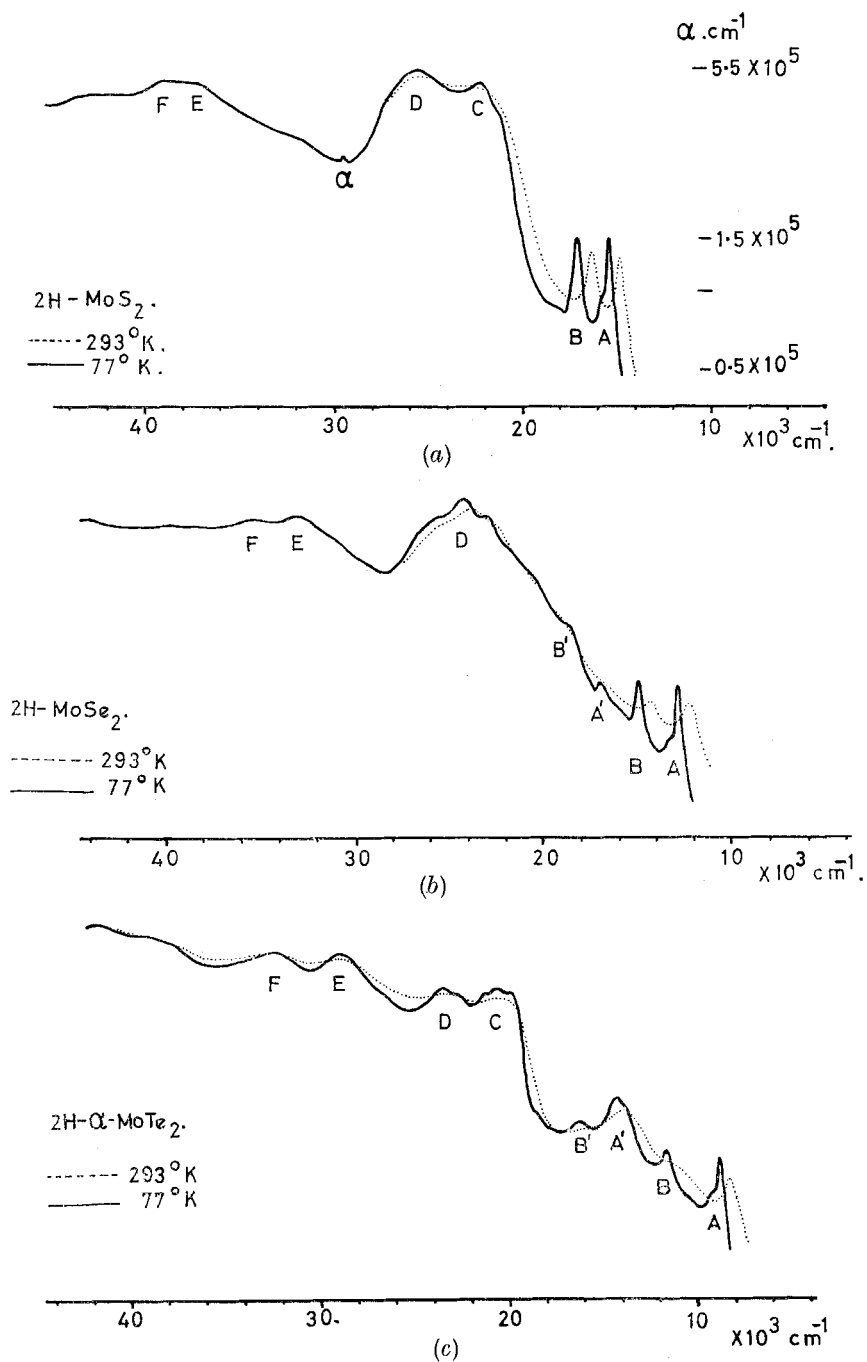
In drawing the following spectra all materials have constantly been referred back to MoS<sub>2</sub>, for which a proper analysis of the absorption and reflection measurements has been made in deriving absorption coefficient values (Evans and Young 1965). The spectra as presented below are with the *y* axis varying approximately as  $\log \alpha$  (see fig. 22 *a*).

The spectra have been divided into the following groupings, the full significance of which will become apparent later :

- A. Regular group VI  
MoS<sub>2</sub>, MoSe<sub>2</sub>,  $\alpha$ -MoTe<sub>2</sub>, WS<sub>2</sub>, WSe<sub>2</sub>.
- B. Distorted group VI  
 $\beta$ -MoTe<sub>2</sub>, WTe<sub>2</sub>.
- C. Regular group V  
NbS<sub>2</sub>, NbSe<sub>2</sub>, TaSe<sub>2</sub>, VSe<sub>2</sub>.
- D. Distorted group V  
NbTe<sub>2</sub>, TaTe<sub>2</sub>, 1T-TaS<sub>2</sub>.
- E. Group VII  
TcS<sub>2</sub>, TcSe<sub>2</sub>, ReS<sub>2</sub>, ReSe<sub>2</sub>.
- F. Group IV  
ZrS<sub>2</sub>, ZrSe<sub>2</sub>, HfS<sub>2</sub>, HfSe<sub>2</sub>, TiSe<sub>2</sub>.

Several other large families of layer compounds exist in addition to the above dichalcogenides. Among transition metal compounds there are many layer dihalides and trihalides (e.g. FeCl<sub>2</sub>, CrBr<sub>3</sub>); also the divalent hydroxides (e.g. Mn(OH)<sub>2</sub>). Among non-transition metal compounds layer structures are found in the dihalides of groups IIA, IIB and IVA

Fig. 22



Transmission spectra for the transition metal dichalcogenides.

Fig. 22 (continued)

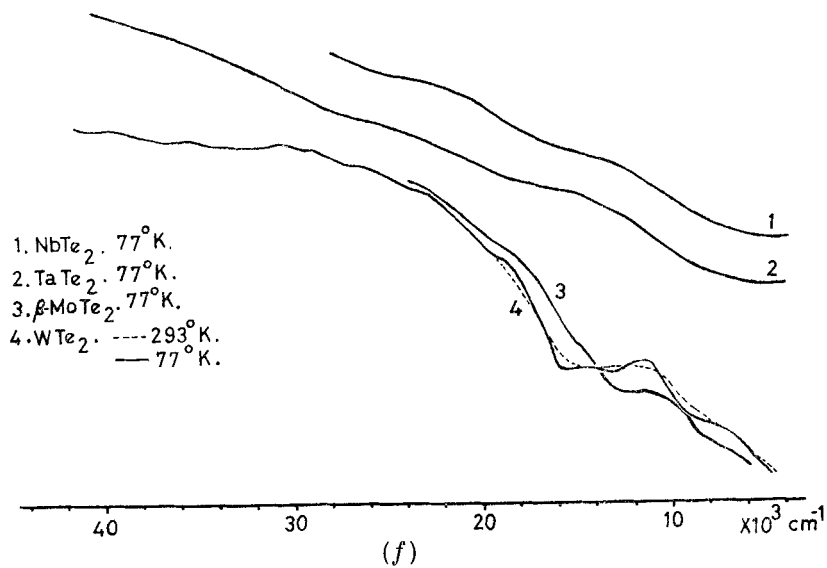
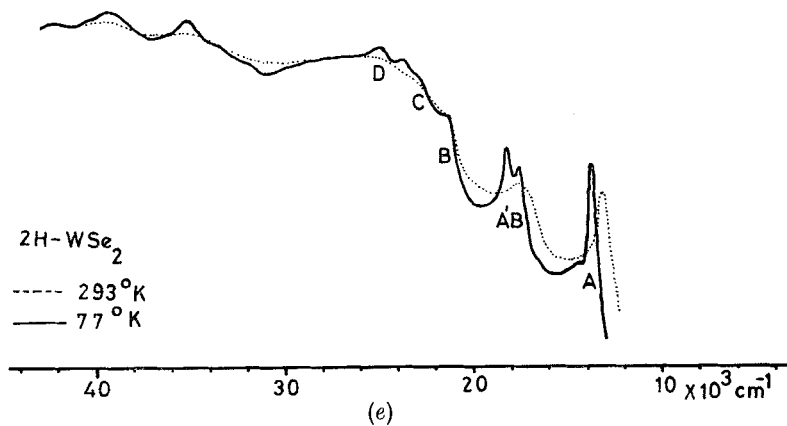
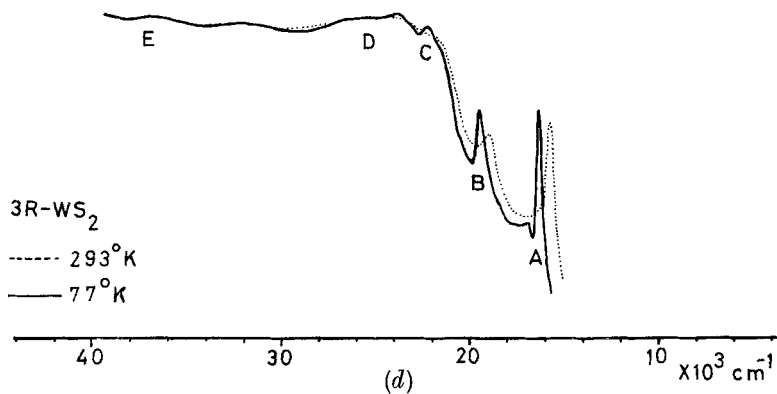


Fig. 22 (continued)

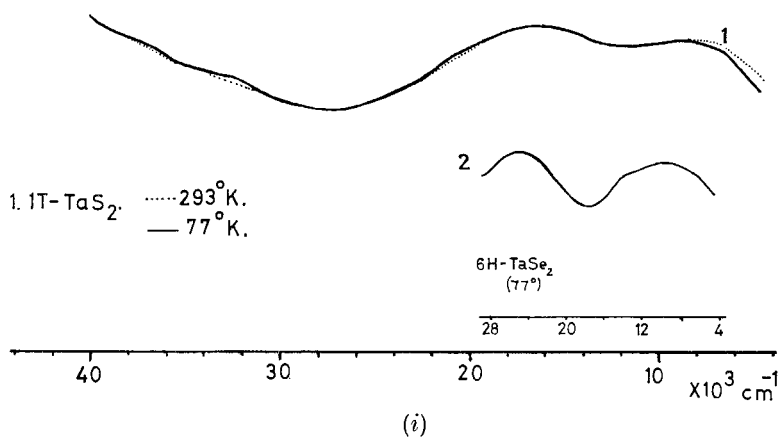
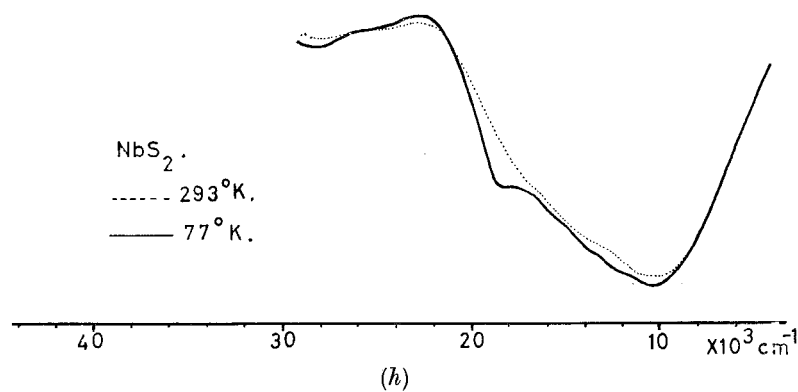
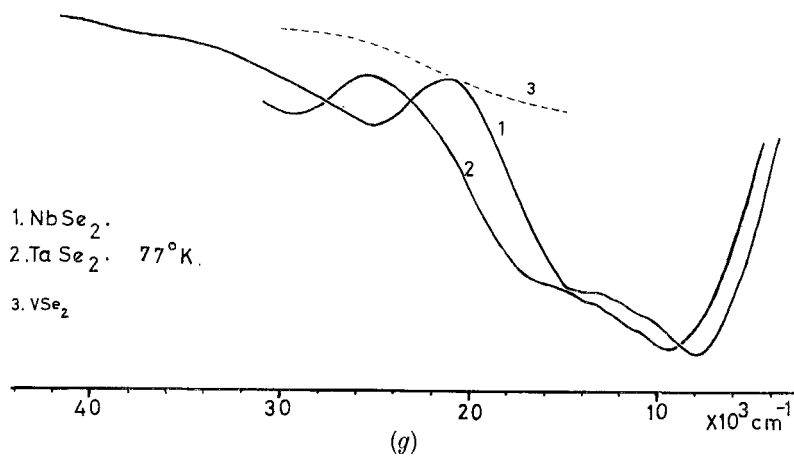
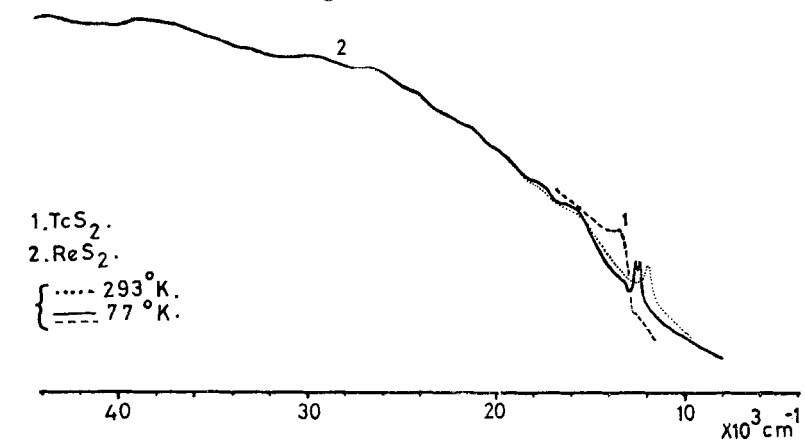
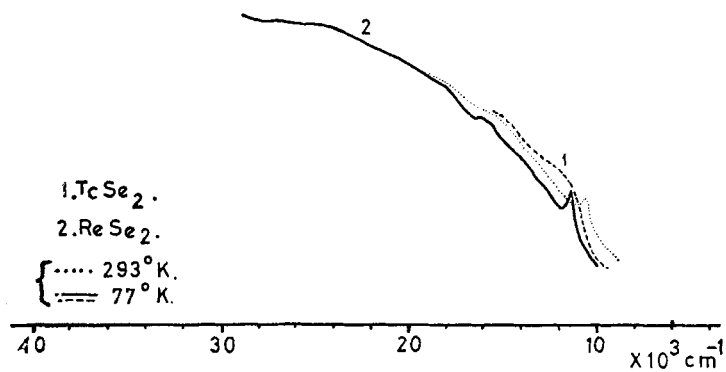


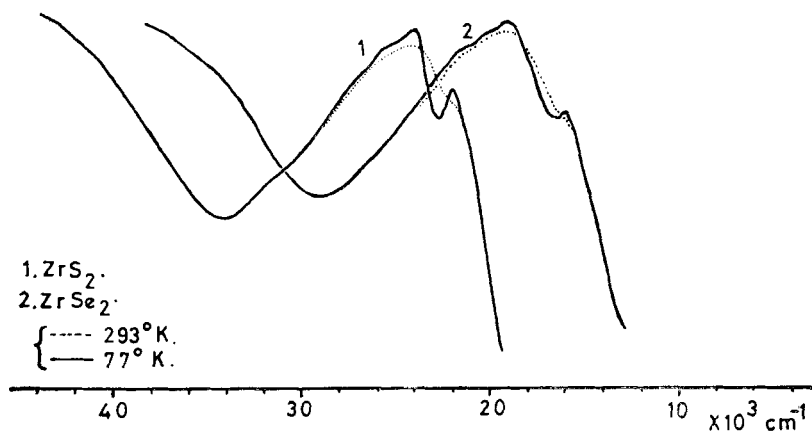
Fig. 22 (continued)



(j)



(k)



(l)

Fig. 22 (continued)

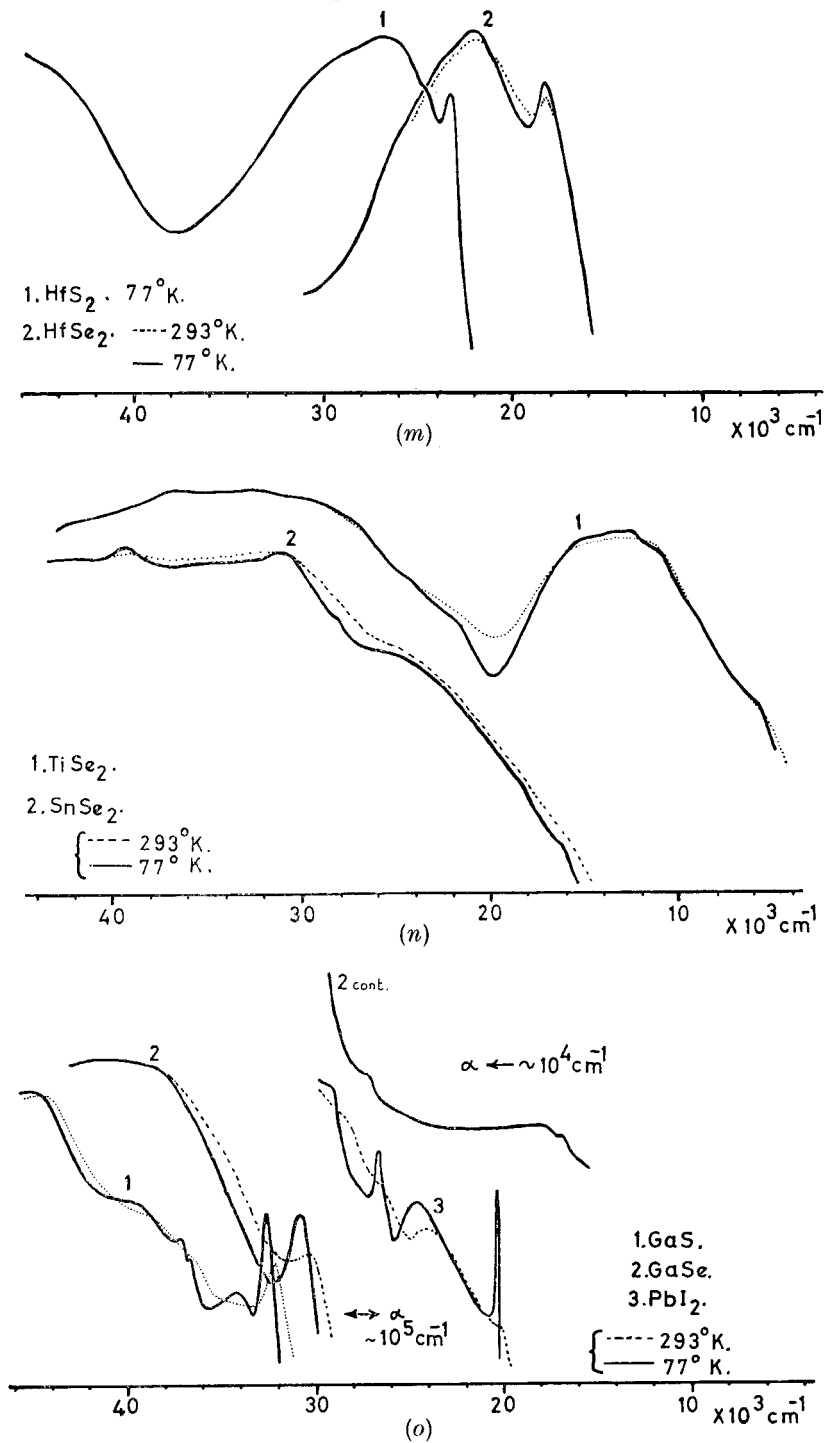
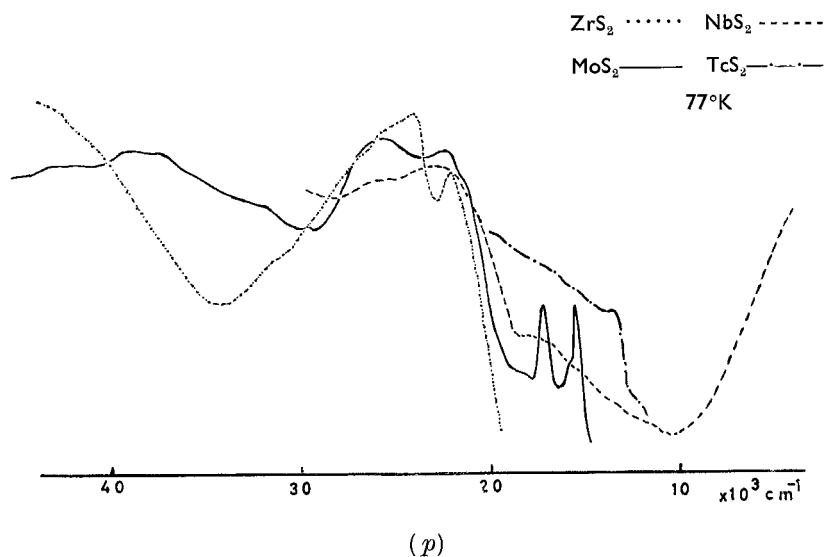


Fig. 22 (continued)

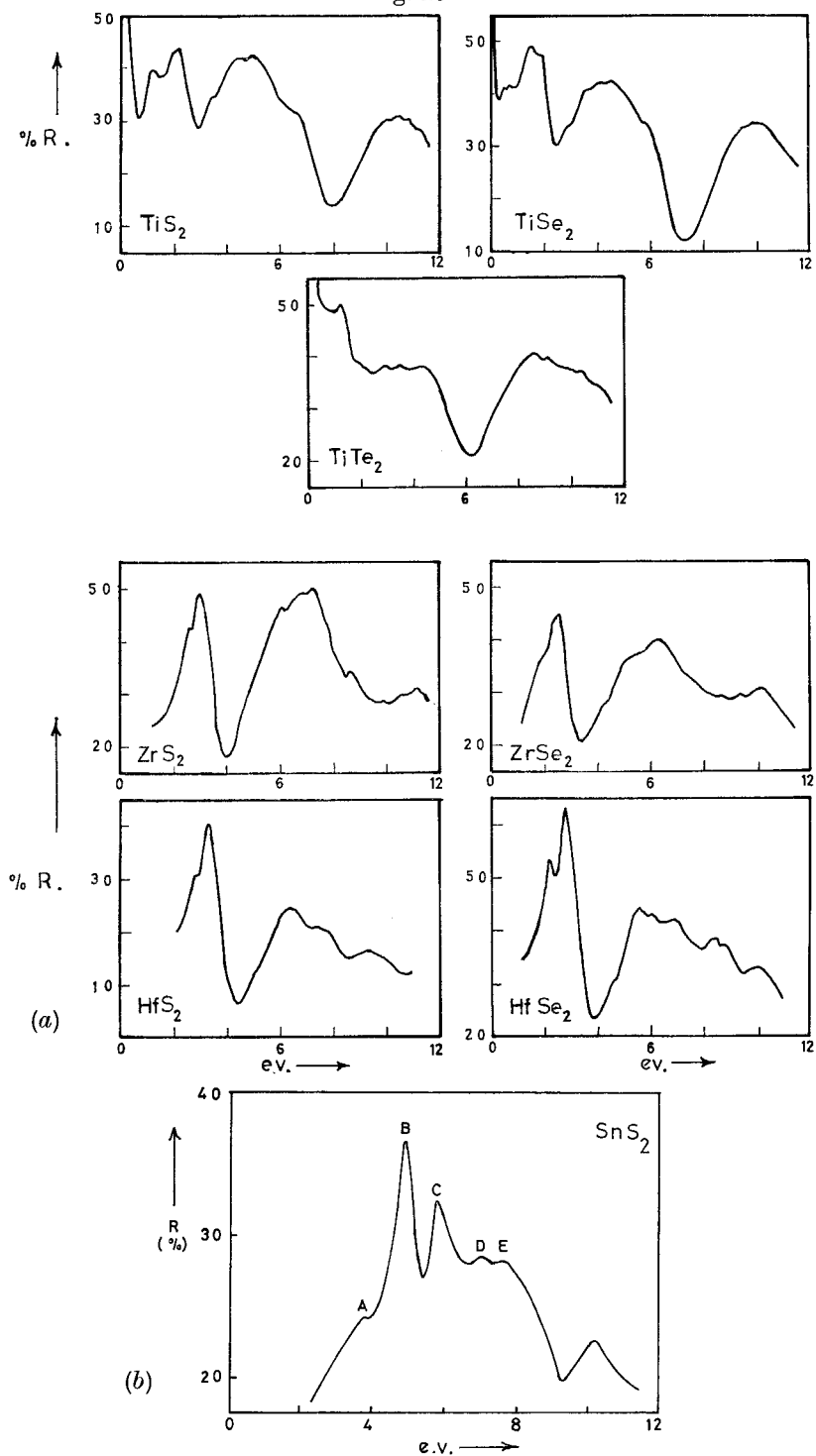


(e.g.  $\text{CaI}_2$ ,  $\text{CdI}_2$ ,  $\text{PbI}_2$ ), the tri-iodides of group VA (e.g.  $\text{BiI}_3$ ), some dichalcogenides of group IVA (e.g.  $\text{SnS}_2$ ), and also the more unusual GaS and  $\text{Bi}_2\text{Te}_3$  families. The transition metal halides are dealt with in detail in § 9.3. Energy gaps are given below for some of the non-transition metal layer compounds. Several points of contact have been made between these latter materials and the layer-type transition metal dichalcogenides, viz.

- (a) Excitons—GaS,  $\text{PbI}_2$ ,  $\text{BiI}_3$ ,  $\text{CdI}_2$ —with  $\text{MoS}_2$  (see §§ 6.1.2. and 7.2.2).
- (b) Defects and polytypism—GaS,  $\text{PbI}_2$ —with  $\text{MoS}_2$  (see §§ 6.1.2 and 7.2.2).
- (c) Indirect edge—GaS,  $\text{CdI}_2$ ,  $\text{SnS}_2$ —with  $\text{MoS}_2$ ,  $\text{ZrS}_2$  (see § 6.1).
- (d) Banding/bonding— $\text{SnS}_2$  versus  $\text{ZrS}_2$ , GaS versus  $\text{MoS}_2$  (see § 5.2).
- (e) Anisotropic electrical data related to band structure— $\text{Bi}_2\text{Te}_3$  (see § 7.2).

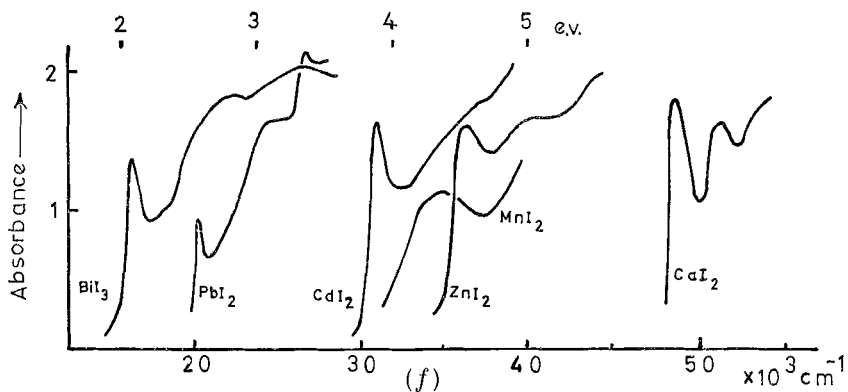
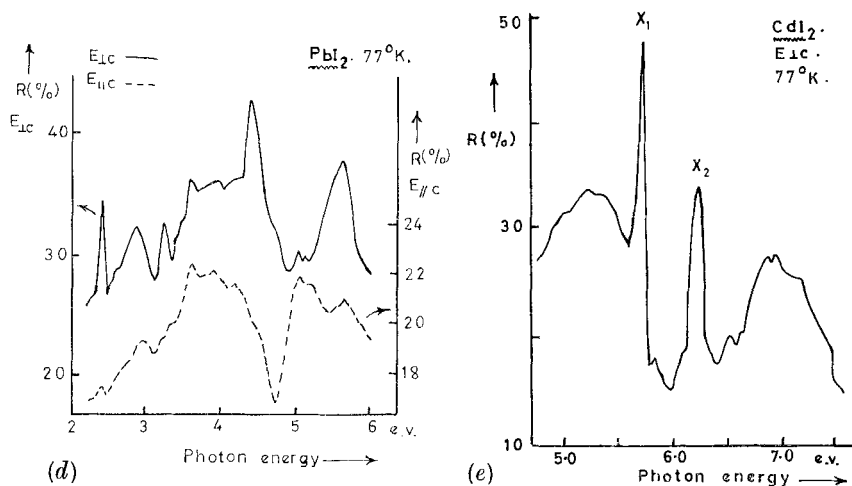
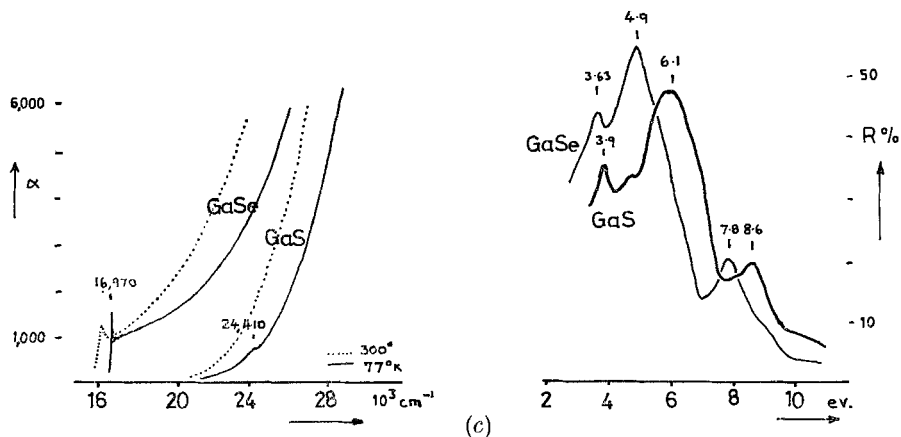
3	Period			Group	Metal atom configuration
	4	5	6		
$\text{MgCl}_2/\text{Br}_2\text{I}_2$	$\text{CaI}_2$	$\text{SrI}_2$	$\text{YbI}_2$	IIA	$s^2(d^0)$
	$\text{ZnCl}_2/\text{Br}_2/\text{I}_2$	$\text{CdCl}_2/\text{Br}_2/\text{I}_2$	—	IIB	$(d^{10})s^2$
	$\text{GeI}_2$	$\text{SnI}_2$	$\text{PbI}_2$	IV	$(s^2)p^2$
	GaS/Se/Te	InSe		IIIA	$s^2p \times 2$
$\text{SiTe}_2$	$\text{GeSe}_2$	$\text{SnS}_2/\text{Se}_2$	$\alpha\text{-PbS}_2/\text{Se}_2$	IVA	$s^2p^2$
	$(\text{As}_2\text{S}_3/\text{Se}_3)$	$\text{Sb}_2\text{Te}_3$	$\text{Bi}_2\text{Se}_3/\text{Te}_3$	VB	$(s^2)p^3$
	$\text{AsI}_3$	$\text{SbI}_3$	$\text{BiI}_3$	VB	$(s^2)p^3$

Fig. 23



Further spectra for various layer compounds.

Fig. 23 (continued)



(a) and (b) from Greenaway and Nitsche 1965, (c) Bassani *et al.* 1964, (d) and (e) from Greenaway and Harbecke 1966, (f) Tubbs 1968.

Optical band gaps, 77°K :

CaI <sub>2</sub>	5.8 (a)	SiTe <sub>2</sub>	1.85 (d)	AsI <sub>3</sub>	~ 2.5 (i)	GaS	3.0 (m)
ZnI <sub>2</sub>	4.4 (a)	GeSe <sub>2</sub>	2.35 (e)	SbI <sub>3</sub>	2.0 (a)	GaSe	2.1 (m)
CdI <sub>2</sub>	3.3 (a), (b), (c)	SnS <sub>2</sub>	2.2 (e), (f)	BiI <sub>3</sub>	1.7 (j)	GaTe	1.75 (n)
PbI <sub>2</sub>	2.5 (a), (b)	SnSe <sub>2</sub>	1.1 (f), (g)	Bi <sub>2</sub> Se <sub>3</sub>	0.16 (k), (l)	InSe	1.3 (o)
		α-PbS <sub>2</sub>	~ 1 (h)	Bi <sub>2</sub> Te <sub>3</sub>	0.14 (l)	Ag <sub>2</sub> F	super- conducting metal (p)

References : (a) Tubbs (1968) ; (b) Greenaway and Harbecke (1966) ; (c) Greenaway and Nitsche (1965) ; (d) Rau and Kanneuf (1966) ; (e) Asanabe (1961) ; (f) Domingo *et al.* (1966) ; (g) Busch *et al.* (1961) ; (h) Silverman (1966) ; (i) Evans, B. L. (private communication) ; (j) Evans (1966) ; (k) Gobrecht *et al.* (1966) ; (l) Greenaway and Harbecke (1965) ; (m) Bassani *et al.* (1964) ; (n) Brebner and Fischer (1962) ; (o) Andriyashik *et al.* (1968) ; (p) Andres *et al.* (1966).

Mentioned in the above is one of the very few 'anti-structure' CdI<sub>2</sub>-type materials, Ag<sub>2</sub>F. Hf<sub>2</sub>S and Hf<sub>2</sub>Se have anti-type MoS<sub>2</sub> structures, and are again metallic (see Franzen *et al.* 1967). Layer structures occasionally occur in the transactinides, e.g. USE<sub>3</sub> (Khodadad 1961), ThI<sub>2</sub> (Guggenberger and Jacobson 1968), and also in the rare earths, e.g. GdCl<sub>3</sub>/Br<sub>3</sub>(f<sup>7</sup>) (Varsanyi *et al.* 1969). In ThI<sub>2</sub> there is an alternating stacking of octahedral and trigonal prism sandwiches, similar to 6H-TaSe<sub>2</sub>. The uranium systems are complex and resemble those of thorium and group IV, rather than group VI. USE<sub>3</sub> and ThSe<sub>3</sub> both have the linear stack structure of ZrSe<sub>3</sub>, mentioned in § 9.3.

## § 5. THE APPROACH TOWARDS A BAND SCHEME FOR THE LAYER-TYPE TRANSITION METAL DICHALCOGENIDES

### 5.1. General Discussion of Band Formation in Transition Metal Compounds

A major problem in discussing transition metal materials is what happens to the metal d states when a compound is formed and a crystal structure built up. The various compounds of nickel or manganese illustrate clearly the gradation from completely localized d states, through various degrees of incipient band formation, to complete delocalization in a wide band. The properties most clearly to show this change are the magnetic susceptibility and the ligand field spectrum. The value of  $\mu_{\text{eff}}$  falls off from the local spin value down through to Pauli-type metallic paramagnetism. At the same time the ligand field intra-atomic d-d transitions lose definition, move to smaller energies and gain rapidly in intensity before being incorporated into stronger inter-band transitions (see § 9.3).

It is not yet clear whether band formation occurs continuously as the relevant conditions are changed (*viz.* d-d intercore overlap), or whether the process suffers some discontinuous cooperative change. It is thought that inter-site electron correlation interactions may favour the latter process, and

Table 8. Growth of covalency in the divalent compounds of manganese and nickel

(a) Magnetic properties of divalent nickel									
	NiCl <sub>2</sub>	NiBr <sub>2</sub>	NiI <sub>2</sub>	NiO	NiS <sub>2</sub>	α-NiS	NiSe <sub>2</sub>	NiTe <sub>2</sub>	
$\chi_{\text{Molar}}$	6150	5600	3900	660	700	240	170	80	$\times 10^{-6}$
$\Theta_{\text{Para}} \text{ } ^\circ\text{K}$	+70°	-18°	—	~ -2500°	~ -750°	—	—	—	
$T_{\text{Néel}} \text{ } ^\circ\text{K}$	50°*	60°*	75°*	520°	—	(263°)	—	—	

\* For a discussion of these values see van Uitert, Williams, Sherwood and Rubbin, 1965, *J. appl. Phys.*, **36**, 1029.

(b) Optical properties of divalent manganese									
	MnF <sub>2</sub>	MnSO <sub>4</sub> ·4H <sub>2</sub> O	MnCO <sub>3</sub>	MnO	MnCl <sub>2</sub>	MnBr <sub>2</sub>	MnI <sub>2</sub>	α-MnS	
Position of ${}^6\text{A}_{1g} \rightarrow {}^4\text{A}_{1g}$	25200	24880	24540	23920	23360	22980	21900	21500	cm <sup>-1</sup>
Oscillator strength	Very low	0.6	7.7	—	7.3	9	12.1	230	$\times 10^{-7}$

(See Lohr and McClure 1968 and Huffman 1969.)

that the d band prior to its full establishment is pinched off into a series of non-conducting (i.e. full) sub-bands (see No. 4, **40**, *Rev. mod. Phys.*, October 1968). At present we are studying the high pressure optical properties of several promising layer compounds from this aspect of the Mott 'metal/insulator transition', viz.  $\text{NiI}_2$ ,  $\text{VI}_2$ ,  $\text{TiI}_2$ ,  $\text{CrI}_3$  and  $\text{TiCl}_3$ .

Returning to the layer-type transition metal dichalcogenides it is clear that d band formation is there well advanced. The semiconductors of groups IV (e.g.  $\text{ZrS}_2$ ), VI ( $\text{MoS}_2$ ) and VIII ( $\text{PtS}_2$ ) are all *diamagnetic*, whilst the spectra in the 1 eV range are not of the ligand-field type, since the absorption coefficients are in excess of  $10^5 \text{ cm}^{-1}$ . The degree of filling of d bands lying within the basic bonding-antibonding band gap ( $\sim 4 \text{ eV}$  in  $\text{MoS}_2$ ) largely determines the electrical character of the various compounds. For example the trigonal prism group V materials ( $d^3$ ) are medium mobility metals ( $\rho \sim 3 \times 10^{-4} \Omega\text{-cm}$ ), superconducting, and with the plasma edge at about 1 eV.

Among the *pyrite* dichalcogenides, however, such d bands are not always formed. Thus, although  $\text{RhSe}_2$  ( $d^7$ ) and  $\text{CuSe}_2$  ( $d^9$ ) are metallic and show Pauli paramagnetism, superconductivity and strong free carrier absorption, the manganese materials ( $d^5$ ), and  $\text{NiS}_2$ , still have local spin moments, which in the case of the manganese compounds become cooperatively aligned to yield antiferromagnetic ordering around liquid air temperature. This antiferromagnetism should be distinguished from the band antiferromagnetism shown by the  $\text{NbSe}_2$  family; the latter is concurrent with free carrier absorption (see § 7.3.1).  $\text{FeS}_2$  and  $\text{CoS}_2$  have magnetic, electrical and optical properties which indicate that a collective narrow d band is achieved. The non-layered transition metal dichalcogenides are discussed in detail in § 9.1.

Several factors affect this question of d band formation :

- (i) internuclear distances, T-X, T-T and X-X (size factor),
- (ii) crystal structure (symmetry factor),
- (iii) (a) ligand electronegativity (energy factor),  
       (b) detailed electronic configuration of metal atom.

These factors are of course inter-related. The extent to which the s and d states of the metal atom can become spatially and energetically distinct is most pronounced for manganese. Compounds like  $\text{MnI}_2$ ,  $\text{MnO}$ ,  $\alpha\text{-MnS}$  and  $\text{MnS}_2$  are all based on the  $\text{Mn}^{2+}$  ion with its contracted  $d^5$  half-shell. They tend to have large interatomic distances in contrast to non-ionic compounds like  $\text{Ni}_2\text{Sn}$ ,  $\text{MnTe}$  and  $\text{MnSb}$ , where the ligand is not sufficiently electro-negative to cause s-d differentiation (collected parameters, Slater 1965, p. 308ff). *Hybridization* of the metal atom s and d states and general

'covalent' mixing of these states into the valence bands, is more common for the early groups of the transition periods, and, again, more so for all groups of the second and third periods than for the first period :

thus we find the decrease in ionicity of $\text{TiCl}_3$ compared with $\text{CrCl}_3$ ,			
and of $\text{TiO}$	,,	,,	$\text{NiO}$ ,
whilst there is an increase in ionicity for $\text{TiCl}_2$	,,	,,	$\text{ZrCl}_2$ ,
for $\text{MnS}_2$	,,	,,	$\text{TeS}_2$ ,
for $\text{NiO}$	,,	,,	$\text{PdO}$ .

(many of these compounds are discussed further in § 9).

Orbital hybridization and the resulting covalency means that in the *crystalline* state we are going to have bands of highly mixed '1' character, which are of greater energy span than for ionic compounds, where the valence bands are very flat. In the *dichalcogenides* of groups IV, V, VI a significant degree of d and p covalent mixing into the valence band along with the metal s state seems feasible. In crystals of the transition *elements* themselves s, d, p mixing is well advanced (e.g. Ti, Altmann and Bradley 1967). When the distance between metal atoms is increased, as in a compound, this direct metal sublattice mixing decreases rapidly, particularly for the elements to the centre right of each series where the atomic radii are small. The metal-metal distances in the above dichalcogenides, with extremes of 3.16 Å for  $\text{MoS}_2$  and 3.95 Å for  $\text{ZrTe}_2$ , correspond to 15% to 25% increases on those distances in the pure metals. In all the *dihalides* these percentage increases are much greater, e.g. 42% for  $\text{TiI}_2$  ( $a = 4.11$  Å), 65% for  $\text{MnI}_2$  ( $a = 4.10$  Å). This general size factor difference plus the electronegativity change means that there will be far greater isolation, energetically and spatially, of the d-states in say  $\text{ZrCl}_2$  than in its isostructural isoelectronic partner  $\text{MoS}_2$ †. The layer halides are discussed further in § 9.3.

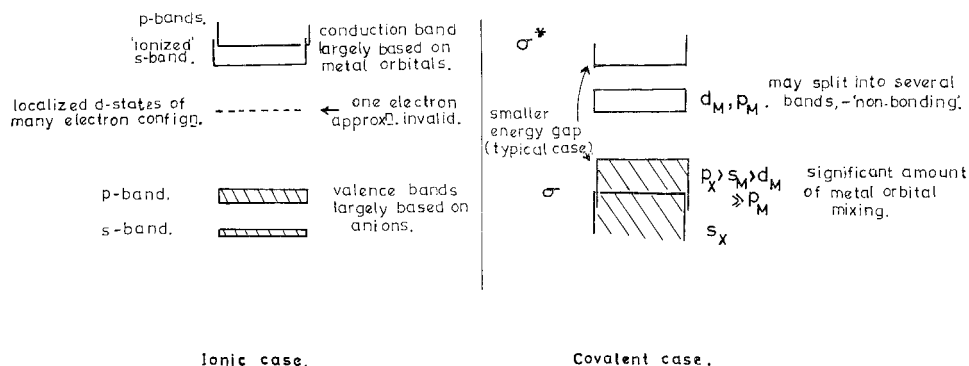
### 5.2. The Proposed Banding Arrays for the Layer-type Transition Metal Dichalcogenides

The effect on the general band scheme for transition metal compounds of the move from ionic to covalent bonding is represented in fig. 24. With covalent bonding the valence band is considerably broader due to T/X state mixing. Au Yang and Cohen's (1969) band diagram for  $\text{SnSe}_2$  ( $C6$ ,  $E_g = 1$  eV) shows this markedly as compared with the isoelectronic isostructural but ionic case for  $\text{CdBr}_2$  ( $E_g \approx 4$  eV; compare  $\text{RbBr}$   $E_g \sim 6.5$  eV, and  $\text{AgBr}$   $E_g \sim 3$  eV). In a transition metal compound like  $\text{ZrS}_2$  or  $\text{MoS}_2$  it is likely that this mixing of metal states into the valence band follows the

† N.B. The above type of orbital differentiation is not completely confined to transition elements; note s/p compounds like  $\text{TlBr}$ ,  $\text{SnTe}$  and  $\text{PbI}_2$ , (also the concomitant long bond lengths, cf.  $\text{MnCl}_2$ ,  $\text{CoO}$ , etc.). A recent attempt at assigning percentage ionic character to non-transition metal compounds has been made by Phillips and van Vechten (1969).

pattern  $s > d \gg p$ . The p states are more likely to be mixed into the energetically closer non-bonding d bands, interposed within the basic  $\sigma\sigma^*$  gap  $\dagger$ . The averaged value of this latter gap is directly related to the heat of formation of the compound, a measure of the chemical binding energy which is often known (Vijh 1969).

Fig. 24



The change in banding character between 'ionic' and 'covalent' transition metal compounds.

In an octahedrally coordinated compound (e.g.  $\text{ZrS}_2$ ) it is well known that out of the five d states the two  $e_g$  states are more suited geometrically to covalent bonding than are the three  $t_{2g}$  states. The latter go to form the basis of a non-bonding band. In a structure with trigonal prism coordination like  $\text{MoS}_2$  (point group  $D_{3h}$ ) the d states split in such a way that the  $d_{yz}$  and  $d_{xz}$  orbitals are the most likely to mix into the valence band. The  $d_{x^2-y^2}$  and  $d_{xy}$  orbitals will mix more with the metal  $p_x$  and  $p_y$  states, and are likely to form a non-bonding band above and detached from a second non-bonding band based on  $d_{z^2}$ . This latter orbital gives poor overlap between near-neighbour metal atoms and the band is likely to be rather narrow.

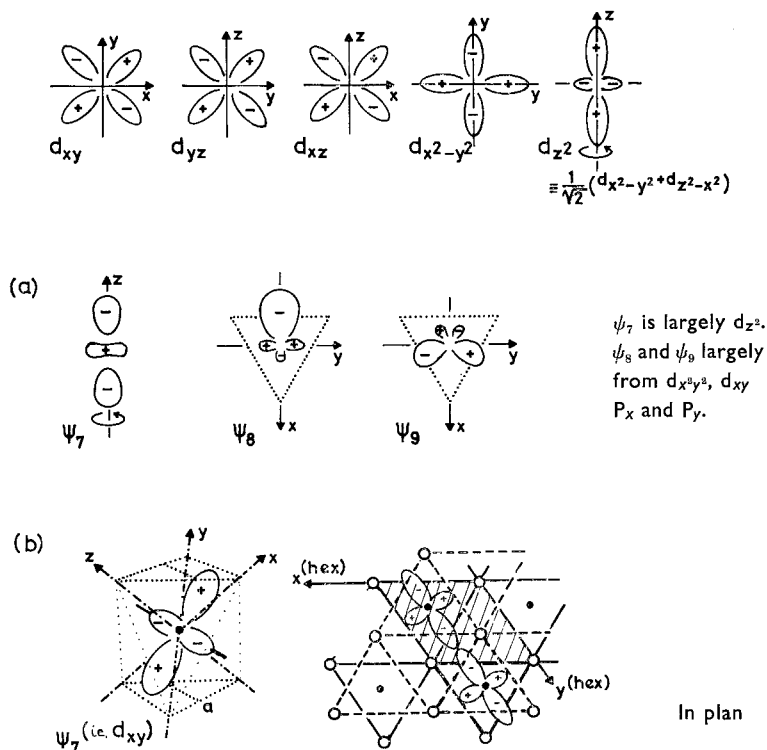
As indicated below in fig. 26 the principal valence band in the  $\text{TX}_2$  layer structures is full with 16 electrons (e.g.  $\text{ZrS}_2$ ), and subsequent electron additions as for  $\text{NbS}_2$ ,  $\text{MoS}_2$ ,  $\text{TeS}_2$  go into the non-bonding d-based bands. It is the degree of filling of these latter bands that then determines the electrical, magnetic and optical properties of these transition metal

$\dagger$  An attempt is being made in this laboratory to calculate the band structures using the tight-binding method by R. A. Bromley.

dichalcogenides. The details will be discussed shortly in §§6 and 7†.

The possible shape and orientation of the non-bonding orbitals for the  $\text{TX}_2$  layer structures is shown in fig. 25. If our interpretation of the spectra is correct (see shortly) the widths and location of the non-bonding bands are as marked on fig. 26(b). Interpretation to this end of the optical results is prompted by the very satisfactory viewpoint that the above

Fig. 25

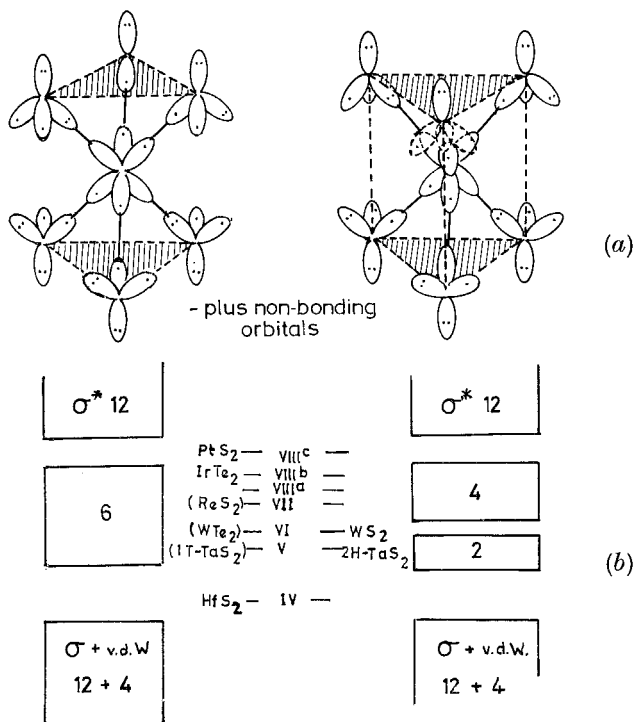


Shape and orientation of the 'non-bonding' orbitals for the  $\text{TX}_2$  layer structures (based largely on metal d and p states). (a) For trigonal prism,  $\psi_7$  yields poor M-M overlap,  $\psi_8$  and  $\psi_9$  degenerate, (b) for octahedron,  $\psi_7$ ,  $\psi_8$ ,  $\psi_9$  degenerate. Lobes bisect bond angles. Good overlap in layers.

† It is hoped from the above discussion we have made clear that in, say,  $\text{ZrSe}_2$ , the zirconium 5p states will be virtually confined to the conduction band. Likewise in  $\text{SnSe}_2$  the tin 5d states will show negligible mixing into the valence band (i.e. as occupied states). The mixing here of p and d states respectively into the valence band is proportionately much less than would be implied from the use of six equivalent metal hybrid bonding functions, of the old octahedral formulation, 'sp<sup>3</sup>d<sup>2</sup>'. The same goes for trigonal prismatic coordination, for which the formulation 'd<sup>4</sup>sp', derived from Hultgren's paper of 1932, is often seen.

banding schemes give of the observed electrical, magnetic and structural properties for the whole  $\text{TX}_2$  dichalcogenide family†.

Fig. 26



(a) Occupation of orbitals in the simple valence bond picture, (b) the proposed band positions and their degree of filling for the regular  $\text{TX}_2$  dichalcogenides.

Figure 26 (a) stylistically represents the arrangement of electrons in the bonded directions for the two types of layer dichalcogenide  $\text{TX}_2$  sandwich. As seen, a simple valence bond picture requires not only hybridization but also 'resonance'. Each chalcogenide atom puts a lone pair into the van der Waals region, and each metal atom then needs to supply four electrons for the bonding states to be completely full (e.g. as in  $\text{ZrS}_2$ ,  $s^2 d^2$ , or  $\text{SnS}_2$ ,  $s^2 p^2$ ). Any further electrons (as in  $\text{MoS}_2$ ,  $s^2 d^4$ ) must enter the non-bonding orbitals which can accommodate up to six electrons (as in  $\text{PtS}_2$ ,  $s^2 d^8$ ). The semiconductivity of octahedral  $\text{ZrS}_2$  and  $\text{PtS}_2$  follows automatically, whilst that of the  $\text{MoS}_2$  family is seen to be a consequence of the adoption of the trigonal prismatic structure. In group V we have metals

† Goodenough has recently published two papers (1968 b, c) discussing the behaviour of the d levels in  $\text{MoS}_2$  and  $\text{WS}_2$  from the aspect of crystal field theory. However, the model seems to be too ionic in character and fails to match much of the experimental data.

for both coordination types,  $\text{VSe}_2$  with the wider octahedral band being a 'better' metal than say  $\text{NbSe}_2$ , where the free carriers lie in the narrow  $d_{z^2}$  band of the trigonal prism scheme. We will look at the electrical properties in some detail group by group in § 7.

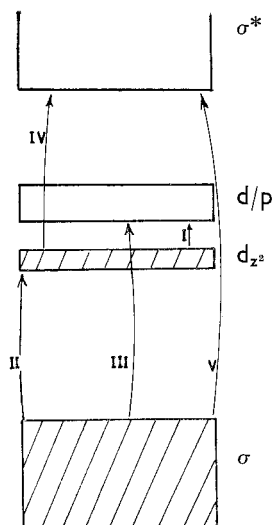
§ 6. THE OPTICAL SPECTRA OF THE *Regular Layered*  $\text{TX}_2$   
DICHALCOGENIDES RELATED TO THE ABOVE BANDING SCHEME

6.1. *The Trigonal Prism Materials*

6.1.1. *Band positions and transition assignments*

Because the non-bonding d band system in the  $\text{MoS}_2$  family is only partially filled, and again because the materials are semiconductors, the group VI spectra are quite complicated. Figure 27 shows the five basic types of inter-band transition to be expected with the trigonal prism set of bands. Transition V is the basic bonding energy gap. Such transitions commence in  $\text{MoS}_2$  with exciton  $\alpha$ . Transition III is the one which gives rise to the strong excitons A and B characteristic of the  $\text{MoS}_2$  family; transitions IV, of somewhat larger energy, yield the broad band topped by peaks C and D. This ordering is seen to be the correct one from a comparison with the group V spectra. There the D transition is absent due to the  $d_{z^2}$  band now being only half full. Furthermore, group V loses the excitons A, B and  $\alpha$  which are screened out by the free carriers of the  $d_{z^2}$  band. A broad hump remains in the A/B region. In group V there is the opportunity also for transitions of type II. These also show up weakly

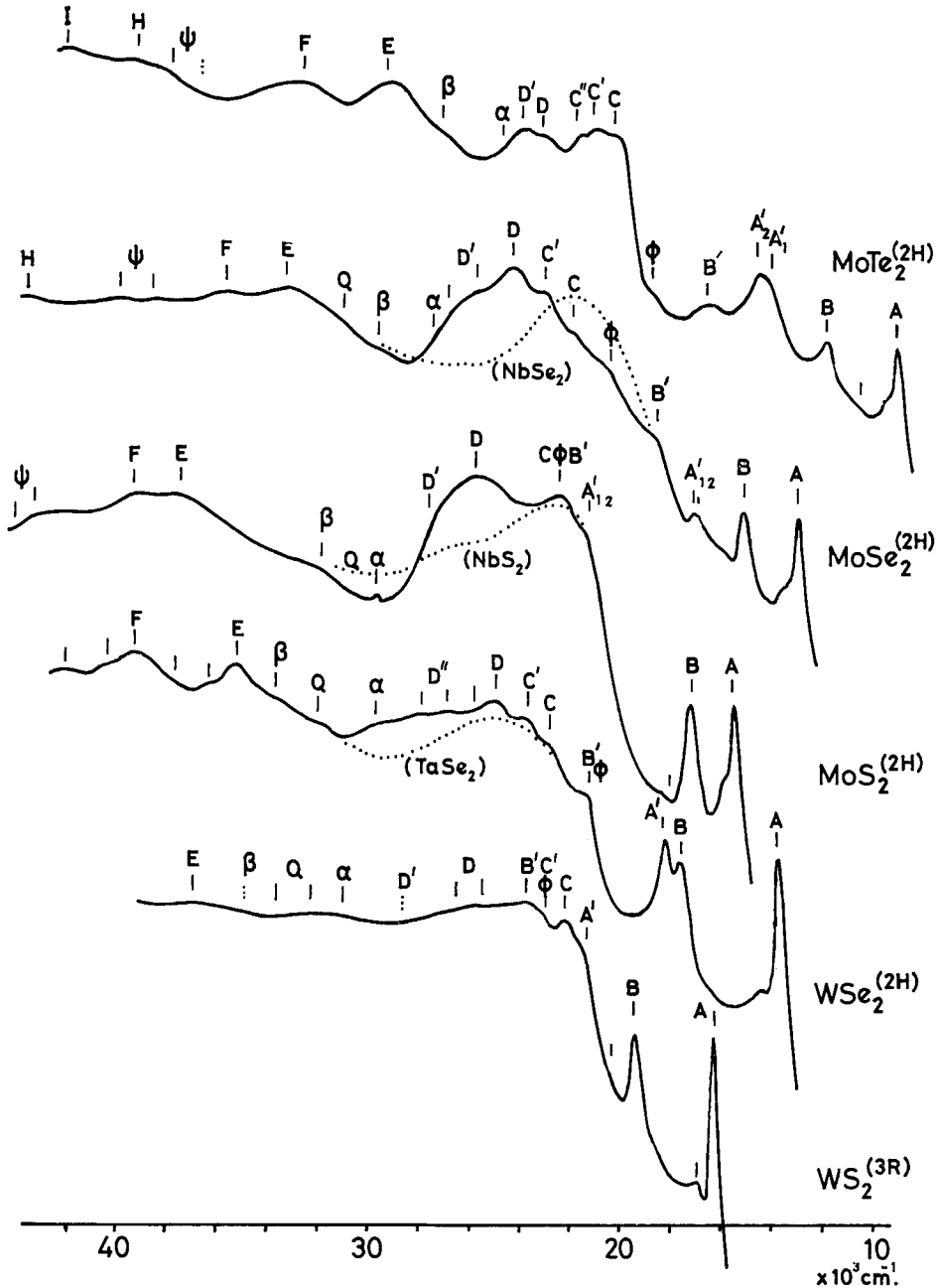
Fig. 27



General types of interband transition for the trigonal prism group VI compounds.

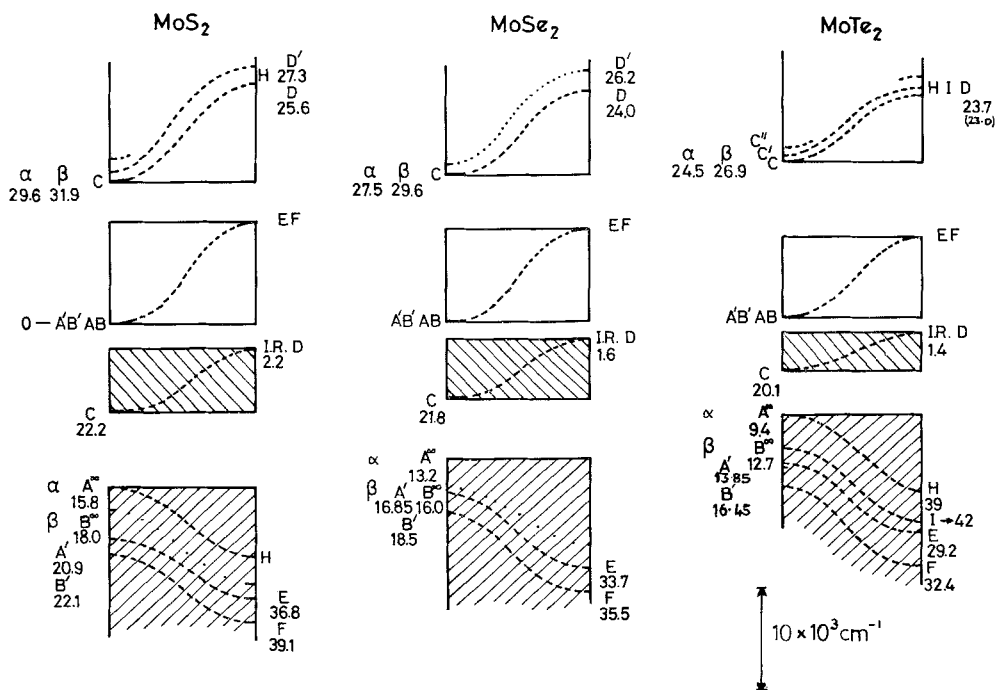
( $\alpha \sim 5000 \text{ cm}^{-1}$ ) to the low energy side of III in p-type  $\text{MoS}_2$  (Evans and Young 1965). Finally, coming to confirm this pattern of bands a weak I.R. edge ( $\alpha \sim 200 \text{ cm}^{-1}$ ) was discovered in  $\text{MoS}_2$  at 0.2 eV. This is the

Fig. 28



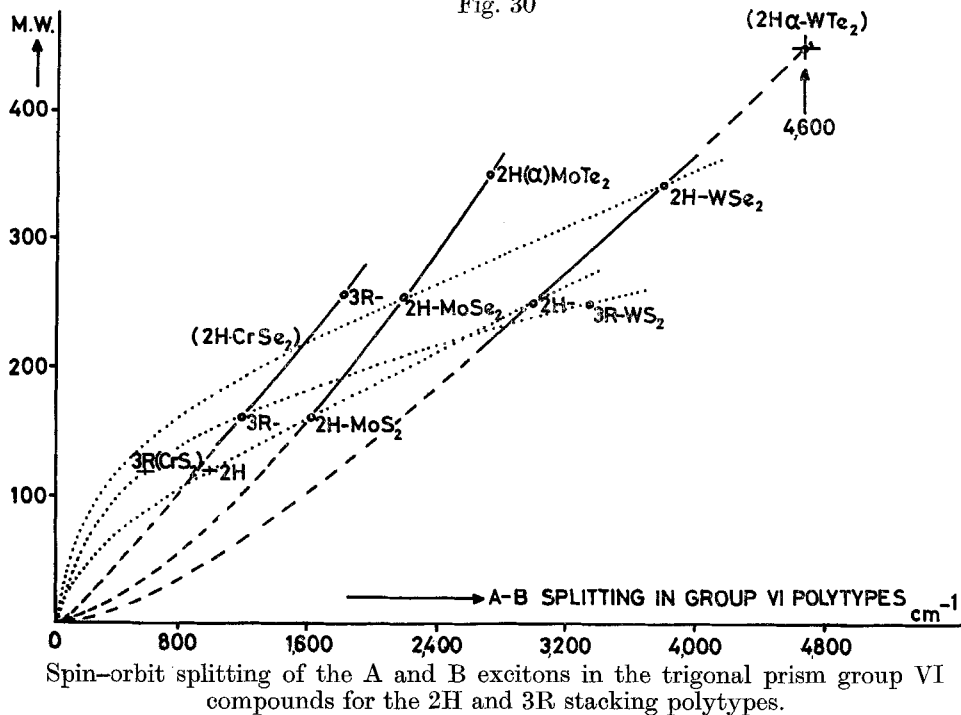
Correlation of the absorption spectra features for the group VI trigonal prism compounds. (Corresponding group V materials also shown in C/D region.)

Fig. 29



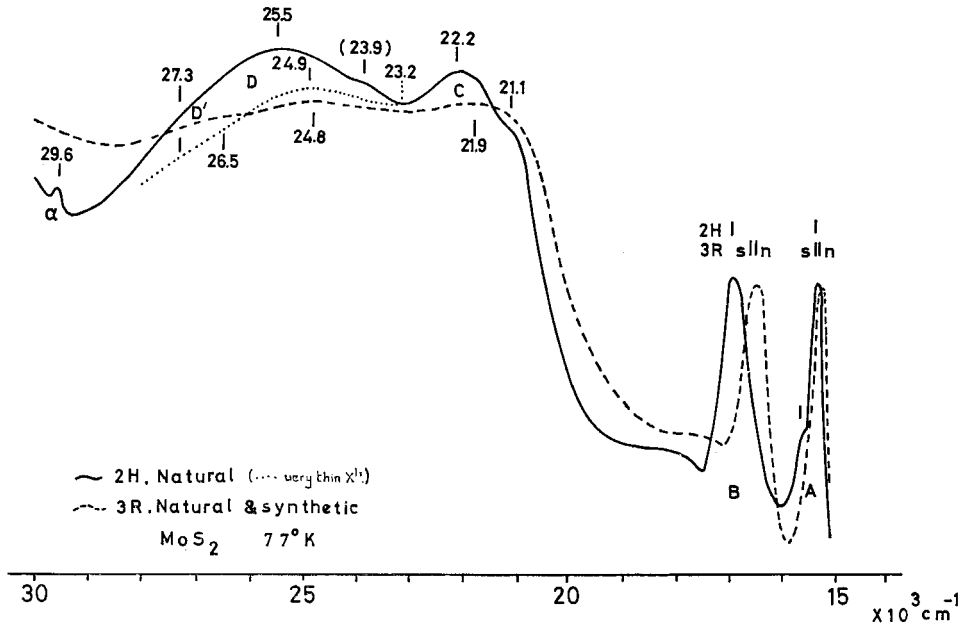
Scale diagram of the band widths of the molybdenum trigonal prism compounds as deduced from experiment. (Tungsten bands almost identical, apart from larger spin-orbit splitting.)

Fig. 30



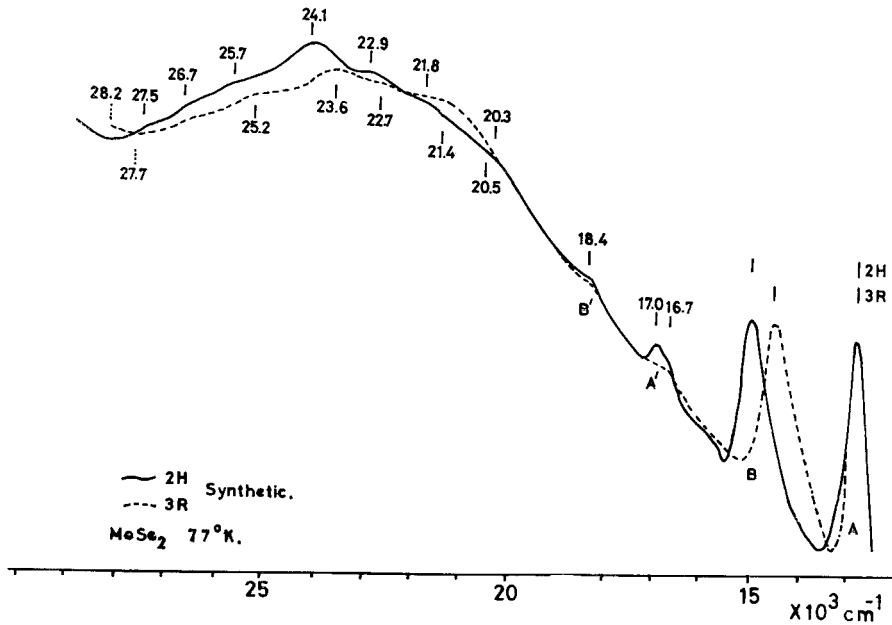
Spin-orbit splitting of the A and B excitons in the trigonal prism group VI compounds for the 2H and 3R stacking polytypes.

Fig. 31



Comparison of optical absorption in 2H and 3R-MoS<sub>2</sub>.

Fig. 32



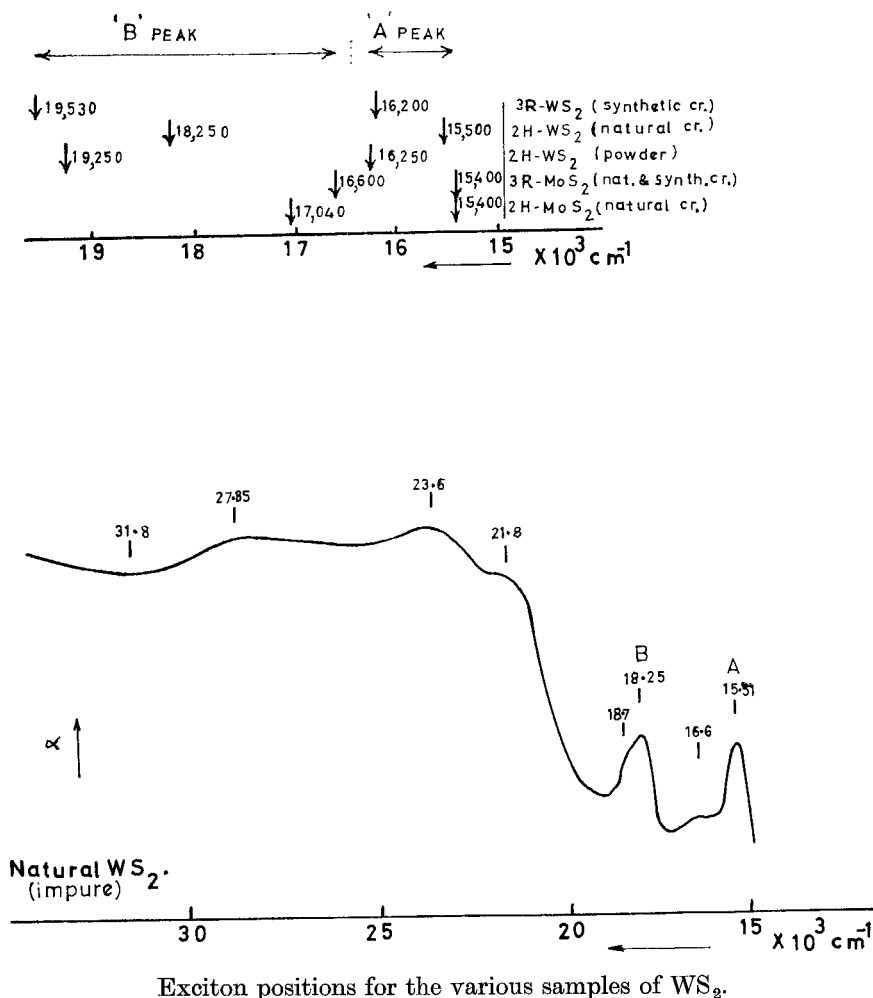
Comparison of optical absorption in 2H and 3R-MoSe<sub>2</sub>.

transition of type I across the d band gap, which it is now realized determines the whole character of the electrical properties of the group VI semiconductors.

The way in which the details of the group VI spectra have been correlated is shown in fig. 28 (note the  $WS_2$  is 3R type). Figure 29 is a scale drawing of the band widths we derive from this assignment. The sequence of operations by which this latter diagram is constructed is given in the experimental paper (Wilson, J. A. 1969).

One of the most noticeable changes in these spectra is the development of the A' and B' exciton peaks in the selenides and tellurides. Exciton  $\alpha$ , conversely, is clearly defined only in 2H-MoS<sub>2</sub>; such high energy excitons are well known in more ionic materials like CdI<sub>2</sub> and PbI<sub>2</sub> (Greenaway and Harbeke 1966, Kübler 1968).

Fig. 33

Exciton positions for the various samples of  $WS_2$ .

6.1.2 The excitons A and B of group VI

The pair of excitons A and B on the leading edge of the strong absorption range are interpreted as resulting from a spin-orbit split valence band. The splitting value of 0.2 eV for MoS<sub>2</sub> (A. W., Mo 96, S 32) is about as expected (compare Cd, same space group, viz. D<sub>6h</sub><sup>4</sup>, A. W. 112, calculated splitting at H<sub>3</sub> of 0.2 eV (Stark and Falicov 1967)). Given also in fig. 30, a plot of spin-orbit splitting versus molecular weight, are the values found for the 3R stacking polytypes. The exact peak positions were recorded in table 7. As seen, there is a remarkable difference in the 2H and 3R splitting values, though the position of the A peak is virtually the same in each case for both polytypes. Figures 31 and 32 show other minor ways in which the spectra from the 2H and 3R polytypes differ for MoS<sub>2</sub> and MoSe<sub>2</sub> respectively. Reflection measurements on WS<sub>2</sub> 2H powder (no 2H transport crystals obtained) seem to indicate that in this case the 2H splitting is less than for the 3R form (transport crystals). In fact a natural crystal of 2H-WS<sub>2</sub> (kindly given to us by Dr. S. Graeser) showed a splitting of only 2750 cm<sup>-1</sup>, as against 3000 cm<sup>-1</sup> for the 2H powder, and 3000 cm<sup>-1</sup> for the 3R transport crystals. However, to confuse matters, the A peak in this natural crystal actually fell at a considerably lower energy (see fig. 33), although said to contain only 6% molybdenum. It is clear that more work on good WS<sub>2</sub> crystals needs to be done.

In the mixed systems (Mo/W)Se<sub>2</sub> and Mo(S/Se)<sub>2</sub> it seems (from preliminary experiments) that the two exciton positions move linearly with composition. It has been found possible by these means to 'tune' the exciton position to match the ruby laser photon output. In this way we hope to study the collective behaviour of the excitons at high densities. A Bose-Einstein condensation and excitonic superfluidity are topics being theoretically explored at the moment (see Gergel *et al.* 1968 *a, b*, Trlifaj 1968, Makarov 1968, Keldysh and Koslov 1968). Mixed crystals have also proved useful in establishing the identity of spectral features between materials (e.g. the A', B' excitons). A further interesting result is obtained

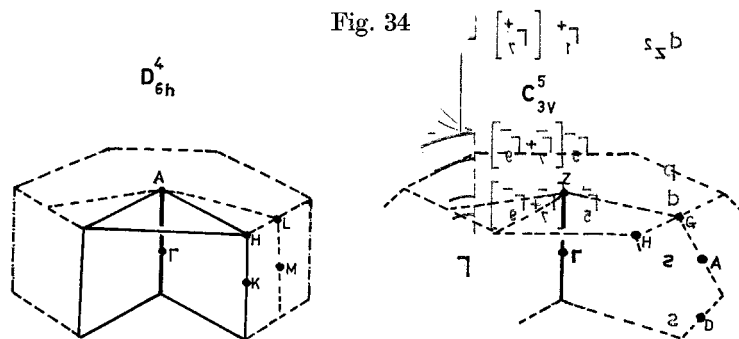
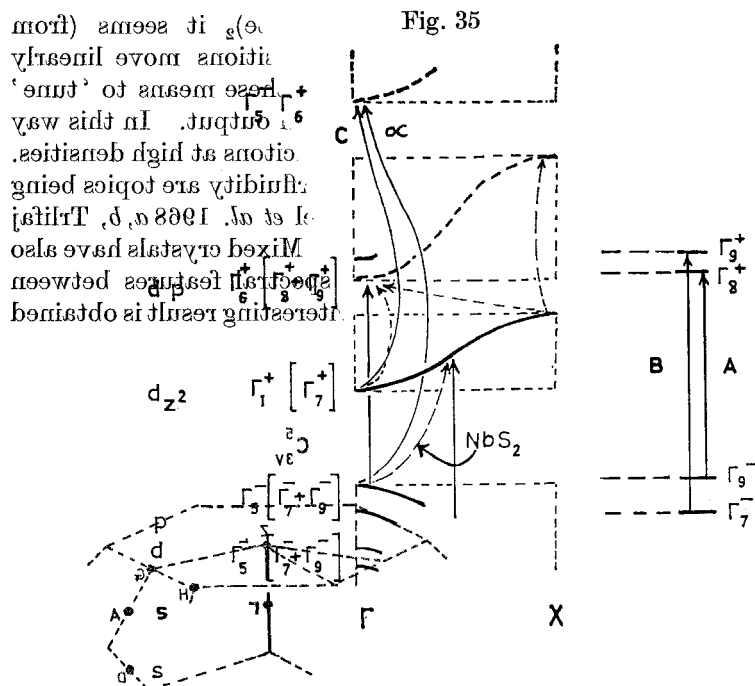


Fig. 34

Indication of permissible positions in the Brillouin zone, for spin-orbit splitting in space groups D<sub>6h</sub><sup>4</sup> and C<sub>3v</sub><sup>5</sup> (marked by continuous lines and bounded planes).

from mixed polytype specimens of a *single* compound. Several crystals of  $\text{MoSe}_2$  seem from the x-ray powder patterns (see p. 219) to have mixed or disordered 2H/3R stacking. The optical spectra of these show an intermediate value for the exciton pair splitting, and, at the temperature ( $77^\circ\text{K}$ ) and resolution used, it did not seem that the B peak was made up of two separate components, as might have been expected.

The position of the A/B exciton pair within the Brillouin zone is fairly well assured. The two polytypes belong to different space groups—2H to  $D_{6h}^2$  ( $P6_3/mmc$ ), 3R to  $C_{3v}^5$  ( $R3m$ )—and fig. 34 shows the theoretical finding that only points on or around the  $k_z$  axis can supply the observed spin-orbit split pair common to both polytypes. Assuming that the various bands, following their tight-binding character, are described by states close to  $\Gamma$  in accord with the molecular orbital scheme of § 5.2, the representation assignment for point group  $D_{6h}$  can be made. Even though the space group  $D_{6h}^4$  is non-symmorphic these point group rules should suffice at the  $\Gamma$  point (see work of Birman 1962, Zak 1962, and Gay *et al.* 1968 on selection rules in such groups). In the less highly symmetric group  $C_{3v}^5$  (symmorphic) the selection rules of  $C_{3v}$  are not so rigid, and in fact appear over-generous.  $D_{3h}$ , the symmetry of the centre point for a



Suggested transitions to explain experimental results. Weak transitions (dashed) fall below 2 ev.

Possible detailed assignment of transitions in  $\text{MoS}_2$ .

single sandwich, seems more appropriate. Some relaxation of  $D_{6h}$  towards  $D_{3h}$  would account for the weak transitions found at  $9000\text{ cm}^{-1}$  in  $\text{MoS}_2$  (possibly  $d_{z^2}$  to  $d_{x^2-y^2}$ ), and also for the weak features that show up between excitons A and B on the leading edge of the B peak (see fig. 22; also Y. Liang 1967,  $\text{MoS}_2$  reflection)†. Figure 35 summarizes this discussion.

At one time it was thought that excitons in layer compounds might be confined to a single sandwich (Shinada and Sugano 1965, Ralph 1965). The resulting two-dimensional exciton series would then go as:

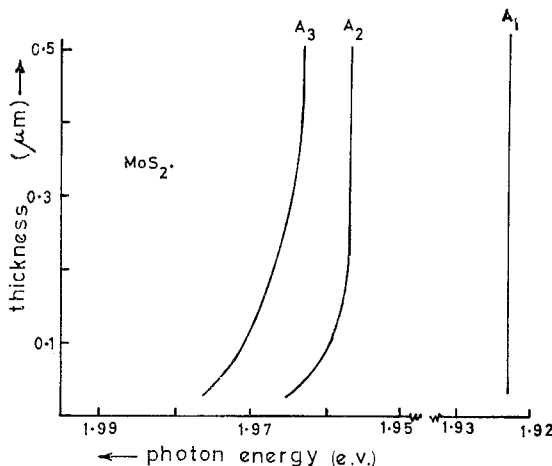
$$-\frac{R}{(n + \frac{1}{2})^2}, \quad n = 0, 1, 2, \dots$$

as against

$$-\frac{R}{n^2}, \quad n = 1, 2, 3, \dots$$

for the standard three-dimensional case. However, for  $\text{MoS}_2$  crystals of thickness greater than  $5000\text{ \AA}$  Evans and Young (1967 a, b, 1968) find that the latter expression fits their optical data very well (at least to  $n=4$ ).

Fig. 36

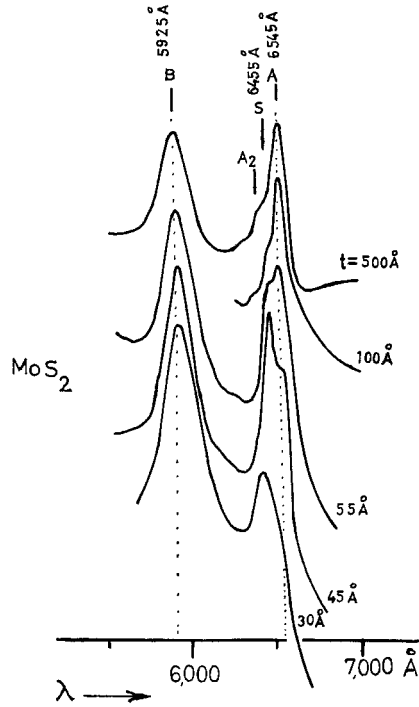


(a)

(a) Behaviour of A exciton peak positions in  $\text{MoS}_2$  as function of crystal thickness. (Evans and Young 1967 a.)

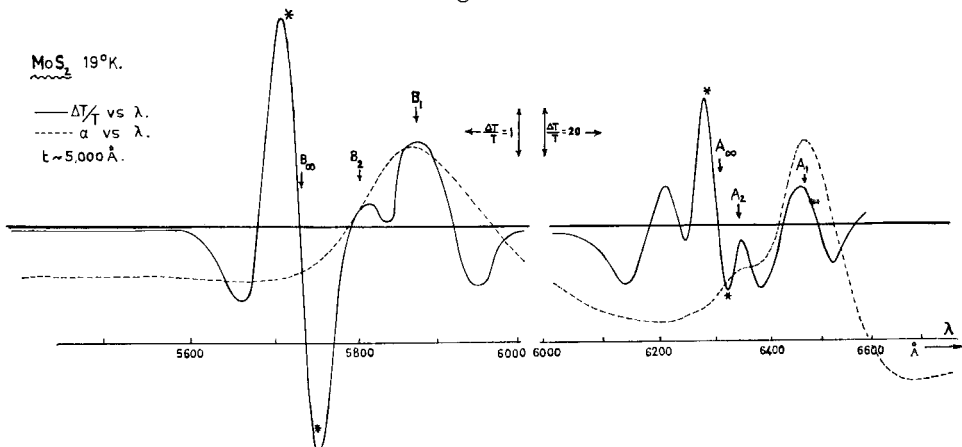
† Reflection measurements which have just been made by Liang on crystals of  $3R\text{-WS}_2$  throw some doubt on the details of the above assignment. The crystals used were of sufficient thickness to allow reflection measurements to be taken from the side faces with the light polarized perpendicular and parallel to the  $c$  axis. In the latter polarization the exciton transitions A and B appear to be completely absent. Previously surface polished specimens had failed to reveal this marked polarization effect because the layers were folded over at the edge during polishing.

Fig. 36 (continued)



(b) Behaviour of the A  $n=1$  exciton peak in ultra thin crystals of  $\text{MoS}_2$ . (Frindt 1965.)

Fig. 37



Electrotransmission spectrum of a crystal of  $\text{MoS}_2$  ( $t \sim 5000 \text{ \AA}$ ). (G. A. N. Connell, paper to be published.)

Harper and Hilder (1968) have now shown theoretically how the  $1/n^2$  relation can hold up to very high degrees of band mass anisotropy. They have also demonstrated how spatial confinement of exciton bound states in crystals of thickness less than  $5000 \text{ \AA}$  should lead to Evans and Young's observation (fig. 36(a)) that the high-order exciton states ( $n > 1$ ) are pushed to energies higher than are given by the  $1/n^2$  expression as the crystal thickness is reduced (i.e. decreased binding). The radii derived by Evans and Young (1967 a) for the A exciton states in thick crystals are:

$$r_{\perp c}^A = 38.5 n^2, \quad r_{\parallel c}^A = 24.5 n^2 \text{ \AA},$$

so that for  $n = 3$ ,

$$r_{\parallel c}^A \sim 200 \text{ \AA}.$$

The  $n = 1$  peak is stable in position for crystals as thin as  $100 \text{ \AA}$  (see fig. 36(b)), though below this the A peak does show a companion to higher energies, (Frindt 1965). Another striking thickness effect, noted in fig. 31, is the marked weakening and red shift of the D transition for  $t < 500 \text{ \AA}$ . This suggests that the D transition occurs away from the  $\Gamma$  point, possibly along the  $k_z$  axis. Again referring back to fig. 31 for  $\text{MoS}_2$ , it is not clear why the transmission well following peak D ( $\sim 3\frac{1}{2} \text{ eV}$ ) shows so much more strongly in 2H- $\text{MoS}_2$  than in 3R- $\text{MoS}_2$ , natural or synthetic, or in 3R- $\text{WS}_2$ . The crystal quality seems no poorer; indeed the excitons in these 3R materials are even sharper than for the 2H form. By contrast to this latter point, however, the  $n = 2$  hump is not seen in direct transmission on the 3R excitons ( $77^\circ\text{K}$ ). Electro-transmission and electro-reflection measurements are currently being carried out in our laboratory to assess the binding energies of all these group VI excitons (G. A. N. Connell, E. A. Davis and J. Bordas). Separate signals of characteristic form are obtained from the exciton states ( $n = 1, n = 2$ ) and from the band edge. The various features in these modulation spectra can be brought out by a suitable choice of field strength. Figure 37 shows a trace obtained for 2H- $\text{MoS}_2$  at  $20^\circ\text{K}$ . The binding energy of the A exciton is found to be  $0.050 \pm 0.004 \text{ eV}$ , or  $400 \pm 30 \text{ cm}^{-1}$ . For 3R- $\text{WS}_2$  this is increased slightly.

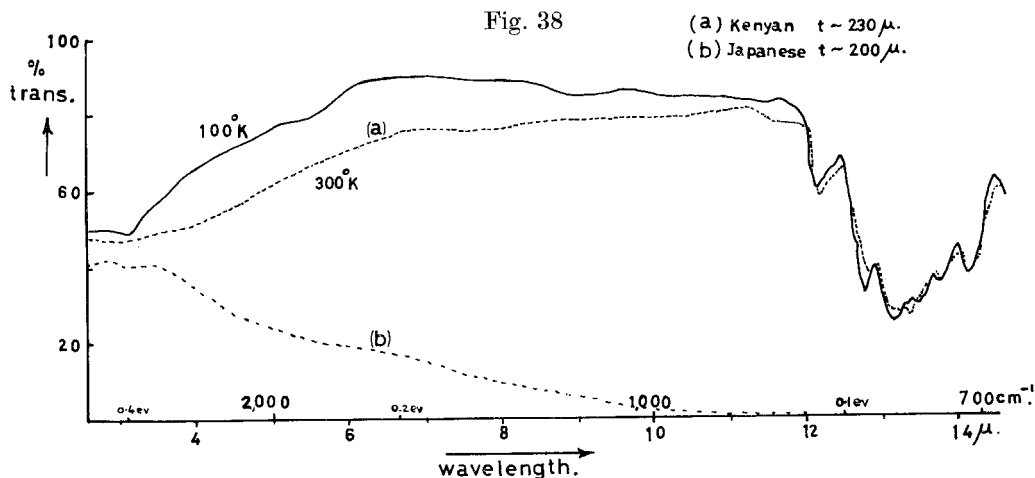
Evans and Young's value for  $\text{MoS}_2$  from direct transmission of  $350 \text{ cm}^{-1}$  compares reasonably with the above modulation value. However, their value for the B exciton of just over  $1000 \text{ cm}^{-1}$  is quite different from the present finding of  $360 \pm 30 \text{ cm}^{-1}$ . Indeed it would seem that the measurements of Evans and Young have been made on the fairly strong 'anti-resonance' feature that follows the B exciton. Features of this latter type have found several explanations (see Phillips 1966, §§ 27 and 28, Shinada and Sugano 1965, Halpern 1966). The fine detail observed on such post-excitonic humps (cf. Liang and Yoffe 1968) has led to the exciton-phonon complex (E.P.C.) interpretation. Coupling occurs between the lattice and the internal field of the exciton (Toyazawa and Hermanson 1968), and is strongest in crystals of medium ionicity where the exciton

binding energy is comparable to longitudinal optic phonon energies (i.e.  $\sim 0.03$  to  $0.05$  eV). Features of this type are particularly apparent in the spectra of fig. 22 following the A peaks in  $\text{WS}_2$ ,  $\text{WSe}_2$  and  $\alpha\text{-MoTe}_2$ . GaSe shows such behaviour following the indirect exciton at 2 eV (Halpern 1966) and GaS shows a very strong hump of this type following the direct exciton at 4 eV (see fig. 20 (o)). This hump in GaS extends over  $2000\text{ cm}^{-1}$ , with its peak at a similar separation from the exciton  $n=1$  peak. Several of the very strong post-excitonic features observed by Tubbs (1968) in layer halides like  $\text{PbI}_2$ ,  $\text{ZnI}_2$ ,  $\text{CaI}_2$ ,  $\text{BiI}_3$  may also be of this E.P.C. origin. The E.P.C. complex gives signals in the electromodulation experiments and one is apparent in the above diagram following the A exciton.

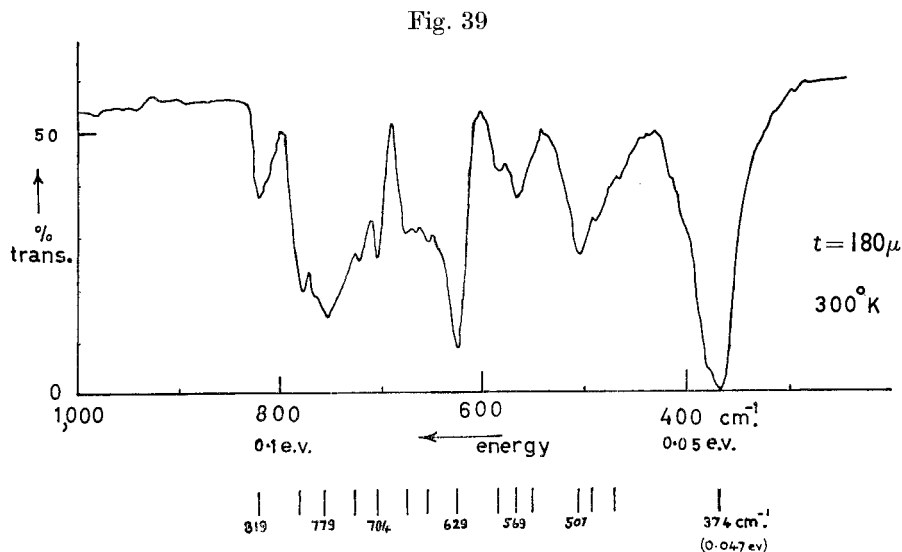
Electro-reflection measurements on the excitons in  $\text{PbI}_2$  at 2.5, 3.3, 3.9 and 4.4 eV have been made by Gahwiller and Harbeke (1968). They failed to obtain clear band edge signals at the field strength employed, although there is a considerable amount of other detail. The exciton on the leading edge in  $\text{PbI}_2$  is very strong and sharp ( $W_{1/2} \sim 150\text{ cm}^{-1}$ ) at  $77^\circ\text{K}$ , but has virtually disappeared at  $300^\circ\text{K}$ . This is similar to the behaviour of the excitons in ZnO, etc. ( $W_{1/2} \sim 100\text{ cm}^{-1}$  at  $77^\circ\text{K}$ ;  $E_b = 0.065$  eV). From direct optical absorption on  $\text{PbI}_2$  (Nikitine *et al.* 1964) it was suggested that the binding energy is *ca.* 0.14 eV, but the poor temperature stability of the  $\text{PbI}_2$  exciton contrasts strongly with that of the  $\text{MoS}_2$  doublet. In  $\text{MoS}_2$  etc., the A peak is still to be seen at  $200^\circ\text{C}$  ( $W_{1/2}$ ,  $400\text{ cm}^{-1}$  at  $77^\circ\text{K}$ ;  $500\text{ cm}^{-1}$ ,  $300^\circ\text{K}$ ). The B peak is, however, more temperature sensitive (particularly in  $\text{WS}_2/\text{Se}_2$  and  $\alpha\text{-MoTe}_2$ ), presumably because of auto-ionization into the degenerate bands. Excitons beyond the absorption edge are not in fact uncommon in more ionic compounds (e.g. the very stable pair in  $\text{CdI}_2$  at 6 eV, Greenaway and Nitsche 1965; also see GaS/Se). The high energy peaks found in  $\text{PbI}_2$  show considerable fine-structure (Greenaway and Harbeke 1966), which has again been attributed to phonon interaction. Fine structure on the exciton peaks can also arise from polytype effects, as Brebner and Mooser (1967) have noted for GaSe. There the indirect exciton at 2 eV suffers splittings of up to 0.004 eV from this cause. This is somewhat smaller than the shift already noted in the position of the A peak for  $\text{MoS}_2$  between the 2H and 3R polytypes ( $\sim 0.010$  eV – see fig. 31.)

In the  $\text{MoS}_2$  family the excitons are not only broadened by phonon collisions at raised temperatures, but also suffer screening of the coulombic binding interaction via the quite appreciable number of free carriers produced by thermal excitation out of the  $d_{z^2}$  band into the d/p conduction band (see § 7.3). Optical experiments at very high pressures ( $\lesssim 60$  kB, Connell, Wilson and Yoffe 1968) suggest that this latter band gap decreases (the peak C reddens), and that the exciton binding energy (i.e. stability) is accordingly reduced through enhanced screening. A factor of this type contributes at all but the very lowest temperatures to the observed *blue* shift of the excitons ( $300^\circ\text{K}$ ,  $2.0 \times 10^{-3}$  eV/kB;  $77^\circ\text{K}$ ,  $1.4 \times 10^{-3}$  eV/kB). The d band gap closure rate is estimated to be  $2.5 \times 10^{-3}$  eV/kB, so that a pressure

of 200 kbar should close completely the d band gap. Indeed Minomura and Drickamer (1963) find a fall of almost three orders of magnitude in  $\rho$  for  $\text{MoS}_2$  between 0 and 200 kbar, with then no further change to 500 kbar. It was not reported whether under these conditions any phase change occurred.  $\text{MoTe}_2$  is known to convert to the  $\beta$  phase (see § 8.1) at high pressures and temperatures. This distorted octahedral layer material is a superconducting semi-metal, ( $\rho_{300^\circ\text{K}} \sim 10^{-3} \Omega\text{-cm}$ ), lacking the d band gap of the  $\alpha$  form. In  $\alpha\text{-MoTe}_2$  this gap under room conditions is  $\sim 0.1$  eV. If this interpretation of the pressure experiments is correct  $\alpha\text{-MoTe}_2$  should be an ideal



Indirect absorption edge in  $\text{MoS}_2$ .



Phonon spectrum of  $\text{MoS}_2$  out to  $40 \mu$ .

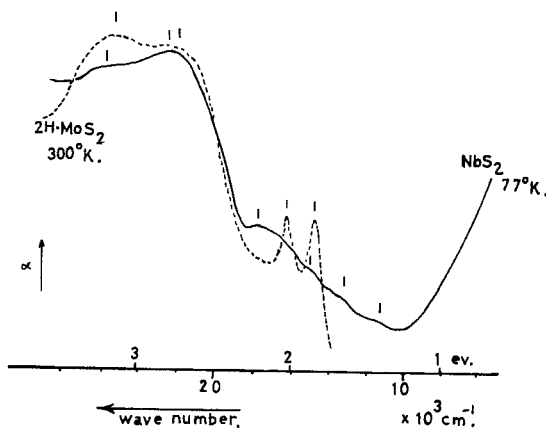
material on which to test the theory of the 'excitonic insulator' (discussed in § 8.2). It is intended to attempt optical experiments under pressure at 4°K on  $\alpha$ -MoTe<sub>2</sub> to see if new phases of the excitonic insulator type are produced when the d band gap is reduced to the order of the excitonic binding energy (i.e.  $\sim 0.03$  eV).

### 6.1.3 Phonon spectra and the indirect edge

Direct infra-red spectroscopic evidence of the above indirect band gap has been secured using large natural MoS<sub>2</sub> crystals  $\sim \frac{1}{4}$  mm thick. Figure 38 shows the weak absorption edge at 0.25 eV. Also evident on this diagram is the start of the phonon spectrum, which is shown in full in fig. 39. The line at 27  $\mu$  still shows up for crystal thicknesses  $\sim 1 \mu$  in classical oscillator form, and is interpreted as the T.O. phonon. The phonon spectra in ZrS<sub>2</sub>, SnS<sub>2</sub> and GaS all appear to have slightly lower energies. As yet similar results on the other members of the MoS<sub>2</sub> family have not been obtained, due to lack of large thick crystals. Measurements on 3R-MoS<sub>2</sub> would be particularly interesting as they would indicate through comparison with the 2H results the degree of inter-sandwich coupling.

Phonon spectra cannot of course be obtained for the group V materials because metallic free-carrier absorption occurs throughout the I.R. In VSe<sub>2</sub> (octahedral) this extends well into the visible, obscuring any direct absorption edge. However, for the trigonal prism materials, like NbSe<sub>2</sub>, the thinned crystals are strongly coloured. Here the free-carrier rise below *ca.* 1 eV is well separated from the direct absorption edge above *ca.* 2 eV. The position of this free-carrier rise so far into the I.R. demonstrates the small width of the band ( $d_{z^2}$ ), in which the metallic carriers lie. This was estimated above from the group VI spectra to be of about 0.5 eV (see fig. 29). Such a value is thought to be very close to the lower limit for

Fig. 40



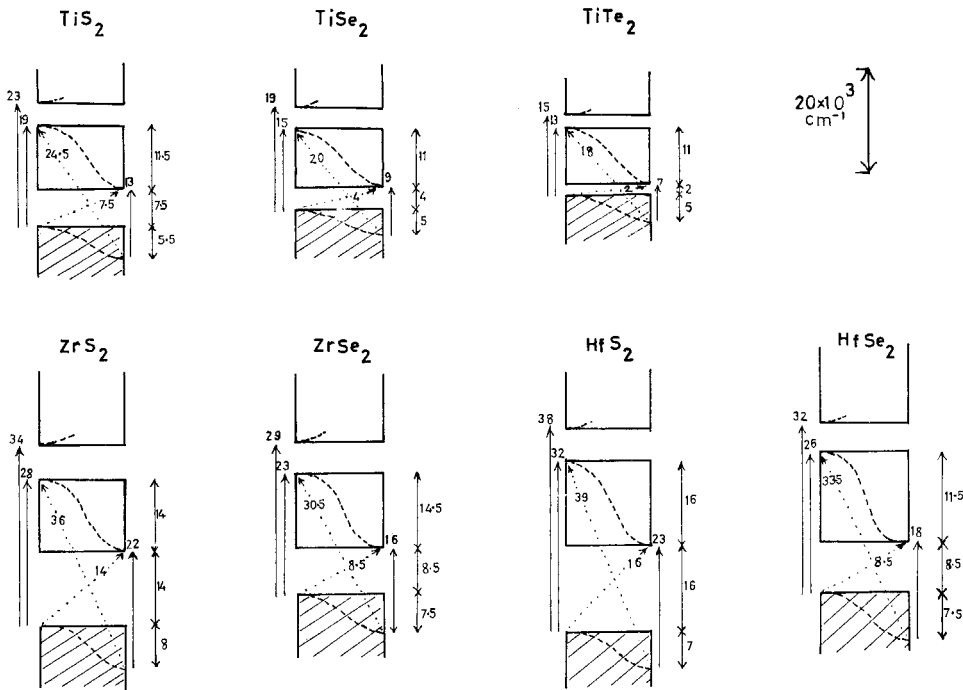
Optical absorption in NbS<sub>2</sub> at 77°K compared with MoS<sub>2</sub> at 300°K.

simple band formation†. Despite the fact that the direct interband transitions are not overlaid by the free carrier absorption, all spectral detail is lost from these group V materials as compared with their group VI counterparts (see fig. 40). The free carriers lead to a general broadening through collision processes, and also to loss of excitonic features through the coulomb screening (see § 7.3).

6.2. The Group IV materials

In contrast to groups VI and V, the 3d dichalcogenides of group IV (Ti) have the same structure type as do its 4d and 5d members (viz. CdI<sub>2</sub>). The transmission spectra show that the 4d (Zr) and 5d (Hf) compounds are energetically very similar (a reflection of the lanthanide contraction), whilst the titanium compound transitions are to considerably lower energies. All are semiconductors but the titanium compounds, and particularly the sulphide, because of the very poor stoichiometry ( $n \approx 10^{20}/\text{cm}^3$ —e.g. Bernard and Jeannin 1962), differ in that free-carrier absorption encroaches

Fig. 41



Scale energy bands in the group IV dichalcogenides, constructed from optical data.

† Contrast even the position for the plasma edge in the metallic oxides CrO<sub>2</sub> and ReO<sub>3</sub>, of 1.4 and 2.0 eV respectively.

almost to 1 eV. Stoichiometry is shown to be better in  $\text{ZrS}_2$  and  $\text{HfSe}_2$ , and in  $\text{HfS}_2$  there is no trace of free-carrier absorption to  $15\ \mu$  (Greenaway and Nitsche 1965). This finding matches the changes in resistivity, etc. for these compounds, as normally prepared (see § 7.1).

It has been found that the group IV materials also possess an indirect edge, but this shows to considerably higher energies than for the group VI case, and with greater oscillator strength. It is the stoichiometry difference which explains why  $\text{MoS}_2$ , etc. are invariably *intrinsic* at room temperature, whilst the group IV materials are always *extrinsic*. The optically determined indirect edge positions are:

$$\text{ZrS}_2\ 1.75, \quad \text{HfS}_2\ 1.95, \quad \text{HfSe}_2\ 1.15\ \text{eV},$$

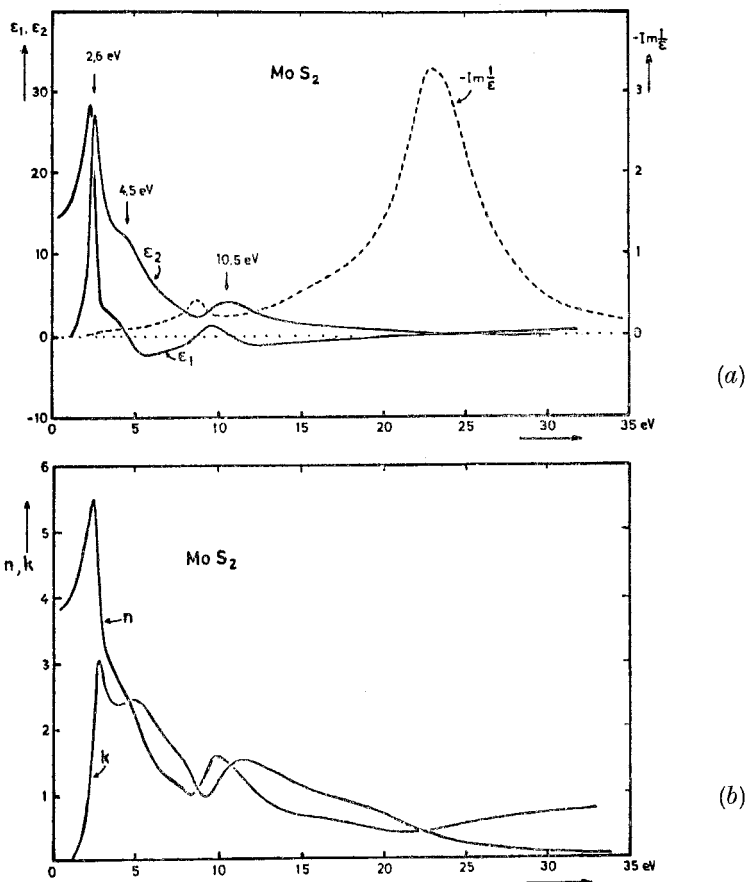
(Greenaway and Nitsche 1965) and these values have been used in constructing the block banding of fig. 41. The construction details are again given in the experimental paper (Wilson 1969 a). As is seen the d band here may be up to 2 eV wide. The width of the top valence band seems to be  $\sim 0.6$  to 1 eV, a value similar to that obtained by calculation for the non-transition metal layer compounds  $\text{GaS}$  (Bassani and Parravicini 1967),  $\text{SnS}_2$  (Au Yang and Cohen 1969) and  $\text{Bi}_2\text{Te}_3$  (Borghese and Donato 1968).

An unusual feature common to all the group IV spectra is the sharp peak topping the leading absorption edge of direct transitions. Though this feature sharpens considerably on cooling, it undergoes no appreciable temperature shift and shows no fine structure. It is not clear then whether it is excitonic in character and measurements at liquid helium temperature together with modulation experiments need to be made. Also sharpening strongly is the peak of maximum absorption, and it may be that this peak, together with the leading feature, form a spin-orbit split pair. If the features are excitons, it is a little strange that in the most stoichiometric compound,  $\text{HfS}_2$ , the peak has not the sharpness shown by  $\text{ZrS}_2$  and  $\text{HfSe}_2$  (see also fig. 23 (a)).

### 6.3. The Group VIII Layer Dichalcogenides

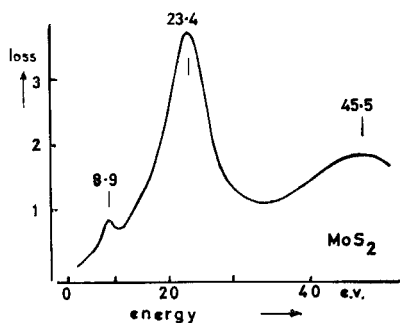
In group VIIIc the d band is completely full and the semiconductivity of  $\text{PtS}_2$  and  $\text{PtSe}_2$  follows. However, because of the relatively low heat of formation ( $< 30$  kcal/mole; Westrum *et al.* 1961), the band gap,  $d \rightarrow \sigma^*$ , accordingly, is small. This is confirmed by electrical measurements ( $E_g^{\text{el}}$ ,  $\text{PtS}_2$  0.7 eV;  $\text{PtSe}_2$  0.1 eV—Hulliger 1965). All the spectra are disappointingly bare. For the tellurides  $\text{NiTe}_2$ ,  $\text{PdTe}_2$  and  $\text{PtTe}_2$  it seems that the  $\sigma^*$  band dips into the d band, as these materials are all metallic, and highly opaque ( $\text{PdTe}_2$  is a superconductor,  $T_s = 1.5^\circ\text{K}$ ). They resemble more the tellurides of group VIIIb,  $\beta\text{-CoTe}_2$ ,  $\beta\text{-RhTe}_2$  and  $\text{IrTe}_2$ , which are expected in any case to be metallic. Again these compounds are extremely opaque. Poor stoichiometry, particularly for  $\text{CoTe}_2$ , seems to contribute to this and the crystals available tended to crack badly during cleaving. For all these group VIII materials  $c/a$  is small, with large  $a$  values and a contracted van der Waals gap (see table 2, and compare  $\text{Bi}_2\text{Te}_3$ ). The cause of this structural deformation is discussed in § 9.2.

Fig. 42



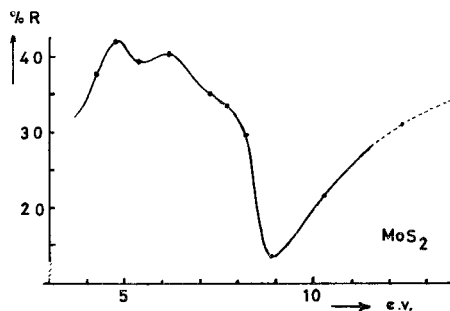
(a) Plots of  $\epsilon_1$ ,  $\epsilon_2$  and  $\text{Im} (1/\epsilon)$  for MoS<sub>2</sub>. (Zeppenfeld, private communication 1969.) (b)  $n$  and  $k$  plots for MoS<sub>2</sub>. (Zeppenfeld, private communication 1969.)

Fig. 43



Measured electron energy loss spectrum for MoS<sub>2</sub>. (Liang and Cundy 1969.)

Fig. 44

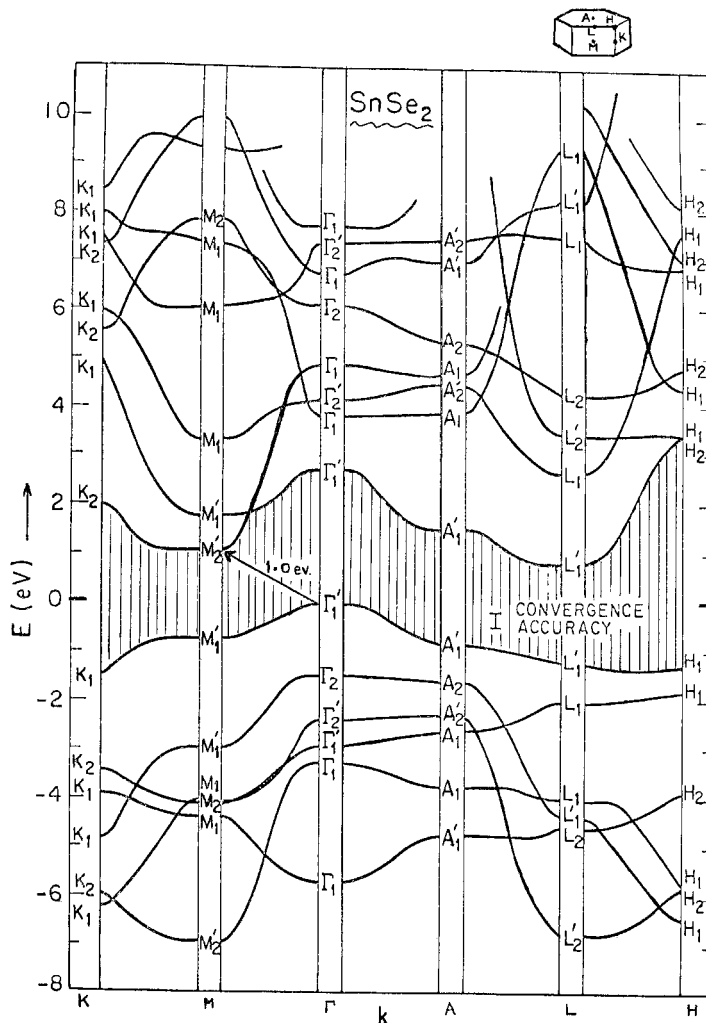


High energy reflection spectrum of MoS<sub>2</sub>. (E. A. Davis, private communication 1968.)

6.4. *U.V. and Electron Energy Loss Spectra*

The above transmission spectra are supplemented by some u.v. reflection work on  $\text{MoS}_2$  (Davis 1968, private communication), and on the group IV materials (Greenaway and Nitsche 1965) out to 12 eV, and also by electron energy loss spectra on the materials of groups IV, V and VI (Liang and Cundy 1969). The latter type of spectra are known to show peaks in regions where both  $\epsilon_1$  and  $\epsilon_2$  move close to zero. This often occurs following one strong absorption band and before the commencement of another.

Fig. 45

Pseudo-potential calculated band structure of  $\text{SnSe}_2$ . (Au Yang and Cohen 1969.)

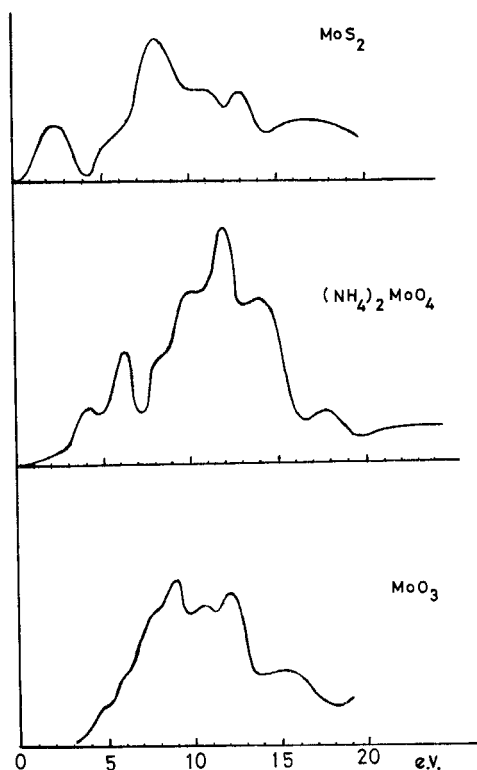
An example of this is shown in fig. 42, where  $\epsilon_1$ ,  $\epsilon_2$ , and the imaginary part of  $1/\epsilon$  (proportional to the 'energy loss') are plotted together for  $\text{MoS}_2$ . These plots follow a Kramers-Kronig analysis. The corresponding  $n$  and  $k$  plots are shown also. The observed electron energy loss spectrum is shown in fig. 43. A direct u.v. reflectivity plot for  $\text{MoS}_2$  is given in fig. 44. The deep absorption well at 9 eV is clearly picked up by the energy loss spectrum. The loss peak at 23.4 eV is that of the plasma resonance response for the 18 valence electrons of  $\text{MoS}_2$ . In  $\text{NbS}_2$  and  $\text{ZrS}_2$  this energy falls to 22.3 eV and to 20.3 eV, as the number of valence electrons falls to 17 and 16 respectively. The 8.9 eV peak for  $\text{MoS}_2$  occurs in  $\text{NbS}_2$  at almost the same energy (8.7 eV), as it should if indeed the band structures are closely similar. In the 5d materials, like  $\text{WSe}_2$  and  $\text{TaSe}_2$ , this peak is not so well defined. Conversely, in group IV the low energy peak which occurs just short of 4 eV is better defined for the hafnium compounds than for the 4d zirconium compounds. Again this is in good agreement with the wells found in both absorption and reflection at this energy. The group IV reflection spectra obtained by Greenaway and Nitsche (1965) were shown in fig. 23.

It is interesting to note that despite the common number of valence electrons the plasma resonance occurs in  $\text{SnS}_2$  at a considerably lower energy than in  $\text{ZrS}_2$ , viz. 18.2 eV as against 20.2 eV. The reflection spectrum for  $\text{SnS}_2$  has been given in fig. 23. The electron energy loss spectrum of  $\text{SnS}_2$  picks out the well at 9.1 eV clearly. These spectra for the group IVA layer dichalcogenides are then quite different from those of the IVB layer compounds, which is not surprising in view of the different character of the states mixed into the valence band.

$\text{SnS}_2$  is the only  $\text{AX}_2$  layer compound for which a complete band structure has been published (Au Yang and Cohen 1969). This is shown in fig. 45. It was obtained by the semi-empirical pseudo-potential method. If the results are to be trusted on this point, it indicates that many of the bands in the  $\Gamma\text{A}$  direction (i.e. for electron waves propagating in the  $c$  direction perpendicular to the sandwiches) are not as flat as might have been expected from the low conductivity in this direction. The same feature is found in the published band structures of  $\text{Bi}_2\text{Te}_3$  (Borghese and Donato 1968, Katsuki 1969).

The similarity between  $\text{MoS}_2$  and  $\text{GaS}$ —which might well be written as  $(\text{Ga}_2)\text{S}_2$  to indicate the common 18 electrons per 'unit' (see § 4)—is again rather superficial, as is revealed by the energy loss measurements. The main plasma resonance occurs in  $\text{GaS}$  at only 17.2 eV, compared with 23.4 eV in  $\text{MoS}_2$ . A small energy loss peak in  $\text{GaS}$  at 7.5 eV marks the sharp dip in reflectivity at this energy; to be seen in fig. 23. The two non-bonding  $d_{z^2}$  electrons of  $\text{MoS}_2$ , which lie within the  $\sigma\sigma^*$  gap, are in  $\text{GaS}$  replaced by the electrons of the metal-metal  $\text{Ga}_2$  bond, and these are mixed into the top of the principal valence band. Various preliminary attempts towards elucidating the band structures of these III-V compounds are now available (see Kamimura and Nakao 1968, Bassani and Parravicini 1967, Andriyashik *et al.* 1968).

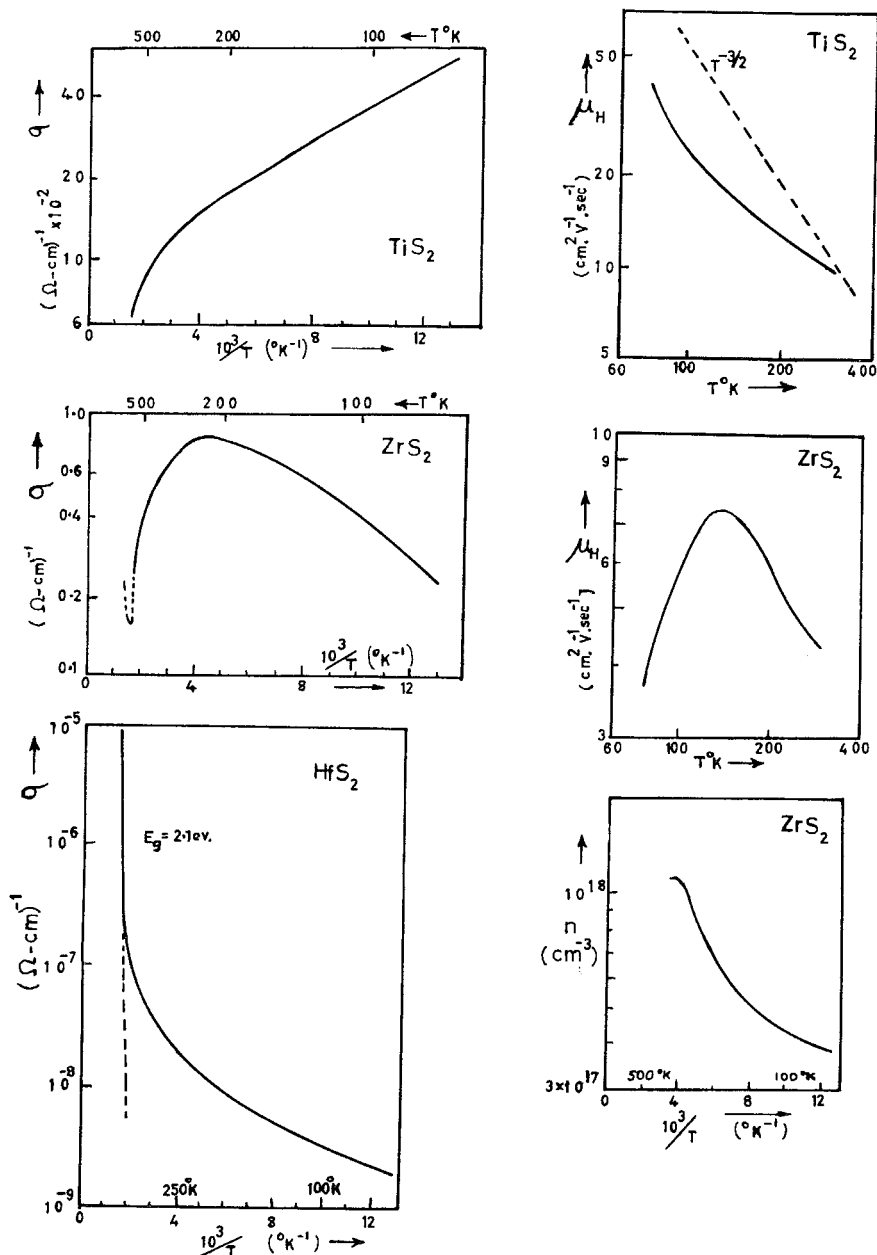
Fig. 46



Soft X-ray absorption spectra (L III) of  $\text{MoS}_2$ ,  $(\text{NH}_4)_2\text{MoO}_4$  and  $\text{MoO}_3$ . (Experimentally, points placed every electron volt with accuracy 0.15 eV—Barinskii and Vainshtein 1957.)

Another high energy technique which can yield useful information on band structures is soft x-ray absorption. The LIII absorption spectra (x-rays generated by 5 kv electrons) involve excitation of the 2p electrons. Accordingly transitions to high energy unoccupied s and d states will show up most strongly. The LIII x-ray spectra of  $\text{MoS}_2$ ,  $\text{MoO}_3$  and  $(\text{NH}_4)_2\text{MoO}_4$  are shown in fig. 46. Transitions into the upper empty non-bonding d band of  $\text{MoS}_2$  appear strongly. Since the points are spaced only every electron volt, and then have an uncertainty of about 0.15 eV, the fine structure must be viewed with some suspicion. However, the leading pair of sharp peaks in  $(\text{NH}_4)_2\text{MoO}_4$  represent typically 'salt-like' d states. The  $\sigma\sigma^*$  gap is known to be about 7 eV (see Muller *et al.* 1967). The edge in  $\text{MoO}_3$  also corresponds with the optical absorption edge of 3 eV (see Dickens and Neild 1968). A very interesting experiment of this type would be with  $\text{NbS}_2$ . Now that experimental techniques have improved somewhat it may

Fig. 47



Electrical data on the group IV  $TX_2$  layer dichalcogenides.  
(From Conroy and Park 1968.)

be possible to pick up a narrow line preceding the first hump of  $\text{MoS}_2$ , corresponding to transitions into the now half empty  $d_{z^2}$  band. A recent example of soft x-ray absorption made on the various oxides of titanium is that by Fischer and Baun (1968).

## § 7. THE ELECTRICAL AND MAGNETIC PROPERTIES OF THE Regular LAYERED $\text{TX}_2$ DICHALCOGENIDES

### 7.1. The Group IV Dichalcogenides

The observed electrical properties of this group of materials are readily understood in terms of the band diagrams of fig. 41, plus a knowledge that they persistently form in non-stoichiometric proportions. This latter tendency is much worse for titanium (cf.  $\text{TiO}_2$ ) than for zirconium or hafnium, (see pp. 213 and 253), and again for the tellurides than for the sulphides. The d band in these compounds must be much better established than in  $\text{TiO}_2$  since the latter, in non-stoichiometric condition, shows the much investigated low-mobility small polaron transport behaviour†. For dichalcogenide specimens on the other hand, the conductivity can quickly rise to  $1 \Omega\text{-cm}^{-1}$  or higher. The electrical character of the dichalcogenides is likely to be determined by the known excess of metal atoms, sited in the van der Waals gap sites, donating electrons through into the otherwise empty d band. n-type behaviour is indeed always observed. Of the whole group only  $\text{HfS}_2$  has been prepared stoichiometrically enough to allow an electrical determination to be made of the intrinsic energy gap. The value obtained by Conroy and Park (1968) (2.1 eV) is close to the value deduced by Greenaway and Nitsche from an analysis of the indirect absorption edge ( $\sigma \rightarrow d$ , see p. 254). For  $\text{TiTe}_2$  this gap has shrunk to close to zero, and indeed  $\text{TiTe}_2$  may just be a semi-metal.

The following data drawn from McTaggart and Wadsley (1958), Grimmeis *et al.* (1961) and Conroy and Park (1968) show some typical results, as also does fig. 47.

	$\text{TiS}_2$	$\text{ZrS}_2$	$\text{HfS}_2$	$\text{TiTe}_2$
$n$	$9 \times 10^{20}$	$10^{18}$	$< 10^{17}$	$\sim 10^{21} \text{ cm}^{-3}$
$\rho$	$5 \times 10^{-3}$	1	$> 10^5$	$2 \times 10^{-5} \Omega\text{-cm}$
$S$	-200	-700	-1000	-20 $\mu\text{V}/^\circ\text{C}$

† The conduction mechanism in  $\text{TiO}_2$  is again being queried—see *Sol. Stat. Comm.*, **7**, 245 (1969). Electrical switching effects similar to those reported in amorphous materials are currently being found in several semiconducting layer crystals, e.g.  $\text{ZrS}_2$ ,  $\text{SnS}_2$ ,  $\text{AsSe}_3$ ,  $\text{Sb}_2\text{Se}_3$ , etc. by a number of investigators.

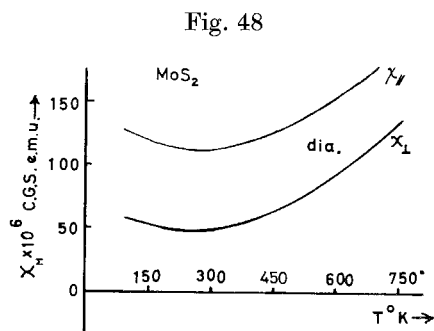
7.2. The Trigonal Prism Group VI Materials

7.2.1. General electrical results

These compounds are diamagnetic and are quite unlike the localized spin paramagnetic layer salts, such as  $\text{FeCl}_2$  or  $\text{VCl}_2$ . All the properties of layer materials are very anisotropic, and for  $\text{MoS}_2$  the molar susceptibility values are :

$$\chi_{\perp} = -50 \times 10^{-6}, \quad \chi_{\parallel} = -115 \times 10^{-6} \text{ c.g.s. e.m.u. at } 300^{\circ}\text{K},$$

see fig. 48. The actual measurements by Paul (née Das, 1968) were of  $\chi_{\perp}$  and  $\chi_{\perp} - \chi_{\parallel}$ .



Magnetic susceptibility of  $\text{MoS}_2$  crystals. (From Das 1968.)

The conductivity values parallel and perpendicular to the layers indicate a ratio possibly even in excess of  $10^3$ . The two values show similar temperature behaviour, the mobilities carrying the  $10^3$  factor and the carrier number changing exponentially with temperature. A majority of group VI samples appear intrinsic in the temperature range  $250^{\circ}\text{K}$  to  $500^{\circ}\text{K}$  with respect to the indirect d-d gap mentioned earlier. In  $\text{MoS}_2$  this band gap is of approximately  $0.25 \text{ eV}$ , and typical self-consistent values at  $300^{\circ}\text{K}$  are :

$$E_g \approx 0.2 \text{ eV}, \quad R_H \approx 100 \text{ cm}^3/\text{coul}, \quad n = 10^{16}\text{--}10^{17}/\text{cm}^3, \quad S \sim 500 \mu\text{V}/^{\circ}\text{K}$$

$$\sigma_{(\perp c)} = 0.1 - 1 \text{ (ohm-cm)}^{-1}, \quad (\mu_H)_e \approx (\mu_H)_h \sim 100 \text{ cm}^2/\text{V-sec. } (\perp c).$$

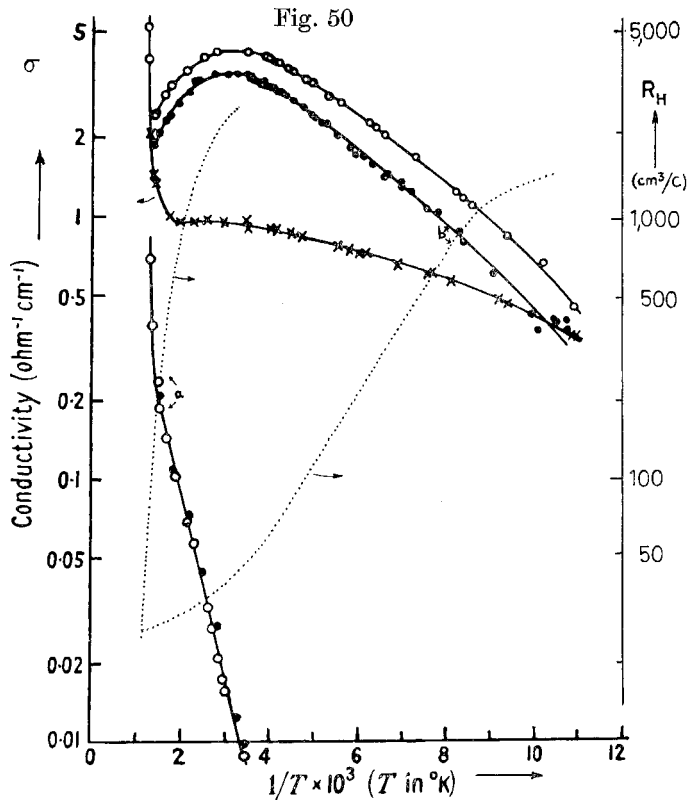
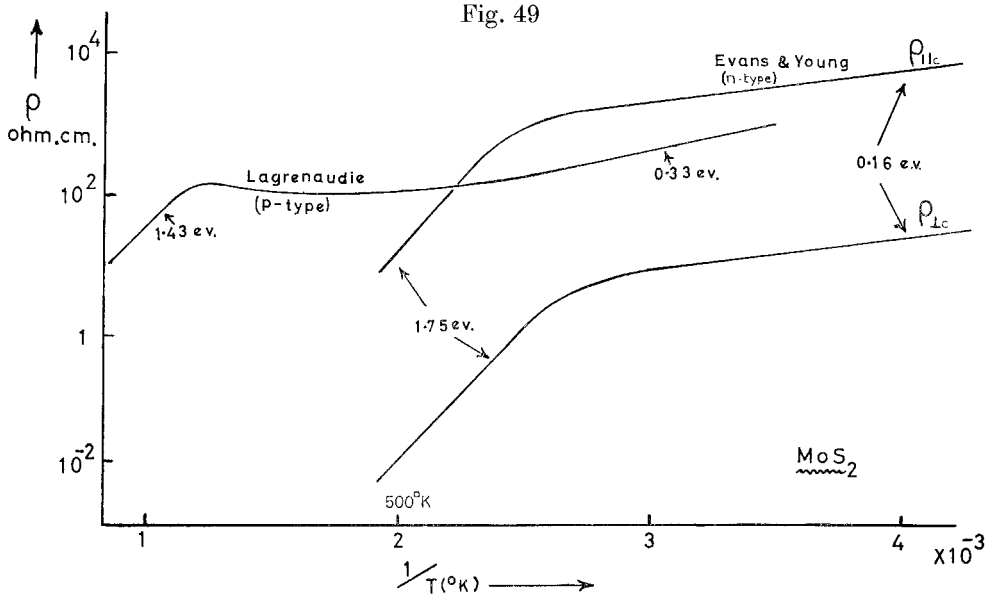
Electrical measurements on single crystals of  $\text{MoS}_2$ , etc. have proved very difficult to obtain satisfactorily, due to the layered character of these materials. The crystal edges are exceedingly soft and any damage on a microscopic level must lead to extensive 'shorting out' of the high crystal-line anisotropy of the sandwiches. Preliminary measurements of a.c. conductivity parallel to  $c$  in which a guard ring technique was used show that the conductivity is proportional to frequency in the range  $10^5$  to  $10^7 \text{ c/s}$ . This is consistent with a hopping mechanism across the layers particularly at low temperatures (Shaw 1969). Several d.c. measurements on the

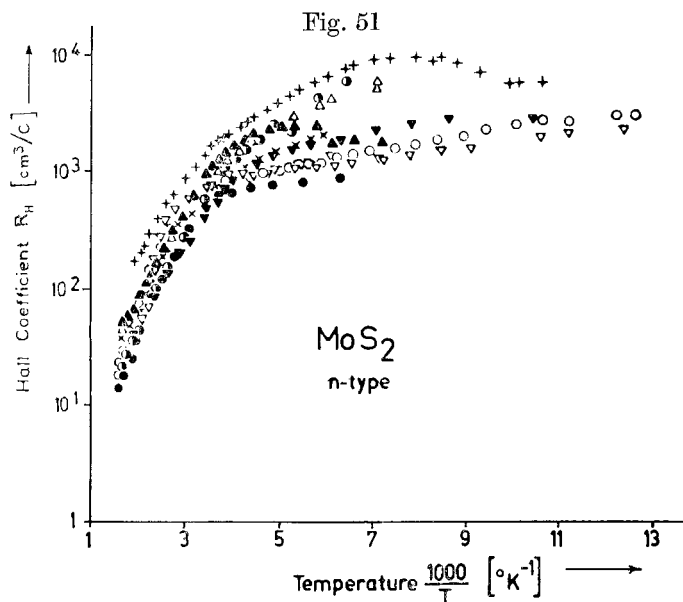
Table 9. Collected electrical data on the

Worker	Date	Substance	Specimen preparation	Carrier type	Resistivities ( $\Omega$ -cm) and activation energies (ev)	Hall coefficient $R_H$ ( $\text{cm}^3/\text{cb}$ )
Lagrenaudie	1954	$\text{MoS}_2$	Natural crystal	p	$E_a < 300^\circ\text{K}$ , 0.03 to 0.06 ev $> 700^\circ\text{K}$ , 0.72 ev	—
Evans and Young	1965	$\text{MoS}_2$	Natural crystal	—	$290^\circ\text{K}$ , $\rho_{  c} = 2 \times 10^3$ $\rho_{\perp c} = 12$ $E_a < 400^\circ\text{K} = 0.87$ ; $> 400^\circ\text{K} = 0.08$ ev	—
Mansfield and Salaam	1953	$\text{MoS}_2$	Natural crystal	Mainly p	$\rho^{300^\circ\text{K}}$ between 3 and 100 $\Omega$ -cm $E_a (< 600^\circ\text{K})$ 0.03 to 0.14 ev $E_a (> 600^\circ\text{K}) \sim 1$ ev	$\sim 50$ at $300^\circ\text{K}$ (two samples with 3000) (see fig. 50)
Regnault	1952	$\text{MoS}_2$	Natural crystal	n+p p	$E_s = 0.14$ , $E_h = 0.14$ ev $E_h^{(1)} = 0.05$ , $E_h^{(2)} = 0.12$ ev	—
Brixner with Teufer	(a) 1962 (b) 1963 (c) 1963	$\text{MoSe}_2$ $\text{WSe}_2$ $\alpha\text{-MoTe}_2$ $\text{WSe}_2$ $\text{WSe}_2$ $\text{MoSe}_2$	Compacts Powder synth. $1100^\circ\text{C}$ , $\text{I}_2/\text{Br}_2$ transport $700^\circ\text{C}$ , sintered $600\text{--}800^\circ\text{C}$ after cold pressing at 7 kb	n p n p p n	$300^\circ\text{K}$ , 3.4 77 $^\circ\text{K}$ , 480 0.5 15 8.5 1350 $300^\circ\text{K}$ , 0.72 77 $^\circ\text{K}$ , 120	— — —
Hicks	1964	$\text{MoSe}_2$ $\text{WSe}_2$ $\alpha\text{-MoTe}_2$	Compacts Reacted at $550^\circ\text{C}$ , sintered at $1000^\circ\text{C}$ , pressed to 92% theoret.	n p n	$100^\circ\text{C}$ $600^\circ\text{C}$ 0.6    0.8 20    1 25    0.1	$300^\circ\text{K}$ -110 +80 -85
Revolinsky and Beerntsen	(a) 1964 (b) 1966	$\text{MoSe}_2$ $\text{WSe}_2$ $\alpha\text{-MoTe}_2$ $\alpha\text{-MoTe}_2$	Compacts Powder synth. $750^\circ\text{C}$ , pressed 5 kb and $300^\circ\text{C}$ to $\sim 85\%$ theoret.  pressed 5 kb and $300^\circ\text{C}$ to $\sim 85\%$ theoret.	p p p p	$\rho \sim 10^3$ at $300^\circ\text{K}$ $\sim 10$ at $550^\circ\text{K}$ $E_a$ $\text{MoSe}_2$ 0.1 ev $\text{WSe}_2$ 0.09 ev well-defined $E_a \sim 0.18$ ev ; $\rho^{300^\circ\text{K}} = 2000$ $\Omega$ -cm	— —
Champion	1965	$\text{MoSe}_2$ $\text{WSe}_2$ $\alpha\text{-MoTe}_2$	$650^\circ\text{C}$ products rather loosely compacted	p p p	$300^\circ\text{K}$ , $\rho$ 10 <sup>6</sup> 400 14000 $\Omega$ -cm	—
Lepetit	1965	$\alpha\text{-MoTe}_2$	Transport crystals $720^\circ\text{C}$ ; $\text{Br}_2$	n  p by Nb doping	$\rho$ peaks at $600^\circ\text{K}$ , $\sim 1$ $\Omega$ -cm $E_a (> 650^\circ\text{K})$ 0.50 ev.  $\left\{ \begin{array}{l} \text{n type } (T < 300^\circ\text{K}) \\ \quad \quad \quad 0.08 \text{ ev} \\ \text{p type } (T < 100^\circ\text{K}) \\ \quad \quad \quad 0.005 \text{ ev} \end{array} \right.$	Gradient break at $600^\circ\text{K}$ . $E_a > 600^\circ\text{K} = 1.23$ ev, others as for $\rho$ . n type $R_H$ ( $300^\circ\text{K}$ ) $\sim 5$ p type $R_H$ ( $300^\circ\text{K}$ ) $\sim 1$
Kershaw <i>et al.</i>	1967	$\text{WSe}_2$	Transport crystal $750^\circ\text{C}$ ; $\text{I}_2$	p	$\rho^{300^\circ\text{K}} \sim 5$ , $\rho^{100^\circ\text{K}} \sim 30$ $\Omega$ -cm	—
Fivaz	1967	$\text{MoS}_2$ $\text{MoSe}_2$ $\text{WSe}_2$	Transport crystals $\text{Br}_2$ growth temperature $\text{MoS}_2$ and $\text{WSe}_2$ $> 900^\circ\text{K}$	All n including $\text{WSe}_2$	$\rho^{300^\circ\text{K}} \sim 10$ $\Omega$ -cm $\sim 1.5$ $\sim 1$	$300^\circ\text{K}$ $> 300^\circ\text{K}$ 1000 $E_a$ 100    0.16 to 100    0.07 ev (see figs. 51 and 53)

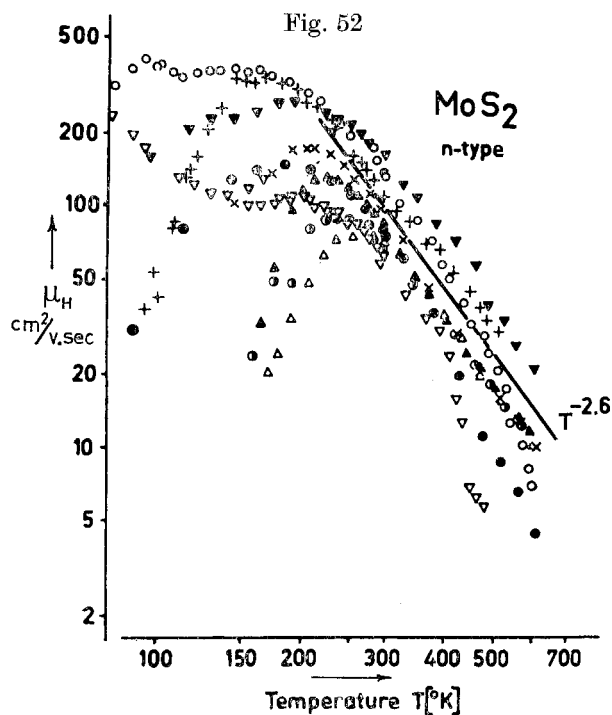
trigonal prism group VI dichalcogenides

Carrier concentration n cm <sup>-3</sup>	Hall mobility $\mu_H$ (cm <sup>2</sup> /v-sec)	Seebeck coefficient $S$ ( $\mu$ V/°C)	Further comments
—	—	—	WS <sub>2</sub> powder also reported to be p type; E <sub>a</sub> 0.04, 0.11, 0.18 ev. Optical absorption above 1.1 ev in both compounds
—	—	—	Resistivity plot (see fig. 49). Evans and Young find weak optical absorption at 1.5 ev
10 <sup>16</sup> at 100°K 2 × 10 <sup>17</sup> at 300°K 5 × 10 <sup>17</sup> at 700°K (two samples with 3 × 10 <sup>15</sup> at 300°K)	$\mu^{300^\circ\text{K}} \sim 150$ varies as $T^{-1.4}$ steepening above 500°K	600, sharp rise below 180°K	Low mobility temperature exponent similar to Lepetit's on p type $\alpha$ -MoTe <sub>2</sub> in this temperature range
'Centre' numbers (i) 10 <sup>19</sup> n, 5 × 10 <sup>14</sup> p. (ii) 1.4 × 10 <sup>16</sup> p <sup>(1)</sup> , 1.7 × 10 <sup>18</sup> p <sup>(2)</sup> .	—	—	—
—	—	300°K -900 +990 -780 +700	Compacts did not achieve densities of much more than 90% theoretical (see Hicks also) Thermal conductivities: $\sim 2 \times 10^{-2}$ w/cm <sup>2</sup> °C
300°K 5.6 × 10 <sup>16</sup> 8.0 × 10 <sup>16</sup> (see fig. 68 (a)) 7.3 × 10 <sup>16</sup>	300°K 15 99 12	100°C 600°C -900 +190 +560 +530 -360 -100	p type WSe <sub>2</sub> may signify that tungsten compounds less likely to be metal-rich than are molybdenum products
—	—	300°K $\sim +400$ +600 +400	Find disorder peak in $\rho$ for mixed system (Mo/W)Se <sub>2</sub> (all p type)
—	—	300°K +450	$\rho$ (300°K) $\sim 10$ composition Mo <sub>1.05</sub> Te <sub>2</sub>
—	—	300°K +300 +600 +400	These resistivities are very high. Prepared in presence of excess chalcogen and at very low temperature
n $\sim 10^{18}$ , falling in n type sample to 10 <sup>14</sup> at 77°K	300°K n type $\sim 50$ below 10 p type $\sim 35$ by 650°K n : $\propto T^{-1.5}$ (80°K) - 330°K $T^{-2.5}$ 330°K - (600°K) p : $\propto T^{-1.4}$ (250°K) - 570°K $T^{-3}$ 570°K - (630°K)	At 300°K $\sim 600$ for both n and p type, falling above 600°K to small positive value at 1000°K	$\rho$ and $R_H$ (see fig. 55) $\mu_H$ (see fig. 56) $S$ (see fig. 57)
—	—	—	—
500°K 300°K 80°K 10 <sup>17</sup> 6 × 10 <sup>15</sup> 10 <sup>15</sup> 10 <sup>17</sup> 5 × 10 <sup>16</sup> 10 <sup>15</sup> 10 <sup>17</sup> 5 × 10 <sup>16</sup> 10 <sup>12</sup>	$\mu$ (300°K) $\sim 100$ $\propto T^{-2.6}$ (or greater) $> 300^\circ\text{K}$ $T^{-2.5} > 250^\circ\text{K}$ $T^{-2.4} > 120^\circ\text{K}$ (see figs. 52 and 54)	—	This sample of WSe <sub>2</sub> appears almost compensated. It is the only case of n type behaviour reported for WSe <sub>2</sub> , and is possibly due to the high growth temperature

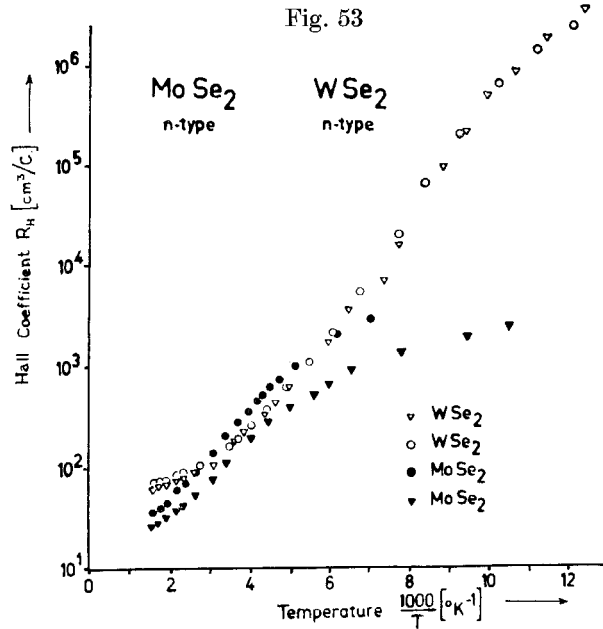




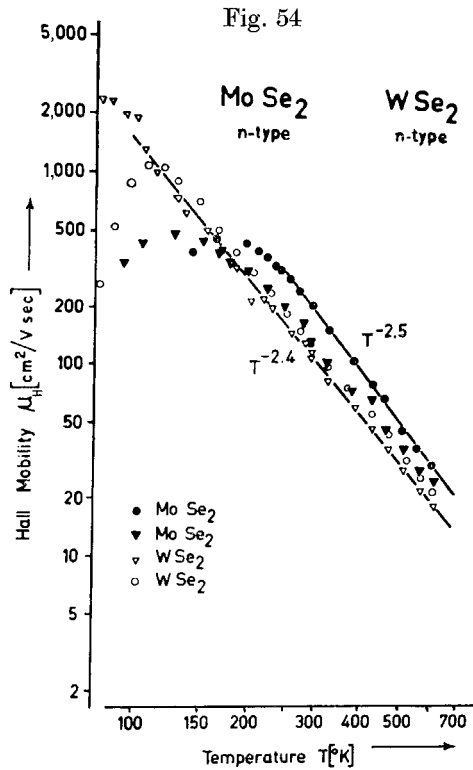
Hall coefficient for MoS<sub>2</sub> transport crystals. (n type ; Fivaz and Mooser 1967.)



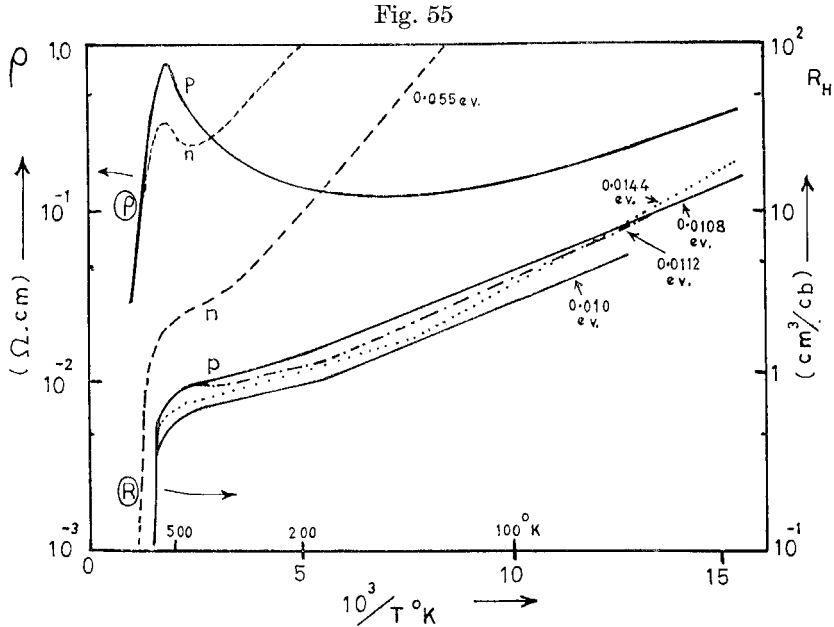
Hall mobility-temperature dependence for MoS<sub>2</sub> crystals.  
(n type ; Fivaz and Mooser 1967.)



Hall coefficient results for n type MoSe<sub>2</sub> and WSe<sub>2</sub> transport crystals. (Fivaz and Mooser 1967.)

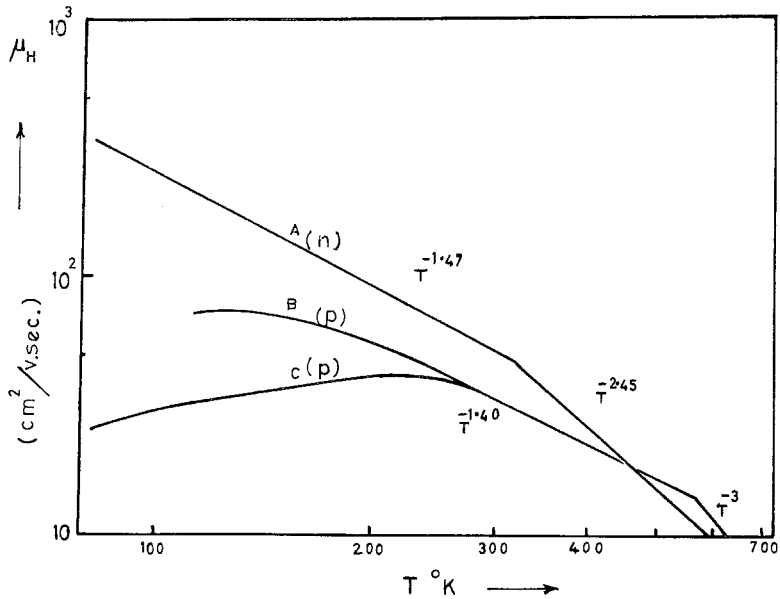


Hall mobility-temperature dependence for MoSe<sub>2</sub> and WSe<sub>2</sub> transport crystals. (Fivaz and Mooser 1967.)



Temperature behaviour of  $\rho$  and  $R_H$  for  $\alpha$ - $\text{MoTe}_2$  transport crystals. (p type crystals obtained by Nb doping; Lepetit 1965.)

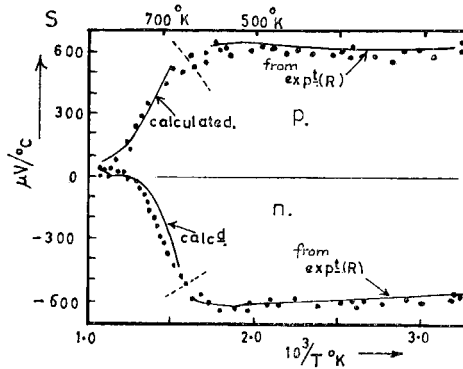
Fig. 56



Hall mobility-temperature dependence for  $\alpha$ - $\text{MoTe}_2$  transport crystals. (Lepetit 1965. Note differences between n and p type specimens.)

selenides and tellurides have been undertaken using sintered compacts, but here again a considerable scatter results. Crystals and compacts of both carrier types have been reported. Table 9 records some of these details.

Fig. 57



Seebeck coefficient-temperature dependence for  $\alpha$ -MoTe<sub>2</sub> transport crystals

Three important points may be abstracted from this collection of data. (a) That a good case can be made for the intrinsic condition detailed above, which would match our small band gap model for the MoS<sub>2</sub> family. Even in crystals close to being compensated (e.g. Fivaz and Mooser's WSe<sub>2</sub> 1967—fig. 53), the resistivity does not reach very high values at room temperature (contrast HfS<sub>2</sub>, SnS<sub>2</sub> and PbI<sub>2</sub>,  $E_g \sim 2.0$  ev). (b) That the hole and electron band masses associated with the  $d_z^2$  and  $d/p$  bands respectively are approximately equal, the room temperature mobility values ( $\mu_{\perp c}$ ) being close to 100 cm<sup>2</sup>/v-sec. Such values are compatible with band widths  $\sim 0.5$  ev (compare SnS<sub>2</sub>,  $\mu_H \approx 300$  cm<sup>2</sup>/v-sec—Busch *et al.* 1961), and are considerably greater than for compounds like VO<sub>2</sub>, NiS or SrTiO<sub>3</sub> ( $\mu \lesssim 10$ ). (c) That the occurrence of mobility temperature exponents greater than 2 is evidence in favour of Fivaz's theory of carrier-phonon interaction in layer compounds. Fivaz (1966, 1967), Fivaz and Mooser (1964, 1967) argue that, because of the sandwich nature of the crystal, homopolar vibration of the sandwiches due to optic phonons traveling in the layers polarized  $\parallel c$  will be strong, and that scattering of the carriers by these phonons leads to an exponent  $n$ , in the relation

$$\mu_{\perp c} \propto \left( \frac{T}{T_0} \right)^{-n},$$

which is dependent on the phonon energy, and always numerically greater than 1.5. (The *acoustic* phonon scattering exponent is deduced to be constant at unity—compare 1.5 in the three-dimensional case.) The predicted homopolar phonon energies for GaSe and MoS<sub>2</sub> (fig. 58) fall at similar positions within the full phonon spectrum of these compounds, but

are difficult to spot exactly as the transition is optically forbidden [GaSe  $345\text{ cm}^{-1}$  (Leung *et al.* 1966); MoS<sub>2</sub>  $490\text{ cm}^{-1}$  (see fig. 39)]. The high temperature exponents obtained on  $\alpha$ -MoTe<sub>2</sub> by Lepetit (1965) would, however, suggest a phonon energy there greater than for MoS<sub>2</sub>. Preliminary infra-red measurements do not support this unlikely eventuality†, and as both Lepetit, and Hicks (1964), point out (see also Champness and Kipling (1965), working on Bi<sub>2</sub>Te<sub>3</sub>, where the exponent can rise to almost 4), these high exponents can arise when  $\mu_e \approx \mu_h$ . This does not seem too unlikely for the MoS<sub>2</sub> family, as the following room temperature results on heavily doped n and p type MoSe<sub>2</sub> suggest:

From Hicks (1964)	$R_H$ (cm <sup>3</sup> /cb)	$n$ (cm <sup>-3</sup> )	$\rho$ ( $\Omega$ -cm)	$\mu$ (cm <sup>2</sup> /v-sec)	Free carriers/substitute atom
Mo <sub>0.99</sub> Ta <sub>0.01</sub> Se <sub>2</sub>	+0.11	$6 \times 10^{19}$	$2.5 \times 10^{-2}$	4	0.4
Mo <sub>0.98</sub> Re <sub>0.02</sub> Se <sub>2</sub>	-0.14	$4.5 \times 10^{19}$	$4.3 \times 10^{-2}$	4	0.15
MoSe <sub>2</sub>	-100	$6 \times 10^{16}$	5	50	—

At temperatures where 'standard' samples of the group VI materials have moved into the intrinsic region (with respect to the d band gap) we will have for the *mixed* carrier situation:

$$\sigma = n_1 e \mu_1 + n_2 e \mu_2 \quad \text{and} \quad R_H = \frac{3\pi}{8e} \left( \frac{n_h \mu_h^2 - n_e \mu_e^2}{(n_h \mu_h + n_e \mu_e)^2} \right)$$

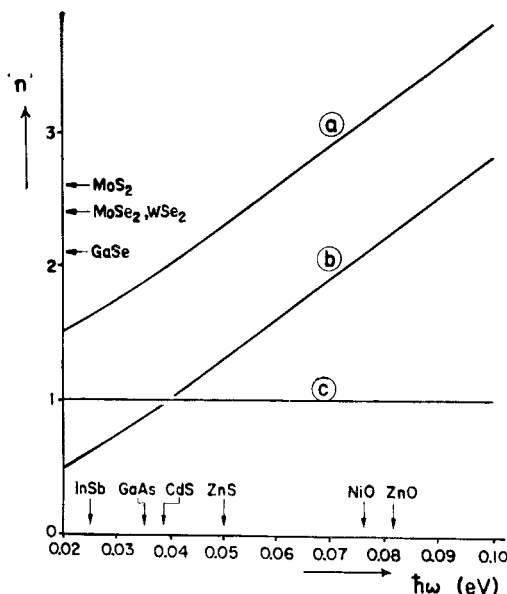
and if  $n_e \Rightarrow n_h$ , then with  $\mu_e \sim \mu_h$ ,  $R_H \rightarrow 0$ . If such a decrease in  $R_H$  when the temperature is raised were to be associated with a *single* free-carrier type via equations  $\sigma = ne\mu$  and  $R_H = 1/ne$ , one would then interpret the carrier mobility as falling rapidly. Fivaz's interpretation of the experimental data may well be faulted over this point. Further details of Lepetit's conclusions concerning the electrical data are given in table 9, and of Hick's work on p. 281.

As mentioned,  $R_H$  for  $\alpha$ -MoTe<sub>2</sub> has been observed to fall very rapidly with increasing temperature above 400°C (Lepetit 1965). This fall is also accompanied by one in resistivity, but the gradient energies do not agree (see fig. 55). The resistivity gradient gives *ca.* 1.0 eV—fairly close to the expected position of the  $\sigma \rightarrow$  d/p absorption edge—whilst the gradient for  $R_H$  gives  $\sim 2.5$  eV. A similar finding was made by Mansfield and Salaam (1953) on p type MoS<sub>2</sub>. Lagrenaudie (1954) and Evans and Young (1965) have also reached a region of rapid fall-off in  $\rho$  for MoS<sub>2</sub> (fig. 49). The

† Abdullaev *et al.* (1967) report also the same mobility temperature coefficient for InS, InSe and GaSe (Moscow Conf., p. 1237 (1968)).

latters' resistivity gradient of 1.75 eV is again close to the extrapolated position of the edge  $A$ , for a working temperature of 200°C. It is not clear by what mechanism excitations of this energy from the  $\sigma$  band should take apparent preference over those from the  $d_z^2$  band in the processes of thermal excitation, though internal radiation and re-absorption may play a part (cf. thermal conductivity in GaSe above 150°C—Guseinov and Rasulov 1966). The materials certainly have very low absorption coefficients at energies up to the direct edge.

Fig. 58

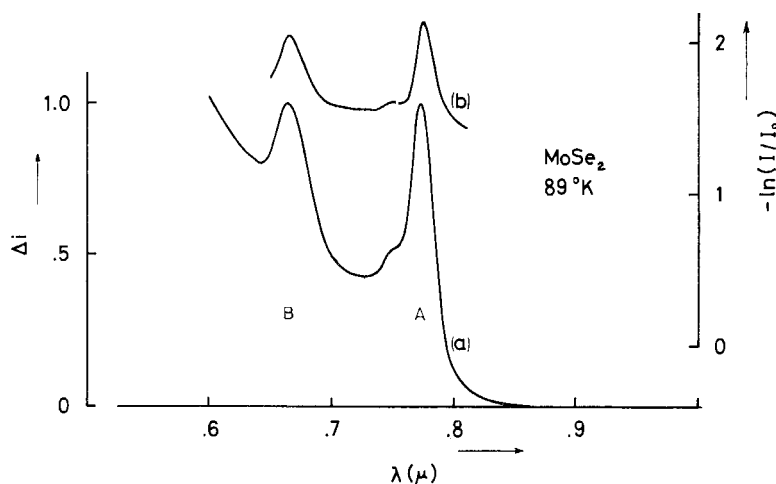


Plots of the mobility temperature exponent to be expected as a function of phonon frequency for various scattering modes according to Fivaz's theory. (Fivaz and Mooser 1967.) The exponent  $n$  in  $\mu = \mu_0(T/T_0)^{-n}$ , where  $T_0 = 300^\circ\text{K}$ , for interaction with (a) homopolar optical modes; (b) polar optical modes; (c) acoustic optical modes.

### 7.2.2. Electromagnetic work on the $A$ and $B$ excitons

A photoconductive response has been obtained from this region of the spectrum (Wieting 1968) which closely matches the optical absorption results (see fig. 59). However, in several specimens the photoconduction peaks are observed in positions slightly shifted towards the blue, and additional small features are observed on the sides of the peaks, some of which were field dependent. The quantum yield was fairly independent of light intensity, but decreased with decreasing temperature. However, sizeable signals were still obtained at 30°K. Conduction band lifetimes were relatively long at  $10^{-2}$  sec.

Fig. 59



Photoconduction in MoSe<sub>2</sub>. (Wieting 1968.) (a) Photoconductive response, (b) optical absorption in same specimen.

Some magneto-optical work on the MoS<sub>2</sub> excitons has been undertaken which leads to interesting exciton and band mass data, complementing that from zero-field measurements. Harper and Hilder (1968) have shown that in anisotropic crystals the exciton Ryberg constant is given by :

$$R_e = f(\gamma) \cdot \frac{\mu}{m_0 \epsilon^2} \cdot R_{Hyd},$$

where

$$\frac{1}{\mu} = \frac{1}{3\mu_{\perp}} \cdot \left( 2 + \frac{\epsilon_{\perp}\mu_{\perp}}{\epsilon_{\parallel}\mu_{\parallel}} \right), \quad \text{with} \quad \frac{1}{\mu_{\perp\parallel}} = \left( \frac{1}{m_e} + \frac{1}{m_h} \right)_{\perp\parallel},$$

$$\epsilon^2 = \epsilon_{\perp}\epsilon_{\parallel},$$

and the scaling parameter

$$\gamma = 3 \left( \frac{1-q}{2+q} \right), \quad \text{with} \quad q = \frac{\epsilon_{\perp}\mu_{\perp}}{\epsilon_{\parallel}\mu_{\parallel}}.$$

The function  $f(\gamma)$  is dependent on the quantum numbers of the bound excitonic state in question.  $\gamma$  ranges from zero to 1.5 (for  $q=0$  in the case of extreme anisotropy) and in MoS<sub>2</sub> is found to be  $\sim 0.8$ . Harper and Hilder show that for such a value of  $\gamma$   $f(\gamma) \approx 1$  for the exciton S states. This allows the simple hydrogenic-like formula to be used to evaluate  $\mu$  (for MoS<sub>2</sub>,  $\epsilon_{\perp} = 6.76$ ,  $\epsilon_{\parallel} = 2.74$ , Evans and Young 1965). It should be noted here that  $\gamma$  is kept below 1, by the partial compensation in  $q$  of the ratios  $\epsilon_{\perp}/\epsilon_{\parallel}$  and  $\mu_{\perp}/\mu_{\parallel}$ . The value of  $\mu$  obtained for the A exciton is  $0.06m_0$ .

Diamagnetic shift measurements on the excitons (Evans and Young 1968) allow a value of  $\mu_{\parallel}^{\Delta}$  to be assessed, giving the exciton mass anisotropy as

$$\mu_{\perp}^{\Delta} = 0.065 m_0, \quad \mu_{\parallel}^{\Delta} = 0.46 m_0 \quad \text{and} \quad \frac{\mu_{\parallel}}{\mu_{\perp}} \approx 7.$$

Magneto-oscillation measurements carried out on the 2 eV exciton in GaSe (see Halpern 1966, Aoyagi *et al* 1966) at helium temperatures yielded there the values :

$$\mu_{\perp} = 0.14 m_0, \quad \mu_{\parallel} = 0.7 m_0 \quad \text{and} \quad \frac{\mu_{\parallel}}{\mu_{\perp}} \approx 5.$$

If the mobility ratio deduced by Fivaz and Mooser (1967)  $\mu_{\perp}$  in n and p type GaSe is valid at 5 to 1, then  $(m_e/m_h)_{\perp} = 1/\sqrt{5}$ , and one obtains there

$$m_e^{\perp} = 0.2 m_0, \quad m_h^{\perp} = 0.44 m_0.$$

This value of  $m_h^{\perp}$  means that the limit deduced by Fivaz (1967) for self-trapping of the exciton is closely approached.

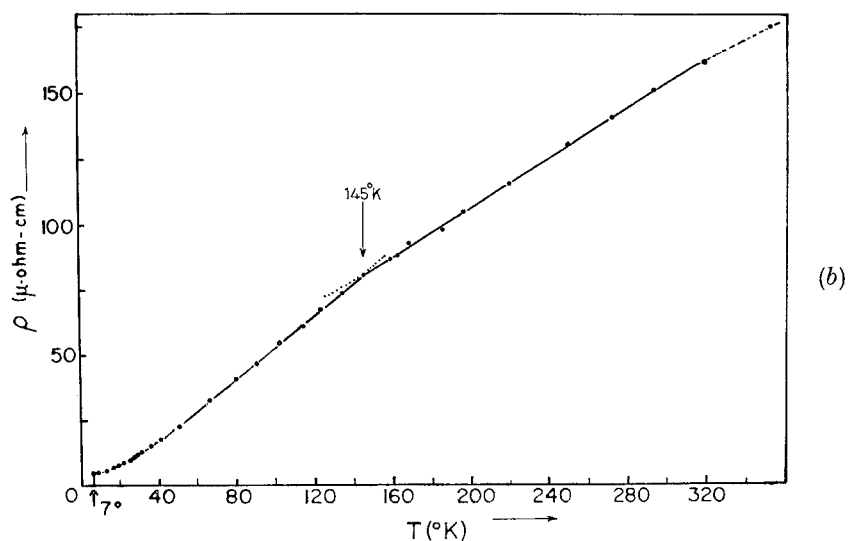
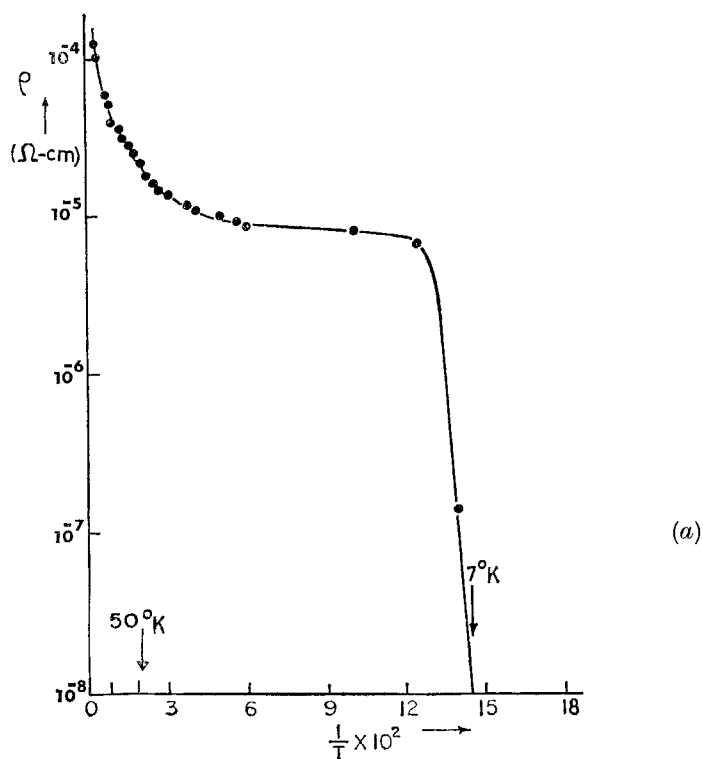
### 7.3. The Regular Group V and Mixed V/VI Materials

#### 7.3.1. Group V materials as antiferromagnetic metals

The layer compounds of group V divide into four classes. The ditellurides have distorted octahedral coordination. These and the unusual octahedral 1T forms of TaS<sub>2</sub> and TaSe<sub>2</sub> are considered separately in § 8. The remaining two classes are undistorted layer structures having octahedral (VSe<sub>2</sub>), or trigonal prism coordination (NbS<sub>2</sub>, NbSe<sub>2</sub>, TaS<sub>2</sub>, TaSe<sub>2</sub>—2H, 3R or 4Ha polytypes—see fig. 3). The band models given above indicate that the materials in each of these latter two classes are d band metals. VSe<sub>2</sub> seems a somewhat better metal than the trigonal prism materials, where the single free-carrier half fills the narrow d<sub>2z</sub> band. The room temperature resistivity of VSe<sub>2</sub> is  $\sim 10^{-4} \Omega\text{-cm}$ , whilst that of NbSe<sub>2</sub>, etc. is  $\sim 4 \times 10^{-4} \Omega\text{-cm}$ . The free-carrier absorption for VSe<sub>2</sub> goes right through into the visible range (cf. the metallic oxide ReO<sub>3</sub>—Feinleib *et al.* (1968)), whilst that for the NbS<sub>2</sub> family dies away in the near I.R. around  $10\,000 \text{ cm}^{-1}$ . In NbS<sub>2</sub>, etc., since the plasma limit occurs at an energy less than that of the direct absorption edge (cf. CoS<sub>2</sub> fig. 84) an exact location of  $\omega_p$  can be made. A calculation of the effective mass from the simple expression†  $\omega_p = (4\pi n e^2/m^*)^{1/2}$  yields  $m^* = 2.6 m_e$ . The high effective mass here is in sympathy with the fact that NbS<sub>2</sub>, etc., are superconductors whilst VSe<sub>2</sub> (and ReO<sub>2</sub>) are not (see p. 309).

† It has recently been confirmed by Hall coefficient measurements that NbSe<sub>2</sub> has indeed one free electron per formula unit (Lee *et al.* 1969). The sign of the Hall coefficient is positive, whilst that of the Seebeck coefficient is negative (see table 18.)

Fig. 60



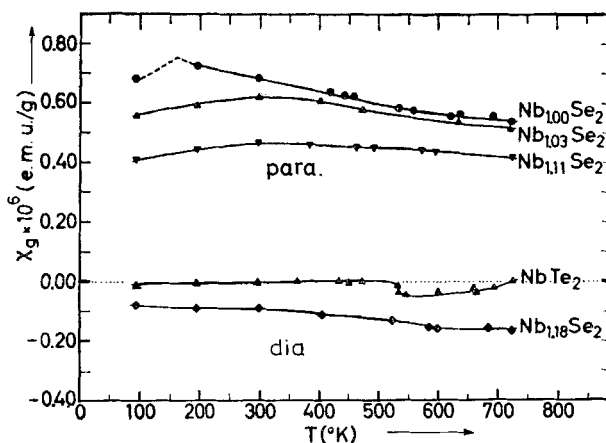
(a)  $\rho$  versus  $1/T$  for  $\text{NbSe}_2$  single crystals. (Kershaw *et al.* 1967.) (b)  $\rho$  versus  $T$  for  $\text{NbSe}_2$  single crystals. (Lee *et al.* 1969.)

Electrical data on single crystals of these materials are very sparse. The resistivity plot of fig. 60 (a) is a single crystal measurement for  $\text{NbSe}_2$ . It indicates clearly the superconducting break. The temperature coefficient of resistance for these metals is  $\sim 4 \times 10^{-3}/^\circ\text{C}$  and in this they are very comparable to, say, silver. Further data, obtained by Brixner on powdered compacts, are given below :

Brixner (1962)	$\rho_{300^\circ\text{K}}$	$\rho_{77^\circ\text{K}}$	$S$	$\kappa_{\text{th}}$
$\text{NbSe}_2$	$3.5 \times 10^{-4}$	$1.8 \times 10^{-4}$	-12	0.021
$\text{TaSe}_2$	$4.0 \times 10^{-4}$	$3.1 \times 10^{-4}$	-13	0.017
	ohm-cm		$\mu\text{V}/^\circ\text{C}$ (compare $\text{VSe}_2$ , +30)	$\text{W}/^\circ\text{C}/\text{cm}$

It is not known what happens at high temperatures, where the considerations of Fivaz's theory of electron-phonon interaction may become important (see p. 268). Examination of the free-carrier rise at raised temperatures is to be attempted.

Fig. 61

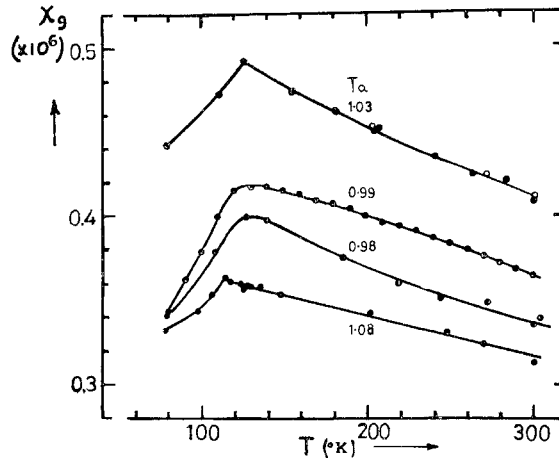


Magnetic susceptibility of  $\text{Nb}_{1+z}\text{Se}_2$  and  $\text{NbTe}_2$ .  
(Selte and Kjekshus 1965.)

The magnetic properties of these compounds are very interesting. From the preliminary susceptibility measurements on  $\text{NbSe}_2$  and  $\text{TaSe}_2$  (figs. 61 to 64) it seems that these compounds show band antiferromagnetism

below 160°K and 130°K respectively (Theory—see Herring 1966, Rice *et al.* 1969). As with chromium ( $T_N = 475^\circ\text{K}$ ) the conductivity is not discontinuous at  $T_N$ , apart from a local anomaly, see fig. 60 (b); (see Arko *et al.* 1968, and Meaden and Sze 1969 for the case of chromium). This contrasts with the behaviour of several other narrow band metallic compounds. NiS for example (two free electrons per formula unit) shows a factor increase of 50 in the resistivity on cooling through the Néel point (268°K), and semi-conducting properties appear. It is clear that in the NbS<sub>2</sub> family band behaviour is better established than it is in say NiS, or VO<sub>2</sub> ( $T_d = 341^\circ\text{K}$ ,  $\rho_{400^\circ\text{K}} \sim 1 \times 10^{-3} \Omega\text{-cm}$ ), where electron–electron and electron–phonon interactions lead to low temperature semiconducting phases. The plasma edge occurs at 8000 cm<sup>-1</sup> in metallic VO<sub>2</sub> (Barker *et al.* 1966) as against 10 000 cm<sup>-1</sup> in NbS<sub>2</sub> and 9000 cm<sup>-1</sup> in NbSe<sub>2</sub>. Many estimates of the effective mass in metallic VO<sub>2</sub> have been made ranging up to 40  $m_e$ , but the typical values quoted seem notably higher than the suggested values for NbSe<sub>2</sub>, etc., viz.  $1 < m^*/m_e < 3^\dagger$ .

Fig. 62

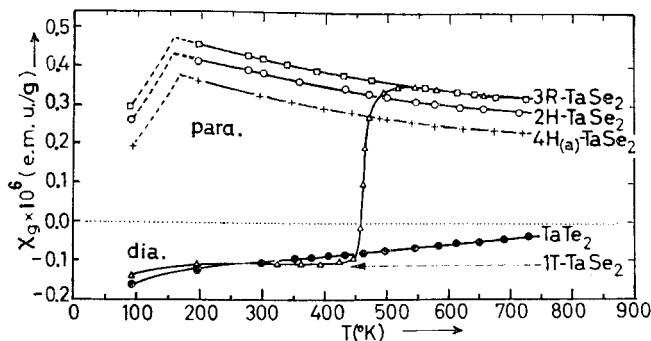


Magnetic susceptibility of trigonal prism Ta<sub>1+x</sub>Se<sub>2</sub>. (Quinn *et al.* 1966.)

Returning to the details of figs. 61 to 64 it is found that application of the Curie–Weiss expression  $\chi = C/T - \theta_p$  to the susceptibility above  $T_N$  gives very odd results.  $\theta_p$  values of *ca.*  $-2100^\circ\text{K}$  and  $-2600^\circ\text{K}$  are found for NbSe<sub>2</sub> and TaSe<sub>2</sub> respectively, with  $n_{\text{eff}}$  values of  $2.4\mu_B$ . The peak susceptibilities are very similar, at  $180 \times 10^{-6}$  e.m.u. units/mole. This

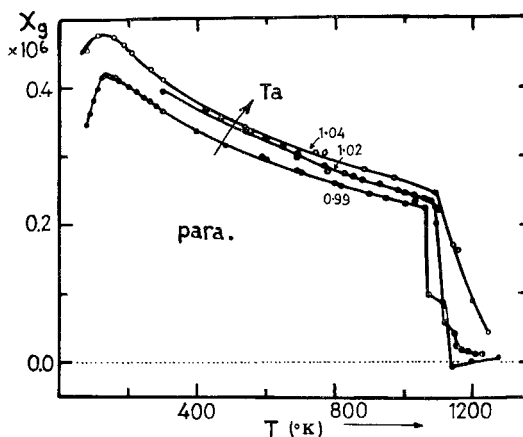
† It has not proved possible to obtain a reliable value of  $m^*$  for NbS<sub>2</sub>, etc. from an analysis of the wavelength dependence of the free-carrier absorption, since the latter rises very quickly to very high values, and not with the classical  $\lambda^2$  form. In the degenerate layer semiconductor Bi<sub>2</sub>Se<sub>3</sub> Gobrecht *et al.* (1966) obtained a dependence as  $\lambda^{3.5}$ , over the range 6 to 12  $\mu$ .

Fig. 63



Magnetic susceptibility of the various polytypes of  $\text{TaSe}_2$ ; also  $\text{TaTe}_2$ . (Bjerkelund and Kjekshus 1967.)

Fig. 64



High temperature susceptibility of several  $\text{TaSe}_2$  specimens. (Quinn *et al.* 1966.)

combination of high  $\theta_p$  and low  $\chi$  is typical of materials far removed from 'ionic' localized d state behaviour. The peak susceptibility value of  $\text{VSe}_2$  ( $T_N \sim 230^\circ\text{K}$ —Røst *et al.* 1964) likewise is only  $340 \times 10^{-6}$  e.m.u. units/mole. These values should be compared with the very much higher susceptibility for the more ionic  $\alpha\text{-TiCl}_3$  ( $T_N = 220^\circ\text{K}$ ) of about  $1000 \times 10^{-6}$ /mole (see § 9.3). Magnetism in all the above compounds is the product of a single electron. The peak susceptibility in Cr metal is down again to  $187 \times 10^{-6}$  e.m.u. units/mole. Values in this latter range are of the order found for straight Pauli paramagnetism in metals, e.g.

Pt  $214 \times 10^{-6}$ , Mg  $134 \times 10^{-6}$ ,  $\text{NiTe}_2$   $88 \times 10^{-6}$  e.m.u./mole.

It is not known what happens to the lattice parameters of the NbSe<sub>2</sub> family below  $T_N$  (there is a 2% volume *increase* in NiS). A neutron diffraction study is awaited. What is known is that the susceptibility depends on the stacking polytypes being used and is also markedly dependent on the stoichiometry of the sample. Metal excess quickly reduces the susceptibility. It is also known to lead to a rapid decrease in the superconducting transition temperature (Van Maaren and Schaeffer 1966, 1967). (This is not so in the superconducting series PdTe<sub>2</sub> ↔ PdTe—Kjekshus and

Table 10. Superconducting transition temperatures of the group V dichalcogenides

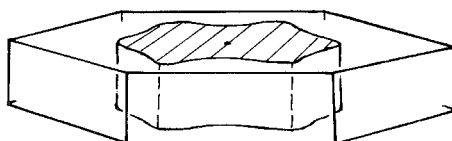
Material	$T_s$ °K	Reference
2H-NbS <sub>2</sub>	6.3	} Van Maaren and Schaeffer (1966)
3R-NbS <sub>2</sub>	5.5	
2H-NbSe <sub>2</sub>	7.0	} Revolinsky <i>et al.</i> (1965)
4H-NbSe <sub>2</sub>	6.3	
NbTe <sub>2</sub>	0.74	} Van Maaren and Schaeffer (1967)
1T-TaS <sub>2</sub>	0.8	
2H-TaSe <sub>2</sub>	0.15	
3R-TaSe <sub>2</sub>	0.22	

$T_s$  not above 0.05°K in V<sub>1+x</sub>Se<sub>2</sub>, V<sub>1+x</sub>Te<sub>2</sub> and TaTe<sub>2</sub>.

Pearson 1965.) What the magnetic properties of these compounds are like close to the superconducting transition should provide an interesting study †. The superconducting temperatures of the group V specimens so far examined are given in table 10. The superconducting temperatures of the tantalum compounds are markedly lower than those of niobium—a not uncommon feature of 5d materials. The properties of the unusual 1T polytypes and of the ditellurides are discussed in § 8.

For the trigonal prism *metals* it is likely that the Fermi surface, if formed from the  $d_{z^2}$  orbital as suggested above, is of the form shown in

Fig. 65



Postulated form of the Fermi surface for 2H-NbS<sub>2</sub>, etc.

† Such behaviour is not entirely unknown, La/Gd alloys showing some coexistence of magnetic and superconducting conditions (cf. Rado and Suhl, Vol. 2B, p. 209).

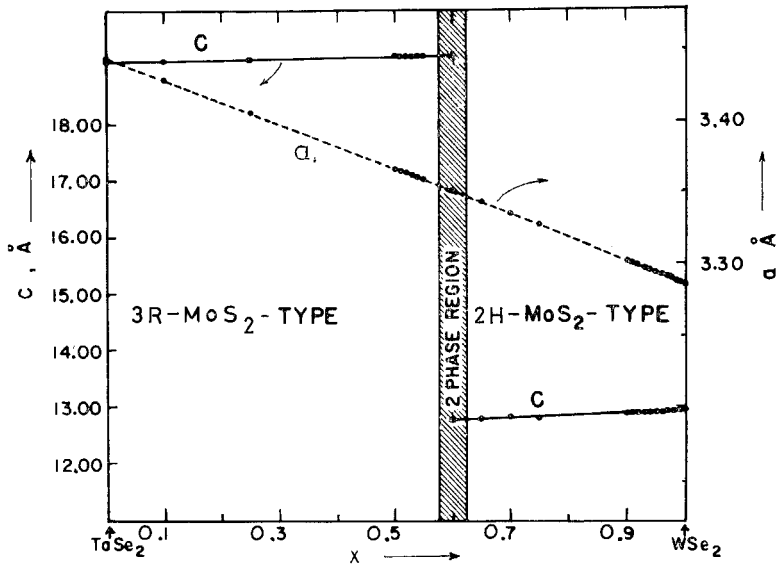
fig. 65. Its 'cylindrical' shape expresses the fact that, as in  $\text{MoS}_2$ , there is likely to be a factor of about  $10^2$ – $10^3$  difference in the carrier mobilities  $\parallel$  and  $\perp$  to  $c$ . It is hoped to confirm this shape by de Haas van Alphen measurements, but the crystals at present available are inadequate in size and perfection to make a proper study. Such measurements have recently been performed on the layer material  $\text{Bi}_2\text{Te}_3$  (Mallinson *et al.* 1969), and on the d band metal  $\text{ReO}_3$  (Marcus 1968).

### 7.3.2. Group V materials as superconductors

An intriguing possibility that this family of compounds offers is of manipulating the superconducting transition temperature over fairly wide limits via substitutional doping, e.g.  $(\text{Nb}/\text{Mo})\text{Se}_2$ . V/VI substitution occurs very readily. Figure 66 shows the steady variation of lattice parameters in the system  $(\text{Ta}/\text{W})\text{Se}_2$ . We see that in the high tantalum range the structure obtained is of the  $3\text{R-MoS}_2$  polytype common to both group V and group VI (see fig. 3). Figure 67 and table II show how  $\sigma$  and  $S$  vary in this system. The carrier type is seen to change from n to p just above the half-filled band concentration (*viz.* 55 at. % W). This suggests a tight-binding sinusoidal form to the  $E$  versus  $k$  bands. B.C.S. theory of superconductivity gives for the transition temperature  $T_S$ , in the phonon mechanism:

$$T_S = 1.14 \Theta_D \cdot \exp [(-1/N(O)V)],$$

Fig. 66



Lattice parameters as a function of composition for the system  $\text{W}_x\text{Ta}_{1-x}\text{Se}_2$ . (Brixner 1963.)

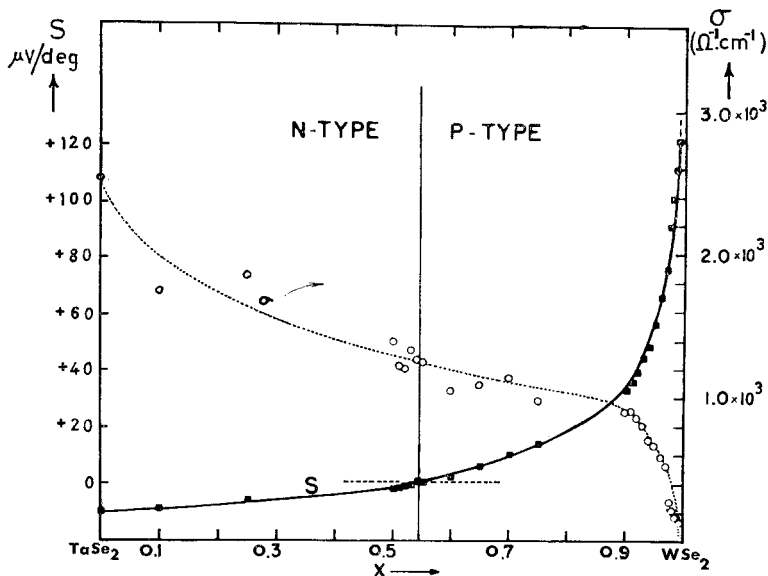
Table 11. Electrical data on (W/Ta)Se<sub>2</sub> for plot of fig. 67. (Brixner 1963)

$x$	$m \cdot \rho$ ohm-cm 25°C	$m \cdot \rho$ ohm-cm -196°C	$S$ $\mu\text{V}/^\circ\text{C}$ 25°C
0 (TaSe <sub>2</sub> )	0.40	0.31	-10
0.10	0.60	0.45	-9
0.25	0.55	0.42	-6
0.50	0.72	0.59	-2 n
0.51	0.82	0.53	-1.5
0.52	0.83	0.51	-1.0
0.53	0.75	0.54	-0.6
0.54	0.79	0.57	-0.2
0.55	0.80	0.58	+0.5
0.60	0.95	0.80	+2.0
0.65	0.92	0.83	+6
0.70	0.88	0.80	+10
0.75	1.01	0.93	+14
0.90	1.10	0.95	+33
0.91	1.10	0.96	+36
0.92	1.15	0.97	+39
0.93	1.23	0.96	+44 p
0.94	1.40	1.09	+48
0.95	1.49	1.18	+56
0.96	1.70	1.58	+65
0.97	1.90	1.83	+75
0.975	3.50	2.90	+90
0.98	4.51	4.00	+100
0.985	5.71	6.02	+110
0.99	6.92	7.21	+120
1 (WSe <sub>2</sub> )	719	$1.2 \times 10^5$	+700

where  $N(O)$  is the density of states at the Fermi energy ( $0^\circ\text{K}$ ), and  $V$  is the effective attractive electron-electron interaction. For MoS<sub>2</sub>  $\Theta_D$  is  $210^\circ\text{K}$  (Salaam 1960), and this is likely to be fairly constant throughout a system like (Nb/Mo)S<sub>2</sub> (N.B. for Nb metal,  $T_S = 9.2^\circ\text{K}$ ,  $\Theta_D = 250^\circ\text{K}$ ). Recently there has been considerable investigation into the superconductivity ( $T_S \lesssim \frac{1}{4}^\circ\text{K}$ ) found in the semiconductors SrTiO<sub>2</sub> (Koonce *et al.* 1967), GeTe and SnTe (Allen and Cohen 1969), when prepared in the degenerate condition. Cohen and Koonce (1966) and Koonce and Cohen (1969) have given expressions for the attractive potential  $V$  in terms of the intra-valley and inter-valley phonon couplings.  $T_S$  is large when these phonon couplings are large, as may well be the case in a layer compound (see Fivaz and Mooser 1967, and p. 268). Also the density of states  $N(O) \sim m^* \cdot n^{1/3}$  will be large in NbS<sub>2</sub>. Actually too many carriers can screen out the superconductive attractive potential, and in SrTiO<sub>3</sub>  $T_S$  passes through a maximum at  $n_c = 8 \times 10^{19}/\text{cm}^3$ . Hence our interest in the mixed systems like (Nb/Mo)S<sub>2</sub>, and possibly (Mo/Tc)S<sub>2</sub>, though this system is not fully

miscible. Further, in the latter system the carriers are in the d/p rather than in the  $d_z^2$  band.

Fig. 67



Variation of  $\sigma$  and  $S$  through the system  $W_xTa_{1-x}Se_2$ . (Brixner 1963.)

Any superconductivity arising in compositions not too far removed from  $MoS_2$  could be of great interest in efforts to obtain very high transition temperatures. The very stable excitons formed in connection with the d/p band (see p. 245) could lead to the occurrence of the recently proposed excitonic mechanism for superconductivity (see Ginzburg 1968). The mechanism is one of direct interaction in the Bose-Einstein gas of excitons, rather than of electron-electron interaction through phonon mediation. Since the  $\Theta$  value in the B.C.S. equation is now an electronic rather than a lattice temperature,  $T_S$  stands the possibility of being raised at least above the liquid hydrogen barrier ( $20.4^\circ K$ ). The quasi two-dimensional character of these layer materials is also thought likely to contribute to this end.

It is not expected that any optical effects will be noted in the visible range when these materials are in their superconducting state (Tinkham 1966), but the crystals are well suited to far infra-red work. There the superconducting energy gap for  $NbS_2$  should lie at about  $20\text{ cm}^{-1}$  (i.e.  $\sim 4kT_S$ ). Alternatively the gap could be studied quite easily using the tunnelling technique. In such experiments the effects of crystal thickness on  $T_S$  could be readily ascertained. It has been found for many systems that  $T_S$  increases markedly as the specimen thickness is reduced. As with lamellar intercalated graphites (Salzano and Strongin 1967) it is presumed

that the crystals become superconducting both  $\parallel$  and  $\perp$  to  $c$  at the same  $T_S$ . Anisotropy is, however, reported in critical current measurements (Spiering *et al.* 1966). It has already been noted that  $T_S$  changes with the different stacking polytypes; in these cases the phonon spectrum may be more significantly altered than is the electronic band structure. It is also likely that the phonon spectrum is strongly modified in very thin specimens.

Moreover, Kogan and Tavger (1966) predict that for thicknesses  $\lesssim 100 \text{ \AA}$ , when the electron states lie virtually in two-dimensional sheets in the Brillouin zone, superconductivity could arise even in *non*-degenerate semiconductors ( $n \sim 10^{17}/\text{cm}^3$ ). Such a material could be obtained by very light doping of  $\text{MoS}_2$  with niobium. Moreover, crystal thicknesses of this order are accessible using layer crystals.

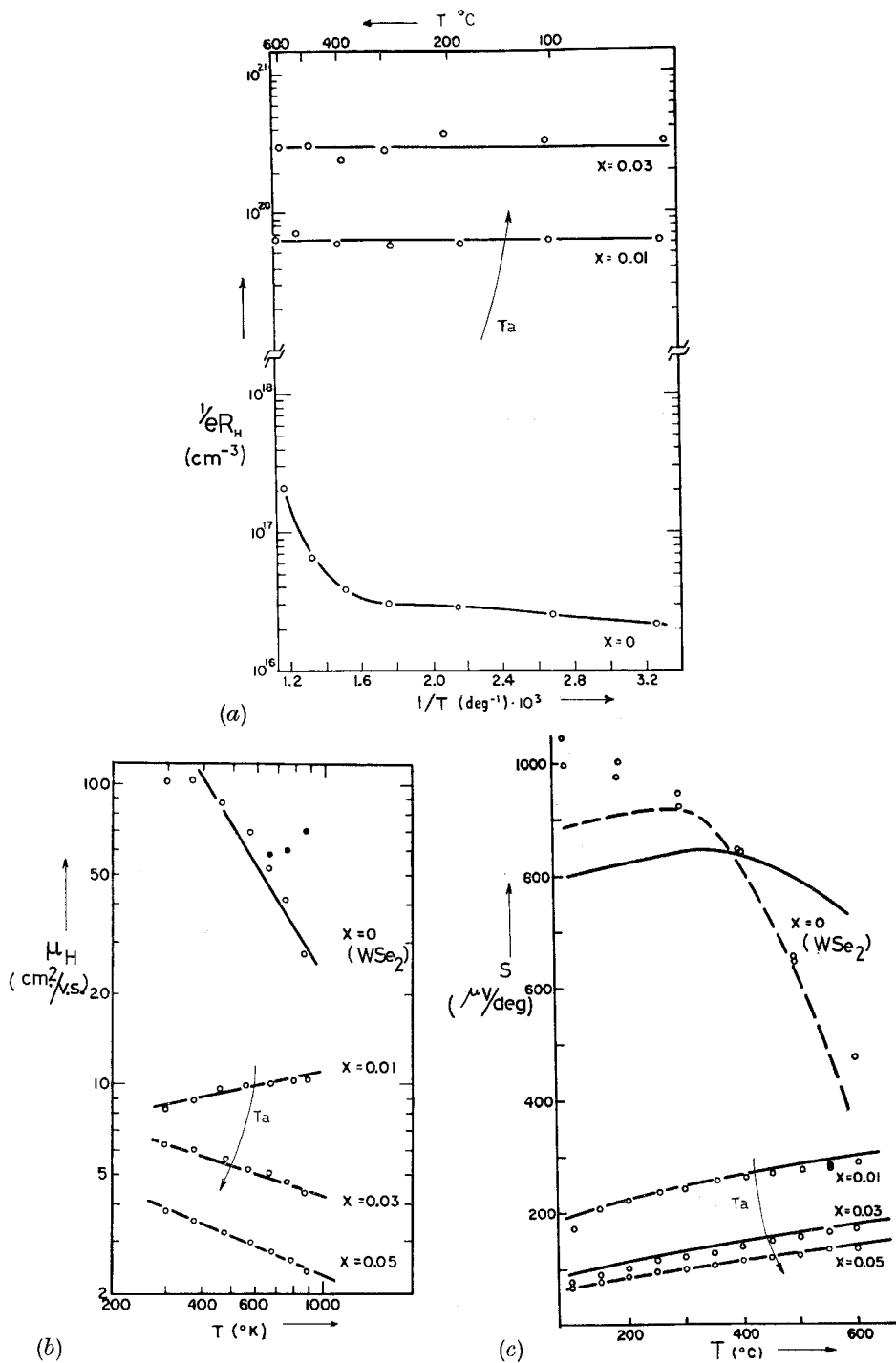
### 7.3.3. Doped materials, intercalates and exciton screening

The main fall in resistivity in a V/VI system like, say,  $(\text{W}/\text{Ta})\text{Se}_2$ , comes of course close to the group VI end, when the small gap semiconductor (here  $\text{WSe}_2$ ) gives way first to highly degenerate semiconducting behaviour ( $\lesssim 1\%$  Ta), and then to complete metallicity. These changes are given in table 12 and figs. 68 and 69. The effective free-carrier yield (holes) per added Ta atom is only one-fifth at doping level  $x = 0.005$  (i.e.  $\frac{1}{2}$  at. %), but rises to approximately unity with 2% doping. At this level the Seebeck coefficient has dropped below  $200 \mu\text{V}/^\circ\text{C}$ . Hicks (1964) obtained quite good fits to his Seebeck data (see fig. 68 (c)) over the doping range 1 to 5% using Johnstone's curves (1956) for scattering in degenerate semiconductors. At 5% doping the scattering is principally as from ion centres ( $\nu_H \propto T^{-0.5}$ ), and the fit leads to the deduction that  $m_h^* \sim m_0$ . The intrinsic zero doping data were only fitted with the additional assumptions that  $\mu_e \sim \mu_h$  and  $m_e^* \sim m_h^*$ , but it is suspected that this fit was attempted using  $E_g = 1.7 \text{ eV}$ , corresponding to the excitonic energy gap ( $\sigma \rightarrow \text{d/p}$ , see fig. 27), rather than the d-d gap which is about 0.1 eV. Fivaz and Mooser (1967), or Revolinsky and Beerntsen's (1964) data show that the smaller gap is the carrier determining gap in intrinsic material at least until  $600^\circ\text{C}$  (see fig. 53, and p. 269).

Table 12. Electrical data on tantalum doped  $\text{WSe}_2$ . (Hicks 1964)

Compound	$x$	$\rho$ <i>m. ohm-cm</i>	$R_H$ $\text{cm}^3/\text{coul}$	$n$ $\text{cm}^{-3}$	$\mu$ $\text{cm}^2/\text{v-sec}$	$\frac{n_e}{n_{\text{at}}}$
$\text{W}_{1-x}\text{Ta}_x\text{Se}_2$	0	780	78	$8.0 \times 10^{16}$	99	—
	0.005	30.2	$3.9 \times 10^{-1}$	$1.6 \times 10^{19}$	12.9	0.2
	0.01	11.7	$7.4 \times 10^{-2}$	$8.4 \times 10^{19}$	6.3	0.6
	0.02	4.3	$2.5 \times 10^{-2}$	$2.5 \times 10^{20}$	5.8	0.9
	0.03	3.2	$1.8 \times 10^{-2}$	$3.5 \times 10^{20}$	5.6	0.8
	0.04	—	$1.5 \times 10^{-2}$	$4.2 \times 10^{20}$	—	—
	0.05	2.5	$9.4 \times 10^{-3}$	$6.6 \times 10^{20}$	3.8	0.9

Fig. 68



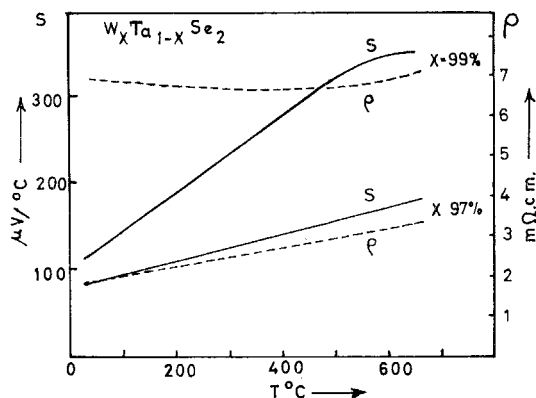
(a) Number of carriers, (b) Hall mobility, (c) Seebeck coefficient. (Hicks 1964.)

Increase of the carrier concentration in a group VI semiconductor through group V doping has an interesting effect on the excitons A and B. The effective two-body electron-'hole' exciton interaction in the carrier sea is:

$$V(r) = - \frac{1}{\epsilon(r)} \cdot \frac{e^2}{r} \cdot \exp(-qr).$$

The exponential screening term arises from the free carriers which are able to respond and to 'dissolve' the bound exciton state. The screening parameter  $q$  will depend on the density of these free carriers and their mobility, and also on the expectation radius of the exciton, which is governed among other things by its effective mass (a function of the bands in which its one-electron state components lie).

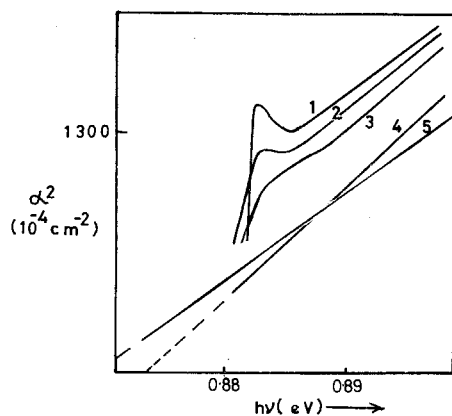
Fig. 69



High temperature measurements of  $\rho$ , and  $S$  for (a) 1% (atomic) Ta in  $WSe_2$ , (b) 3%. (Brixner 1963.)

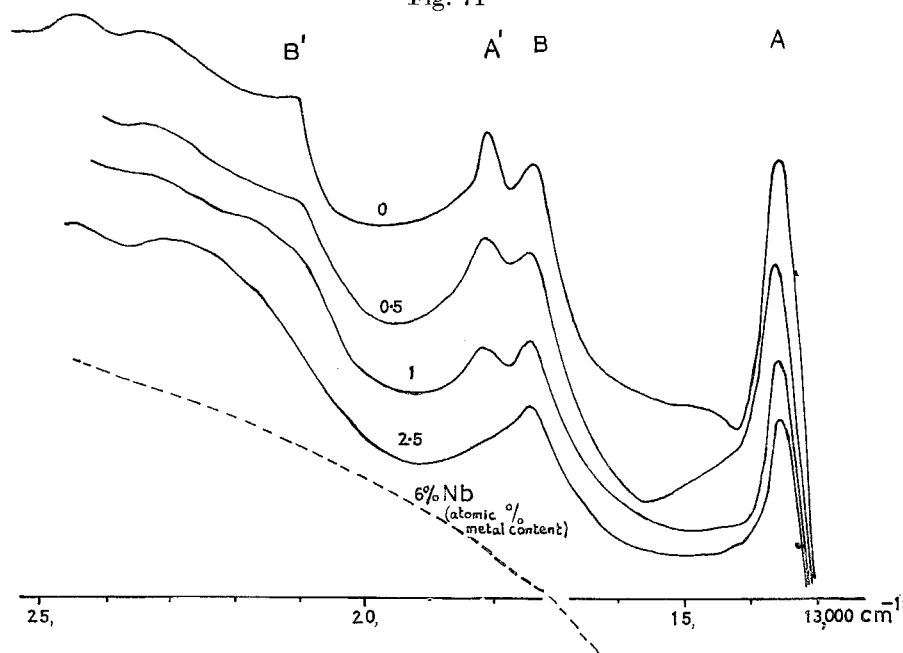
The course of free-carrier screening may be followed through by controlled doping. The exciton binding energy in germanium is very small ( $\sim 10^{-3}$  eV) and the peak is accordingly very temperature dependent (see fig. 39, Phillips 1966). Asnin and Rogachev (1967) have recently succeeded in progressively screening out this feature from the transmission spectrum by using doping concentrations from  $10^{13}$  up to  $10^{17}/\text{cm}^3$ . Their results are shown in fig. 70. Because of the much larger exciton binding energy for  $MoS_2$  ( $\sim 0.05$  eV) and the smaller radius (20 Å as against 200 Å) it has been found possible to parallel their experiment at much more convenient doping levels. As seen in table 12, doping  $WSe_2$  with 1% Nb, say, will increase the conductivity by  $10^2$  or more whilst the carrier concentration changes from  $10^{17}$  to  $10^{20}/\text{cm}^3$ . Figure 71 shows the spectra obtained for such systems. The disappearance of the excitons is not due to poor crystal quality, as is seen from electron micrographs and also from the results on other mixed

Fig. 70



Effect on the exciton in germanium of arsenic doping. (1)  $3 \times 10^{13}$ , (2)  $2 \times 10^{15}$ , (3)  $1 \times 10^{16}$ , (4)  $2 \times 10^{17}$ , (5)  $1.5 \times 10^{18}/\text{cm}^3$ . (Asnin and Rogachev 1967.)

Fig. 71



Effect on the excitons in  $\text{WSe}_2$  of niobium doping (curves staggered—common level of absorption at energies greater than  $B'$ ).

systems such as  $(\text{W}/\text{Mo})\text{Se}_2$  or  $\text{Mo}(\text{S}/\text{Se})_2$ , where the excitons still show strongly (see p. 245). It could be, though, that the doping concentrations used in the VI/V system are high enough for exciton-electron collisions to

be very important. The free carriers, however, are *not* introduced into a band occupied by either the electron or the hole of the exciton.

Finally it should be noted that even in  $\text{NbS}_2$  itself there is some trace of peaking in the exciton energy range (see fig. 22 (*h*)). It remains to be seen what happens at liquid helium temperatures (actually at 4°K,  $\text{NbS}_2$  would be a superconductor—see p. 277). The most surprising thing in these compounds is that any excitonic interaction persists at all in the presence of such high carrier concentrations—even though these carriers are not very mobile. Recently Mahan has published two theoretical papers (1967 a, b) discussing such remanent excitonic interaction in highly degenerate semiconductors and poor metals.

A further very interesting means of doping these layer structures is by the process known as ‘intercalation’. In intercalation atoms of an additional element are taken up into the vacant van der Waal’s sites. The take-up of the alkali metals from liquid ammonia solution in particular has been studied (Rudorff 1965). Intercalation compounds of graphite, like  $\text{C}_3\text{K}$ , have recently been shown to be superconducting (Salzano and Strongin 1967). It seems that in such compounds the alkali metal donates its outer electron into an existing energy band of the matrix. In this the intercalates closely resemble the ‘bronzes’ of which the tungsten bronzes,  $\text{A}_x\text{WO}_3$ , are the simplest and best known (e.g. Sienko 1962). The tungsten bronzes are based on a cubic cell, body-centred by tungsten, face-centred by the oxygens, and accommodating any added alkali metal atoms at cube corner sites. The tungsten  $t_{2g}$  orbitals are not involved in the  $\sigma$  bonding of the  $\text{WO}_3$  octahedra, and go to form an empty non-bonding band. It is this band which accepts any electrons donated by added alkali atoms, so yielding a situation akin to that for the metallic compound  $\text{ReO}_3$  (Feinleib *et al.* 1968). This sequence is very much like that of, say,  $\text{TiSe}_2$ , intercalated  $\text{TiSe}_2$ , and  $\text{VSe}_2$ . Alkali metal intercalation by  $\text{TiS}_2$  (group IV) or  $\text{MoS}_2$  (group VI) is known to produce a metallic product, as witnessed

Table 13. Properties of intercalated  $\text{TiS}_2$ , ‘ $\text{VS}_2$ ’ and ‘ $\text{CrS}_2$ ’.  
(Rudorff 1965)

Compound	$\text{Na}_{0.3}\text{TiS}_2$	$\text{NaVS}_2$	$\text{NaCrS}_2$
Colour	Black	Black	Orange
Lattice constants (Å)			
<i>a</i>	3·5 <sub>3</sub>	3·5 <sub>7</sub>	3·5 <sub>3</sub>
<i>c</i>	20·0 <sub>4</sub>	19·6 <sub>5</sub>	19·4 <sub>9</sub>
Magnetic moment B.M.			
$\mu_{\text{eff}}$ ( $T = 293^\circ\text{K}$ )	0·61	2·1	3·7
$\mu_{\text{theoretical}}$	1·73	2·83	3·87
Specific resistivity			
Ω-cm	Small	0·2	> 10 <sup>8</sup>
Reaction with water	H <sub>2</sub> liberated	Slow hydrolysis	Stable

by the low resistivity and Pauli paramagnetism (Rudorff 1965). Intercalation tends to run to a product  $A_xTX_2$ , where  $x$  is fixed for a given compound  $TX_2$ , but is usually less than 1, e.g. for potassium in  $WS_2$ ,  $MoS_2$ ,  $ReS_2$ ,  $x=0.5$ ,  $0.6$  and  $0.8$  respectively. The  $a$  and particularly the  $c$  parameters are increased by such intercalation, but the  $c$  expansion is noted to be smaller for larger  $x$ , e.g.  $2.01$ ,  $1.95$  and  $1.65$  Å in the above-mentioned cases. This could mark an increasing tendency towards ionic behaviour. Certainly such a tendency is very marked through the intercalated products of  $TiS_2$ , 'VS<sub>2</sub>', 'CrS<sub>2</sub>' as table 13 from Rudorff 1965) shows. Indeed,  $NaCrS_2$  has optical and magnetic properties which indicate the presence of  $Cr^{3+}$  ions (Holt and Wold 1967, Bongers *et al.* 1968). This compound is more like a standard perovskite or spinel than an intercalation product. In fact  $CrS_2/Se_2/Te_2$  do not exist (as either layer compounds or pyrites) even under high pressures and temperatures—see p. 321. The progressive increase in ionicity and the breakdown of band behaviour through the series  $NaTiS_2$ ,  $NaVS_2$ ,  $NaCrS_2$  is very similar to that in a perovskite series such as  $LaTiO_3$ ,  $LaVO_3$ ,  $LaCrO_3$ ,  $LaMnO_3$ . Collective to localized transitions in such series have been much investigated lately (e.g. Goodenough 1966, 1967 a, b). Returning to the non-stoichiometric 'bronzes' and 'intercalates' these too are of interest as regards the metal-insulator transition. It is well known (Mott 1967, Shanks *et al.* 1962) that in some cases metallic type conductivity does not appear until the alkali content is quite substantial. The intercalates of  $MoS_2$ , etc., have yet to be investigated from this aspect. If progressive intercalation can be secured it might be possible to observe the steady disappearance of the A and B excitons due to screening. Also of interest are the superconducting properties of the intercalates. Several of the 'bronzes' are known to be superconductors (Sleight *et al.* 1969), as of course is degenerate  $SrTiO_3$  (Koonce *et al.* 1967). The intriguing possibilities for superconductivity in the  $TX_2$  layer dichalcogenides have been mentioned already in § 7.3.2.

#### 7.4. The Group VIII Layer Materials

The layer tellurides of group VIIIb,  $CoTe_2$ ,  $RhTe_2$ , and  $IrTe_2$ , are all very metallic. The metallic character seems better established as compared with that of the non-layered selenides. Thus  $CoTe_2$  (Haraldsen *et al.* 1956) does not show the cooperative magnetism of  $CoS_2$  or  $CoSe_2$  (see § 9.1), and layered  $RhTe_2$  is not a superconductor, unlike the pyrite forms of  $RhSe_2$  and  $RhTe_2$ .  $IrTe_2$  contrasts strongly with orthorhombic  $IrSe_2$ , which is a semiconductor (see Hulliger 1964). These layer tellurides like those of Group VIIIc (viz.  $NiTe_2$ ,  $PdTe_2$ ,  $PtTe_2$ ) all have a very small  $c/a$  parameter (see fig. 14 and table 2). Resistivities of  $\sim 10^{-5}$  Ω-cm for  $PtTe_2$ , etc. again contrast strongly with the semiconductivity obtained in  $PtS_2$  and  $PtSe_2$ . Semiconductivity was to be expected for group VIIIc in the light of the band diagram of fig. 26 (b). The very small band gap observed for  $PtSe_2$  ( $\sim 0.1$  eV, Hulliger 1965) would indicate that for all

six tellurides the non-bonding d band now overlaps the  $\sigma^*$  conduction band. The degree of overlap must be just right to produce superconductivity in  $\text{PdTe}_2$  ( $T_s$  1.8°K, Kjekshus and Pearson 1965), but not in either  $\text{NiTe}_2$  or  $\text{PtTe}_2$  (Guggenheim *et al.* 1966). The  $c/a$  contraction is to be expected as the non-bonding orbitals, which have the geometry shown in fig. 25, become highly occupied. In fact it is likely that there is heavy mixing of all the states in these tellurides.  $c/a$  has its minimum value of 1.27 in  $\text{PdTe}_2$ , as against 1.30 in  $\text{PtTe}_2$  and 1.37 in  $\text{NiTe}_2$ .  $\text{PdTe}_2$  should also be compared with  $\text{ZrTe}_2$  from group IV, where the d band is empty.

	$a$	$c$	$\frac{2r_{\text{at.}}}{d_{\text{M-M}}}$	$c/a$
$\text{ZrTe}_2$	3.950	6.630 Å	81%	1.678
$\text{PdTe}_2$	4.037	5.126 Å	68%	1.270

$(c/a \text{ ideal} = 1.633)$

Further details of the electrical and structural properties for the whole of group VIII are given later in § 9.

## § 8. THE OPTICAL AND ELECTRICAL PROPERTIES OF THE *Distorted* LAYER COMPOUNDS OF GROUPS V, VI AND VII

### 8.1

The compounds with which we are concerned here are :

- (1) Group VII. 3 'non-bonding' electrons,  $\text{ReS}_2$ ,  $\text{ReSe}_2$ ,  $(\text{ReTe}_2)$ ,  $\text{TcS}_2$ ,  $\text{TcSe}_2$  ( $\text{TcTe}_2$ ).
- (2) Group VI. 2 'non-bonding' electrons,  $\text{WTe}_2$ ,  $\beta\text{-MoTe}_2$ .
- (3) Group V. 1 'non-bonding' electron,  $\text{TaTe}_2$ ,  $\text{NbTe}_2$ .

These  $\text{TX}_2$  layer compounds are all based on the octahedral sandwich but with the metal atoms displaced from the coordination unit centres. This causes the X atom sheets to buckle somewhat. The detailed crystal structures have been given in figs. 4, 5 and 6. The pattern of metal atom displacements changes from group to group with the number of spare electrons not involved in  $\sigma$  bonding. The resulting metal-metal interactions make for the establishment of filled sub-bands, i.e. we have homopolar metal-metal bonding. Figure 25 shows the geometry of the orbitals involved.  $\text{ReS}_2$  with three non-bonding electrons would be a metal in either trigonal prism or octahedral coordination *if* regular (see fig. 26 (b)). Actually the material is a semiconductor showing a sharp excitonic feature on the absorption edge (see fig. 22 (j)). The distortion is particularly strong

in this case. The Re atoms cluster into units of 4, with the shortest Re-Re distance less than that in the h.c.p. metal itself†. Figure 72 and table 14 compare the structures for the three groups together, and also with the distorted rutile VO<sub>2</sub> (see fig. 73). In VO<sub>2</sub> (below  $T_d$ ) we have discrete pairs of vanadium atoms, whilst in the layer compounds we have strands of linked atoms.

Table 14. Comparison of the distortions in NbTe<sub>2</sub>, WTe<sub>2</sub>, ReSe<sub>2</sub> and VO<sub>2</sub>

	NbTe <sub>2</sub>	WTe <sub>2</sub>	ReSe <sub>2</sub>	VO <sub>2</sub>
Shortest M-M	3.33	2.86	2.65	2.65
Average M-M	$\frac{3.33}{3.83} = 0.87$	$\frac{2.86}{3.58} = 0.80$	$\frac{2.65}{3.35} = 0.79$	$\frac{2.65}{2.88} = 0.92$
Shortest M-M	3.33	2.86	2.65	$\frac{2.65}{\parallel c}$
Longest M-M	$\frac{3.33}{4.51} = 0.74$	$\frac{2.86}{4.38} = 0.65$	$\frac{2.65}{4.13} = 0.64$	$\frac{2.65}{3.12} = 0.85$
Shortest M-M	3.33	2.86	2.65	2.65
Shortest in metal	$\frac{3.33}{2.86} = 1.165$	$\frac{2.86}{2.74} = 1.045$	$\frac{2.65}{2.75} = 0.965$	$\frac{2.65}{2.63} = 1.009$
Area of sheet in bonding region	58%	36%	44% (strips) or 20% (diamonds)	—
Shortest M-X	2.690	2.708	2.382	1.86
Longest M-X	$\frac{2.690}{2.908} = 0.925$	$\frac{2.708}{2.820} = 0.962$	$\frac{2.382}{2.665} = 0.893$	$\frac{1.86}{2.05} = 0.906$

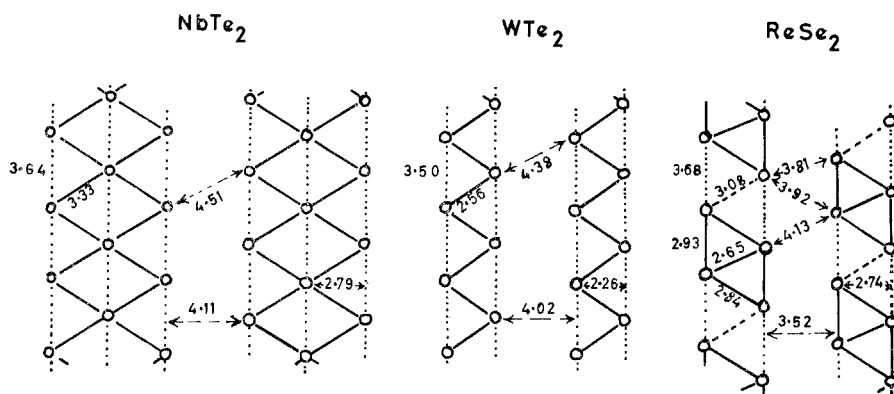
Electrical and optical polarization measurements have as yet failed to reveal any anisotropy *in* the layers, but this may be due to twinned domain formation (see later). The energy derived from the metal-metal bonding and from a number of shortened T-X distances must more than compensate for the increased length of the other T-X bonds in the coordination units. The energy difference between a distorted and regular phase is clearly small. MoTe<sub>2</sub> moves from the regular  $\alpha$  to the distorted  $\beta$  form above 900°C, whilst VO<sub>2</sub> becomes regular above 68°C. Perhaps the best indication of the strength of the metal-metal bonding comes from the ratio of the shortest and longest M-X distances since these bonds are of prime energetic importance. This places ReS<sub>2</sub> > VO<sub>2</sub> > NbTe<sub>2</sub> > WTe<sub>2</sub> (see table 14).

This type of metal sub-lattice distortion is fairly common among oxides, halides and chalcogenides possessing narrow d bands. When the room temperature carrier mobility for a band drops below about 10 cm<sup>2</sup>/v-sec,

† This is typical of many rhenium compounds—see Canterford and Colton (1968) for halide examples. ReTe<sub>2</sub> has a very complex distorted layer structure—see Sorrell (1968). It is reported to be a p type semiconductor (see Johnson *et al.* 1965).

the entropy term causes delocalization to be unfavourable (Mott 1969). Several mechanisms are known which then tend to produce filled band insulators. In several cases, a sharp semiconductor  $\leftrightarrow$  metal transition is obtained at temperatures easily accessible to experiment. In  $\text{VO}_2$  a  $10^5$  drop in  $\rho$  from 10 to  $10^{-4}$   $\Omega\text{-cm}$ , occurs on warming at  $68^\circ\text{C}$  (Ladd and Paul 1969). The  $\text{VO}_2$ -type distortion transition can be described in terms of electron-phonon interaction. It is a 'fixation' of the small polaron effect (Appel 1969) when the structure and number of electrons are favourable to permanent distortion. The distortion causes a previously degenerate band to split into sub-bands. If the distortion is severe as in  $\text{VO}_2$  or  $\text{ReS}_2$  the splitting can separate the bands throughout the zone so that a semiconductor results. Neither a structure analysis nor electrical measurements have been made on  $\text{TcS}_2$  and  $\text{TcSe}_2$ , but from the absence of the exciton peaks on the direct edge, as compared with  $\text{ReS}_2$  and  $\text{ReSe}_2$  (fig. 22 (*j, k*)) it would seem that the distortion is less severe. The transition temperatures,  $T_d$ , etc. are known to be very sensitive to the degree of band overlap (cf.  $\text{NbO}_2$ ,  $T_d \sim 1000^\circ\text{C}$  as compared with  $\text{VO}_2$ ,  $T_d = 68^\circ\text{C}$ —see Adler 1968).

Fig. 72

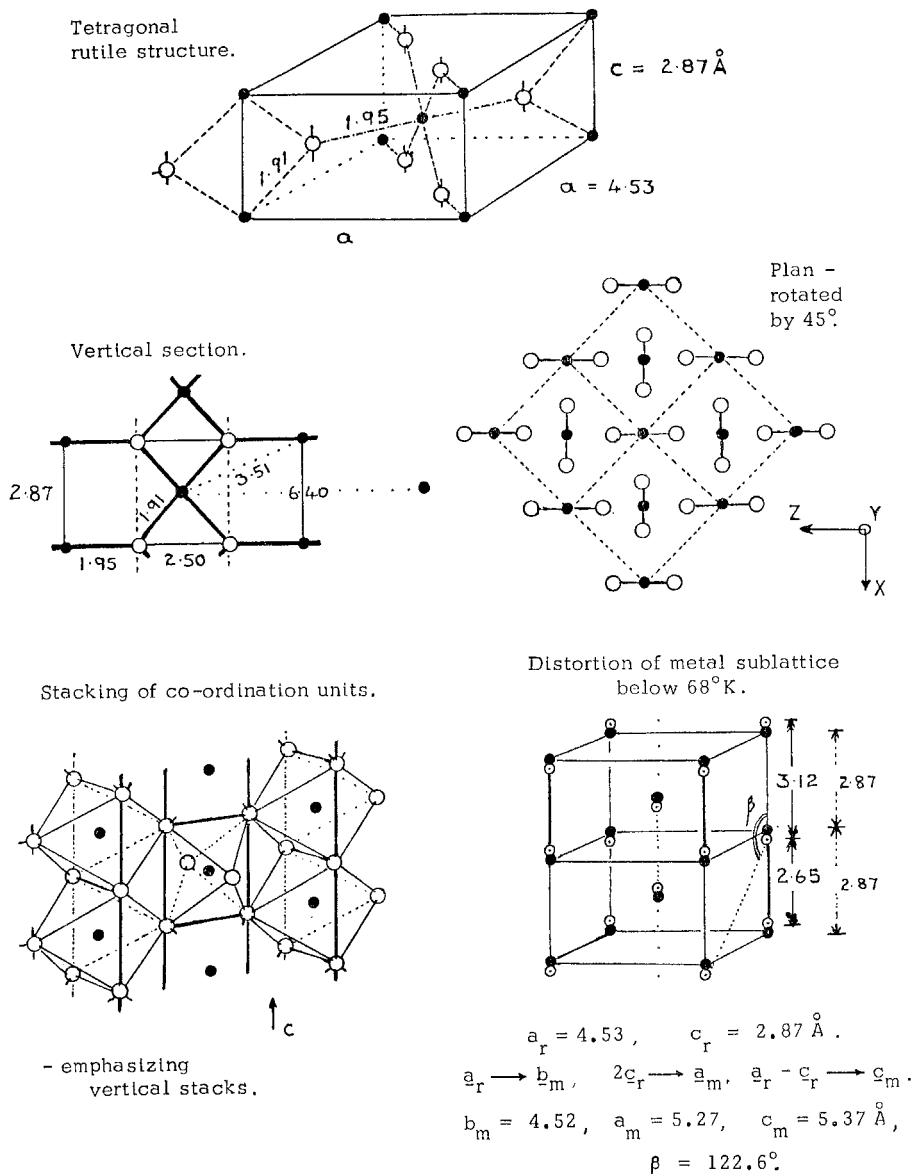


Comparison of the distortion in the metal atom sheets for the layer structures of  $\text{NbTe}_2$ ,  $\text{WTe}_2$  and  $\text{ReSe}_2$ . (The sheets are actually slightly buckled—see figs. 4, 5 and 6.)

In group VI the 5d compound ( $\text{WTe}_2$ ) again seems more distorted than the 4d counterpart ( $\beta\text{-MoTe}_2$ )—a fact which the relative definition of their spectra supports (fig. 22 (*f*)). Figure 29 indicates that the overall width of the d band in  $\text{MoTe}_2$  is *ca.* 1.5 eV, of which about one-third is occupied. In fact the  $\alpha$  form of  $\text{MoTe}_2$ , with its unusual trigonal prism coordination and concomittant split-off  $d_{2^2}$  band, may be viewed as a special type of distortion semiconductor. This again would emphasize the very unusual position of the trigonal prism metals like  $\text{NbSe}_2$  (contrast  $\text{VSe}_2$  or 1T- $\text{TaSe}_2$ ,

see § 8.2). Actually  $\text{WTe}_2$  and  $\beta\text{-MoTe}_2$  are not semiconductors but semi-metals (cf.  $\text{MoO}_2$ ), with the result that their resistivities have rather low values  $\sim 2 \times 10^{-3} \Omega\text{-cm}$ ; the room temperature Seebeck coefficients are  $\sim 30 \mu\text{V}/^\circ\text{C}$ . These values are higher than for  $\text{NbS}_2$ , etc., but very considerably less than for semiconductors like  $\text{MoS}_2$ . The resistivity plot of

Fig. 73

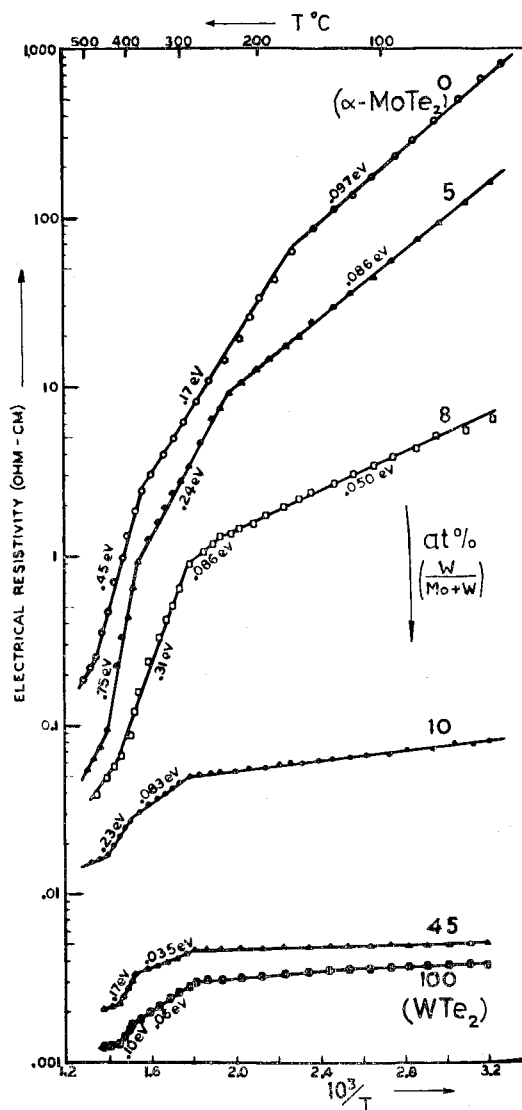


The structure of  $\text{VO}_2$  above and below its distortion temperature.

fig. 74 shows the large and rapid change over from the  $\alpha$  to the  $\beta$  phase on replacing Mo by W in the mixed system (Mo/W)Te<sub>2</sub>. Figure 75 indicates that WSe<sub>2</sub> is considerably more removed from adopting the  $\beta$  form than is MoTe<sub>2</sub>. From such mixed crystals it has been possible to estimate the position of the A and B excitons in the unknown  $\alpha$  form of WTe<sub>2</sub>.

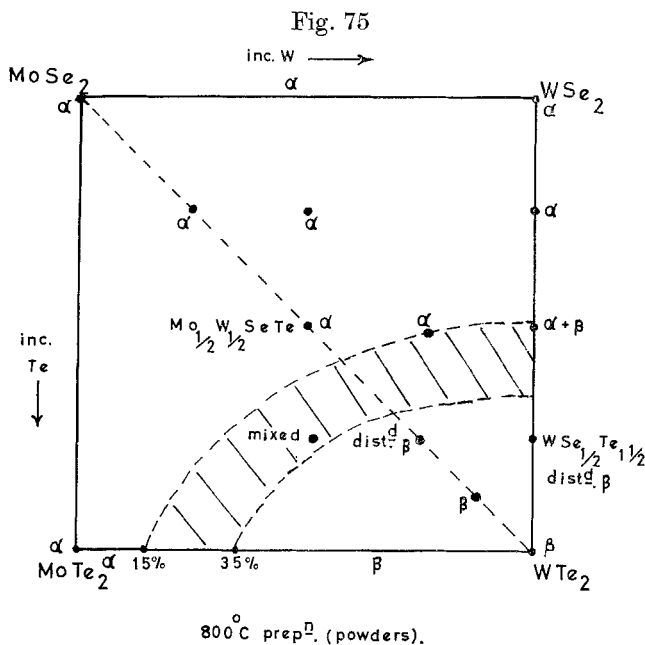
No attempts have yet been made to see if any of these distorted layer compounds undergo a reversion within the octahedral  $\beta$  phase to an undistorted condition at very high temperatures. A specimen of ( $\beta$ -) WTe<sub>2</sub>

Fig. 74



Resistivity in the (Mo/W)Te<sub>2</sub> system. (From Revolinsky and Beerntsen 1964.)

showed no change in its orthorhombic electron diffraction pattern to 800°C. This is not really surprising as the  $\beta$  phase of  $\text{MoTe}_2$  is only prepared using high temperatures (Revolinsky and Beerntsen 1966) and/or pressures (Silverman 1967).



Choice of the  $\alpha$  and  $\beta$  structure between  $\text{MoSe}_2$ ,  $\text{WSe}_2$ ,  $\text{MoTe}_2$  and  $\text{WTe}_2$ .  
(Based on data of Champion 1965—sintered powders.)

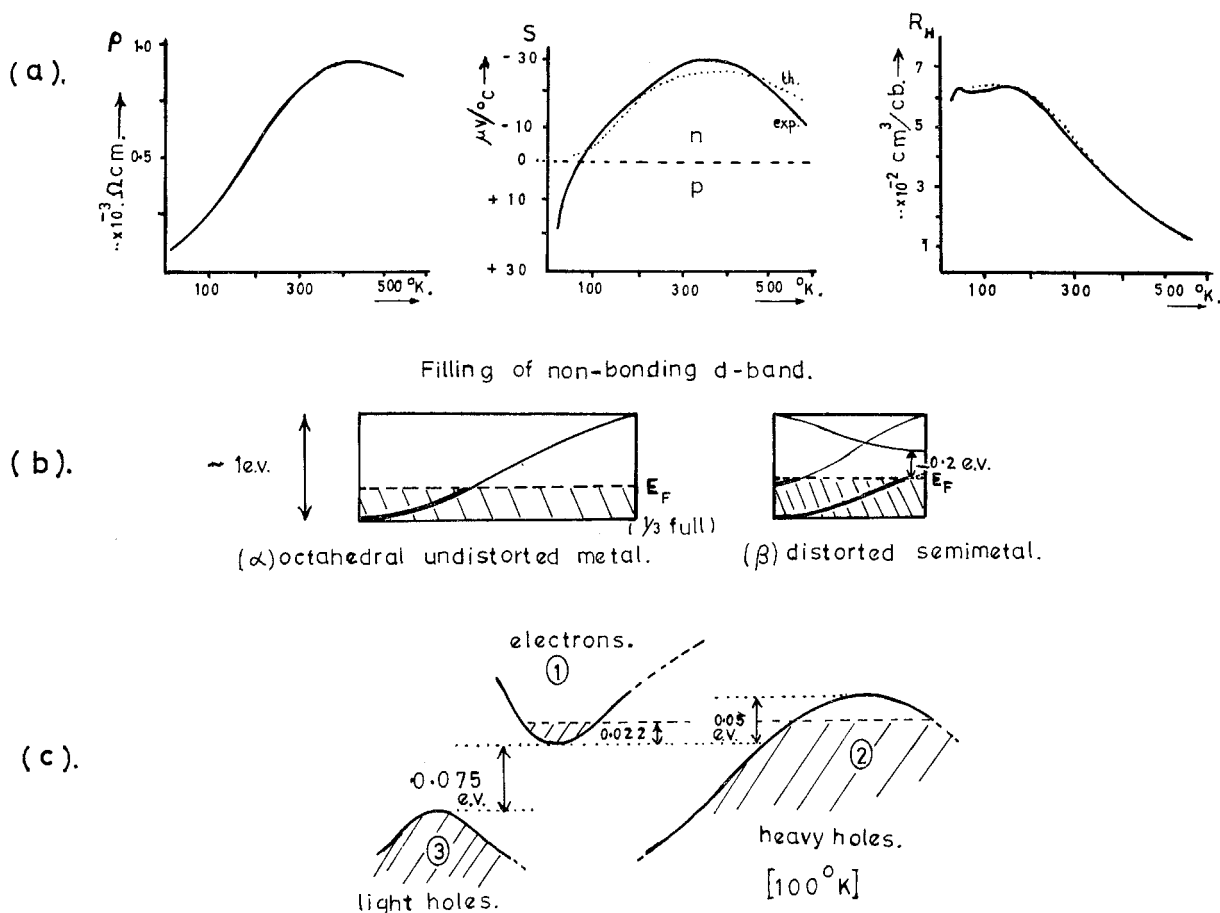
The electrical properties of  $\text{WTe}_2$  (Brixner 1962, Kabashima 1966) are very interesting and may be explained, as mentioned earlier, using a semi-metal band model, shown in fig. 76. Above room temperature high thermal excitation from the lower to the upper d sub-bands ( $E_a \sim 0.1$  eV) causes the material to behave like a highly degenerate semiconductor, with falling resistivity and Seebeck coefficient. The fall in Hall coefficient cannot be simply interpreted due to the mixed carrier situation (cf. p. 269), but Kabashima obtained the fitted curve shown in fig. 76 with the data given below it. The high excess of p type carriers ( $\sim 10^{20}/\text{cm}^3$ ) which determines the low temperature properties, corresponds to Brown's metal deficient finding (1966) on the stoichiometry of transport crystals of these compounds.

The group V compounds  $\text{NbTe}_2$  and  $\text{TaTe}_2$  again are semi-metals similar to  $\text{WTe}_2$ , but their conductivity (Brixner 1962) is an order of magnitude higher, being  $\sim 10^{-4} \Omega\text{-cm}$  rather than  $10^{-3}$ , as one might expect with an odd electron number †. The conductivity continues falling metal-wise to at

†  $\text{VTe}_2$  is also a distorted layer compound though little as yet is known about it (see Røst *et al.* 1964).

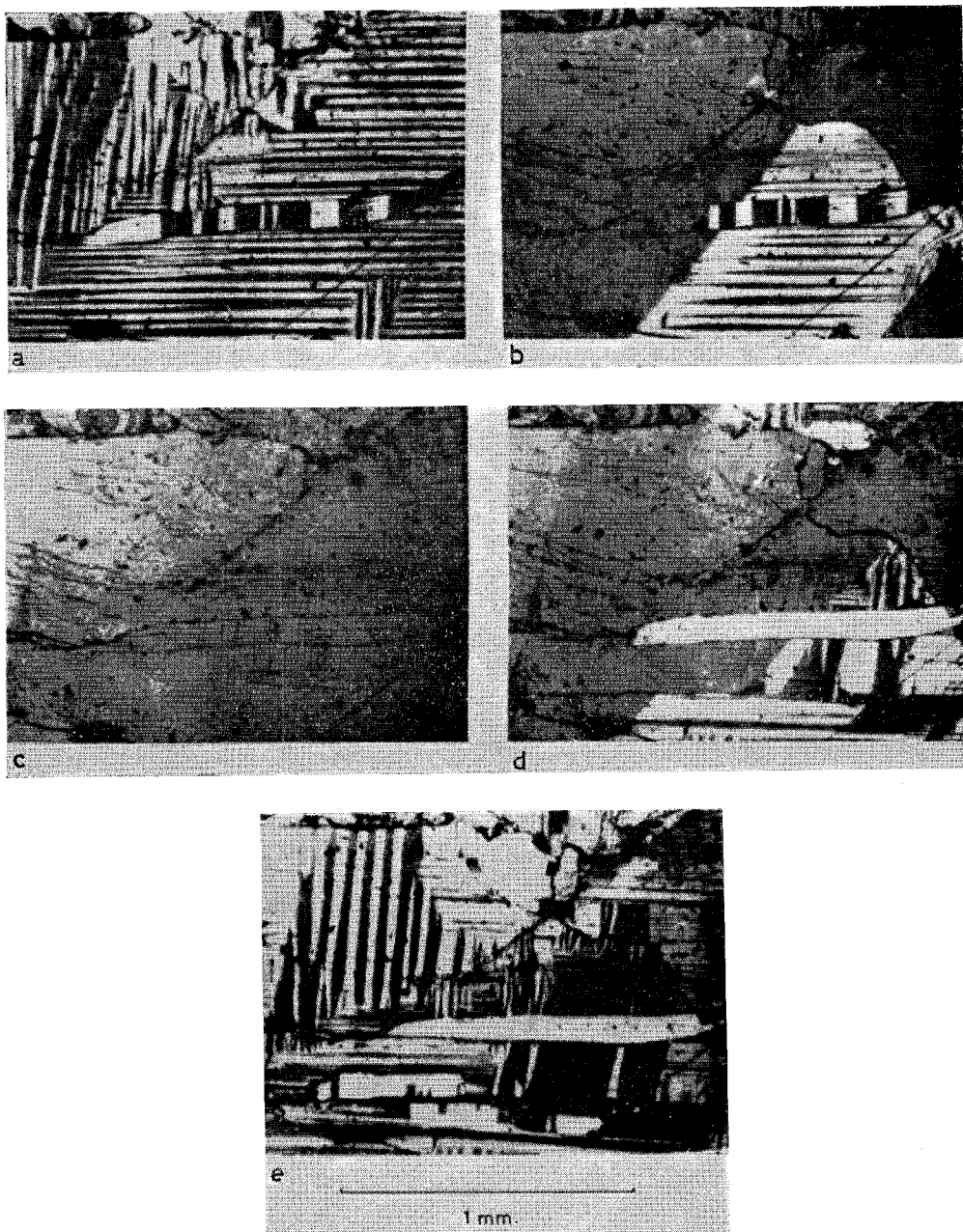
least 600°C. Crystals of NbTe<sub>2</sub> and TaTe<sub>2</sub> are very opaque in the visible part of the spectrum, indicating possibly that free-carrier absorption encroaches into this region. This was not the case for the trigonal prism full metals, like NbS<sub>2</sub>, but resembles octahedral VSe<sub>2</sub>. WTe<sub>2</sub> was quite highly transparent at 2 μ; presumably a free-carrier absorption edge is to be found in this case at about 5 μ, as is appropriate for a material with ~ 10<sup>20</sup> carriers per cm<sup>3</sup>. Despite its distorted structure NbTe<sub>2</sub> is reported to be a superconductor, T<sub>s</sub> = 0.74 °K (van Maaren and Schaeffer 1967). Like WTe<sub>2</sub> and ReS<sub>2</sub>, NbTe<sub>2</sub> and TaTe<sub>2</sub> are diamagnetic (see figs. 61 and 63). VTe<sub>2</sub>

Fig. 76



Electrical data and band model for WTe<sub>2</sub>. (a) ρ, S and R<sub>H</sub> versus T (Kabashima 1966), (b) possible effect of distortion on the 'non-bonding' d band of WTe<sub>2</sub>, (c) model used by Kabashima to fit experimental data. [ $\mu_1/\mu_2=6$ ,  $\mu_3/\mu_2=25$ ,  $m_1=m_0$ ,  $m_2=3m_0$ ,  $m_3=0.8m_0$ .]

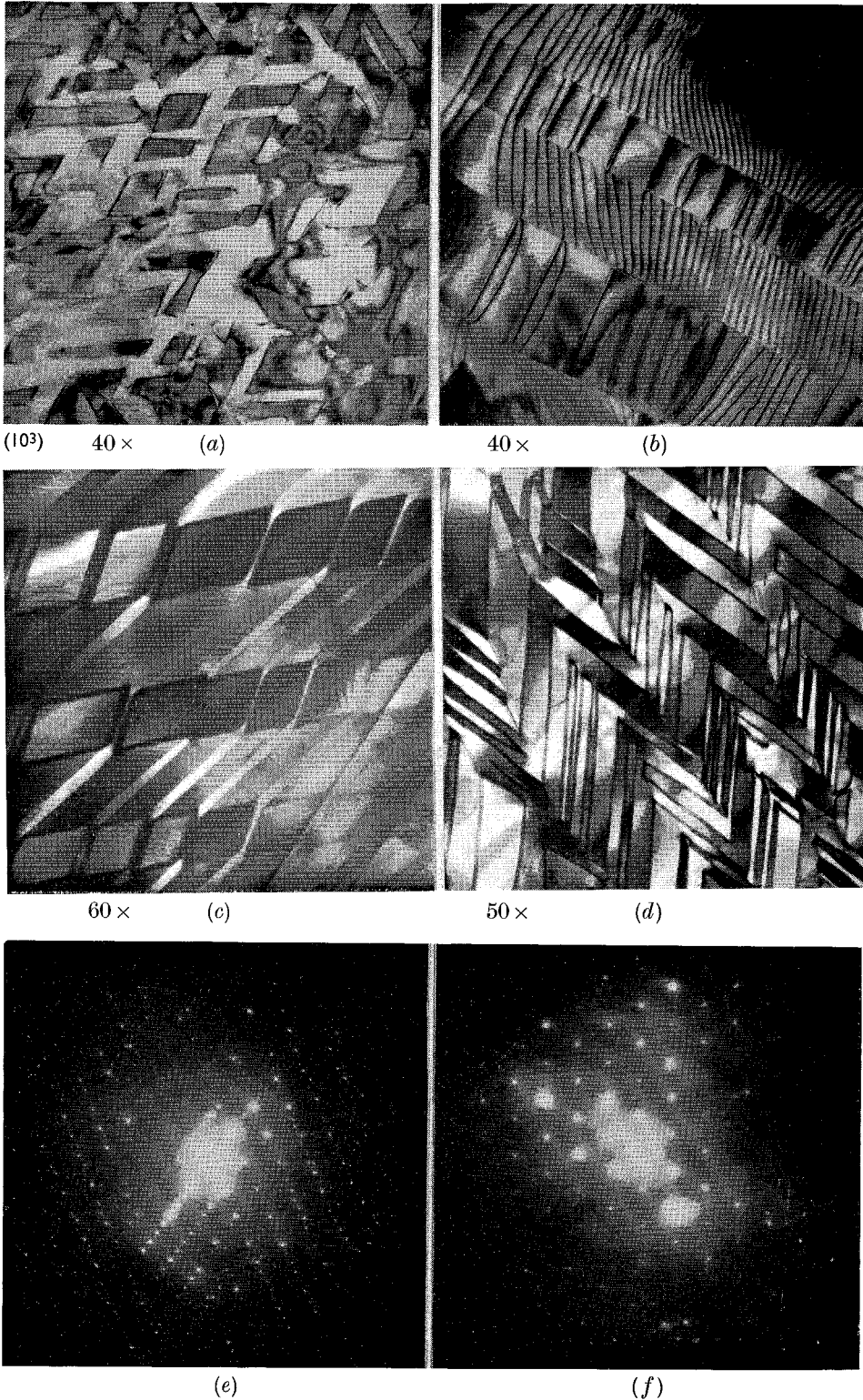
Fig. 77



Domain patterns and movement of phase boundary. (011) face of  $\text{VO}_2$ . (a) At room temperature, (b) phase boundary moving across sample near  $70^\circ\text{C}$ , (c) high temperature phase, transition complete, (d) during cooling through transition, and (e) after cooling, at room temperature. (Viewed by polarized light.)

NbTe<sub>2</sub>

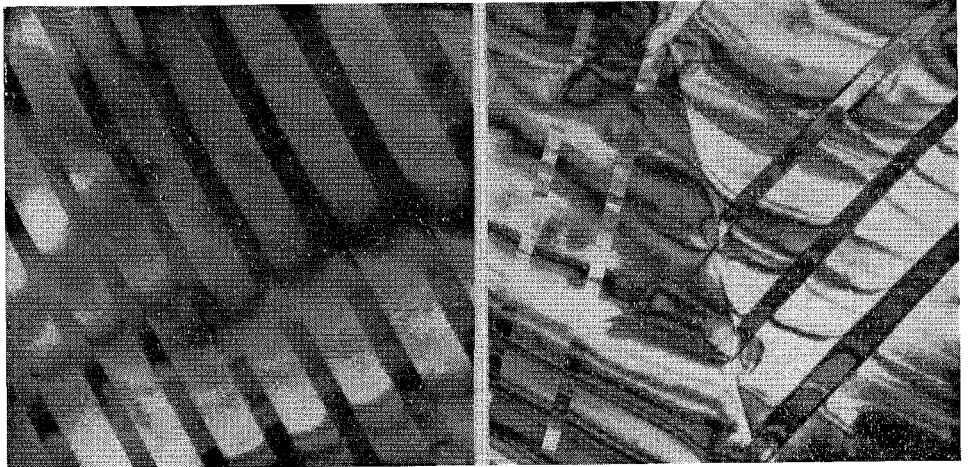
Fig. 78 (i)



Distortion twin 'domains' in NbTe<sub>2</sub> and TaTe<sub>2</sub>. (i) NbTe<sub>2</sub>. Diffraction pattern (f) comes from the region shown in (d), but (e) is more typical.

TaTe<sub>2</sub>

Fig. 78 (ii)

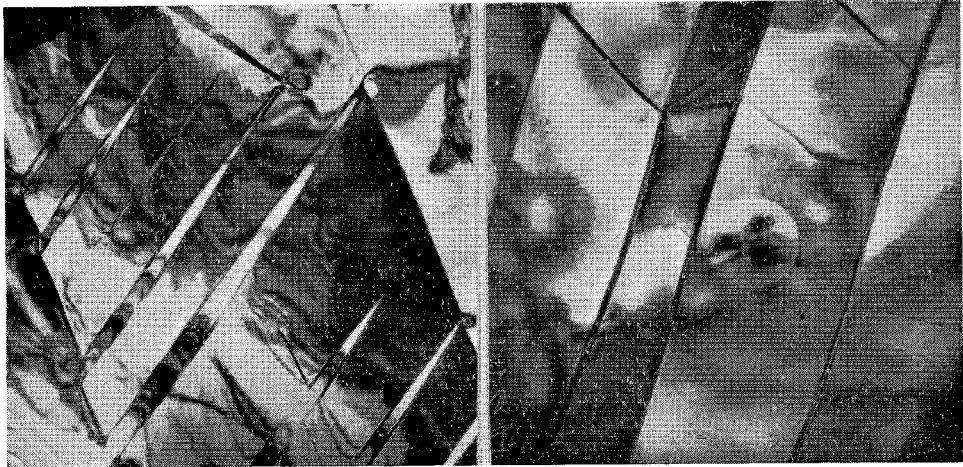


(103) 20 ×

(a)

16 ×

(b)

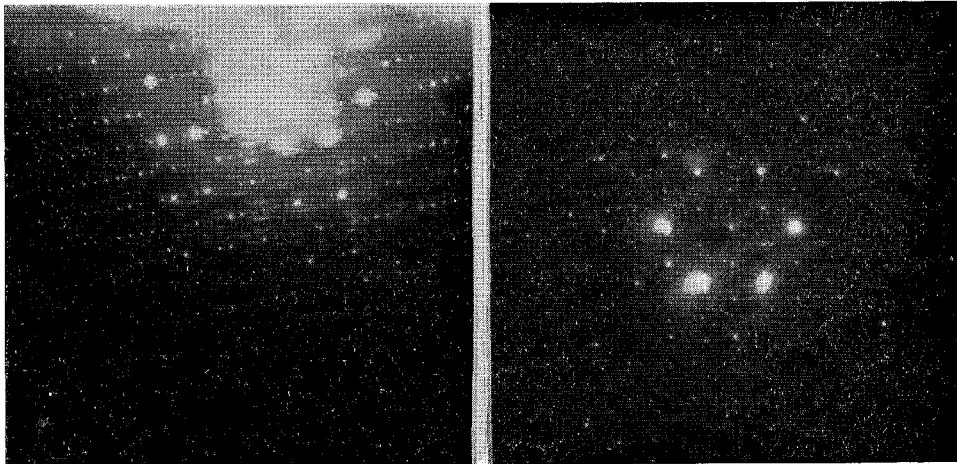


(103) 13 ×

(c)

20 ×

(d)



(e)

(f)

(ii) TaTe<sub>2</sub>. Larger domains than NbTe<sub>2</sub>. Pattern (f) comes from region shown in (d) but (e) is more typical.

differs in being paramagnetic with a break in  $\chi$  at 200 °C, somewhat resembling the behaviour in  $VSe_2$  and  $VO_2$ , the latter being paramagnetic in both in semi-metallic and distorted semiconducting phases†. Paramagnetism in 3d compounds giving way to diamagnetism in 4d and 5d compounds is not an uncommon feature (see p. 308).

$NbTe_2$ ,  $TaTe_2$  and  $VO_2$  are similar in that they show marked twinned distortion domain formation. Fillingham (1967) has obtained (using reflected polarized light) the fascinating sequence of pictures on  $VO_2$  which are shown as fig. 77. No undistorted domain free phase has been obtained for  $NbTe_2$  and  $TaTe_2$ . Domains have been observed throughout all samples of these layer dichalcogenides and some electron micrographs of these are shown in fig. 78. The domains tend to be smaller in  $NbTe_2$  than in  $TaTe_2$  and very complex diffraction patterns can result. The absence of domains in our specimens of  $ReS_2$  and  $WTe_2$  may mean that these crystals were grown below the distortion temperature, whereas the  $NbTe_2$  and  $TaTe_2$  had been quenched from above this temperature. High temperature electron microscopy should resolve this point. Ferromagnetic domain patterns in the insulating layer compound  $CrBr_3$  show up very similar to the above (Fischer 1969). As yet antiferromagnetic domains have not been looked for in  $NbSe_2$ , etc. between the Néel and superconducting transition temperatures.

### 8.2. The Properties of 1T-TaS<sub>2</sub> and TaSe<sub>2</sub>

We have discussed above cases where distortion of the metal atom sub-lattice leads to the formation of sub-bands from a fairly narrow degenerate d band. A similar removal of free carriers from the system may also be achieved through magnetic coupling and the appearance of anti-ferromagnetic order.  $\alpha$ -NiS is a material of this type, showing a resistivity that rises metal-wise with temperature above the Néel point of 268°K, but rises semiconductor-wise on cooling below this temperature (Sparks and Komoto 1968). There is also a sharp resistivity discontinuity factor of about 50 at  $T_N$ . This is unlike the behaviour of  $NbSe_2$ , etc. which remain metals in the antiferromagnetic phase (see fig. 60 (b)). Behaviour like that of NiS may possibly be found in the group IV layer halides  $\alpha$ -TiCl<sub>3</sub>/Br<sub>3</sub> (see § 9.3), but in a group V layer dichalcogenide like  $NbSe_2$  (where there is also one non-bonding electron), delocalization just prevails. The word 'just' has been added here because it is known that TaS<sub>2</sub>, TaSe<sub>2</sub> (and recently  $NbSe_2$ ) may be obtained by quenching from high temperatures in an octahedral modification which promises to show very unusual properties.

Structure analyses (Jellinek 1962, Bjerklund and Kjekshus 1967, Huisman and Jellinek 1969) on these 1T forms have hitherto indicated that they are regular CdI<sub>2</sub> type materials, like  $VSe_2$ , and an x-ray powder pattern to this effect is included in fig. 18. However, the spectrum of

†  $VTe_2$  (Røst *et al.* 1964);  $VSe_2$  (Røst and Gjertsen 1964);  $VO_2$  (Hyland 1968).

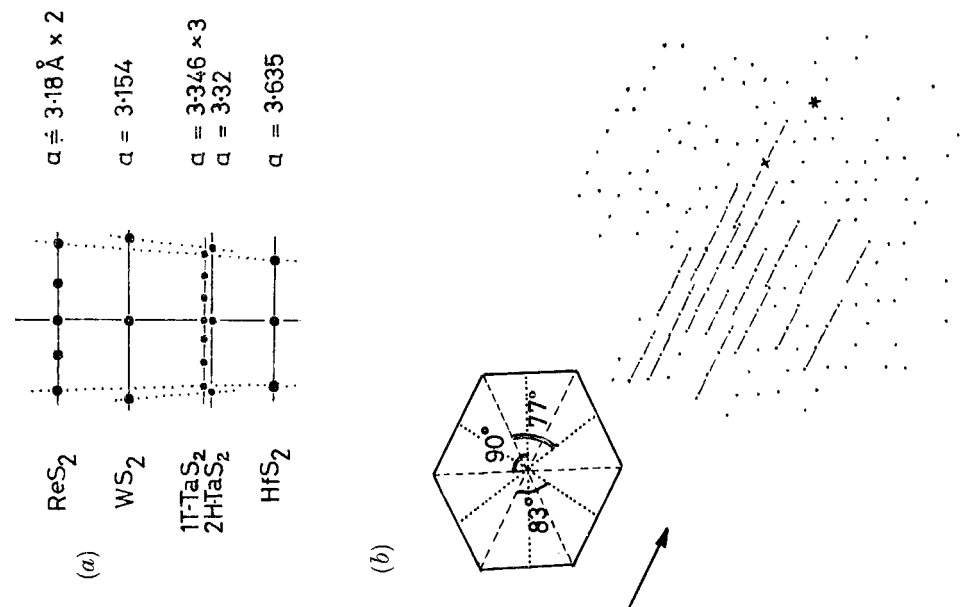
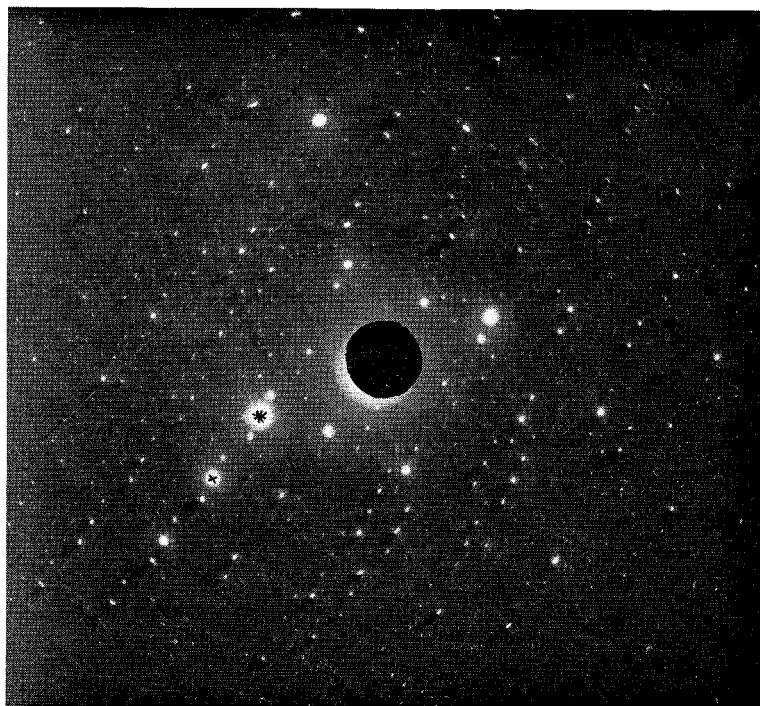


Fig. 79



(a) Comparison of electron diffraction spot spacing from crystals of HfS<sub>2</sub>, TaS<sub>2</sub>, WS<sub>2</sub> and ReS<sub>2</sub>. (b) Electron diffraction spot misalignment in 1T-TaS<sub>2</sub>.

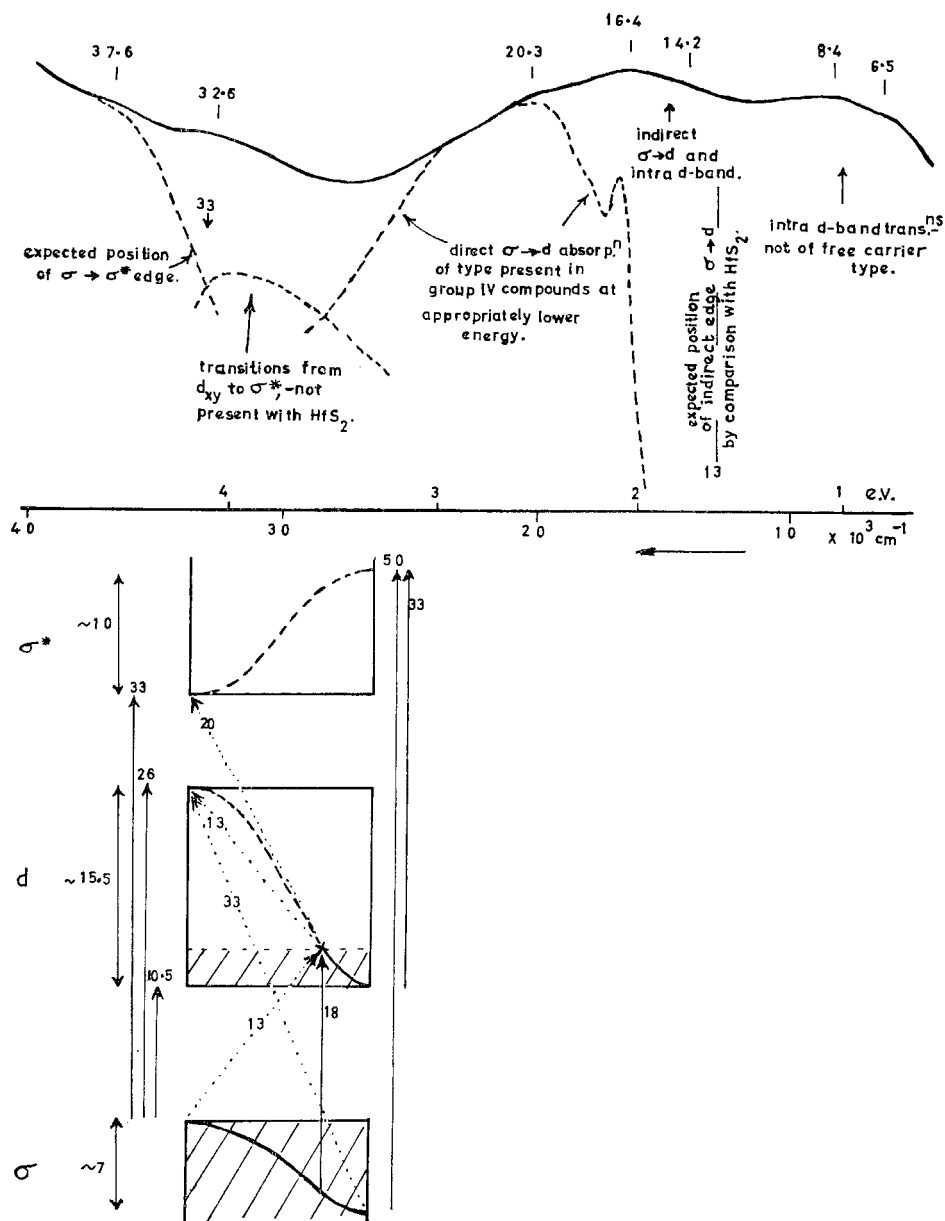
1T-TaS<sub>2</sub> given in fig. 22 (*i*) shows that there is no similarity with the metal VSe<sub>2</sub> (or indeed with 2H-TaS<sub>2</sub>); the optical absorption of the 1T form is actually falling rapidly in the region of 2  $\mu$ . This recalls the behaviour of the semi-metal WTe<sub>2</sub>. As yet no infra-red or electrical measurements have been made on these 1T materials, but the resistivity is considerably higher than for the trigonal prism forms †. Further to the above, the 1T form of TaSe<sub>2</sub> is known to be diamagnetic (see fig. 63), unlike VSe<sub>2</sub> and 2H-TaSe<sub>2</sub> which are Pauli paramagnetic. One possibility to account for the non-metallic properties is that electron-electron correlation in the d band secures at high temperatures (where the mobility is low) a condensation of carriers into electron-hole pairs, i.e. into something like the Mott condition. Certainly for the quenched high temperature 1T phase the metal-metal atom distance is slightly greater than it is in the various trigonal prism polytypes (see table 3). This is compatible with a somewhat smaller band width and greater correlation. However, a simple comparison is not possible; in the 1T case the d band in question is only one-sixth full, in the trigonal prism case it is just half-full. The 1T materials are only metastable at room temperature, and revert to a trigonal prism phase on warming to about 200 °C (see fig. 82). The ease of formation of the 1T phase seems to rise along with the degree of ionic character through the sequence NbSe<sub>2</sub>, TaSe<sub>2</sub>, TaS<sub>2</sub>. Despite the apparent lack of metallic properties 1T-TaS<sub>2</sub> is reported to be a superconductor below 0.8°K.

Some relief to this impasse comes from an electron microscope investigation of these materials. In spite of the accumulated x-ray data it is clear from the electron diffraction patterns that the structure is not a simple CdI<sub>2</sub> type. The pattern for 1T-TaS<sub>2</sub>, included in fig. 19, shows evidence of a hexagonal super-cell with sides perpendicular to *c* of about 10 Å. This super-cell incorporates nine basic cells—see fig. 79. However, whatever process defines the superlattice it must be slight as the simple x-ray pattern fails to detect it. A neutron diffraction result is awaited with interest. One feature which is to be noticed on the electron diffraction patterns is that the strings of spots do not appear to be quite colinear but fall into groups of six or so ending in slight mis-matches. This type of diffraction pattern has been noted for 'shear structures' (cf. 'Nb<sub>2</sub>O<sub>5</sub>', 'Ta<sub>2</sub>O<sub>5</sub>'), Spyridelis *et al.* (1968). Goodenough (1967 b) has given a preliminary outline of the reasons for shear structure occurrence in compounds with narrow d bands. Another possibility for the explanation of the properties of 1T-TaS<sub>2</sub> is that it is an example of a so-called 'excitonic insulator' phase. The possibility of such a phase is the subject of a recent review article by Halperin and Rice (1968), but it is as yet without a representative; its feasibility has indeed been queried by Kübler (1969). The basic condition required for the appearance of the phase is that there exists in the material a pair of bands with an energy separation which is less than the binding energy of the

---

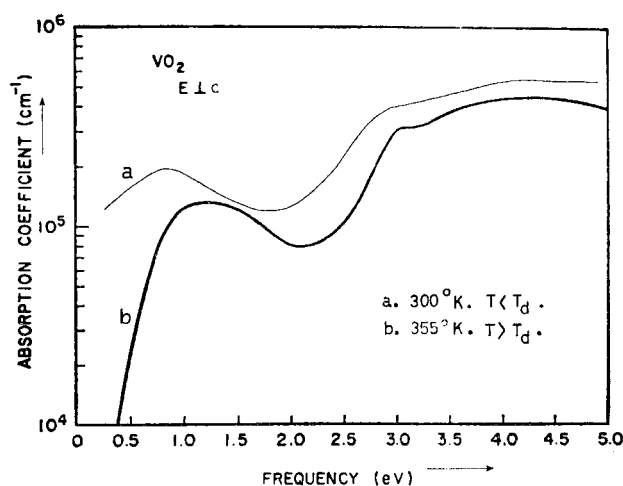
† See for example van Maaren and Harland.

Fig. 80

Transmission spectrum of 1T-TaS<sub>2</sub> compared with that of HfS<sub>2</sub>.

excitons formed from the band extrema in question†. A new ground state is formed in such conditions with insulating properties, and based on a supercell that has its repeat unit determined by the  $k$  separation in the Brillouin zone of the two-band extrema. Clearly the super-cell may thus be incommensurate with the units of the basic cell. Superconductivity in such a system could well arise through Ginzburg's exciton mechanism. The two closely adjacent bands which are required could arise in 1T-TaS<sub>2</sub> following a Mott type condensation of the electron gas, a narrow filled d band separating off from the bulk of empty d states.

Fig. 81



Absorption coefficient of VO<sub>2</sub>. (Calculated from reflectivity measurements—Verleur *et al.* 1968.)

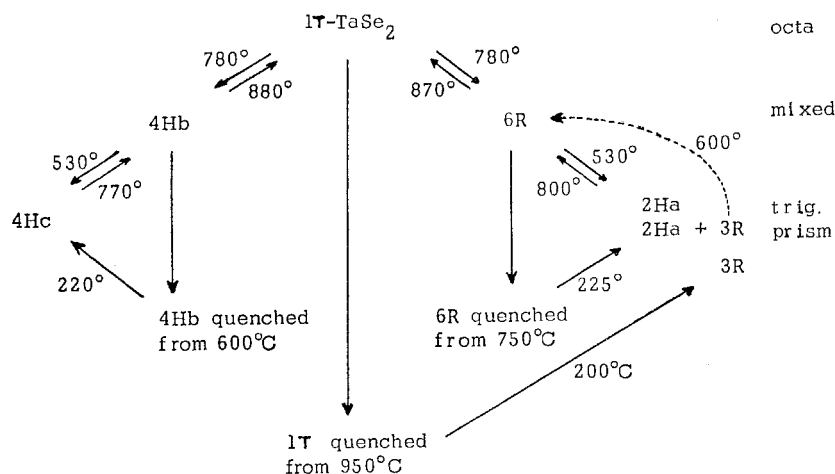
As mentioned above, the optical spectrum of 1T-TaS<sub>2</sub> sheds interesting light on this problem. It is seen by reference to fig. 80 that the spectrum above 1.8 eV can be satisfactorily accounted for using the band diagram for HfS<sub>2</sub> (suitably scaled down in energy), now with the d band partially occupied. Absorption occurs then in 1T-TaS<sub>2</sub> around 30 000 cm<sup>-1</sup> which is absent in HfS<sub>2</sub>, involving d to  $\sigma^*$  transitions. The additional absorption found below 13 000 cm<sup>-1</sup> can only arise *within* the d band system. However, this fairly strong absorption does not appear to be of the normal free-carrier type, as obtained for the trigonal prism metals. In fact absorption falls steeply in 1T-TaS<sub>2</sub> for energies below 1 eV. This was quite unexpected since the 1T carriers should lie in a band that is considerably wider than the trigonal prism d<sub>2</sub> band. In VSe<sub>2</sub>, indeed, absorption does remain strong at 2 microns (though the stoichiometry of this compound is somewhat suspect).

† For the possibility of excitonic insulator phases occurring in MoTe<sub>2</sub> see p. 251.

This fall in absorption for 1T-TaS<sub>2</sub> is reminiscent of that for the absorption coefficient of VO<sub>2</sub> over this region when in its so-called 'metallic' high temperature state—see fig. 81 (Verleur *et al.* 1968—following an analysis of reflection data). It is becoming clear that this latter compound too is not a simple metal; Hall coefficient measurements indicate a free-carrier density only one-tenth of that expected (see Barker *et al.* 1966, and contrast 2H-NbSe<sub>2</sub>, p. 272). Optical absorption measurements on 1T-TaS<sub>2</sub>/Se<sub>2</sub> are shortly to be carried further into the infra-red.

Another puzzling result has been the optical absorption of the 6R form of TaSe<sub>2</sub> (fig. 22 (*i*)). This polytype has alternating trigonal prism and octahedral sandwiches (see fig. 3). However, although the spectrum fits closely to the 2H form above 2.5 eV, below 2.5 eV it resembles that of the 1T form; in particular the free-carrier rise is absent. Huisman and Jellinek (1969) find that the magnetic properties are also intermediate between the 2H (paramag) and 1T (diamag) forms. These workers have carefully investigated the conditions under which the various polytypes occur, and they find that the mixed coordination 4Hb and 6H types are indeed intermediates

Fig. 82



	4Hc	4Hb	1T	6R	2Ha	3R	4Ha
Vol./formula unit.	65.27	65.07	65.66	65.20	64.90	65.31	64.93
a	3.436	3.455	3.477	3.456	3.436	3.435	3.436
c	4 × 6.383	4 × 6.287	6.272	6 × 6.304	2 × 6.348	3 × 6.392	4 × 6.350
c/a	4 × 1.858	4 × 1.820	1.804	6 × 1.824	2 × 1.847	3 × 1.861	1.848

4Hc and 2Ha are stable room temperature forms.

Polytypic transformations in the TaSe<sub>2</sub> system. (Based on data by Huisman and Jellinek 1969.)

between the 1T and the 4Hc and 2Ha forms (fig. 82). 3R appears to be metastable at all temperatures. The irreversible 1T $\rightarrow$ 3R transition makes itself apparent in fig. 63. One interesting finding is that given samples are reversible in one or other of the two channels 4Hb $\leftrightarrow$ 1T, and 6R $\leftrightarrow$ 1T. This 'memory' return from the 1T form could possibly arise from slight stoichiometric differences or from the stacking defect patterns. Clearly a detailed single crystal structure analysis of 1T-TaS<sub>2</sub> at high and low temperatures is called for on all counts. The possible effects of high pressures on polytype stability are also not clear. From the lattice parameters alone, it would seem that uniaxial pressure ||c favours octahedral coordination, whereas isotropic pressure would favour trigonal prism coordination.

We also hope to gain further insight into the octahedral state by studying the mixed IV-V system (Ta/Ti)S<sub>2</sub>. It is possible that the unusual properties of 1T-TaS<sub>2</sub> only arise when there is exactly the integral electron number per metal atom (cf. NiS<sub>2</sub>, § 9.1).

#### § 9. CAUSE AND EFFECT OF CRYSTAL STRUCTURE CHOICE AMONG THE TRANSITION METAL DICHALCOGENIDES AND HALIDES

##### 9.1. Survey of the Properties of the Transition Metal Dichalcogenides beyond Group VII

It is in this part of the family that the non-layered structures are found. Actually the manganese compounds of group VII take the pyrites structure, but they form a special case unique to the whole family, in that they possess a high degree of ionicity, based on the very stable Mn<sup>2+</sup>d<sup>5</sup> half-shell. All three manganese compounds are insulators, despite the odd electron number, so reflecting the localized character of the d electrons. This is also supported by their magnetic properties. They show the full paramagnetism of the d<sup>5</sup> ion, and only become antiferromagnetic on the low side of 100°K (Hastings *et al.* 1959, Lin and Harker 1968). It is not known whether they give salt-like ligand field spectra as exhibited by MnO (Iskenderov *et al.* 1968) and  $\alpha/\beta/\gamma$  MnS (Ford *et al.* 1963)—compounds which again are much more ionic than their immediate neighbours in the Periodic Table. MnS<sub>2</sub> is in fact deep red. Two is not a stable valency for the heavier elements of group VII, Tc and Re, and as was seen in § 8 the dichalcogenides of these elements are completely different from those of Mn.

MnTe<sub>2</sub> is the least ionic of the manganese compounds, and has a room temperature resistivity of only *ca.* 1  $\Omega$ -cm (always p type—Johnston *et al.* 1965). Under pressure the conductivity rises, and the Néel temperature quickly shifts to temperatures above 100°K (Sawaoka *et al.* 1966). Indeed the break in the latter plot at 100 kb may mark the onset of collective band behaviour in MnTe<sub>2</sub>.

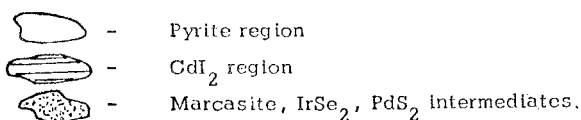
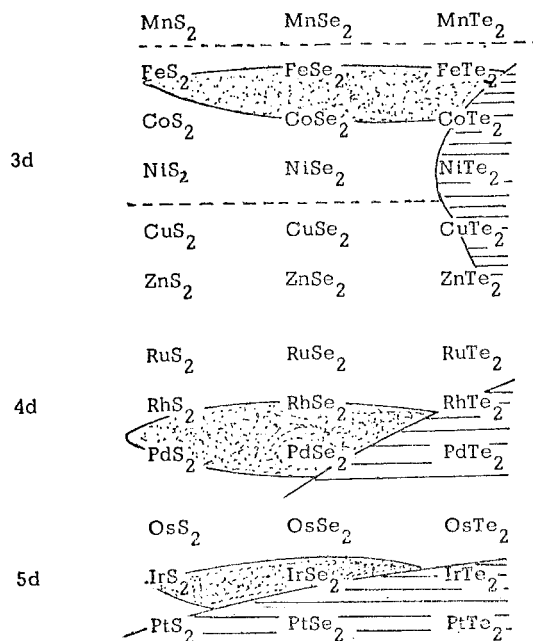
The remaining compounds in question are set out in table 15. There the crystal structures are given, and heavy type has been used to indicate the semiconductors. The first part of the table, (a), arranges these materials

Table 15. Structures of the group VIII transition metal dichalcogenides classified by (a) group number, (b) period number

VIII a d <sup>6</sup>	FeS <sub>2</sub> <b>M, P</b> RuS <sub>2</sub> <b>P</b> OsS <sub>2</sub> <b>P</b>	FeSe <sub>2</sub> <b>M, (P-H.P.)</b> RuSe <sub>2</sub> <b>P</b> OsSe <sub>2</sub> <b>P</b>	FeTe <sub>2</sub> <b>M, (P-H.P.)</b> RuTe <sub>2</sub> <b>P</b> OsTe <sub>2</sub> <b>P</b>
VIII b d <sup>7</sup>	CoS <sub>2</sub> <b>P</b> (RhS <sub>2</sub> ) <b>P</b> IrS <sub>2</sub> <b>X, (P-H.P.)</b>	CoSe <sub>2</sub> <b>P, M</b> RhSe <sub>2</sub> <b>X, (P-H.T.)</b> IrSe <sub>2</sub> <b>X</b>	CoTe <sub>2</sub> <b>M, (C-H.T.), (P-H.P.)</b> RhTe <sub>2</sub> <b>P, (C-H.T.)</b> IrTe <sub>2</sub> <b>C</b>
VIII c d <sup>8</sup>	NiS <sub>2</sub> <b>P</b> PdS <sub>2</sub> <b>Y, (Y'-H.P.)</b> PtS <sub>2</sub> <b>C</b>	NiSe <sub>2</sub> <b>P</b> PdSe <sub>2</sub> <b>Y</b> PtSe <sub>2</sub> <b>C</b>	NiTe <sub>2</sub> <b>C, (P-H.P.)</b> PdTe <sub>2</sub> <b>C</b> PtTe <sub>2</sub> <b>C</b>
I d <sup>9</sup>	CuS <sub>2</sub> (P-H.P.)	CuSe <sub>2</sub> M, (P-H.P.)	CuTe <sub>2</sub> (P, C-H.P.)
II d <sup>10</sup>	ZnS <sub>2</sub> (P-H.P.) CdS <sub>2</sub> (P-H.P.)	ZnSe <sub>2</sub> (P-H.P.) CdSe <sub>2</sub> (P-H.P.)	ZnTe <sub>2</sub> (P-H.P.) (C-H.P.)

Structures: P: pyrite, M: marcasite, X: IrSe<sub>2</sub>, Y: PdS<sub>2</sub>, C: cadmium iodide. Unusual preparation conditions: H.T.: high temperature > 900°C, H.P.: high pressures ~ 50 kb, often coupled with high temperatures. Semiconductors are printed in heavy type.

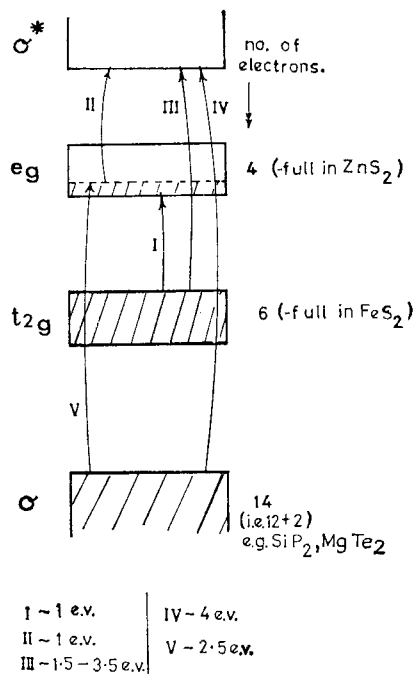
(b)



by group number, and the second part, (b), indicates the development of structure type over the periods 3, 4 and 5. As mentioned earlier (see figs. 7 to 11), the marcasite,  $\text{IrSe}_2$  and  $\text{PdS}_2$  structures are intermediate between those of cadmium iodide and pyrites. The prominence of the pyrite structure among the 3d materials is lost in the 'heavier' periods.

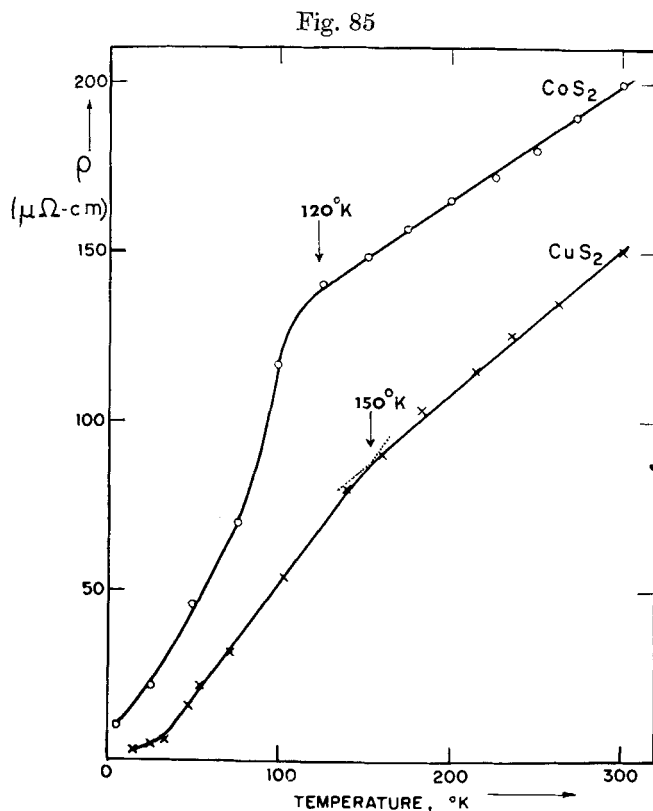
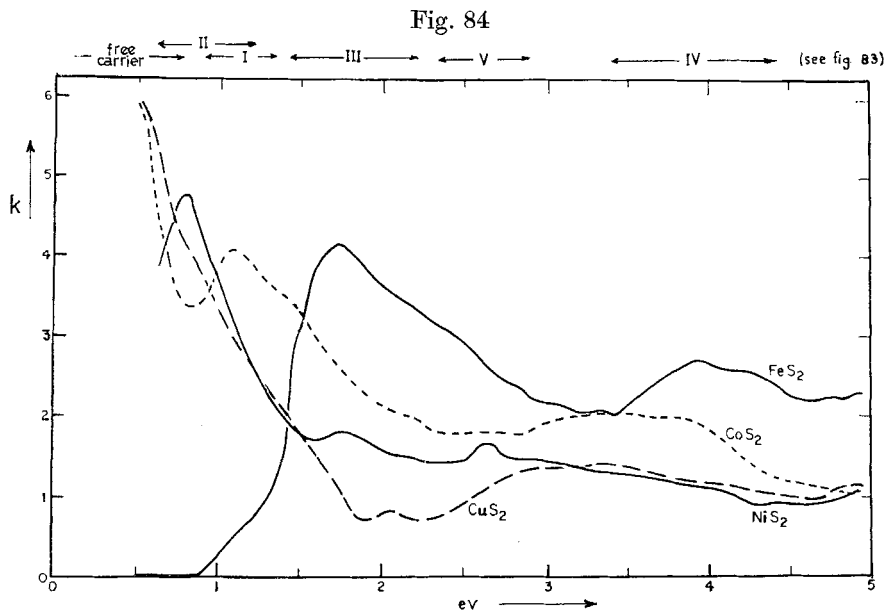
A considerable amount of fairly detailed work has appeared recently on the 3d materials, particularly in the pyrite phase†, but there is little published as yet on several of the heavier compounds. The pyrite structure is not one confined to transition metal elements (e.g.  $\text{SiP}_2$ , Donohue *et al.* 1968), but represents a general geometrical 'attempt' at high density 6 : 4 packing. As seen from the above example the structure requires 14 valence electrons, 12 being equivalent to the M-X bonding of the octahedra, and two to the X-X link (see fig. 7).  $\text{FeS}_2$  with 20 electrons, then has six surplus electrons which enter the d bands inserted within the basic  $\sigma\sigma^*$  gap. This gap is likely to be about 3-4 eV wide. The  $t_{2g}$  orbitals form a true non-bonding band, but the upper band based on the  $e_g$  orbitals will take on a slight anti-bonding character due to the covalent participation in the M-X

Fig. 83



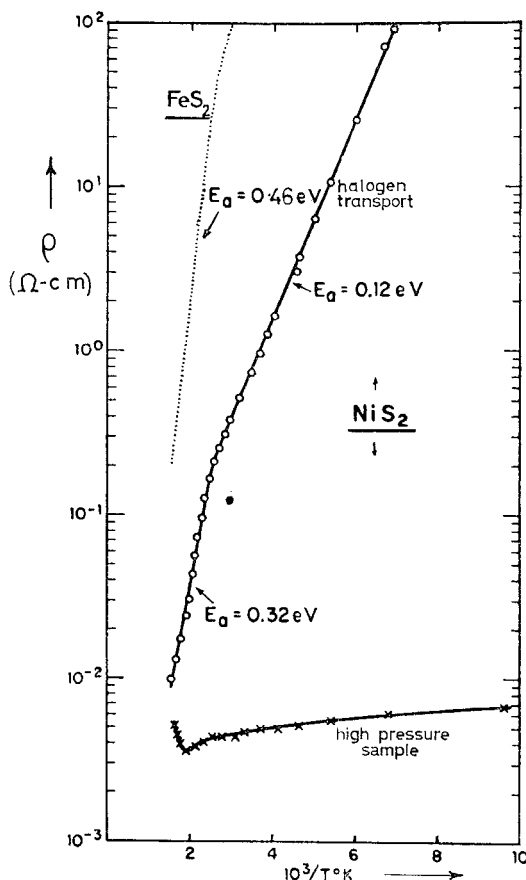
Postulated banding for the pyrite disulphides. (Based on optical and electrical data from Bither *et al.* 1968.)

† See Miyahara and Teranishi (1968); Jarrett *et al.* (1968); Bither *et al.* (1968); Adachi *et al.* (1969).



bonding, the  $e_g$  orbitals being suitably oriented. Thus in the  $\text{FeS}_2$  group (VIIIa) we arrive at a semiconducting condition with the  $t_{2g}$  band completely filled. Depending on impurity content the specimens can either be n or p type. Electron mobilities are  $\sim 200 \text{ cm}^2/\text{V}\cdot\text{sec}$ , with hole mobilities substantially smaller. From optical (fig. 84) and electrical data (see, for example, Bither *et al.* 1968) the inter d band gap is seen to be just under 1 eV wide.  $\text{FeS}_2$ , then, is in many ways reminiscent of  $\text{MoS}_2$ . This is even more true of say  $\text{RuTe}_2$  by which stage the band gap has closed to 0.25 eV (Hulliger 1963, Johnston *et al.* 1965). The band properties of these semiconductors are clearly quite different from the properties of the manganese compounds. The very large lattice parameters of the manganese dichalcogenides (see fig. 12) contrast their high ionicity. Also they share the rather high compressibility of other  $\text{Mn}^{2+}$  compounds (see Clendenen and Drickamer

Fig. 86

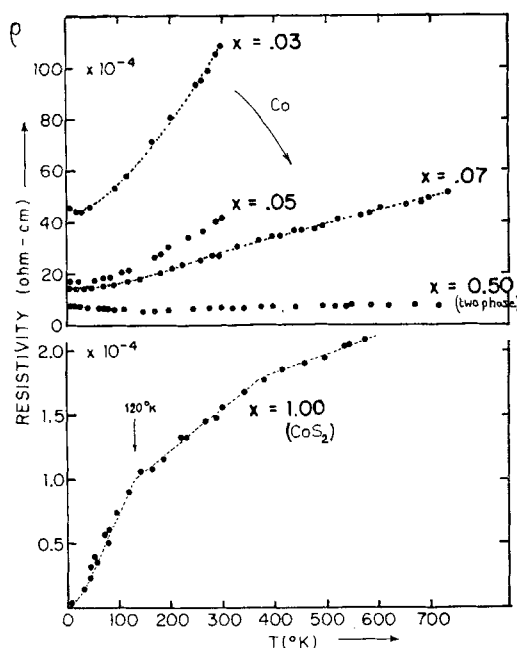


$\rho$ - $T$  plot for the pyrite semiconductors  $\text{FeS}_2$  and  $\text{NiS}_2$ . (Single crystals—Bither *et al.* 1968.)

1966)—compared with which  $\text{FeS}_2$  is much more rigid (linear compressibility  $2.3 \times 10^{-7}/\text{bar}$ —(Sato *et al.* 1969)†.

Those pyrites with more electrons than  $\text{FeS}_2$  take these up into the  $e_g$  band (fig. 83). Since this has some anti-bonding character their formation becomes progressively more difficult. Thus the pyrite tellurides of Fe, Co, and Ni, and all the Cu and Zn compounds require high pressures for their formation (Bither *et al.* 1968). The  $e_g$  band is full at Zn ( $d^{10}$ ), and the zinc compounds are diamagnetic insulators ( $\text{ZnS}_2$ ,  $E_g \sim 2.5 \text{ eV}$ ,  $\rho \sim 10^6 \Omega\text{-cm}$ ). For Co ( $d^7$ ) and Cu ( $d^9$ ) the band is one-quarter and three-quarters full respectively, and accordingly metals result. The properties of these metals will be compared shortly with those of group V like  $\text{NbS}_2$ . The nickel compounds ( $d^8$ ) in the half-filled band position seem to have very interesting potentialities with regard to the metal-insulator transition. The reflection spectra of these pyrites are shown in fig. 84, and the various features are interpreted there in terms of the banding arrangement of fig. 83.

Fig. 87

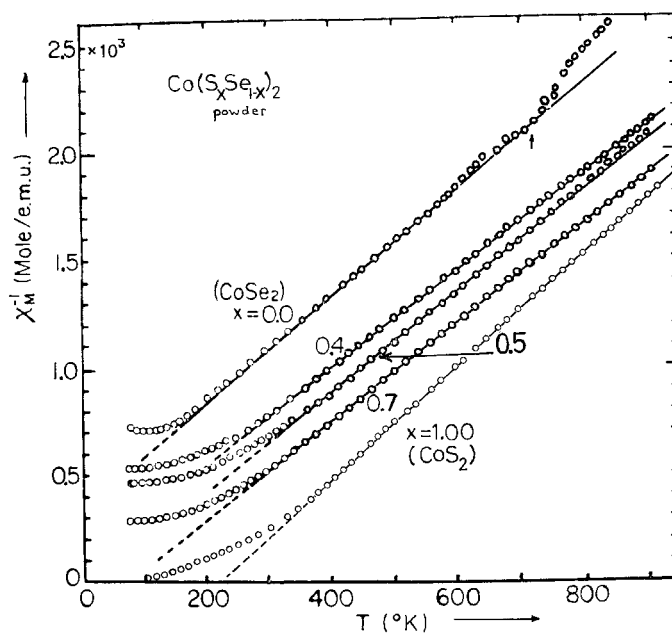


$\rho$ - $T$  plots for  $\text{FeS}_2$  doped with Co. (Single crystals—Bither *et al.* 1968.)

† N.B. The low temperature-independent paramagnetism ( $\chi_M \sim 10 \times 10^{-6}$  cgs/mole—Miyahara and Teranishi 1968) of  $\text{FeS}_2$  is to be found in other narrow band 3d semiconductors (e.g.  $\text{FeAs}_2^a$ ,  $\text{TiO}_2^b$ ) and is absent from their broader band diamagnetic 4d and 5d counterparts. (Ref. 'a', Holseth and Kjekshus 1968; Ref. 'b', Senftle and Thorpe 1968.)

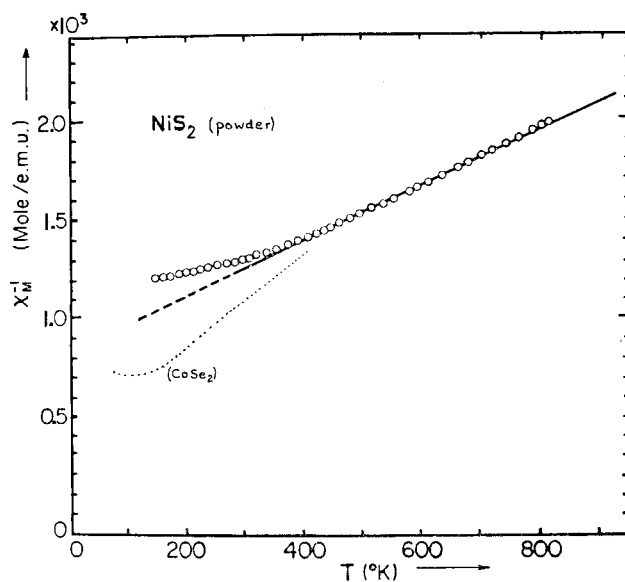


Fig. 88



$1/\chi$ - $T$  plot for  $\text{CoS}_2$ ,  $\text{CoSe}_2$  and mixed crystals. (Adachi *et al.* 1969.)

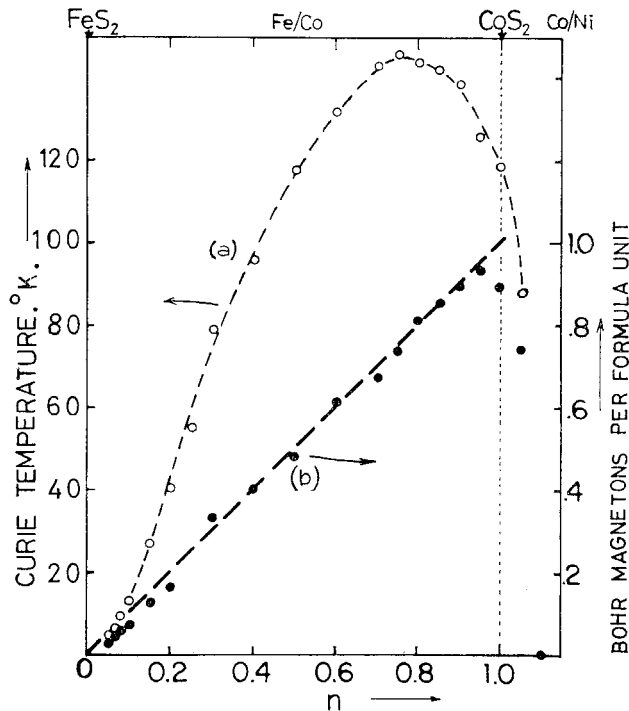
Fig. 89



$1/\chi$ - $T$  plot for  $\text{NiS}_2$ . (Adachi *et al.* 1969.)

Mixed crystals such as  $(\text{Fe/Co})\text{S}_2$ ,  $(\text{Co/Ni})\text{S}_2$ ,  $(\text{Ni/Cu})\text{S}_2$ ,  $(\text{Cu/Zn})\text{S}_2$  have been prepared (Bouchard 1968) and show very interesting gradations of property. As for say  $\text{MoS}_2$  with Nb doping (§ 7.3.3), additions of small amounts of Co to  $\text{FeS}_2$  rapidly reduce the resistivity, and metallic type

Fig. 90



Ferromagnetism in the  $(\text{Fe/Co})\text{S}_2$  and  $(\text{Co/Ni})\text{S}_2$  systems. (a) Curie temperature versus electron number, (b) saturation moment versus  $n$ . (From Bither *et al.* 1968.)

temperature coefficients are produced (see fig. 87). Ferromagnetism appears with about 5% Co added, and the magnetic saturation moment,  $\mu_s$ , corresponds closely to one 'active' electron per added cobalt atom over the composition range 10 to 95%. Beyond this limit  $\mu_s$  begins to fall rapidly. If we now consider the  $\text{CoS}_2/\text{Ni}$  system this value moves to zero for the addition of only 10% Ni (see fig. 90). The ferromagnetism of  $\text{CoS}_2$  is the subject of a recent series of papers (Adachi *et al.* 1969). The Curie temperature  $T_c$  falls quite quickly under pressure and particularly so following the replacement of sulphur by selenium (limit of 12% Se).  $\text{CoS}_2$  follows the  $T^{3/2}$  law for saturation magnetization quite well up to 40°K, leading to an exchange interaction value of  $0.3 \times 10^{-2}$  eV per cobalt pair ( $J_{s.w.}$ —see Kittel 1967, p. 468).  $\text{CoSe}_2$  is antiferromagnetic, and as fig. 88 shows,  $T_N$  is about 90°K with  $\theta_p \sim -160^\circ\text{K}$ . From fig. 89,  $\text{NiS}_2$  would also appear

Table 16. Summary of the properties of the pyrite sulphides and selenides of Fe, Co, Ni and Cu

	Electrical	Magnetic
FeS <sub>2</sub>	Semiconductor, $E_g \sim 0.9$ eV $\rho^{300^\circ\text{K}} = 1 \Omega\text{-cm}$ $S = 500 \mu\text{V}/^\circ\text{C}$	Van Vleck temperature independent paramagnetism, $\chi \sim 10 \times 10^{-6}$ c.g.s. units/mole (Miyahara and Teranishi 1968)
CoS <sub>2</sub>	Metal, $\rho^{300^\circ\text{K}} = 2 \times 10^{-4} \Omega\text{-cm}$ $S = -30 \mu\text{V}/^\circ\text{C}$	Ferromagnetic, $T_c = 124^\circ\text{K}$ (118°) $\mu_s = 0.84\mu_B$ (0.89) $\theta_p = +220^\circ\text{K}$ (193°) $p_{\text{eff}} = 1.76\mu_B$ (1.84) $\frac{\theta_p}{T_c} = 1.64$ (1.77) $\chi^{300^\circ\text{K}} = 4000 \times 10^{-6}$ c.g.s. units/mole
NiS <sub>2</sub>	Semiconductor, (a) Sulphur deficient : $E_a > 400^\circ\text{K} = 0.32$ eV $E_a < 400^\circ\text{K} = 0.12$ eV $\rho^{300^\circ\text{K}} \sim 0.5 \Omega\text{-cm}$ $S = +300 \mu\text{V}/^\circ\text{C}$ (b) Sulphur rich : $E_a \sim 0.01$ eV $\rho^{300^\circ\text{K}} \sim 5 \times 10^{-3} \Omega\text{-cm}$ $S = +9 \mu\text{V}/^\circ\text{C}$	Paramagnetic, $\theta_p = -740^\circ\text{K}$ (1800°) $p_{\text{eff}} = 2.48\mu_B$ (3.65) $\chi^{300^\circ\text{K}} = 700 \times 10^{-6}$ c.g.s. units/mole
CuS <sub>2</sub>	Metal, $\rho^{300^\circ\text{K}} = 1.5 \times 10^{-4} \Omega\text{-cm}$ $S = +3 \mu\text{V}/^\circ\text{C}$ superconductor $T_s = 1.5^\circ\text{K}$	Pauli paramagnetic, $\chi^{300^\circ\text{K}} \sim 40 \times 10^{-6}$ c.g.s. units/mole
FeSe <sub>2</sub>	Semiconductor, $\rho^{300^\circ\text{K}} \sim 0.1 \Omega\text{-cm}$	' Non-magnetic '
CoSe <sub>2</sub>	Metal, $\rho^{300^\circ\text{K}} = 1 \times 10^{-4} \Omega\text{-cm}$ $S = -20 \mu\text{V}/^\circ\text{C}$	Antiferromagnetic, $T_N = 90^\circ\text{K}$ $\theta_p = -160^\circ\text{K}$ (-450°K) $p_{\text{eff}} = 1.72\mu_B$ (2.44) $\chi^{300^\circ\text{K}} = 900 \times 10^{-6}$ c.g.s. units/mole
NiSe <sub>2</sub>	Metal, $\rho^{77^\circ\text{K}} = 0.7 \times 10^{-4} \Omega\text{-cm}$ $\rho^{300^\circ\text{K}} = 2.2 \times 10^{-4} \Omega\text{-cm}$ $S = -7 \mu\text{V}/^\circ\text{C}$	Pauli paramagnetic, $\chi^{300^\circ\text{K}} = 170 \times 10^{-6}$ c.g.s. units/mole
CuSe <sub>2</sub>	Metal, $\rho^{300^\circ\text{K}} = 0.8 \times 10^{-4} \Omega\text{-cm}$ $S = +2 \mu\text{V}/^\circ\text{C}$ superconductor $T_s = 2.4^\circ\text{K}$	Pauli paramagnetic, $\chi^{300^\circ\text{K}} \sim 90 \times 10^{-6}$ c.g.s. units/mole

Based on papers of Bither *et al.* (1968) and Adachi *et al.* (1969). Magnetic data from first paper appear bracketed for CoS<sub>2</sub>, NiS<sub>2</sub> and CoSe<sub>2</sub>.

to be antiferromagnetic, but although  $\chi$  stops rising below 200°K no sharply defined ordering temperature has been found, and indeed no order is observed by neutron diffraction, even at 4°K (Adachi *et al.* 1969).† As mentioned above the semiconducting properties of NiS<sub>2</sub> are unusual and contrast strongly with the metallic properties of NiSe<sub>2</sub> (see table 17). The semiconductivity disappears at the intermediate composition Ni(S<sub>0.8</sub>Se<sub>0.2</sub>)<sub>2</sub> (Hulliger 1965). In the mixed sulphides studied by Bouchard (1968), the

† J. Hastings is about to publish a paper contradicting this finding.

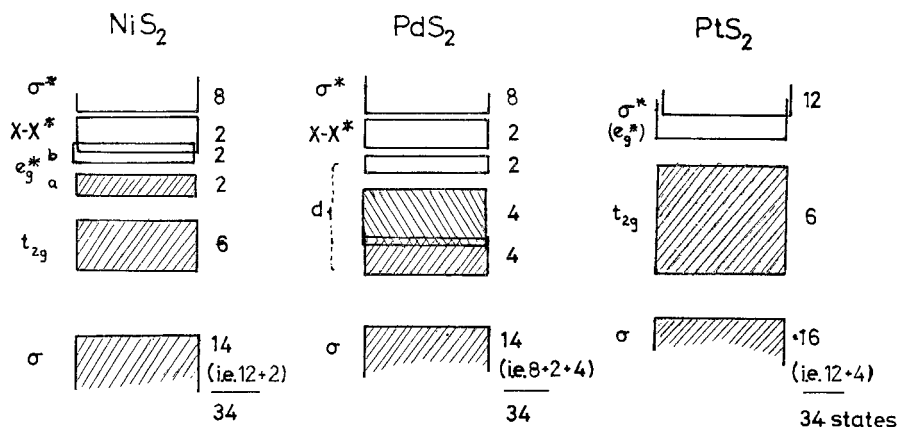
Table 17. Properties of various metallic d band dichalcogenides and oxides

	CoS <sub>2</sub>	CoSe <sub>2</sub>	CuS <sub>2</sub>	NiSe <sub>2</sub>	NbSe <sub>2</sub>	VO <sub>2</sub>	CrO <sub>2</sub>	RuO <sub>2</sub>	ReO <sub>3</sub>
n	1	1	3	2	1	1	2	3	1
$\rho^{4^\circ\text{K}}$ ( $\Omega\text{-cm}$ )	$0.08 \times 10^{-4}$		$0.05 \times 10^{-4}$		$0.1 \times 10^{-4}$		$0.03 \times 10^{-4}$	$< 0.2 \times 10^{-6}$	
$\rho^{77^\circ\text{K}}$ ( $\Omega\text{-cm}$ )	$0.7 \times 10^{-4}$		$0.3 \times 10^{-4}$	$0.7 \times 10^{-4}$	$0.4 \times 10^{-4}$		$0.08 \times 10^{-4}$	$0.03 \times 10^{-4}$	$0.3 \times 10^{-6}$
$\rho^{300^\circ\text{K}}$ ( $\Omega\text{-cm}$ )	$1.6 \times 10^{-4}$	$1 \times 10^{-4}$	$1.5 \times 10^{-4}$	$2.2 \times 10^{-4}$	$1.6 \times 10^{-4}$	[10 <sup>2</sup> ]	$2.5 \times 10^{-4}$	$0.4 \times 10^{-4}$	$8 \times 10^{-6}$
$\rho^{400^\circ\text{K}}$ ( $\Omega\text{-cm}$ )	$1.8 \times 10^{-4}$					$1 \times 10^{-4}$	$10 \times 10^{-4}$		
$\alpha$ °K <sup>-1</sup> (300°K)	$1.7 \times 10^{-3}$		$2.8 \times 10^{-3}$	$\sim 4 \times 10^{-3}$	$2.8 \times 10^{-3}$		$9.4 \times 10^{-3}$		
$R_H$ cm <sup>3</sup> /Cb	$-1.1 \times 10^{-3}$		$-1.9 \times 10^{-3}$		$4.5 \times 10^{-4}$				
$S$ $\mu\text{V}/^\circ\text{C}$	$\equiv 0.24$		$\equiv 0.16$		$\equiv 0.96$	$\equiv 0.1$			
$\chi_M^{300^\circ\text{K}}$	$-28$	$-23$	$+3$	$-7$	$-13$	$+30$			
$T_{N/C/d}$ °K	$+4000$	$900$	$40$	$170$	$180$	$630_{(40^\circ\text{K})}$		$200$	(very low)
$T_s$ °K	(C) $120^\circ$	(N) $90^\circ$	(N?) $155^\circ$		(N) $145^\circ$	(d) $341^\circ$	(C) $394^\circ$		
Plasma edge	$0.9$ eV		$1.5$ eV		$1.0$ eV				$2.0$ eV

† A recent band structure calculation for ReO<sub>3</sub> by L. F. Mattheis, *Phys. Rev.*, 1969, **181**, 987 puts the width of the carrier holding d-band in that case at 2.5 to 3 eV.

pyrite lattice constant shows a marked peak at  $\text{NiS}_2$ . This would seem to be absent for the selenides, and could well be an indicator of the quasi-ionic localized character of the electrons close to  $\text{NiS}_2$ , where the  $e_g^*$  band is in the half-filled condition. The semiconductivity and paramagnetism could arise from a breakdown in band behaviour under high correlation at this point. The very high value of  $\theta_P$  ( $\sim -750^\circ\text{K}$ ), and the low value of  $\chi$  and  $p_{\text{eff}}$  (2.48 in place of 2.83 ideally, or 3.2 more typically for the  $\text{Ni}^{2+}$  ion) are characteristic of materials leaving the ionic regime, cf.  $\text{NiO}$ ,  $\text{NiI}_2$ ,  $\text{NiS}$ ,  $\text{Cr}_2\text{S}_3$ ,  $\text{TiBr}_3$ ,  $\text{TiI}_2$ . An examination of the electrical properties of  $\text{NiS}_2$  under pressure would be interesting. Of course it is possible that under the action of the crystal field in the somewhat distorted octahedra of the pyrite structure a normal band gap opens up in the  $e_g^*$  band. This, however, would leave the magnetic properties unexplained.

Fig. 91



Possible banding arrays for the triplet of group VIIIc semiconductors  $\text{NiS}_2$ ,  $\text{PdS}_2$ ,  $\text{PtS}_2$ .

Such a band gap does provide a satisfactory account of the diamagnetic semiconducting behaviour of  $\text{PdS}_2$  and  $\text{PdSe}_2$ . Here the pyrite structure has been quite severely distorted by elongation along one of the cube axes (see fig. 11). Figure 91 contrasts the proposed banding diagrams for the triplet of VIIIc semiconductors  $\text{NiS}_2$ ,  $\text{PdS}_2$ ,  $\text{PtS}_2$ . A second form of  $\text{PdS}_2$ , reverting towards a pyrite structure, is obtained under high pressure, in which the  $a$  and  $b$  axes are expanded somewhat and the  $c$  axis is contracted by almost  $\frac{1}{2}$  Å (Munson and Kasper 1969). The metallic nature of this form contrasts with the high resistivity and Seebeck coefficient of the normal semiconducting form ( $E_g^{\text{elec}} \sim 0.8$  eV—Hulliger 1965). Semiconductivity

and diamagnetism is also surprisingly obtained in the rather complex low temperature structures of the group VIIIb materials  $\text{IrSe}_2$ ,  $\text{RhSe}_2$ ,  $\text{IrS}_2$ . This contrasts strongly with the metallic character of the rest of group VIIIb, including the alternative pyrite forms of  $\text{RhSe}_2$  and  $\text{IrS}_2$ . The  $\text{IrSe}_2$  structure is built on units of the marcasite structure, and the semi-conductivity seems to result from the stacking break of the anion layers (see fig. 10), resulting in fewer X-X pairs than would otherwise occur. Orbitals then drop from the X-X\* band and absorb the surplus electrons into the valence bands. The straight group VIIIb marcasite  $\text{CoSe}_2$  is a metal (Ramdohr 1955).

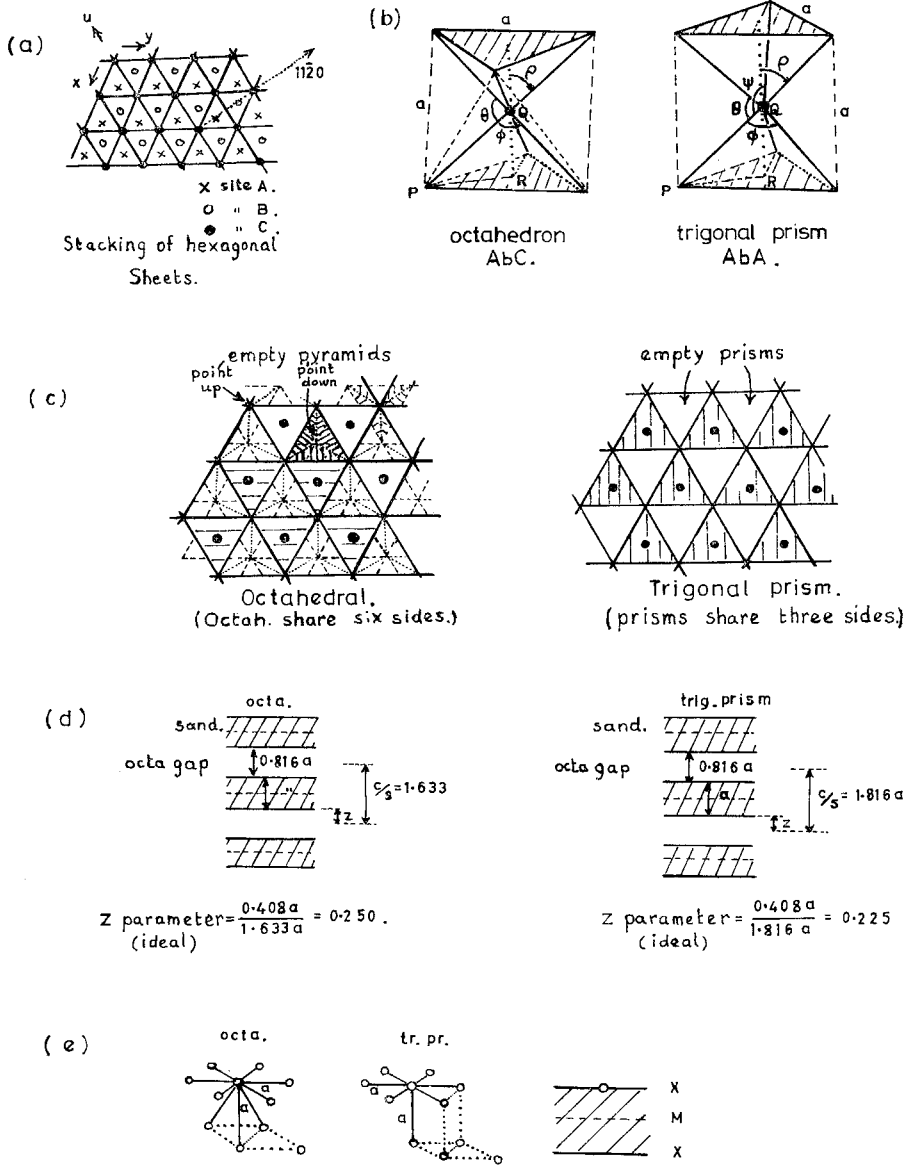
The marcasites of group VIIIa (viz.  $\text{FeS}_2/\text{Se}_2/\text{Te}_2$ ) are small gap semi-conductors similar to the corresponding pyrites. There is still an X-X pair per unit, and the two band structures are likely to be similar, with 14 deep valence electrons and six in the non-bonding  $t_{2g}$  band. In the marcasite structure the octahedra share a couple of edges (see fig. 8), rather than being linked by the corners as in the pyrite form, with the result that rows of metal atoms are formed parallel to  $c$  as in the rutile structure (fig. 73). When one electron is removed from the  $t_{2g}$  band (as in  $\text{FePS}$  or  $\text{CoAs}_2$ —Hulliger and Mooser 1965) metal-metal *pairing* occurs in this chain yielding the distorted arsenopyrite structure ( $E0_7$ ). The semiconductivity and diamagnetism here resemble that of low temperature  $\text{VO}_2$ . When two electrons are removed, as in  $\text{RuP}_2$  (isoelectronic with  $\text{MoS}_2$ ), the marcasite structure shows a *regular* contraction parallel to  $c$ , and semi-conductivity again results. The same occurs for  $\text{CrSb}_2$ , where now only the lower third of the non-equivalent  $t_{2g}$  states are occupied. With yet two fewer electrons again, as in  $\text{TiP}_2$ , we obtain a metallic  $\text{PbCl}_2$ -like material, and not an insulating marcasite or pyrite (at least not at normal pressure), despite the precedent of the pyrite  $\text{SiP}_2$ .

In general the properties of the pnictides are likely to be more difficult to interpret than those of the corresponding chalcogenides, because of the smaller energy separations and the more general state mixing. In their band structures of the three rocksalt materials  $\text{TiO}$ ,  $\text{TiN}$  and  $\text{TiC}$ , Ern and Swittendick (1965) show the sort of progression in mixing to expect.

### 9.2. *The Development of Crystal Structure through the Transition Metal Dichalcogenides*

In the above sections we have dealt with most of the transition metal dichalcogenides and noted how the structure type moves from layered structures, first regular, then distorted, through to marcasite and pyrites, finally to return via the intermediates  $\text{IrSe}_2$  and  $\text{PdS}_2$  to the flattened layer structures like  $\text{PtS}_2$ . The movement is influenced by both group number and period number—that is, electron configuration and atom size. By looking at the structure parameters in detail we can study these changes more closely.

Fig. 92



Comparison of the geometry of the ideal octahedral and trigonal prism  $TX_2$  layer structures.

Downloaded by [18.140.1.248] at 15:50 06 April 2015

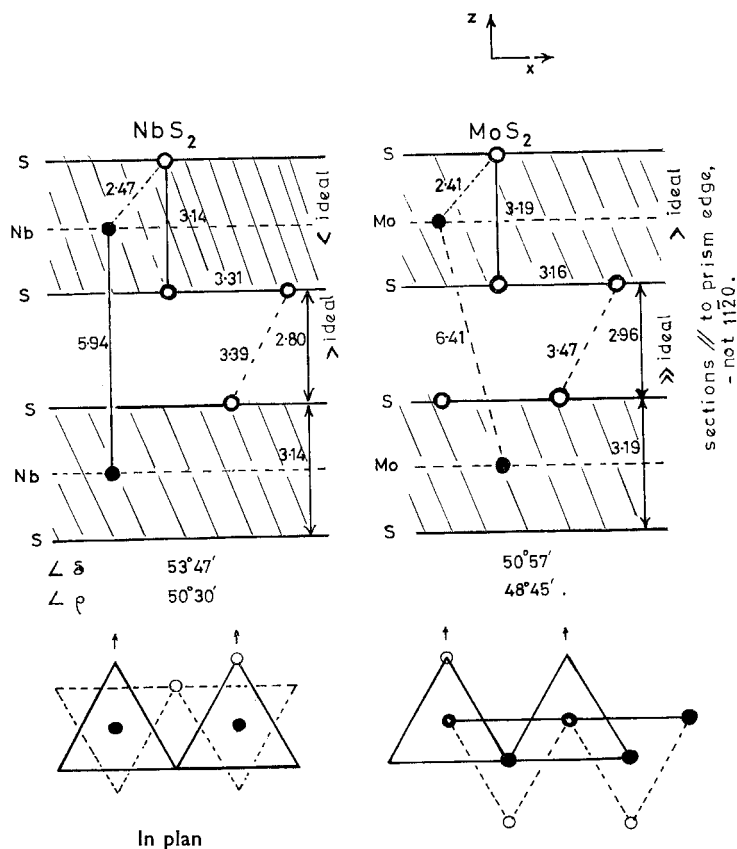
Table 18. Comparison of the geometry of the ideal octahedral and trigonal prism TX<sub>2</sub> layer structures (see fig. 92)

	Octahedron		Trigonal prism
(a) With common lattice constant <i>a</i> . All coordination unit sides = <i>a</i>			
Bond length	$B_0 = 0.707a$	<	$B_p = 0.763a$
Unit height	$h_0 = 0.816a$	<	$h_p = a$
Unit volume	$V_0 = 0.471a^3$	>	$V_p = 0.434a^3$
Coordination units as fraction of sandwich	$\frac{2}{3}$	>	$\frac{1}{2}$
Gap height	$g_0 = h_0 = 0.816a$	=	$g_p = g_0 = 0.816a$
Cell parameter	$c_0 = 1.633a_0$	<	$c_p = 1.816a_p$
(b) With common bond length of $0.763a_p$			
Lattice constant	$a_0 = 1.08a_p$	>	$a_p$
Unit height	$h_0 = 0.882a_p$	<	$h_p = a_p$
Gap height	$g_0 = h_0 = 0.882a_p$	>	$g_p = h_0 = 0.816a_p$
$c_0 = h_0 + g_0$	$= 1.764a_p$	<	$c_p = h_p + g_p = 1.816a_p$
(c) Angles in structure			
(i) In coordination unit			
$\angle$ XMX, $\theta$ and $\phi = 90^\circ 00'$ (12)	>		$81^\circ 47'$
$\angle$ XMX, $\psi = 180^\circ 00'$ (3)	>		$135^\circ 35'$ (fig. 92 (a))
$\angle$ zMX, $\rho = 54^\circ 45'$	<		$49^\circ 07'$
(ii) In gap, octahedral sites			
$\angle$ zOX, $\delta = 54^\circ 45'$	=		$54^\circ 45'$
(d) Number of X-X close neighbours within single sandwich			
9 (i.e. 6 + 3) at <i>a</i>	>		7 (i.e. 6 + 1) at <i>a</i> (fig. 92 (d))
(e) Further parameters			
(i) <i>z</i> (taken from middle of gap)	0.250	>	0.225 (fig. 92 (c))
(ii) $\chi = \frac{\text{X-X measured across gap}}{\text{X-X standard v.d.W.}}$			Standards S 3.7 Å Se 4.0 Å Te 4.4 Å

First we shall look at the changes which occur in the layer structures of groups IV, V, VI and VII. The parameters were collected in tables 2 and 3. These should be compared with the ideally coordinated situation, as represented in table 18 and fig. 92. As is seen in part (a) of this table, for a common lattice constant *a*, the bond length is shorter with the octahedral coordination than for the trigonal prism. Since the bond length is of primary energetic importance, part (b) of the table shows the data converted to a common bond length. Under these conditions the octahedral *a* parameter is the greater of the two by about 8%. We begin by comparing materials which exist in both octahedral and trigonal prism forms. The *a* parameters of 1T-TaS<sub>2</sub> and TaSe<sub>2</sub> are indeed found to be greater than

those of the trigonal prism forms (e.g. 2H, 3R), but in fact by only 1%. As mentioned in § 8.2, a refined structure analysis of the 1T materials is not available, but for the trigonal prism tantalum materials it is known that  $a$  is greater than for ideal coordination (from the angles X-M-X). Furthermore, in the octahedral 1T forms the very large values of  $c/a$  might indicate that there  $a$  is a little less than ideal.

Fig. 93



A comparison of the structure deformations in 2H-MoS<sub>2</sub> and 2H-NbS<sub>2</sub>.  
(Note not 1120 sections.)

A major cause in the build up of the  $c/a$  ratios above ideality is likely to be 'c' expansion due to the repulsive X-X interaction between the top and bottom layers of each individual MX<sub>2</sub> sandwich. This is seen by noting that

- (i)  $c/a$  for Ti > Zr or Hf materials; also for VSe<sub>2</sub> > 1T-TaSe<sub>2</sub>,
- (ii)  $c/a$  for all tellurides > corresponding selenides > sulphides.

i.e. the bigger the X atoms in proportion to the M atom, the bigger is the value of  $c/a$  for the resulting structure. From the existing trigonal prism data of table 2 it is seen that both the sandwich coordination units and also the van der Waals gap heights are likely to follow these same sequences, e.g.

	MoS <sub>2</sub>	$\alpha$ -MoTe <sub>2</sub>	
Unit $\angle\rho$	48° 45'	48° 15'	(A smaller angle means greater elongation $\parallel c$ )
Gap $\angle\delta$	50° 57'	50° 29'	

Unfortunately no refined data are available for the group IV materials, other than TiS<sub>2</sub>. The increase in the *gap* elongation on passing from sulphide to telluride is likely to occur as a reaction to the relative reduction in  $a$ . Actually this 'riding up' effect appears to be somewhat offset by a second effect. The van der Waals force parameter  $\chi$  shows in fact that the attractive force across the gap is a little *stronger* in proportion in the telluride than in the sulphide. The latter effect presumably arises because the interacting X-sheets are individually packed more densely in the telluride than in the sulphide. Figure 14 shows the interesting results obtained by plotting  $c/a$  for all these compounds against the separation between the outer electrons of neighbouring X-atoms in such a sheet. Effective orbit radii for this purpose are drawn from Slater (1965, p. 103). The plot reveals the much greater distinction that exists *between* the groups of the Periodic Table than within them. The following data make the contrast between group IV and group V :

	$a$	$c$	$c/a$	Atomic radii of metal
HfSe <sub>2</sub>	3.75	6.16	1.643	1.59 Å
↑		↓		↑
1T-TaSe <sub>2</sub>	3.48	6.27	1.804	1.46
↓		↑		≈
.....				
TiSe <sub>2</sub>	3.53	6.00 Å	1.698	1.47

The expansion in the value of the  $c$  parameter of 1T-TaSe<sub>2</sub> is not solely an atom size effect, as is seen from the comparison with TiSe<sub>2</sub>. It is also the product of the single non-bonding electron of 1T-TaSe<sub>2</sub> lying in the orbital, shown in fig. 25 (b), where the horizontal lobes force the X-atom sheets apart. In  $\beta$ -MoTe<sub>2</sub> and ReSe<sub>2</sub>, with two or three non-bonding electrons respectively, the averaged value of  $c/a$  rises to over 1.9. It is to be remembered that these two materials are in addition distorted somewhat by metal-metal bonding in the layers, as also are the group V tellurides. The effective anisotropy in these compounds due to the

contraction in the chains (measured by the ratio of ' $a_{\text{effective}}$ ' taken perpendicular and parallel to the chains) is for  $\text{NbTe}_2$  2.5%, for  $\text{WTe}_2$  3.8%, and for  $\text{ReSe}_2$  11.5% (see fig. 72)†.

It is also noteworthy that the octahedral and trigonal prismatic forms of  $\text{TaS}_2$  and  $\text{TaSe}_2$  are more closely similar in  $c/a$  ratio, than are the trigonal prism compounds of group V to those of group VI. Indeed it seems that the 1T forms pass over smoothly into the 2H, 3R and  $4\text{H}_a$  forms via the intermediate  $4\text{H}_b$  and 6R, where octahedral and trigonal prismatic coordination coexist (see p. 302). Figure 93 outlines the marked change in shape which occurs between 2H-NbS<sub>2</sub> (group V) and 2H-MoS<sub>2</sub> (group VI). When it is recalled that, for 'ideal' trigonal prism coordination, the height of the coordination unit and the van der Waals length should both equal the lattice parameter, it is seen that the MoS<sub>2</sub> coordination unit is somewhat extended [ $c$ , particularly relative to that of NbS<sub>2</sub>]. In fact the group V value is below 'ideal', so accounting for the affinity to the 1T form. Further, in MoS<sub>2</sub> the van der Waals length is seen to be very large in comparison to  $a$ , though the absolute value of this length remains less than 'standard' (see  $\chi$  parameter, table 2). The elongated character of MoS<sub>2</sub>/Se<sub>2</sub>/Te<sub>2</sub> is in part due to the very small size of the molybdenum atom; indeed it is one of the smallest atoms to form a layered chalcogenide. The plot of fig. 14 reveals the highly compacted character of the sandwiches, for  $\alpha\text{-MoTe}_2$  in particular. A second factor causing elongation parallel to  $c$  in the MoS<sub>2</sub> family is the action of the filled non-bonding  $d_{z^2}$  orbital (see fig. 25), pushing the X-atom sheets apart. Conversely in NbS<sub>2</sub> this orbital is only half-filled, and the relative contraction of the sandwich and gap in this case may be in part due to intersandwich bonding. Indeed in several of the group V polytypes there is a tendency for the metal atoms to line up parallel to  $c$ , which is not shown in the two group VI polytypes—see fig. 3. (N.B. 3R is only metastable for group V.)

The very large value of  $c/a$  for  $\alpha\text{-MoTe}_2$  marks the limit for the regular structures, and the value is relaxed somewhat in the distorted octahedral layer structures of  $\beta\text{-MoTe}_2$ ,  $\text{WTe}_2$ , and the technetium and rhenium compounds. It has been reported that a pyrite form of  $\text{ReS}_2$  also exists. The lattice parameter at 5.57 Å is a little smaller than that of  $\text{OsS}_2$ , and a whole  $\frac{1}{2}$  Å smaller than that of  $\text{MnS}_2$ , indicating that it does not share the quasi-ionic character of its 3d analogue. In the pyrite structure the coordination octahedra are linked by the corners only, with the metal atoms falling on a regular three-dimensional face-centred cubic array (fig. 7). This produces a much denser structure in general (Mn compounds excluded) than does a layer type arrangement, with its 'wasted' van der Waals space. The arrangement of octahedra to achieve the pyrite packing necessitates close X-X approaches, so that the manganese compounds in particular

† N.B. A comparison between  $\text{TiTe}_2$  and  $\text{TaTe}_2$  quickly reveals the contraction present in the latter which is absent from the selenide. As mentioned in § 8.2 the structure of 1T-TaS<sub>2</sub>/Se<sub>2</sub> is a little strange, but it retains a much higher degree of pseudo-hexagonal symmetry than does the telluride.

finish by resembling the NaCl structure (shown by  $\alpha$ -MnS), with the X-X pairs acting as a divalent group. In all three manganese dichalcogenides the X-X distance is very close to that in the elementary form of the respective chalcogen. Such pairings could well contribute 50 kcal/mole ( $> 2$  eV) to the total binding energy. Similar pairings are also present in marcasite (where the octahedra share edges) and in the IrSe<sub>2</sub> structure. Table 5 shows how towards the edge of the non-layered domain—as defined by table 15 (b)—the X-X pairings are weakened, to allow a material like RhTe<sub>2</sub> to move through to the cadmium iodide structure (contrast RuTe<sub>2</sub>).

The *layer* compounds of group VIII all have in common a very low value of  $c/a$ . In PtS<sub>2</sub>, for example, although the platinum atom is the same size as the molybdenum atom, the  $a$  parameter is 10% greater than for MoS<sub>2</sub>. The sandwich flattening in PtS<sub>2</sub> is likely to result from the completely filled non-bonding d orbitals. The tilted lobes of these orbitals lie closer to the  $c$  axis than do the bonding orbitals (see fig. 25), so forcing the latter to splay out somewhat. The two sulphur planes of each sandwich now lie closer together, to produce S-S distances *through* the sandwich that are quite small (3.06 Å, as compared with 3.19 Å for MoS<sub>2</sub>). This is reminiscent of the behaviour in the pseudo-layer structure of PdS<sub>2</sub> (see fig. 11) where this distance has shrunk to 2.13 Å. The gap height also in PdS<sub>2</sub> is only 2.6 Å compared with 2.75 Å in PtS<sub>2</sub>. The van der Waals gap parameter  $\chi$  for PtS<sub>2</sub> is quite high at 0.93, but because of the large value of  $a$  angle  $\delta$  appears rather large. However, as one goes to the selenide and telluride the gap contracts strongly. Indeed all the group VIII tellurides have a gap height of only about 2.5 Å as compared with 3.35 Å in  $\alpha$ -MoTe<sub>2</sub>†. The metallic properties of Pt/Pd/NiTe<sub>2</sub> indicate that the conduction band is overlapping the d bands, and the energetics of the situation are far from simple. Structure determining factors are in general known to be a very small fraction of the total energy locked in any compound, as the heats of formation of polymorphic forms reveal.

Finally we return to groups V and VI to mention the only transition metal dichalcogenides not to exist—viz. VS<sub>2</sub> and CrS<sub>2</sub>/Se<sub>2</sub>/Te<sub>2</sub>. (N.B. the pyrite RhS<sub>2</sub> is very metal deficient.) Chromium and vanadium form a whole series of chalcogenides (see Jellinek 1963), e.g. M<sub>5</sub>X<sub>6</sub>, M<sub>3</sub>X<sub>4</sub>, M<sub>2</sub>X<sub>3</sub>, converting a NiAs-type structure through towards a CdI<sub>2</sub> type (see fig. 15) by the progressive abstraction of metal atoms from alternate metal sheets. However, the most chalcogen rich products obtained, even under high pressure, have only the composition M<sub>5</sub>X<sub>8</sub> (Sleight and Bither 1969). The

† PtS<sub>2</sub> displays a very large disparity in expansion coefficient  $\parallel$  and  $\perp c$

Expansion coefficients		PtS <sub>2</sub>	PtSe <sub>2</sub>	PdTe <sub>2</sub>	CdI <sub>2</sub>	
$\alpha$	$\parallel c$	37	20	30	40	$\times 10^{-6} \text{ } ^\circ\text{C}^{-1}$
	$\perp c$	2.3	5.7	12	10	

(Kjekshus and Grønvold 1959).

effective  $c/a$  ratio of  $\text{Cr}_5\text{Se}_8$ , reckoned as a non-stoichiometric layer structure, is 1.605, the very low value of which is an indication as to why the end product  $\text{CrSe}_2$  does not form†. Certainly a nominal valency of 4 for chromium is not impossible, as  $\text{CrO}_2$  shows. This latter compound is a rutile, and closely similar to  $\text{MoO}_2$ , but without the metal-metal bonding of the latter. '4' is of course a more acceptable valency for molybdenum, and  $\text{MoS}_2$  forms its natural ore, 'molybdenite'. The stability of  $\text{Cr}_2\text{S}_3$  relative to the instability of  $\text{Mo}_2\text{S}_3$  underlines the preference of chromium for trivalency. This also serves to explain why pressure does not lead to production of a pyrite form of  $\text{CrS}_2$ . The pseudo-divalency required for the pyrite form is not in line with the high degree of s-d mixing still present in chromium compounded with a chalcogen. Divalency can be induced by chlorine, and  $\text{CrCl}_2$  forms as a Jahn-Teller distorted marcasite (Tracy *et al.* 1961). The absence of Jahn-Teller type distortion in the octahedra of the pyrite and marcasite structures of the  $d^7$  cobalt dichalcogenides of course underlines that these chalcogenides are not ionic in the standard sense, there being a fair degree of d mixing into the valence band as discussed in § 9.1.  $\text{MoCl}_2$  is again quite different from  $\text{CrCl}_2$ , being a distorted layer structure, and without ligand field spectra (Clark 1964). The layer halides will be discussed in the next section, but the plot of fig. 14 shows how similar the simple ionic dihalide structures are irrespective of group number—in sharp contrast to the dichalcogenides.

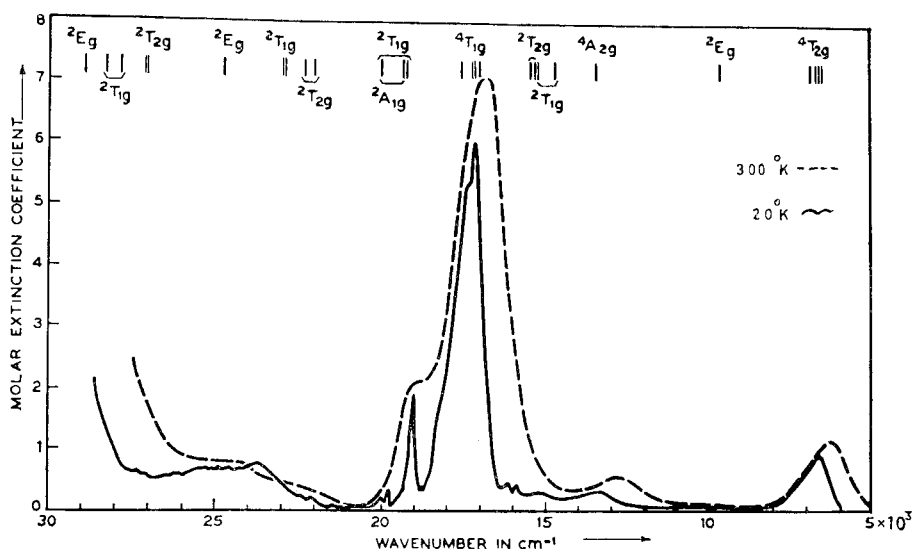
### 9.3. Survey of the Properties of the Layer-type Transition Metal Halides

The majority of the transition metal dihalides (in anhydrous form) adopt the layer structure of  $\text{CdCl}_2$  or  $\text{CdI}_2$ ‡. As seen earlier all the layered dichalcogenides are of covalent rather than ionic character, i.e. they do not show the low intensity many-electron d state 'crystal field' spectra, are not salt-like paramagnetics, and in appropriate cases exhibit metallic conduction. Among the dihalides, however, compounds such as  $\text{CoCl}_2$ ,  $\text{MnCl}_2$  and  $\text{VCl}_2$  are all typically salt-like by such criteria. Furthermore, they show the long 'bond' lengths typical of ionic materials (e.g.  $\text{CoCl}_2$ , experiment 2.52 Å, sum of atomic radii 2.35 Å—Slater 1965, p. 308ff). The pyrite dichalcogenides are intermediate between these groups,  $\text{MnS}_2$  being salt-like, but  $\text{CoS}_2$  showing delocalization and metallic properties. As in the monoxide and monosulphide families the greatest degree of localization is to be expected for manganese, this tendency decreasing towards the edges of the period (3d), viz. towards nickel and particularly towards titanium. The origins of this effect were discussed in § 5.1. Indeed the superconducting metallic properties of TiO (Denker 1964) tempt one to look at  $\text{TiCl}_2/\text{Br}_2/\text{I}_2$  for possible metallic properties, whilst the metal/insulator

†  $c/a$  for the isostructural  $\text{V}_5\text{Se}_8$  is 1.715, and  $\text{VSe}_2$  goes on to form with  $c/a = 1.82$  (Røst and Gjertsen 1964). In these  $\text{T}_5\text{X}_8$  products the metal deficient sheets are only one-third full.

‡ Excluding the fluorides.

Fig. 94



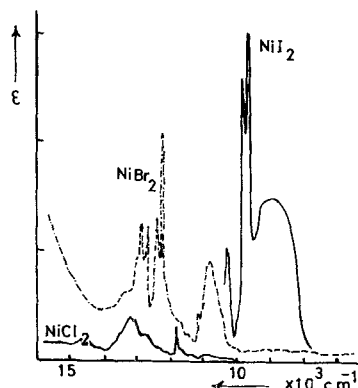
Ligand field spectrum of  $\text{CoCl}_2$ . (Ferguson *et al.* 1963.)

transition in  $\text{NiS}$  (Sparks and Komoto 1968) and also possibly  $\text{NiS}_2$  point to  $\text{NiCl}_2/\text{Br}_2/\text{I}_2$  as an interesting series. What data there are at present available supports this. The following table shows the run of the bond length and susceptibility criteria through the nickel halide series.

	Ni-X distance		$\chi^{300^\circ\text{K}}$ Molar (c.g.s.)	Colour
	Experiment	Atom sum		
$\text{NiCl}_2$	2.51	2.35	6150	Yellow
$\text{NiBr}_2$	2.64	2.50	5600	Brown
$\text{NiI}_2$	2.78	2.75 Å (ref. above)	$3880 \times 10^{-6}$	Black

The melting point of these nickel halides is also  $300^\circ\text{C}$  higher than those of the corresponding manganese, iron and cobalt salts. The ligand field spectra of the latter halides have been reported in several papers (see Hush and Hobbs 1968) and show nothing like the red shift and gain in intensity for these transitions that is found in the nickel case (see fig. 95). This is reminiscent of the behaviour observed in the series  $\text{MnO}/\text{MnS}/\text{MnSe}$  (Lohr and McClure 1968), or the layer compounds  $\text{CrCl}_3/\text{Br}_3/\text{I}_3$  (Dillon *et al.* 1966).

Fig. 95



Ligand field spectra of  $\text{NiCl}_2$ ,  $\text{NiBr}_2$  and  $\text{NiI}_2$  (as the gaseous  $\text{TX}_2$  linear molecule species). (De Kock and Gruen 1967.)

The Néel point in  $\text{TiI}_2$  ( $d^2$ ) appears to be in the region of  $200^\circ\text{K}$  and the susceptibility is of low magnitude ( $\sim 1800 \times 10^{-6}$  c.g.s./mole at  $300^\circ\text{K}$ —Klemm and Grimm 1942 b—compare for the  $(d\gamma)^6 (d\epsilon)^2 \text{Ni}^{2+}$  ion in  $\text{NiCl}_2$  above, where the value is much higher). For  $\text{TiCl}_2\text{T}_\text{N}$  is reported as  $85^\circ\text{K}$  (Lewis *et al.* 1962). Such values should be compared with  $\text{MnCl}_2$   $2^\circ\text{K}$ ,  $\text{CoCl}_2$   $25^\circ\text{K}$ ,  $\text{NiBr}_2$   $60^\circ\text{K}$  (collected data, Goodenough 1963). Both  $\text{TiI}_2$  and  $\text{TiCl}_2$  are black with high continuous absorption in the photon energy range 1 to 4 eV (Clark 1964). We intend to investigate these compounds directly and under pressure to see whether they exhibit metallic properties above or below the Néel point. If they are metallic only above this temperature they would resemble  $\alpha\text{-NiS}$ ; if metallic only below this temperature they may provide the first clear cut example of a Mott-type insulator to metal transition. In these compounds where band formation is in a critical stage the effect of pressure could be very marked (cf.  $\text{MnTe}_2$ —see § 9.1). Pressure has been shown (via detailed analysis of the ligand field spectra—Zahner and Drickamer 1961) to increase the degree of covalency in the salts  $\text{MnCl}_2$ ,  $\text{NiCl}_2$ , etc.

In  $\text{VCl}_2$  the d overlap is less than for  $\text{TiCl}_2$  (cf.  $\text{VO}$  versus  $\text{TiO}$ ) and ligand field spectra are obtained from the pale yellow crystals (Clark 1964). Crystals of  $\text{VBr}_2$  are red, and of  $\text{VI}_2$  again black †, following the covalency rise. The covalency rise on moving to the 4d zirconium dihalides is matched by a marked drop in susceptibility to  $\sim 150 \times 10^{-6}$  c.g.s. units/mole (Lewis *et al.* 1962). This is less than that of  $\text{NiS}$  ( $\sim 220 \times 10^{-6}$  c.g.s. units/mole—Sparks and Komoto 1968). As always in these cases of incipient band formation, there is at the moment some doubt concerning the stability of the regular structure (Klemm and Grimm 1942 a), but an electron diffraction

† Two forms exist for  $\text{VI}_2$ , black and red (Juza *et al.* 1969), but the structural difference is slight and as yet undetermined.

pattern would readily detect a distortion of the type found in  $\beta$ -MoTe<sub>2</sub> (also with 18 valence electrons). Many of the 4d and 5d dihalides, such as NbCl<sub>2</sub>, MoCl<sub>2</sub>, WI<sub>2</sub>, PdCl<sub>2</sub>, do indeed have more complex structures than their 3d counterparts, so denying simple comparisons (Canterford and Colton 1968).

An interesting comparison can be made between VBr<sub>2</sub> and VSe<sub>2</sub>, both CdI<sub>2</sub>-type materials. The former is salt-like, the latter a metal. The metal-metal spacings in the sandwiches are 3.77 and 3.35 Å amounting to 41 and 25% increases respectively on the spacing in elemental vanadium. These percentages should be compared with the following :

MnI <sub>2</sub>	NiI <sub>2</sub>	VI <sub>2</sub>	TiI <sub>2</sub>	·	Zr/Nb/MoTe <sub>2</sub>	·	Zr/Nb/MoS <sub>2</sub>	·	MnS <sub>2</sub>	FeS <sub>2</sub> <sup>P</sup>	FeS <sub>2</sub> <sup>M</sup>
·	·	·	·	·	·	·	·	·	·	·	·
65	56	54	40	·	25	·	14	·	71	52	34%
·	·	·	·	·	·	·	·	·	·	·	·

Of course the non-metallic properties of VBr<sub>2</sub> are not just induced by the larger metal atom separation, but also by the more electronegative role of the halide ligand in causing d shell contraction (see § 5.1). The band properties apparent in the pyrites FeS<sub>2</sub>, CoS<sub>2</sub>, etc. emphasize moreover, that the formation of these bands, though prominently based on the metal d states, is mediated to some extent by the chalcogenide states.

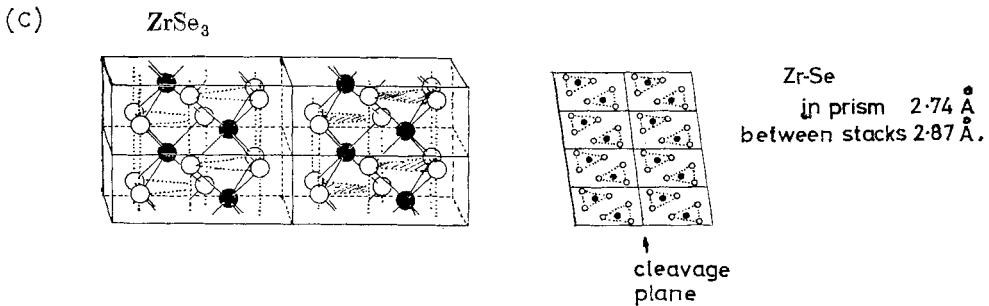
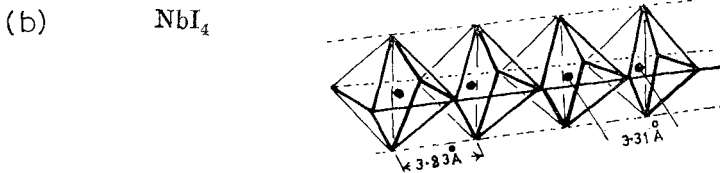
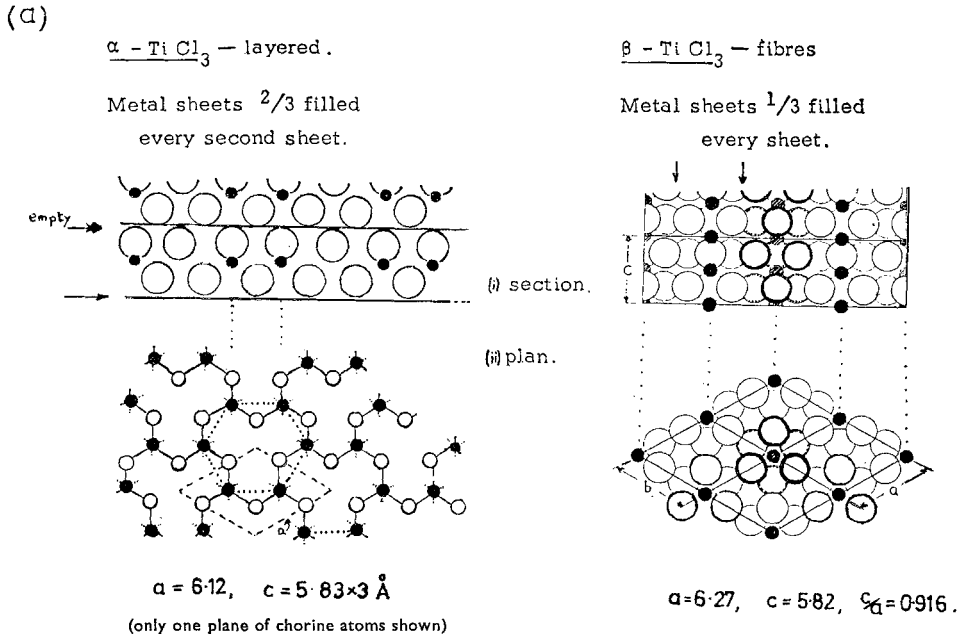
Such mixing is dependent on the basic  $\sigma\sigma^*$  ('charge transfer') energy. We can get a fair idea of what energies of this kind will be from the spectra of the corresponding manganese and zinc compounds, where d transitions are either weak or absent, e.g.

MnS/ZnS, $E_g \approx 3.9$ ev ; (Ford <i>et al.</i> 1963)	MnI <sub>2</sub> /ZnI <sub>2</sub> , $E_g \approx 3.2$ ev ; (Tubbs 1968)	MnS <sub>2</sub> /ZnS <sub>2</sub> , $E_g \approx 3$ ev. (Bither <i>et al.</i> 1968)
--	---	---

For ZnCl<sub>2</sub>,  $E_g \sim 7$  ev, and so throughout the transition metal dichlorides halide mixing with the metal states will be at a minimum. Hence our interest in possible isolated d band metallic properties for ZrCl<sub>2</sub>, etc. It is not only the dihalides but also the tri-halides of group IV which offer interesting possibilities in this respect.

The metal-metal spacing is only a little closer (3.555 Å versus 3.561 Å) in  $\alpha$ -TiCl<sub>3</sub> than in the divalent TiCl<sub>2</sub>. No refined data are available on the Ti-Cl bond lengths.  $\alpha$ -TiCl<sub>3</sub> has the 'honey-comb' metal layer sandwich structure shown in fig. 96 (a). With one non-bonding electron per metal atom it is in a condition deserving comparison with VO<sub>2</sub>, NbSe<sub>2</sub> or CoSe<sub>2</sub>. There is a very sharp drop in its susceptibility occurring at 217°K (Ogawa 1960). Just above this temperature  $\chi$  reaches a value of  $1100 \times 10^{-6}$  c.g.s. units/mole—a fairly salt-like value (cf.  $\chi_M^{300^\circ}$  for the more ionic TiF<sub>3</sub> (d<sup>1</sup>) and Cu(NO<sub>3</sub>)<sub>2</sub> · 6H<sub>2</sub>O (d<sup>9</sup>  $\equiv$  d<sup>1</sup>) of  $1300 \times 10^{-6}$  and  $1625 \times 10^{-6}$  respectively) ;

Fig. 96



Crystal structures of the linear chain compounds. (a)  $\beta\text{-TiI}_3$ , based on Dahl *et al.* 1964. (b)  $\text{NbI}_4$ , based on Dahl *et al.* 1962. (c)  $\text{ZrSe}_3$ , based on Kronert and Plieth 1965.

below  $217^\circ\text{K}$ ,  $\chi$  for  $\alpha\text{-TiCl}_3$  quickly drops to one-tenth the value. For further comparison the peak susceptibilities of some 'one-electron' *band* compounds are for  $\text{CoSe}_2$  ( $90^\circ\text{K}$ )  $1400 \times 10^{-6}$ , for  $\text{VO}_2$  ( $340^\circ\text{K}$ )  $700 \times 10^{-6}$ , and for  $\text{NbSe}_2$  ( $160^\circ\text{K}$ ) only  $200 \times 10^{-6}$ . From optical absorption (Baldini *et al.* 1968) it would seem that  $\alpha\text{-TiCl}_3$  is an insulator both above and below the discontinuity temperature, since the single ligand-field peak of the  $d^1$  'ion' is seen in both ranges. Infra-red, pressure and conductivity measurements at low temperatures would be valuable. There is also a possibility of structure distortion below  $T_d$ —certainly the volume contracts by almost 2% (Ogawa 1960)—a value equal but *opposite* to that in NiS (Sparks and Komoto 1963).

Again the materials tend to opt out of this critical condition by adopting an alternative structure.  $\beta\text{-TiCl}_3$  has the very interesting structure shown in fig. 96 (*a*). It seems that this is the normal form adopted by  $\text{TiI}_3$  and the Zr and Hf trihalides (Dahl *et al.* 1964). All these  $\beta$  materials appear at first sight to have the possibility of being metals as they show low constant paramagnetism  $\sim 200 \times 10^{-6}$  c.g.s./mole (Lewis *et al.* 1962, Llemm and Krose 1947) and no longer exhibit the ligand field peak (Clark 1964, Baldini *et al.* 1968). Indeed it is possible in the Zr and Hf compounds that absorption is rising into the infra-red, as if from free carriers (Schläfer and Wille 1967). No electrical or optical absorption measurements on single crystals have as yet been made. As is seen from fig. 96 (*a*) the  $\beta\text{-TiCl}_3$  structure consists of 'independent' linear stacks of face-sharing octahedra, and this raises the interesting possibilities of linear chain metals in general. In particular superconductivity may occur at highish temperatures (see Dzyaloshinskii and Katz 1969—contrast Ginzburg 1968, p. 367 ff). ( $\beta$ )- $\text{HfI}_3$  would seem to offer an excellent chance for linear chain metal behaviour, since the metal-metal distance in the chains at  $3.3 \text{ \AA}$  is only  $0.1 \text{ \AA}$  larger than the distance in hafnium metal itself. Indeed in  $\text{ZrCl}_3$  this distance is  $\sim 0.1 \text{ \AA}$  shorter than in the element. There are, however, some slight indications of metal-metal bonding and a superstructure forming within the chains (Struss and Corbett 1969, Watts 1966, Schnering 1966). In  $\text{NbI}_4$  and  $\text{TaI}_4$ , where chains of octahedra share edges, the metal atoms are definitely grouped in displaced pairs (fig. 96 (*b*)), but there (as with l.t.  $\text{VO}_2$ ) the compound is diamagnetic (Schnering 1963). In the  $\text{ZrSe}_3$  family, where we have stacks of trigonal prisms (fig. 96 (*c*)), we again end with diamagnetic semiconductors (McTaggart and Wadsley 1958, Kronert and Plieth 1965) due to some cross-linking between the stacks. Hence the  $\beta\text{-TiCl}_3$  family could possibly stand in a unique position.

We do not wish to enter into further discussion of these halides until our experimental work on these systems is more advanced, but the above survey does serve to show in what manner the halides usefully complement the chalcogenides in any investigation of bonding and banding in transition metal compounds. On the experimental and practical side, however, there is one great disadvantage that the halides suffer relative to most of the chalcogenides. They are extremely susceptible to chemical attack by moist air.

## § 10. SUMMARY AND CONCLUSION

Our own experimental work has been based on optical studies of the  $\text{MoS}_2$  type layer dichalcogenides. Because of the unique properties of such structures we automatically have taken an interest in layer materials in general. Further, since the layered dichalcogenides like  $\text{ZrS}_2$ ,  $\text{NbS}_2$ ,  $\text{MoS}_2$ ,  $\text{ReS}_2$  and  $\text{PtS}_2$  show a wide range of electrical and optical properties of the narrow d band type, we have also looked in this paper for comparisons with the neighbouring non-layered transition metal dioxides (e.g.  $\text{TiO}_2$ ,  $\text{VO}_2$ ,  $\text{CrO}_2$ ) and dichalcogenides (e.g.  $\text{MnS}_2$ ,  $\text{FeS}_2$ ,  $\text{CoS}_2$ ,  $\text{NiS}_2$ ). Both halves of the dichalcogenide family, layered and non-layered, have much in common and take up an interesting position in the general progression of transition metal compounds. This progression is one of d state participation in crystal binding and band formation. The dichalcogenides fall between the 'ionic' localized d state materials such as the halides and oxysalts on the one hand, and the binary 'alloy materials' such as  $\text{CrSb}$ ,  $\text{V}_3\text{Si}$  or  $\text{MoAl}_2$  on the other. In fact they just span the critical overlap condition for d band conduction,  $\text{MnS}_2/\text{Se}_2/\text{Te}_2$  alone behaving quasi-ionically.  $\text{NiS}_2$  seems to sit right on the dividing line. In  $\text{CoS}_2/\text{Se}_2$  and  $\text{VSe}_2$  overlap conditions are just sufficient to allow itinerant band magnetism to develop. In the layered  $\text{NbS}_2$  family band antiferromagnetism occurs along with superconductivity (cf. M. H. Cohen 1967).  $\text{CuSe}_2$ ,  $\text{RhSe}_2$ ,  $\beta\text{-MoTe}_2$ ,  $\text{PdTe}_2$  are among the other superconductors.

Much theoretical effort has of late gone into describing the narrow d band condition and incipient band formation, via the Hubbard Hamiltonian and the strong correlation problem (see Kemeny, Arai, Caron, etc. Int. Conf. on Metal/Non-metal Transition, *Rev. mod. Phys.*, **40**, No. 4 (Oct. 1968)). Two simpler effective one-electron descriptions of this complex situation have been developed at M.I.T. and by J. C. Slater's group (see Adler and Feinleib 1969— $\text{NiO}$ ; T. M. Wilson 1969— $\text{MnO}$ ). Slater's spin-polarized A. P. W. procedure (Slater 1968) in a case like that of  $\text{MnO}$  will allow a good estimate to be obtained of the ligand field d-d transition energies. The method is identical with that used on magnetic metals, e.g. ferromagnetic Ni (Connolly 1967) and antiferromagnetic Cr (Yamashita *et al.* 1968). It would be very interesting to see a calculation of this type made for the band antiferromagnets like  $\text{NbS}_2$ , particularly in view of their superconducting properties. A recent paper by Rice *et al.* (1969) has stressed the formal similarity in the theories of band antiferromagnetism and superconductivity.

Temporary band models for the  $\text{TX}_2$  layer compounds have been produced above, which explain satisfactorily the present optical and electrical data. These involve fairly 'pure' d bands with widths ranging from 0.4 to 2 eV. The models were derived with the aid of the chemical bond molecular orbital approach. Indeed a more localized valence band model is now receiving considerable attention from theoretical physicists (see Anderson 1968, Jarós 1968, Heine and Jones 1969).

A most interesting feature of  $\text{NbS}_2$  is its intimate relation to the semiconductor  $\text{MoS}_2$  (cf.  $\text{CoS}_2$ , which is a metal, relative to  $\text{FeS}_2$ , which is a

semiconductor). Complete solid solution between the two allows the electron concentration to be manipulated at will, and offers wide scope to the magnetic and superconducting properties. The very strong excitonic features in the optical absorption spectrum of  $\text{MoS}_2$  have been observed under conditions of controlled screening via Nb doping. The excitons in pure  $\text{MoS}_2$  have rather large binding energy ( $\sim 0.05$  eV) and are very temperature stable. Remanent humps even occur in the spectrum of  $\text{NbS}_2$ . Indeed it is possible that the excitonic interaction may contribute to the cause of superconductivity in these compounds. The Bose-Einstein condensation and superfluidity of excitons seems also to be a possibility for these materials (see Gergel *et al.* 1968). The strongly two-dimensional character of layer crystals adds to the possibility of finding new extremal states of matter.

Perhaps the most unusual material of this family of compounds is the 1T form of  $\text{TaS}_2$ . This appears to be superconducting and yet possibly not even a semi-metal.  $\beta\text{-MoTe}_2$  is similar in being diamagnetic and superconducting, but is definitely a semi-metal, although the free-carrier absorption does not start until well into the infra-red. A preliminary investigation of 1T- $\text{TaS}_2$  would seem to indicate a much smaller lattice distortion than that of  $\beta\text{-MoTe}_2$ , and one moreover which appears incommensurate with the basic lattice. It is just possible that the state may arise from an excitonic insulator type of effect, across a small inter d band gap, created when a narrow closed d band falls away from the bulk of empty d states under strong correlation. Certainly, in  $\alpha\text{-MoTe}_2$ , we seem to have a set of bands that will allow the excitonic insulator theory (Halperin and Rice 1968) to be tested at high pressures and low temperatures.

The various stacking polytypes of a given layer compound have interesting small variations in lattice parameter, but unexpectedly large variations can occur in certain other properties, e.g. in group VI, the spin-orbit splitting of exciton states; and in group V, the superconducting transition temperatures. This indicates that there remains considerable interaction between the sandwiches of the layer structures despite the very large electrical and thermal anisotropy in these materials. The same is likely to be true also for a linear chain material like  $\text{ZrI}_3$ , and indeed such cross interaction is essential if superconductivity is to be found in such a material.

Clearly a considerable amount of effort is likely to be expended in the near future on these materials, the spot light most probably falling on the group V dichalcogenide metals. The group IV layer and chain halides would also look to be a field which could be studied with profit.

#### ACKNOWLEDGMENTS

We would like to thank past and present members of this laboratory for their help and advice. In particular we thank Dr. Connell, Dr. Liang and

Mr. Bromley for allowing us to use their unpublished results. We have benefited greatly from stimulating discussions with Professor Sir Nevill Mott, F.R.S.

## REFERENCES

- ABDULLAEV, G. B., GUSEINOVA, E. S., and TAGIEV, B. G., 1967, *Phys. Stat. Sol.*, **20**, 421.
- ADACHI, K., SATO, K., and TAKEDA, M., 1969, *J. phys. Soc. Japan*, **26**, 631.
- ADLER, D., 1968, *Solid St. Phys.*, **21**, 1.
- ADLER, D., and BROOKS, H., 1967, *Phys. Rev.*, **155**, 826.
- ADLER, D., and FEINLEIB, J., 1969, *J. appl. Phys.*, **40**, 1586.
- ALCOCK, N. W., and KJEKSHUS, A., 1965, *Acta chem. scand.*, **19**, 79.
- ALLEN, P. B., and COHEN, M. L., 1969, *Phys. Rev.*, **177**, 707.
- ALTMANN, S. L., and BRADLEY, C. J., 1967, *Proc. phys. Soc.*, **92**, 764.
- AMELINCKX, S., 1964, *Phys. Stat. Sol. suppl.*, **6**, §10.
- ANDERSON, P. W., 1968, *Phys. Rev. Lett.*, **21**, 13.
- ANDRES, K., KUEBLER, N. A., and ROBIN, M. B., 1966, *J. Phys. Chem. Solids*, **27**, 1747.
- ANDRIYASHIK, M. V., SAKHNOVSKII, M., TIMOFEEV, V. B., and YAKIMOVA, A. S., 1968, *Phys. Stat. Sol.*, **28**, 277.
- AOYAGI, K., MISU, A., SHINADA, M., *et al.*, 1966, *J. phys. Soc. Japan*, **21**, 174.
- APPEL, J., 1968, *Solid St. Phys.*, **21**, 193.
- ARCO, A. J., MARCUS, J. A., and REED, W. A., 1968, *Phys. Rev.*, **176**, 671.
- ASANABE, S., 1961, *J. phys. Soc. Japan*, **16**, 1789.
- ASNIN, V. M., and ROGACHEV, A. A., 1967, *Phys. Stat. Sol.*, **20**, 755.
- ASNIN, V. M., ROGACHEV, A. A., and RYVKIN, S. M., 1968, *Soviet Phys. Semicond.*, **1**, 1447.
- AU YANG, M. Y., and COHEN, M. L., 1969, *Phys. Rev.*, **178**, 1279.
- BALDINI, G., POLLINI, I., and SPINOLO, G., 1968, *Phys. Stat. Sol.*, **27**, 95.
- BARINSKII, R. L., and VAINSHTEIN, E. E., 1957, *Izv. Akad. Nauk SSSR. Ser. Fiz.*, **21**, 1375.
- BARKER, A. S., VERLEUR, H. W., and GUGGENHEIM, H. J., 1966, *Phys. Rev. Lett.*, **17**, 1286.
- BARRICELLI, L. B., 1958, *Acta crystallogr.*, **11**, 75.
- BARSTAD, J., GRØNVOLD, F., RØST, E., and VESTERSJO, E., 1966, *Acta chem. scand.*, **20**, 2865.
- BASSANI, F., GREENAWAY, D. L., and FISCHER, G., 1964, *VIIIth Conf. on Semiconductors*, Paris, p. 51.
- BASSANI, F., and PARRAVICINI, G. P., 1967, *Nuovo Cim. B*, **50**, 95.
- BENNEMANN, K. H., GARLAND, J. W., and MUELLER, F. M., 1969, *Phys. Rev. Lett.*, **23**, 169.
- BERNARD, J., and JEANNIN, Y., 1962, *Adv. in Chem. 'Non-stoichiometric Compounds'*, p. 191.
- BIEMAN, J. L., 1962, *Phys. Rev.*, **127**, 1093.
- BITHER, J. A., BOUCHARD, R. J., CLOUD, W. H., DONOHUE, P. C., and SIEMONS, W. J., 1968, *Inorg. Chem.*, **7**, 2208.
- BJERKELUND, E., and KJEKSHUS, A., 1967, *Acta chem. scand.*, **21**, 513.
- BONGERS, P. F., *et al.*, 1968, *J. Phys. Chem. Solids*, **29**, 977.
- BORGHESE, F., and DONATO, E., 1968, *Nuovo Cim. B*, **53**, 283.
- BOUCHARD, R. J., 1968, *Mat. Res. Bull.*, **3**, 563.
- BREBNER, J. L., and FISCHER, G., 1962, *Vith Int. Conf. Semiconductors*, Exeter, p. 760.
- BREBNER, J. L., and MOOSER, E., 1967, *Physics Lett. A*, **24**, 274.

- BRIXNER, L. H., 1962, *J. Inorg. nucl. Chem.*, **24**, 257 ; 1963, *J. electrochem. Soc.*, **110**, 289.
- BRIXNER, L. H., and TEUFER, G., 1963, *Inorg. Chem.*, **2**, 992.
- BROWN, B. E., 1966, *Acta crystallogr.*, **20**, 264.
- BROWN, B. E., and BEERNTSEN, D. J., 1965, *Acta crystallogr.*, **18**, 31.
- BUSCH, G., FROHLICH, C., HULLIGER, F., and STEIGMEIER, E., 1961, *Helv. Phys. Acta*, **34**, 359.
- CANTERFORD, J. H., and COLTON, R., 1968, *Halides of the Transition Elements* (Wiley Interscience).
- CHAMBERLAND, B. L., 1967, *Mater. Res. Bull.*, **2**, 827.
- CHAMPION, J. A., 1965, *Br. J. appl. Phys.*, **16**, 1035.
- CHAMPNESS, C. H., and KIPLING, A. L., 1965, *Can. J. Phys.*, **44**, 769.
- CLARK, R. J. H., 1964, *J. chem. Soc.*, p. 417.
- CLENENDEN, R. L., and DRICKAMER, H. G., 1966, *J. chem. Phys.*, **44**, 4223.
- COHEN, M. H., 1967, *Fermi School Physics*, **37**, 403.
- COHEN, M. L., and KOONCE, C. S., 1966, *VIIIth Conf. on Semiconductors*, Kyoto, p. 633. *J. phys. Soc. Japan*, **21**, Suppl.
- CONNELL, G. A. N., WIETING, T., WILSON, J. A., and YOFFE, A. D., 1968, *IXth Conf. on Semiconductors*, Moscow, p. 414.
- CONNELL, G. A. N., WILSON, J. A., and YOFFE, A. D., 1968, *J. Phys. Chem. Solids*, **30**, 287.
- CONNOLLY, J. W. D., 1967, *Phys. Rev.*, **159**, 415.
- CONROY, L. E., and PARK, K. C., 1968, *Inorg. Chem.*, **7**, 459.
- DAHL, L. F., CHIANG, T. I., SEABURGH, P. W., and LARSEN, E. M., 1964, *Inorg. Chem.*, **13**, 1236.
- DAHL, L. F., and WAMPLER, D. L., 1962, *Acta crystallogr.*, **15**, 903.
- DAS, D. (now Mrs. Paul), 1968, *Indian J. Phys.*, p. 943.
- DEKOCK, C. W., and GRUEN, D. M., 1967, *J. chem. Phys.*, **46**, 1096.
- DENKER, S. P., 1964, *J. Phys. Chem. Solids*, **25**, 1397.
- DEXTER, D. L., and KNOX, R. S., 1965, *Excitons* (New York : Interscience).
- DICKENS, P. G., and NEILD, D. J., 1968, *Proc. Faraday Soc.*, **64**, 13.
- DILLON, J. F., KAMIMURA, H., and REMEIKI, J. P., 1966, *J. Phys. Chem. Solids*, **27**, 1531.
- DOMINGO, G., ITOGA, R. S., and KANNEWUF, C. R., 1966, *Phys. Rev.*, **143**, 536.
- DONOHUE, P. C., SIEMONS, W. J., and GILLSON, J. L., 1968, *J. Phys. Chem. Solids*, **29**, 807.
- DZYALOSHINSKII, I. E., and KATZ, E. I., 1969, *Soviet Phys. JETP*, **28**, 178.
- ERN, V., and SWITENDICK, A. C., 1965, *Phys. Rev. A*, **137**, 1927.
- EVANS, B. L., 1966, *Proc. R. Soc. A*, **289**, 275.
- EVANS, B. L., and YOUNG, P. A., 1965, *Proc. R. Soc. A*, **284**, 402 ; 1967 a, *Ibid.*, **298**, 74 ; 1967 b, *Proc. phys. Soc.*, **91**, 475 ; 1968, *Phys. Stat. Sol.*, **25**, 417.
- FEINLEIB, J., SCOULER, W. J., and FERRETTI, A., 1968, *Phys. Rev.*, **165**, 765.
- FERGUSON, J., WOOD, D. L., and KNOX, K., 1963, *J. chem. Phys.*, **39**, 881.
- FILLINGHAM, P. J., 1967, *J. appl. Phys.*, **38**, 4823.
- FISCHER, F., 1969, *Phys. Stat. Sol.*, **31**, 601.
- FISCHER, D. W., and BAUN, W. L., 1968, *J. appl. Phys.*, **39**, 4757.
- FIVAZ, R., 1966, *Helv. Phys. Acta*, **39**, 247 ; 1967, *J. Phys. Chem. Solids*, **28**, 839.
- FIVAZ, R., and MOOSER, E., 1964, *Phys. Rev. A*, **136**, 833 ; 1967, *Ibid.*, **163**, 743.
- FORD, R. A., KAUER, E., RABENAU, A., and BROWN, D. A., 1963, *Bunsenges*, **67**, 460.
- FRANZEN, H. F., SMEGGIL, J., and CONARD, B. R., 1967, *Mater. Res. Bull.*, **2**, 1087.
- FRINDT, R. F., 1965, *Phys. Rev. A*, **140**, 536 ; 1966, *J. appl. Phys.*, **37**, 1928.

- FRINDT, R. F., and YOFFE, A. D., 1963, *Proc. R. Soc. A*, **273**, 69.
- FURUSETH, S., SELTE, K., and KJEKSHUS, A., 1965, *Acta chem. scand.*, **19**, 257.
- GAHWILLER, C., and HARBEKE, G., 1968, March. Am. Phys. Soc. Meeting, Berkeley.
- GAY, J. G., ALBERS, W. A., and ARLINGHAUS, F. J., 1968, *J. Phys. Chem. Solids*, **29**, 1449.
- GELLER, S., 1955, *J. Am. chem. Soc.*, **77**, 2641.
- GERGEL, V. A., KAZARINOV, R. F., and SURIS, R. A., 1968 a, *Soviet Phys. JETP*, **26**, 354; 1968 b, *Ibid.*, **27**, 159.
- GINZBURG, V. L., 1968, *Contemp. Phys.*, **9**, 355.
- GOBRECHT, H., SEECK, S., and KLOSE, T., 1966, *Z. Phys.*, **190**, 427.
- GOODENOUGH, J. B., 1963, *Magnetism and the Chemical Bond* (Interscience); 1966, *J. appl. Phys.*, **37**, 1415; 1967 a, *Mater. Res. Bull.*, **2**, 37; 1967 b, *Ibid.*, **2**, 165; 1967 c, *Czech. J. Phys. B*, **17**, 304; 1968 a, *J. appl. Phys.*, **39**, 403; 1968 b, *Phys. Rev.*, **171**, 466; 1968 c, *Mater. Res. Bull.*, **3**, 409.
- GRAESER, S., 1964, *Schweiz Min. Pet. Mitt.*, **44**, 121.
- GREENAWAY, D. L., and HARBEKE, G., 1965, *J. Phys. Chem. Solids*, **26**, 1585; 1966, *VIIIth Conf. on Semiconductors*, Kyoto, p. 151.
- GREENAWAY, D. L., and NITSCHKE, R., 1965, *J. Phys. Chem. Solids*, **26**, 1445.
- GRIMMEIS, V. H. G., RABENAU, A., HAHN, H., and NESS, P., 1961, *Bunsenges*, **65**, 9.
- GRØNVOLD, F., HAGBERG, O., and HARALDSEN, H., 1958, *Acta chem. scand.*, **12**, 971.
- GRØNVOLD, F., and RØST, E., 1957, *Acta crystallogr.*, **10**, 329.
- GUGGENBERGER, L. J., and JACOBSON, R. A., 1968, *Inorg. Chem.*, **7**, 2257.
- GUGGENHEIM, J., HULLIGER, F., and MULLER, J., 1966, *Helv. phys. Acta*, **34**, 408.
- GUSEINOV, G. D., and RASULOV, A. I., 1966, *Phys. Stat. Sol.*, **18**, 911.
- HALPERIN, B. I., and RICE, T. M., 1968, *Solid St. Phys.*, **21**, 116.
- HALPERN, J., 1966, *J. phys. Soc. Japan*, **21**, 180. (Kyoto Conf.)
- HARALDSEN, H., 1966, *Angew. Chem.* (int. ed.), **5**, 58.
- HARALDSEN, H., GRØNVOLD, F., and HURLEN, T., 1956, *Z. Anorg. allg. Chem.*, **283**, 143.
- HARPER, P. G., and HILDER, J. A., 1968, *Phys. Stat. Sol.*, **26**, 69.
- HASTINGS, J. M., ELLIOTT, N., and CORLISS, L. M., 1959, *Phys. Rev.*, **115**, 13.
- HATTORI, M., ADACHI, K., and NAKANO, H., 1969, *J. phys. Soc. Japan*, **26**, 642.
- HEINE, V., and JONES, R. O., 1969, S. 2, *Proc. R. Soc., Sol. Stat. Phys.*, **2**, 719.
- HICKS, W. T., 1964, *J. electrochem. Soc.*, **111**, 1058.
- HOCKINGS, E. F., and WHITE, J. G., 1960, *J. phys. Chem.*, **64**, 1042.
- HOLSETH, H., and KJEKSHUS, A., 1968, *J. less-common Metals*, **16**, 472.
- HOLT, S. L., and WOLD, A., 1967, *Inorg. Chem.*, **6**, 1595.
- HUFFMAN, D. R., 1969, *J. appl. Phys.*, **40**, 1334.
- HUISMAN, R., and JELLINEK, F., 1969, *J. less-common Metals*, **17**, 111.
- HULLIGER, F., 1960, *Helv. Phys. Acta*, **33**, 959; 1963, *Nature, Lond.*, **200**, 1064; 1964, *Ibid.*, **204**, 644; 1965, *J. Phys. Chem. Solids*, **26**, 639.
- HULLIGER, F., and MOOSER, E., 1965, *Prog. Solid St. Chem.*, **2**, 330.
- HULTGREN, R., 1932, *Phys. Rev.*, **40**, 891.
- HUSH, N. S., and HOBBS, R. J. M., 1968, *Prog. Inorg. Chem.*, **10**, 259.
- HYLAND, G. J., 1968, *Proc. phys. Soc.*, S. 2, **1**, 189.
- ISKENDEROV, R. N., DRABKIN, I. A., EMELYANOVA, L. T., and KSENDZOV, M., 1968, *Soviet Sol. Stat.*, **10**, 2031.
- JAMES, P. B., and LAVIK, M. T., 1963, *Acta crystallogr.*, **16**, 1183.
- JARRETT, H. S., CLOUD, W. H., BOUCHARD, R. J., BUTLER, S. R., and FREDERICK, C. G., 1968, *Phys. Rev. Lett.*, **21**, 617.

- JELLINEK, F., 1962, *J. less-common Metals*, **4**, 9 ; 1963, *Arkiv Kemi*, **20**, 447.
- JELLINEK, F., BRAUER, G., and MULLER, H., 1960, *Nature, Lond.*, **4710**, 376.
- JOHNSTON, W. D., MILLER, R. C., and DAMON, D. H., 1965, *J. less-common Metals*, **8**, 272.
- JOHNSTONE, V. A., 1956, *Prog. in Semiconductors* (ed. Gibson), **1**, 65 (London : Heywoods).
- JORGENSEN, K. C., 1967, *Prog. inorg. Chem.*, **8**, 120.
- JUZA, D., GIEGLING, D., and SCHÄFFER, H., 1969, *Z. anorg. allg. Chem.*, **366**, 121.
- KABASHIMA, S., 1966, *J. phys. Soc. Japan*, **21**, 945.
- KAMIMURA, H., and NAKAO, K., 1968, *J. phys. Soc. Jap.*, **24**, 1313 (68).
- KATSUKI, S., 1969, *J. phys. Soc. Japan*, **26**, 58.
- KELDYSHE, L. V., and KOZLOV, A. N., 1968, *Soviet Phys. JETP*, **27**, 521.
- KERSHAW, R., VLASSE, M., and WOLD, A., 1967, *Inorg. Chem.*, **6**, 1599.
- KHODADAD, P., 1961, *Bull. Soc. Chim. France*, p. 133.
- KITTEL, C., 1967, *Introduction to Solid State Physics*, 3rd edition (Wiley).
- KJESKSHUS, A., and GRØNVOLD, F., 1959, *Acta chem. scand.*, **13**, 1767.
- KJESKSHUS, A., and PEARSON, W. B., 1964, *Prog. Sol. Stat. Chem.*, **1**, 83 ; 1965, *Can. J. Phys.*, **43**, 438.
- KLEMM, W., and GRIMM, L., 1942 a, *Z. Anorg. allg. Chem.*, **249**, 198 ; 1942 b, *Ibid.*, **249**, 209.
- KLEMM, W., and KROSE, E., 1947, *Z. Anorg. allg. Chem.*, **253**, 209.
- KNOX, R. S., 1963, *Theory of Excitons* (Academic Press).
- KOGAN, V. G., and TAVGER, B. A., 1966, *Soviet Phys. Solid St.*, **8**, 808.
- KOONCE, C. S., and COHEN, M. L., 1969, *Phys. Rev.*, **177**, 707.
- KOONCE, C. S., COHEN, M. L., SCHOOLEY, J. F., HOSLER, W. R., and PFEIFFER, E. R., 1967, *Phys. Rev.*, **163**, 380.
- KRONERT, W., and PLIETH, K., 1965, *Z. Anorg. allg. Chem.*, **336**, 207.
- KÜBLER, J., 1968, *Z. Phys.*, **208**, 249.
- KÜBLER, J. K., 1969, *Physics Lett. A*, **29**, 43.
- LADD, L. A., and PAUL, W., 1969, *Solid St. Commun.*, **7**, 425.
- LAGRENAUDIE, J., 1954, *J. de Physique*, **15**, 299.
- LEE, H. N. S., MCKINZIE, H., TANNHAUSER, D. S., and WOLD, A., 1969, *J. appl. Phys.*, **40**, 602.
- LEPETIT, P. A., 1965, *J. de Physique*, **26**, 175.
- LEUNG, P. C., ANDERMANN, G., SPITZER, W. G., and MEAD, C. A., 1966, *J. Phys. Chem. Solids*, **27**, 849.
- LEWIS, J., MACHIN, D. J., NEWNHAM, I. E., and NYHOLM, R. S., 1962, *J. chem. Soc.*, p. 2036.
- LIANG, W. Y., 1967, *Physics Lett. A*, **24**, 573.
- LIANG, W. Y., and CUNDY, S. L., 1969, *Phil. Mag.*, **19**, 1031.
- LIANG, W. Y., and YOFFE, A. D., 1968, *Phys. Rev. Lett.*, **20**, 59.
- LIN, M. S., and HARKER, H., 1968, *Solid St. Commun.*, **6**, 687.
- LOHR, L. I., and McCLURE, D. S., 1968, *J. chem. Phys.*, **49**, 3516.
- McTAGGART, F. K., and WADSLEY, A. B., 1958, *Aust. J. Chem.*, **11**, 445.
- MAHAN, G. D., 1967 a, *Phys. Rev.*, **153**, 882 ; 1967 b, *Phys. Rev. Lett.*, **18**, 448.
- MAKAROV, V. P., 1968, *Soviet Phys. JETP*, **27**, 173.
- MALLINSON, R. B., RAYNE, J. A., and URE, R. W., 1969, *Phys. Rev.*, **175**, 1049.
- MANSFIELD, R., and SALAAM, S. A., 1953, *Proc. phys. Soc. B*, **66**, 377.
- MARCUS, S. M., 1968, *Physics Lett. A*, **27**, 585.
- MEADEN, G. T., and SZE, N. H., 1969, *Physics Lett. A*, **29**, 162.
- MINOMURA, S., and DRICKAMER, H. G., 1963, *J. appl. Phys.*, **34**, 3043.
- MIYAHARA, S., and TERANISHI, T., 1968, *J. appl. Phys.*, **39**, 896.
- MOTT, N. F., 1967, *Adv. Phys.*, **16**, 49 ; 1968, *Rev. mod. Phys.*, **40**, 677 ; 1969, *Phil. Mag.* **20**, 1.

- MULLER, A., KREBS, B., GLEMSEK, O., and DIEMANN, E., 1967, *Z. Naturf. B*, **22**, 1235.
- MUNSON, R. A., 1968, *Inorg. Chem.*, **7**, 389.
- MUNSON, R. A., DE SORBO, W., and KOUVEL, J. S., 1967, *J. chem. Phys.*, **47**, 1769.
- MUNSON, R. A., and KASPER, J. S., 1969, G.E.C. Report 69-C-047.
- NEBENZAHL, I., 1969, *Phys. Rev.*, **177**, 1001.
- NIKITINE, S., SCHMITT-BURKEL, J., BIELLMAN, J., and RINGEISSEN, J., 1964, *J. Phys. Chem. Solids*, **25**, 951.
- OGAWA, S., 1960, *J. phys. Soc. Japan*, **15**, 1901.
- PHILLIPS, J. C., 1966, *Solid St. Phys.*, **18**, 55.
- PHILLIPS, J. C., and VAN VECHTEN, J. A., 1969, *Phys. Rev. Lett.*, **22**, 705.
- PUOTINEN, D., and NEWNHAM, R. E., 1963, *Acta crystallogr.*, **16**, 1183.
- QUINN, R. K., SIMMONS, R., and BANEWICZ, J. J., 1966, *J. phys. Chem.*, **70**, 230.
- RADO, G. T., and SUHL, S., 1963/6, *Magnetism*, 4 vols. (Academic Press).
- RALPH, H. I., 1965, *Solid St. Commun.*, **3**, 303.
- RAMDOHR, P., 1955, *Chem. Abs.*, **49**, 13,027 f.
- RAU, J. W., and KANNEWUF, C. R., 1966, *J. Phys. Chem. Solids*, **27**, 1097.
- REGNAULT, F., AIGRAIN, P., DUGAS, C., and JANCOVICI, B., 1952, *C. r. hebd. Séanc. Acad. Sci., Paris*, **235**, 31.
- REVOLINSKY, E., and BEERNTSEN, D., 1964, *J. appl. Phys.*, **35**, 2086 ; 1966, *J. Phys. Chem. Solids*, **27**, 523.
- REVOLINSKY, E., BROWN, B. E., BEERNTSEN, D., and ARMITAGE, C. H., 1965, *J. less-common Metals*, **8**, 63.
- RICE, T. M., BARKER, A. S., HALPERIN, B. J., and McWHAN, D. B., 1969, *J. appl. Phys.*, **40**, 1337.
- ROGERS, D. B., SHANNON, R. D., SLEIGHT, A. W., and GILLSON, J. L., 1969, *Inorg. Chem.*, **8**, 841.
- RØST, E., and GJERTSEN, L., 1964, *Z. Anorg. allg. Chem.*, **328**, 299.
- RØST, E., GJERTSEN, L., and HARALDSEN, H., 1964, *Z. Anorg. allg. Chem.*, **333**, 301.
- RUDORFF, W., 1965, *Chimia*, **19**, 489.
- SALAAM, S. A., 1960, *Proc. Math. Phys. Soc. U.A.R.*, **24**, 41.
- SALZANO, F. J., and STRONGIN, M., 1967, *Phys. Rev.*, **153**, 533.
- SATO, K., ADACHI, K., OKAMOTO, T., and TATSUMOTO, E., 1969, *J. phys. Soc. Japan*, **26**, 639.
- SAWAOKA, A., MINOMURA, S., and MIYAHARA, S., 1966, *J. phys. Soc. Japan*, **21**, 1017.
- SCHAFER, H., 1964, *Chemical Transport Reactions* (Academic Press).
- v. SCHLÄFER, H. L., and WILLE, H. W., 1967, *Z. Anorg. allg. Chem.*, **351**, 279.
- v. SCHNERING, H. G., 1966, *Naturwissenschaften*, **53**, 359.
- SCHOOLEY, J. F., and THURBER, W. R., 1966, *J. phys. Soc. Japan*, **21**, 639.
- SELTE, K., BJERKELUND, E., and KJEKSHUS, A., 1966, *J. less-common Metals*, **11**, 14.
- SELTE, K., and KJEKSHUS, A., 1964, *Acta chem. scand.*, **18**, 697 ; 1965, *Ibid.*, **19**, 258.
- SENTLE, F. E., and THORPE, A. N., 1968, *Phys. Rev.*, **175**, 1144.
- SHANKS, H. R., SIDLES, P. H., and DANIELSON, G. C., 1962, *Adv. in Chem.* 'Non-stoichiometric Compounds', p. 237.
- SHAW, R. F., 1969, Ph.D. Thesis, Cambridge University.
- SHINADA, M., and SUGANO, S., 1965, *J. phys. Soc. Japan*, **20**, 1274.
- SIENKO, M. J., 1962, *Adv. in Chem.* 'Non-stoichiometric Compounds', p. 224.
- SILVERMAN, M. S., 1966, *Inorg. Chem.*, **5**, 2067 ; 1967, *Ibid.*, **6**, 1063.
- SLATER, J. C., 1965, *Quantum Th. of Molecules and Solids*, Vol. 2 (McGraw-Hill) ; 1968, *J. appl. Phys.*, **39**, 761.

- SLEIGHT, A. W., and BITHER, T. A., 1969, *J. Inorg. Chem.*, **8**, 566.
- SLEIGHT, A. W., BITHER, T. A., and BIERSTEDT, P. E., 1969, *J. Phys. Chem. Solids*, **30**, 299.
- SORRELL, C. A., 1968, *J. Am. ceram. Soc.*, **51**, 285.
- SPARKS, J. T., and KOMOTO, T., 1963, *J. appl. Phys.*, **34** (II), 1191 ; 1968, *Rev. mod. Phys.*, **40**, 752.
- SPIERING, G. A., REVOLINSKY, E., and BEERNTSEN, D. J., 1966, *J. Phys. Chem. Solids*, **27**, 535.
- SPYRIDELIS, J., DELAVIGNETTE, P., and AMELINKCX, S., 1968, *Mater. Res. Bull.*, **3**, 31.
- STARK, R. W., and FALICOV, L. M., 1967, *Phys. Rev. Lett.*, **19**, 795.
- STRUSS, A. W., and CORBETT, J. D., 1969, *Inorg. Chem.*, **8**, 227.
- SWANSON, H. E., *et al.*, 1955, N.B.S. Structure Circ. No. 529, MoS<sub>2</sub>, **5**, 47 ; 1958, *Ibid.*, WS<sub>2</sub>, **8**, 65.
- TAKEUCHI, Y., and NOWACKI, W., 1964, *Schweiz Min. Pet. Mitt.*, **44**, 105.
- TINKHAM, M., 1966, *Optical Properties of Metals and Alloys*, edited by Abeles (North-Holland), p. 431.
- TOWLE, L. C., OBERBECK, V., BROWN, B. E., and STAJDOHAR, R. E., 1966, *Science, N.Y.*, **154**, 895.
- TOYAZAWA, Y., and HERMANSON, J., 1968, *Phys. Rev. Lett.*, **21**, 1637.
- TRACY, J. W., DUNITZ, J. D., RUNDLE, R. E., YANKEL, H. L., *et al.*, 1961, *Acta crystallogr.*, **14**, 927.
- TRLIFAJ, M., 1968, *Czech. J. Phys. B*, **18**, 1576.
- TUBBS, M. R., 1968, *J. Phys. Chem. Solids*, **29**, 1191.
- UYEDA, R., 1968, *Acta crystallogr.*, A, **24**, 175.
- UYEDA, R., and NONOYAMA, M., 1968, *J. appl. Phys.*, **7**, 200.
- VAND, V., and HANOKA, J. I., 1968, *J. appl. Phys.*, **39**, 5288.
- VAN MAAREN, M. H., and SCHAEFFER, G. M., 1966, *Physics Lett*, **20**, 131; 1967, *Ibid.*, **24A**, 645.
- VAN MAAREN, M. H., and HARLAND, H. B., 1969, *Phys. Lett.*, **29A**, 571.
- VARSAANYI, F., ANDRES, K., and MAREZIO, M., 1969, *J. chem. Phys.*, **50**, 5027.
- VERLEUR, A. W., BARKER, A. S., and BERGLUND, C. N., 1968, *Phys. Rev.*, **172**, 788.
- VIJH, A. K., 1968, *J. Phys. Chem. Solids*, **29**, 2233 ; 1969, *J. Phys. Chem. Sol.*, **30**, 1999.
- WATTS, J. A., 1966, *J. inorg. Chem.*, **5**, 281.
- WESTRUM, E. F., CARLSON, H. G., GRØNVOLD, F., and KJEKSHUS, A., 1961, *J. chem. Phys.*, **35**, 1670.
- WIETING, T., 1968, Ph.D. Thesis, Cambridge.
- WILDERVANCK, J. C., and JELLINEK, F., 1964, *Z. Anorg. allg. Chem.*, **328**, 309.
- WILSON, J. A., 1969, *J. Phys. Chem. Solids* (to be published).
- WILSON, T. M., 1969, *J. appl. Phys.*, **40**, 1588.
- YAMASHITA, J., ASANO, S., and WAKOH, S., 1968, *J. appl. Phys.*, **39**, 1274.
- ZAHNER, J. C., and DRICKAMER, H. G., 1961, *J. chem. Phys.*, **35**, 1483.
- ZAK, J., 1962, *J. Math. Phys.*, **3**, 1278.
- ZEPPENFELD, K., 1968, unpublished.
- ZVYAGIN, B. B., and SOBOLEVA, S. V., 1967, *Soviet Phys. crystallogr.*, **12**, 46.